Life-Cycle Assessment and Co-Benefits of Cool Pavements

Contract # 12-314
April 2017

Prepared for the California Air Resources Board and the California Environmental Protection Agency

Prepared by

Lawrence Berkeley National Laboratory (LBNL) - Prime contractor
Ronnen Levinson (Principal Investigator)
Haley Gilbert
Ling Jin
Benjamin Mandel (former staff)
Dev Millstein
Pablo Rosado

University of California Pavement Research Center (UCPRC)
John Harvey
Alissa Kendall
Hui Li
Arash Saboori
Jon Lea

University of Southern California (USC)
George Ban-Weiss
Arash Mohegh

thinkstep, Inc. (formerly PE International)
Nicholas Santero (former staff)

Disclaimer

The statements and conclusions in this report are those of the contractor and not necessarily those of the California Air Resources Board. The mention of commercial products, their source, or their use in connection with material reported herein is not to be construed as actual or implied endorsement of such products.

Acknowledgements

The authors thank the California Air Resources Board for funding this project under Contract 12-314. We especially thank Maggie Witt, Annalisa Schilla, and Annmarie Rodgers of the California Air Resources Board and Courtney Smith and Tabetha Willmon, formerly of the California Air Resources Board, for their guidance and management of the project. In addition, we are thankful to the California Department of Transportation for co-funding the project and to staff members Joe Holland, Nick Burmas, and Deepak Maskey for their feedback. We are thankful for the expertise and thoughtful reviews from our voluntary Advisory Team members: Donna Chralowicz, City of San Diego; Yvonne Hunter, Institute of Local Governments; Jan Kleissl, University of California at San Diego; Ash Lashgari, California Air Resources Board; Matt Machado, Stanislaus County; Eric Masanet, Northwestern University; Haider Taha, Altostratus, Inc.; Craig Tranby, Los Angeles Department of Water and Power; and Tom Van Dam, NCE.

We also thank Ramon Abueg, Glendale Water and Power; Ryan Bullard, Riverside Public Utilities; Harlan Coomes, Sacramento Municipal Utility District; Frederic Fletcher, Burbank Water and Power; Greg Green, Analytics Systems Computing & Engineering; and Eric Klinkner, Pasadena Water and Power. The cities of Bakersfield, Berkeley, Chula Vista, Fresno, Los Angeles, Richmond, Sacramento, and San Jose who provided information regarding their pavement management practices are also thanked for their time and effort. We wish to thank Mark Modera, University of California at Davis, for his review of the building energy modeling efforts. And lastly, we want to recognize the critical review team for the pavement life-cycle inventories who provided invaluable feedback during the inventory review process: Robert Karlsson (chair), Swedish National Road and Transport Research Institute; Jeremy Gregory, Massachusetts Institute of Technology; and Amlan Mukherjee, Michigan Technical University.

This project was funded by the California Air Resources Board under Contract 12-314. It was also supported by the Assistant Secretary for Energy Efficiency and Renewable Energy, Office of Building Technology, State, and Community Programs, of the U.S. Department of Energy under Contract No. DE-AC02-05CH11231. The statements and conclusions in this report are those of the authors and not necessarily those of the California Air Resources Board.

Table of Contents

List of Figures

List of Tables

Abstract

Alongside other strategies such as urban forestry, solar PV, and cool roofs, the use of high-albedo "cool" pavements can be considered in programs intended to help cities, regions, and the state meet California's greenhouse gas (GHG) emission reduction and sustainable community goals. While cool pavements can mitigate urban heat islands, improve urban air quality, and in some cases reduce GHG emissions from building energy use, it is also important to consider the environmental consequences of pavement materials and pavement construction, and thus the life-cycle environmental impacts.

Recognizing this, the researchers developed a pavement life-cycle assessment for California cities and translated it into a dynamic decision support tool. Local officials can use this tool to evaluate the life-cycle environmental impacts of various pavements, both conventional (lower albedo) and cool (higher albedo). The tool compares the primary energy demand (without feedstock energy), feedstock energy, and environmental effects of two possible pavement treatment scenarios over a 50-year life cycle, spanning the extraction and manufacturing of pavement materials to the removal and disposal or recycling of the material at the end of its service life. Users can determine, based on outputs from the tool, which options translate to reductions or increases in global warming potential, smog formation potential, generation of particulate matter, and energy demand. Local governments may use the tool as they evaluate pavement-related strategies for reducing their carbon footprints, which will in turn help the state meet its climate goals. It may also be useful as they weigh the potential public health impacts of different pavement options.

It is important to note that the tool does not consider the interaction of other cool community measures, such as urban forestry, with cool pavements; however, the researchers recommend examining these interactions in future research. We also recommend that the tool be transferred to a web-based platform to make it more accessible. In addition, a panel of local government and pavement stakeholders should develop local pavement scenarios to evaluate with the tool. This would provide real-world results to analyze for California cities.

Executive Summary

To maximize benefits and minimize environmental degradation, it is important that decisions about urban infrastructure consider potential life-cycle environmental impacts. Management of a city's pavement network is one of these important infrastructure decisions. While "cool" (high albedo) pavements have the potential to reduce greenhouse gas emissions, mitigate urban heat islands, and improve air quality in cities, it is also important to consider any environmental consequences that might accrue from the production and construction of cool pavement systems.

California has established significant greenhouse gas (GHG) reduction goals—to lower greenhouse gas (GHG) emissions to 1990 levels by 2020, and to 80% below 1990 levels by 2050. We know that the construction, use, and maintenance of California's roadways consume energy and produce GHGs. Such ambitious targets require cities and the state to decrease GHG emissions across all sectors. Therefore, California needs tools to help cities understand the global warming implications of different pavement management practices.

Heat transfer from pavements, which cover about one-third of a typical U.S. city, can also influence local temperatures and air quality. Most cities in California maintain city streets with low-albedo products, such as traditional slurry seals (albedo 0.07 to 0.10). However, pavement products with higher albedo (typically 0.20 to 0.35) are available.

Recognizing the GHG-reducing potential of increasing pavement albedo (solar reflectance), we developed a pavement life-cycle assessment (pLCA) decision support tool. Local officials can use this tool to evaluate the life-cycle environmental impacts of various pavements, both conventional (lower albedo) and cool (higher albedo).

The pLCA tool assesses the energy, GHG emission, air temperature, and air quality consequences of urban pavement choice over a 50-year life cycle. Users of the tool choose a city of interest, specify the fraction of that city's pavement area to be modified, and two pavement scenarios (each specifying pavement type, thickness, service life, and albedo). With this input information, the tool computes (for each scenario) the following:

1. Two life-cycle impact indicators—global warming potential (CO_2e) and smog potential (O_3e) and
2. Three life-cycle flows: particulate matter smaller than or equal to 2.5 micrometers, primary energy demand without feedstock energy, and feedstock energy.

The tool also calculates annual site electricity and gas energy consumed by the city's building stock.

These calculations consider the contributions to the indicators and flows from the following:

1. Extraction/manufacturing of the pavement materials (the "materials and construction" stage),
2. Transportation of the materials to the city where the pavement treatment will take place (the "materials and construction" stage),
3. Pavement construction (the "materials and construction" stage),
4. Removal and transport of the materials to a landfill or to a recycling center at the end of the pavement system's life (the "materials and construction" stage), and
5. Building cooling, heating, and light energy uses (the "use" stage).

The indicators and flows in the tool are based on California-specific pavement life-cycle inventories for pavement materials, construction, and energy sources.

The use-stage contributions to the impact indicators and flows include the cooling, heating, and lighting site energy uses of the buildings in the city. These contributions are calculated for both the "indirect" effect of pavement albedo—the influence of citywide mean pavement albedo on citywide mean air temperature and the variation of building energy use with that air temperature—and the "direct" effect of pavement albedo—the influence of local road albedo on the energy uses of buildings exposed to sunlight reflected from the road. The tool calculates the indirect effect by applying a regional climate model to California to derive the sensitivity of citywide air temperature to pavement albedo change. The air temperature changes are then included in simulations of the energy use of the building stock in California cities. The tool simulates the direct effect with building energy prototypes that incorporate local road albedo.

Each indicator, flow, and site energy use is tallied by stage element (material, transport, construction, cooling, heating, or lighting), subtotaled by stage (materials and construction, or use), and totaled over the life cycle. The tool then reports the difference of these values between the two scenarios.

The tool also reports differences in two additional instantaneous environmental metrics: seasonal values of city-mean hourly air temperature near the top of the urban canopy (derived from the regional climate model) and city-mean daily maximum 1-hour ozone concentration. The tool calculates the latter metric from the change in air temperature, coupled with an air basin specific sensitivity of ozone concentration to air temperature (derived from scientific literature).

The tool's evaluation of use-stage environmental effects is limited to those that result from changing pavement albedo. Therefore, it does not include other environmental effects from the use of pavements, such as the influence of pavement-vehicle interaction on fuel consumption.

We achieved the project objective by developing the first version of a tool that can inform local governments in California of the environmental effects of their pavement practices. It was beyond the scope of this project to analyze tool results for real-world scenarios. However, we found that the pavement design was very important and could significantly change the life-cycle assessment results. For example, portland cement concrete with supplementary cementitious materials generated less than half of the GHGs produced by the conventional portland cement concrete mix with the same thickness.

A very important next step before the tool is widely distributed will be the convening of a panel of local government and pavement stakeholders and the development of realistic local pavement scenarios that the panel can use to evaluate the tool. This would guide further development of scenarios and the interpretation of tool results.

Since this is the first version of the tool, it would benefit from further refinements to make it accessible for general use, including the development of a web-based tool and revisions to improve the presentation and communication of results.

1. Introduction

California has one of the most extensive paved transportation networks in the country. Table 1 illustrates the centerline miles and lane-miles of state- and federally-maintained streets.[1] Dark, dry paved surfaces tend to aggravate the urban heat island effect (UHIE), which is the elevation of air temperatures in a city above those experienced in less-developed surrounding areas. Rising urban temperatures threaten the health and well-being of Californians, particularly those of the most vulnerable populations, such as children, seniors, low-income individuals, and families (CalEPA & CDPH 2013). In addition to increasing heat-related sickness and death, higher air temperatures accelerate smog formation (CEC 2006) and increase air conditioning demand. The latter leads to greater power plant emissions and may destabilize the electricity grid on the highest demand days (USEPA 2008).

Table 1. Maintained public road networks in California, by jurisdiction (Caltrans, 2016).

Jurisdiction	Centerline Miles	Lane-Miles
Cities	76,915	174,929
Counties	64,441	131,508
State	15,100	51,900
Federal	14,915	29,829

All else being equal, pavements with lower albedo (solar reflectance) contribute more to the UHIE than pavements with higher albedo (Pomerantz et al. 2000). Raising pavement albedo lowers its temperature in the sun, which can in turn mitigate the UHIE and slow the formation of smog (Rosenfeld et al. 1998). Currently, most cities in California maintain city streets with low albedo, deploying slurry seals that traditionally have albedos in the range of 0.07 to 0.10. However, there are pavement products available with higher albedos, in the range of 0.20 to 0.35. This report refers to these higher-albedo pavements as "cool pavements."

It is important for cities to understand the consequences of deploying cool pavements to help them manage and meet their sustainability goals. However, switching pavement management practices may also change upstream environmental burdens. The extraction, production, and transportation of pavement materials and the construction of pavements generate pollution and consume energy. Life-cycle assessment (LCA) provides a comprehensive evaluation of the environmental burdens from a product or service by quantifying the environmental effects of a product throughout its life cycle. In LCA, the inputs (such as energy and resource consumption) and outputs (such as pollutant emissions) are identified and inventoried over the product's entire life cycle, which usually includes material production, material transport, construction, use, and end-of-life (Harvey et al. 2016).

Since the potential benefits and penalties of cool pavements can vary widely by region and because substituting cool pavement materials for conventional materials may produce undesired effects, we developed a first version of a pavement life-cycle assessment (pLCA) decision tool for cities in California. The tool is intended to evaluate citywide pavement system choices and focuses on the life-cycle environmental impacts of substituting cool pavement materials for business-as-usual pavement systems.

[1] A "centerline mile" is one mile of road, independent of its number of lanes, while a "lane-mile" is one mile of lane. A two-lane road would have twice as many lane miles as centerline miles.

We designed the pLCA tool to help cities in California understand the global warming and air quality implications of different pavement management practices. Global warming-related implications are particularly important in the context of statewide goals to lower greenhouse gas (GHG) emissions to 1990 levels by 2020 (CARB 2014a) and to further reduce emissions 80% below 1990's level by 2050 (CARB 2014b). Local actions to reduce GHGs are essential for the state to meet this goal, and as such, many cities have set their own GHG reduction targets. For example, the city of Los Angeles plans to reduce its annual GHG emissions to 20 megatons (Mt; also known as million metric tons, or MMT) CO_2e by 2025 and to 7.2 Mt CO_2e by 2050. These values are 45% and 80%, respectively, below its 1990 baseline (Mayor's Office Sustainability 2015). Such ambitious targets require that cities and the state decrease GHG emissions across all sectors, including emissions related to pavement systems.

This tool is intended to help local governments consider the life-cycle impacts of pavement systems as they make construction and maintenance decisions. It illuminates potential air quality and urban heat island effects of pavement systems and provides a snapshot of the potential global warming implications of different pavement treatments. We, along with our ARB partners, hope that cities and localities use the tool to make better-informed decisions and find it helpful in the development of climate action plans or other planning documents that summarize local actions for reducing GHGs.

1.1. Cool pavement literature review

Readers can find the full literature review in Appendix A. Here we include excerpts that touch on the environmental impacts of cool pavements, which we subsequently included in the scope of the pavement life-cycle assessment tool.

As a first step, we consulted cool pavement research literature to determine how these pavements interact with the environment. Pavement systems such as streets, sidewalks, parking lots, and hardscape playgrounds cover 30 to 40 percent of the urban surface in United States cities[2] (Akbari et al. 1999; Akbari and Rose 2008). Historically, most paved surfaces (over 80 percent) are made of asphalt concrete, which has characteristically low albedo (Pomerantz et al. 1997). Hot surfaces warm the city air through convection, so using materials that absorb less solar energy, such as high-albedo pavements, can reduce the flow of heat into the urban environment and moderate the UHIE.

Specifically, increasing pavement albedo decreases convective heating of the outside air. Meteorological simulations indicate that cool pavements, whether deployed in isolation or in conjunction with cool roofs and/or urban vegetation, can reduce urban temperatures. We summarize here previous studies that use mesoscale numerical weather prediction models to investigate the urban climate impacts of increasing albedo. Sailor (1995) found that increasing the albedo of the Los Angeles basin by an average of 0.08 reduced peak summer temperatures by up to 1.5 °C. Rosenfeld et al. (1995) used a mesoscale meteorological model to simulate the effect of increasing albedo and found a peak temperature reduction exceeding 3 °C in the afternoon over Los Angeles after increasing albedo in developed urban areas by 0.13 on average. Rosenfeld et al. (1998) investigated the impacts of increasing the albedo of roofs and pavements by 0.35 and 0.25, respectively. They found that peak maximum temperature decreased by 1.5 °C in Los Angeles. Taha (2008a) found that increasing the albedo of urban surfaces in Sacramento, CA could reduce temperatures by up to 3 °C. Taha (2008b) simulated many scenarios of surface albedo perturbation and found that resulting changes in temperatures depend on the scenario assumed and the

[2] Above-canopy urban fabric fractions characterize the surfaces that are not covered by the tree canopy and therefore can receive sunlight.

city under investigation. Maximum spatial-mean temperature reductions for most cities investigated were up to 1-2 °C. Taha (2008c) simulated the meteorology of Houston, Texas using the MM5 mesoscale model and found temperature reductions of up to 3.5 °C in some locations with decreases in albedo of 0.2, 0.18, and 0.05 for roofs, pavements and walls, respectively. Using a modified mesoscale model, Lynn et al. (2009) investigated mitigation strategies in New York City and found temperature decreases of about 1.5 °C and 2 °C at 12:00 and 18:00h local standard time (LST), respectively, after increasing albedo of impervious areas by 0.35. The larger nighttime cooling found by Lynn et al. was in contrast to some of the aforementioned previous studies that had found maximum cooling from albedo increases during the day. Millstein et al. (2011) modeled the climate of the entire United States and found city-mean afternoon temperature reductions of 0.1 to 0.5 °C after increasing roof and pavement albedo by 0.25 and 0.15, respectively. Georgescu et al. (2013) suggested that cool roof adoption could counter future urbanization-induced warming in Arizona's sun corridor by 50%. Georgescu et al. (2014) studied the effects of heat mitigation scenarios and compared them with projected air temperature increases caused by multiple scenarios of future urbanization over the United States. The results for California showed a reduction in surface air temperature of 1.5 °C after increasing roof albedo to 0.88 from their assumed baseline roof albedo. Using an updated urban canopy model that can resolve multiple ground and roof types per grid cell (Li et al. 2014a), Li et al. (2014b) investigated the effects of cool (and green) roofs for the Baltimore-Washington region. They found that increasing the albedo of all roofs to 0.7 from 0.3 reduced the city-mean surface and near surface air temperature urban heat island by up to about 3 °C and 0.7 °C respectively. The researchers simulated maximum surface temperature and surface air temperature reductions in both the afternoon and evening. Santamouris (2014) reviewed past studies on cool materials and suggested that urban albedo increases of 0.1 leads to a mean reduction in ambient air temperature of about 0.3 °C. Zhang et al (2016) investigated the climate impacts of adopting cool roofs in various cities around the world and found a 0.4 °C reduction in the mean urban heat island effect

The cool pavement literature further revealed the potential for multifaceted effects of reflective pavements on building energy use. Akbari et al. (2001) estimated that additional energy use for cooling attributable to the UHIE accounts for 5 to 10 percent of urban peak electricity demand. By lowering local air temperatures, cool pavements may reduce the cooling energy demands of buildings during summer (the "indirect" energy effect). However, the same properties that allow reflective pavements to keep cities cooler during the cooling season also keep them colder during the heating season, producing a "winter heating penalty" in colder climates. Still, simulation studies generally find that the indirect cooling effect generally results in larger annual cooling energy cost savings than heating energy cost penalties.

Pomerantz et al. (2015) developed a method that estimates the maximum annual indirect electrical energy saving resulting from a change of surface albedo for an entire city. The method uses simple linear equations and parameters that characterize the city, such as hourly power demand, daily temperature swing, annual hours of cooling, and albedo change. It assesses the total power demand of an entire city (i.e., the rate of electricity use for all purposes) to determine citywide air conditioning (A/C) power demand on a hot day. Pomerantz's method then calculates the maximum dependence of the A/C power on air temperature. The increase in air temperature due to changes in surface albedos is calculated with a simple interpolation method using the diurnal air temperature range, the size of the area modified, and the albedo changes (Pomerantz et al. 2000). Lastly, the maximum air temperature dependence of the A/C demand is combined with the maximum air temperature change caused by the albedo increase to estimate the maximum change in annual citywide A/C energy demand. For warm cities in California, such as Sacramento, the research found that the maximum electrical energy saving for an albedo increase of 0.20 was less than 2 kilowatt-hours (kWh) per year per square meter of city surface changed.

In addition to the indirect building energy use effect of high-albedo materials, there are also building energy use consequences from the increased scattering of sunlight. Higher-albedo pavements reflect

more sunlight onto walls and through windows of adjacent buildings, which increases solar absorption by building surfaces. This can increase a building's cooling load and reduce its heating load.

Another potential consequence of lower outdoor air temperatures from using more reflective pavement materials is improved urban air quality. Many cities have high concentrations of nitrogen oxides (NO_x) and volatile organic compounds (VOCs). These react in the presence of ultraviolet radiation from sunlight to form ozone (O_3), a principal component of smog. Because these photochemical reactions increase at higher temperatures, lower air temperatures can slow the formation of smog. As an example, Rosenfeld et al. (1998) simulated the air quality effects of deploying cool community strategies (higher albedo roofs and pavements as well as increasing tree cover) in Los Angeles, which resulted in a 12 percent reduction in smog exceedance (the population-weighted, eight-hour average ozone concentration above 90 ppb). About one-fifth of this effect was attributable to pavements that are more reflective.

The work performed to date leaves room for new research related to the use of cool pavements. This project focuses on several of those areas, including how building energy use for cooling, heating, and lighting is affected by sunlight reflected onto buildings from adjacent streets. While the literature contains research on the effects of cool pavements on outdoor lighting energy use, pedestrian comfort, and negative radiative forcing, these topics were not included in the scope of the pavement life-cycle assessment tool.

1.2. Pavement LCA literature review

Appendix A contains the full literature review. The following provides an overview of the pavement LCA literature.

Changing pavement albedo and the pavement system can affect upstream environmental burdens. Therefore, a life-cycle perspective is necessary to examine the net impact of substituting higher albedo pavement systems for conventional ones. We reviewed the research literature on pavement LCA to build a complete picture of the environmental impacts associated with cool pavement systems and to compare these impacts with those from conventional pavement practices.

LCA is an approach to investigate and quantify the potential environmental burdens of a product. In LCA, the inputs (such as energy and resource consumption) and outputs (such as pollutant emissions) are identified and inventoried over the product's entire life-cycle, which usually includes material production, material transport, construction, use, and end-of-life.

For pavements, the system boundary of the material production stage includes the extraction and initial processing of aggregates, asphalt, cement, and other supplementary materials. This stage also includes the transport between the mining site and the processing facilities, such as oil refineries, cement plants, and aggregate crushing operations, as well as mixing processes at the mixing plants.

One previously contentious topic in energy flow accounting in the material production stage was "feedstock energy," or the chemical energy embodied in a material that is not converted into work or heat. Due to the relatively large amount of feedstock energy stored in asphalt (~40 MJ/kg)—compared to other non-oil-based construction materials such as cement and aggregate—including this value in primary energy consumption can significantly change the result of comparisons with other pavement materials (Santero et al. 2011). The recently published Federal Highway Administration (FHWA) "Pavement Life Cycle Assessment Framework" calls for the separation of primary energy at least into energy that is used as fuel and energy that is used as a material, as is asphalt (Harvey et al. 2016).

The use-stage system boundary can include the following:

- impacts from additional vehicle fuel use from pavement-vehicle interaction,
- changes to the urban heat island effect and building energy use from modifications to pavement albedo and structure,
- non-GHG climate change effect from the pavement albedo,
- changes to roadway lighting due to the pavement albedo,
- carbonation of concrete pavement (the sequestration of CO_2 by the concrete as it reacts with CO_2 in the air or water over time to form calcium carbonate), and
- water pollution from leachate (the extraction of pollutants by water as it passes through pavements) and runoff (Harvey et al. 2011).

For this study, the use-phase system will only include changes related to alterations in pavement albedo. This includes changes to building heating, cooling, and lighting energy consumption, and effects on outdoor air temperature and quality.

The end-of-life (EOL) stage for pavements may consist of recycling or landfilling. Recycling of a pavement system requires the input of some virgin materials and energy and the output of pollutants, and may involve removal and transportation to a processing plant if not recycled in place. Impacts from landfilling primarily include the burdens of transporting waste to the landfill site. The scope of this study includes the EOL stage.

LCA can provide a comprehensive evaluation of the environmental burdens from a product or service, making it a useful tool in decision-making. Although there are established standards for conducting LCAs on industrial products, the intricacy of pavement design makes pavement LCA much more complex than analyses of typical consumer products. This complexity has led to many deficiencies in the existing studies, including: unrepresentative functional units and analysis periods; incomplete scope (e.g., omission of life-cycle stages, typically the use stage); lack of state-of-the-art models for many sub-processes in the pavement life cycle; and lack of uncertainty analysis (Santero et al. 2011). Many of these concerns have been addressed in the recently published FHWA framework (Harvey et al. 2016). This study helps fill one of the gaps related to the proper use of state-of-the-art models to characterize sub-processes in the pavement life cycle.

This research project is unique in its investigation of the use-stage effects of pavements, specifically their contributions to the urban heat island effect and associated energy use and air quality consequences. It supplements best practices from the pavement LCA literature with cool pavement research methods to fill research gaps.

1.3. Project scope and assumptions

A diagram of the scope of the pavement life-cycle assessment (pLCA) decision tool is presented in Figure 1. The pLCA tool assesses the energy and environmental consequences of citywide pavement system choices over a 50-year life cycle. It is not designed for specific pavement project comparisons and does not address the cost of pavement materials, construction, and maintenance. The tool focuses on city streets only. Sidewalks, parking areas, and pedestrian areas are outside its scope. City streets represent about 45 percent of the paved lane-miles of motor vehicle roadway in California (Caltrans 2011).

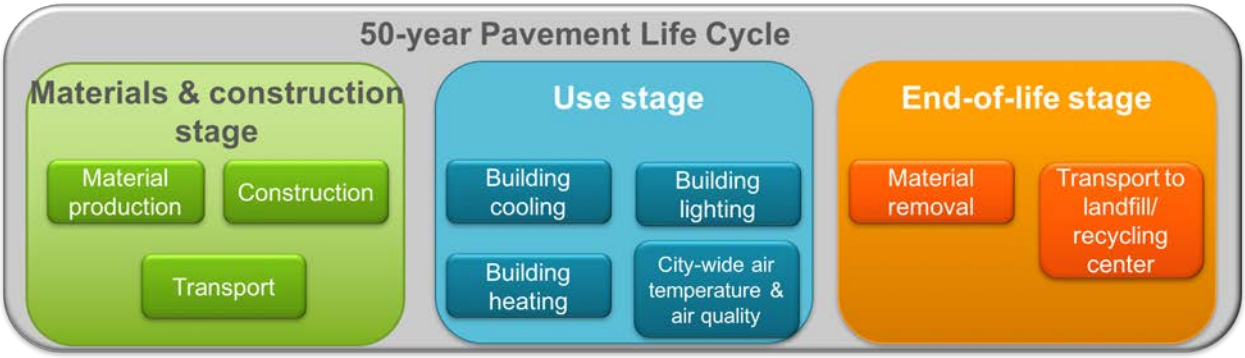

Figure 1. The scope of the pavement life-cycle assessment includes materials and construction stage and use-stage environmental effects over the 50-year life cycle. The end-of-life stage impacts are captured in the materials and construction stage.

The scope includes the material production, construction, and transportation in the materials and construction (MAC) stage, albedo-related environmental effects in the use stage (including building heating, cooling, and lighting, and changes to outdoor air temperature and quality) and the end-of-life stage for the pavement materials. The EOL stage impacts are captured in the MAC stage results. It is important to note that the pLCA tool does not include the negative radiative forcing effect from a rise in pavement albedo.

The following project assumptions and limitations bound the scope of the pLCA tool and the research to develop it:

- The tool excludes any cost analysis and comparisons of different pavement systems.
- We chose to assess the following five life-cycle impacts and flows:
  - Global warming potential
  - Photochemical ozone creation (smog) potential
    - Emission of smog precursors is a local issue and therefore emission location matters. However, this study disaggregates emissions by component, but not by location.
  - Particulate matter with aerodynamic diameter smaller than or equal to 2.5 micrometers (PM2.5)
    - Similar to the smog potential impact, the location of particulate emissions matters. While PM2.5 may be emitted in various locations throughout the life cycle of the pavement treatment, this study aggregates emissions and presents them independent of location.
  - Primary energy demand from renewable and non-renewable resources (net calorific value excluding feedstock energy)
  - Feedstock energy (also referred to as primary energy demand from non-renewable resources used as a material)
- We selected a 50-year analysis period, which is about two to five times longer than the typical interval between pavement maintenance treatments (treatments to seal or restore the pavement surface). It also exceeds the typical interval between local government rehabilitation treatments (treatments that add structural capacity by adding layers or replace sufficient existing damaged

layers to add structural capacity). Thus, the 50-year period captures the repeat time for most possible scenarios.

- The tool assumes that each pavement is replaced with the same type of system at the end of its service life.
- The pavement materials and construction impacts of the final treatment in the 50-year analysis period are linearly pro-rated if any service life remains. In other words, life-cycle materials and construction stage impact is calculated by scaling impact per service life by the ratio of the analysis period (50 y) to the treatment service life.
- The electrical energy production mix used in the analysis is consistent with the California Renewables Energy Portfolio Standard, which requires 33% renewable energy by 2020. (The analysis mix is actually 28% renewable, based on utility projections.) Electricity imported into the state is not considered.
- Most of the pavement treatments considered in the tool were identified through consultations with local governments. However, we also included alternative treatments with higher albedo, permeable pavement (although the evaporative cooling effects of permeable pavements are not considered), and concrete pavement with supplementary cementitious materials.
- The pLCA tool user assigns to each pavement system a constant (presumably aged) albedo over the entire life cycle. This is not what happens in practice, where a generally small percentage of the pavements in a network would be changed each year, slowing changing albedo from year to year. However, this assumption was needed to provide a constant pavement albedo for urban climate modeling.
- The tool does not consider carbonation of concrete material when it is removed from the existing pavement. Carbonation is the reabsorption of CO_2 from the atmosphere by the hydrated cement to form calcium carbonate. Although studies using analytical chemical models have indicated that over long periods and under the right conditions carbonation can potentially result in a significant reduction in the long-term carbon emissions from cement production (Xi et al. 2016). However, most concrete material reclaimed at the end of its life in existing pavement is quickly processed and re-used in new pavement, limiting exposure to the atmosphere, and the practice of sequestering reclaimed concrete will result in the need to replace this material with virgin aggregate (Santero et al. 2013). Further research is warranted to better evaluate and validate carbonation models and the potential impact and cost-efficiency of sequestration considering California conditions.
- The tool does not track the spatial distribution of environmental effects. The tool totals the results without distinguishing location of the effects.
- The climate model methodology in this study used long simulations that represent a variety of meteorological regimes. Therefore, the air temperature reductions reported here would be different from those experienced during an extreme heat event.
- The climate modeling methodology focused on citywide air temperature changes. The effects of higher albedo pavements in a specific neighborhood, at the micrometeorological scale, could vary from what is reported here.
- For the climate model, we use area monthly mean values derived from satellite observations to create an annual cycle of vegetation parameters (e.g., vegetation fraction and albedo).
- Researchers performed building energy simulations with building prototypes that are compliant with California's 2008 Title 24 Standards (CEC 2008a and CEC 2008b). These standards require higher HVAC efficiency and better envelope insulation than what is found in most of the state's

current building stock—the median year of construction of residential buildings is 1975, and that of existing commercial buildings falls between 1970 and 1979. Hence, the simulations may have underestimated the direct and indirect building energy effects of cool pavements.

- The study did not account for shading of streets by vehicles or trees. It also did not consider the ability of trees to shade buildings from pavement-reflected sunlight.
- We do not consider the effect of pavement albedo change on sensible or latent heating of the city by building cooling equipment.
- The global warming potential calculations treat all greenhouse emissions over the analysis period as if they were released today. Kendall (2012) has developed time-adjusted warming potentials that consider when emissions take place.

1.4. Project structure

The pavement life-cycle assessment (pLCA) tool outlined above requires an interdisciplinary approach that entails several discrete but complementary research efforts. Our investigation included the following:

- local governments' pavement management and maintenance practices, to inform tool options and assumptions and allow for tool output to be comprehensible and actionable by its users;
- pavement material life-cycle inventories, to ensure that the pavement options presented in the tool utilize the most current figures for environmental flows that result from materials and construction life-cycle components and the end-of-life stage;
- modeling of urban climate to estimate citywide air temperature reductions induced by cool pavement adoption;
- estimates of urban ozone concentration decreases induced by air temperature reductions from cool pavement adoption; and
- city-scale building energy modeling, to capture the potentially nontrivial contributions to the life-cycle indicators and flows from pavement-related changes in building energy use.

Section 2 of the report details the materials and methods used to perform the research tasks listed above. Section 0 presents the results, Section 4 discusses the results, Section 5 summarizes and draws conclusions, and Section 6 provides recommendations for future research.

2. Materials and Methods

2.1. Overview

The indirect and direct effects of increasing pavement albedo contribute to the "use stage" impacts of the pavement life cycle, while the pavement's material production, construction, and transportation contribute to its "materials and construction stage" impacts. The contribution of the "end-of-life (EOL) stage" impacts is from the removal of the pavement materials and transportation of the materials to the landfill or recycling center. Increasing the albedo of pavement reduces convective heating of the outdoor air, reducing its temperature. This lowers the air temperature difference across the building envelope, decreasing heat gain via conduction and infiltration. This "indirect" effect of reflective pavement can reduce annual cooling load and increase annual heating load. Raising pavement albedo also increases the solar flux incident on walls and windows. This "direct" effect of reflective pavement can increase annual cooling load and reduce annual heating load.

Development of the pLCA tool involved the following, which are described in more detail in the following sections.

- assessment of local government pavement management practices in California
- assessment of pavement albedo
- calculation of life-cycle inventories for pavement materials and energy sources in California
- assessment of building stock in California
- urban climate modeling in California
- literature review of ozone temperature sensitivities in California
- building energy modeling in California
- tool coding
- tool input and output quality assurance

2.2. Assessment of local-government pavement management practice

We surveyed the cities of Bakersfield, Berkeley, Chula Vista, Fresno, Los Angeles, Richmond, Sacramento, and San Jose to learn about the size of their pavement networks and their pavement management practices. Specifically, we asked what percent of their network is treated in a typical year, what surface treatments are used, and what is the typical service life of treatments. Some local governments provided average data and most provided a detailed report with statistics for a number of years. The cities of Chula Vista, Los Angeles, Richmond, and Sacramento provided the last five years of data (2009-2013 or 2008-2012), and the remaining cities provided the most recent data available. We used both detailed and average city data to determine ranges of values for the pLCA tool, such as which pavement treatments to include and expected service lives for the treatments.

2.3. Assessment of pavement albedo

2.3.1. Pavement albedo measurement technique

The American Society for Testing and Materials International (ASTM) provides several standard test methods to measure pavement albedo, including the following:

- ASTM C1549: Standard Test Method for Determination of Solar Reflectance Near Ambient Temperature Using a Portable Solar Reflectometer (ASTM International 2014)
- ASTM E903: Standard Test Method for Solar Absorptance, Reflectance, and Transmittance of Materials Using Integrating Spheres (ASTM International 2012)
- ASTM E1918: Standard Test Method for Measuring Solar Reflectance of Horizontal and Low-Sloped Surfaces in the Field (ASTM International 2006)

For example, the UC Pavement Research Center (UCPRC) follows ASTM E1918 using a first-class albedometer (back-to-back first-class pyranometers) and a data logger, as shown in Figure 2. The UCPRC implementation of ASTM E1918 is detailed by Li et al. (2013).

Figure 2. Albedo measurement system with a dual-pyranometer albedometer. Note that the albedometer is normally placed closer to pavement than shown here.

2.3.2. Lawrence Berkeley National Laboratory pavement albedo database

The Heat Island Group at Lawrence Berkeley National Laboratory (LBNL) has compiled a pavement albedo database. This database includes laboratory measurements performed on samples of various cool pavement treatments using either a PerkinElmer Lambda 900 UV-vis-NIR spectrophotometer with Labsphere 15 cm integrating sphere (ASTM E903) or a Devices & Services Solar Spectrum Reflectometer (ASTM C1549). It also includes field measurements performed with an Eppley Precision

Spectral Pyranometer (first class), a Kipp & Zonen CMP6 first-class pyranometer, or a Kipp & Zonen CMA6 first-class albedometer (ASTM E1918). Many of the measurements in the laboratory were taken as part of iterative product development processes with manufacturers. Measurements taken mid-development are not presented in this report.

The field measurements were recorded mostly at LBNL's UC Davis demonstration site using ASTM C1549 and/or ASTM 1918 (Gilbert et al. 2014). Information recorded about the ages of each measured pavement were used to develop time series data for albedo. The pavement materials characterized in these field measurements include asphalt concrete, asphalt concrete with a reflective coating, chip seal, portland cement concrete, and portland cement concrete with a reflective coating.

2.3.3. Federal Highway Administration pavement albedo database

An ongoing Federal Highway Administration (FHWA) project, "Quantifying Pavement Albedo" (Solicitation Number: DTFH61-12-R-000050), has been measuring the albedo of different pavement materials. Albedo data was provided to us for a number of sections with asphalt and cement materials at different ages measured with ASTM E1918.

2.3.4. University of California Pavement Research Center pavement albedo database

The UCPRC pavement albedo database includes measurements from an on-going onsite pavement study, and several offsite field measurements. The pavement materials included in the albedo database for development of the pLCA tool are summarized in Table 2. All albedo measurements followed the UCPRC implementation of ASTM E1918 as detailed in Li et al. (2013). The ages of the pavement materials included in the database vary significantly.

The UCPRC database includes pavement albedo data from an ongoing cool pavement study. The ongoing study features nine test pavement sections, including three specimens of interlocking concrete pavement (commonly referred to as "pavers" and designated as surfacing type A in the UCPRC study); three specimens of asphalt concrete (AC, or surfacing type B); and three specimens of portland cement concrete (PCC, or surfacing type C). One impermeable paver and two different types of permeable pavers were used within surfacing type A. Dense-graded hot mix asphalt was used on one section within surfacing type B, and open-graded asphalt was used for the other two type B sections. One impermeable concrete mix was used within type C, and two different pervious concrete mixes were used for the remaining two type C sections. The first pervious concrete mix had a higher sand content and smaller maximum aggregate size than the second pervious mixture. Each section was 4 m by 4 m.

The pavement albedo measurements followed ASTM E1918 but the test sections were small than specified in the standard. However, the measurements were performed in the center of each pavement section (2 m from the edge) with the pyranometer 0.5 m above the pavement section. Additionally, since the pavement sections were smaller than the size specified in ASTM E1918, extra albedo measurements were performed on larger pavement sections to check the edge effect. These extra measurements demonstrated that there was no significant difference between the albedo values made from 2 m from the edge to those with up to 4 m separation from the edge with the pyranometer at 0.5 high. More details on the measurement methodology can be found in Li et al. (2013).

Table 2. Summary of albedo measurements of pavement materials included in UCPRC pavement albedo database (Li et al. 2013).

Surface category	Permeable type	Binder/cement/color type	Code [a]	Measurement date (mm/dd/yy) (Pavement age at measurement)
Asphalt	Impermeable	Conventional	B1 [b]	09/19/11, 10/13/11, 02/15/12, 05/02/12 [c]
	Permeable	Polymer modified	B2 [b]	09/19/11, 10/13/11, 02/15/12, 05/02/12 [c]
	Permeable	Polymer modified	B3 [b]	09/19/11, 10/13/11, 02/15/12, 05/02/12 [c]
	Impermeable	Polymer modified	PMA	10/13/11 (3 years)
	Impermeable	Rubberized	RHMA	10/13/11 (3 years)
	Impermeable	Warm mixed asphalt	RWMA	10/13/11 (2 years)
	Permeable	Polymer modified	OGFC	10/13/11 (1 year)
	Impermeable	Conventional	Aged AC	10/13/11 (5 years)
	Impermeable	Conventional (parking lot)	Aged AC	05/21/14 (5 years)
Concrete	Impermeable	Conventional	C1 [b]	09/19/11 10/13/11, 02/15/12, 05/2/12 [c]
	Permeable	Conventional	C2 [b]	09/19/11 10/13/11, 02/15/12, 05/2/12 [c]
	Permeable	White	C3 [b]	09/19/11 10/13/11, 02/15/12, 05/2/12 [c]
	Impermeable	Conventional	PCC	10/13/11 (3 years)
	Impermeable	Conventional (parking lot)	PCC	05/21/14 (5 years)
Interlocking Concrete Paver	Impermeable	Conventional - orange	A1 [b]	09/19/11 10/13/11, 02/15/12, 05/2/12 [c]
	Permeable	Conventional - champagne	A2 [b]	09/19/11 10/13/11, 02/15/12, 05/2/12 [c]
	Permeable	Conventional - orange	A3 [b]	09/19/11 10/13/11, 02/15/12, 05/2/12 [c]
Treatment	Impermeable	Conventional	Slurry Seal	05/21/14 (5 years)
	Impermeable	Conventional	Chip Seal	05/21/14 (5+ years)
	Impermeable	Conventional	Cape Seal	05/21/14 (3+ years)
	Impermeable	Conventional	Fog Seal	05/21/14 (0.1 and 3 years)
Gravel	Permeable	-	Gravel	10/13/11 (0.5 year)
Soil	Permeable	-	Soil	10/13/11
Grass	Permeable	-	Grass	10/13/11

[a] A1-A3, B1-B3, and C1-C3 are experimental test sections described previously. PMA is Polymer Modified Asphalt, RHMA is Rubberized Hot Mixed Asphalt, WMA is Warm Mixed Asphalt, OGFC is Open Graded Friction Course, AC is Asphalt Concrete, and PCC is Portland Cement Concrete.

[b] Monitored continuously over time.

[c] Ages for A1-A3, B1-B3, C1-C3: 9/19/11 (1 month), 10/13/11 (2 months), 02/15/12 (6 months), 05/02/12 (9 months).

The UCPRC pavement albedo database includes some additional field measurements that were performed in 2011 and 2012 (Li et al. 2013). The pavements measured were conventional asphalt concrete and portland cement concrete. Li et al. (2014) also reported the albedos of other land cover materials, including gravel, soil, and grass. These have been included in Table 2 for comparison.

Lastly, the UCPRC pavement albedo database includes a third set of field albedo measurements conducted around Davis, CA in May 2014. Albedo measurements were recorded for the following pavement treatments: slurry seal, fog seal, cape seal, chip seal, conventional asphalt concrete, and portland cement concrete.

Table 3 provides a list of the ranges of albedo gathered from the various sources discussed in Section 2.3. The albedo ranges are matched with the pavement treatments identified by the local government survey and additional alternative treatments identified by UCPRC.

Table 3. Summary of pavement treatment materials.

Treatment type	Range of albedo	Typical range of service life (years) [a]	Allowable thickness range (cm)
Bonded Concrete Overlay on Asphalt (BCOA) OP139SCM139	0.2 - 0.35	10 - 20	6.25 - 17.5
Bonded Concrete Overlay on Asphalt (BCOA) OP267SCM71	0.2 - 0.35	10 - 20	6.25 - 17.5
Bonded Concrete Overlay on Asphalt (BCOA) OP448SCM0	0.2 - 0.35	10 - 20	6.25 - 17.5
Cape Seal	0.05 - 0.15	2 - 15	n/a
Chip Seal	0.1 - 0.24	1 - 10	n/a
Fog Seal	0.04 - 0.07	1 - 5	n/a
Conventional Asphalt Concrete, Hveem (mill and fill)	0.05 - 0.15	5 - 20	2.5 - 37.5
Conventional Asphalt Concrete, Hveem (overlay)	0.05 - 0.15	5 - 20	2.5 - 37.5
Conventional Asphalt Concrete, Superpave (mill and fill)	0.05 - 0.15	5 - 20	2.5 - 37.5
Conventional Asphalt Concrete, Superpave (overlay)	0.05 - 0.15	5 - 15	2.5 - 37.5
Conventional Interlocking Concrete Pavement (Pavers)	0.2 - 0.35	5 - 20	n/a
Permeable Asphalt Concrete (Only the Asphalt Layer)	0.08 - 0.15	5 - 20	10 - 37.5
Permeable Portland Cement Concrete (Only the PCC Layer)	0.2 - 0.3	5 - 20	10 - 37.5
Permeable Rubberized Asphalt Concrete (Only the Asphalt Layer)	0.08 - 0.15	5 - 20	10 - 37.5
Permeable Section (Only the Crushed Agg Base Layer)	0.2 - 0.3	5 - 20	15 - 60
Permeable Asphalt Concrete (with Crushed Agg as Base Layer)	0.08 - 0.15	5 - 20	n/a
Permeable Portland Cement Concrete (with Crushed Agg as Base Layer)	0.2 - 0.3	5 - 20	n/a
Permeable Rubberized Asphalt Concrete (with Crushed Agg as Base Layer)	0.08 - 0.15	5 - 20	n/a
Portland Cement Concrete (PCC) OP139SCM139	0.2 - 0.3	10-60 depending on design	15 - 37.5
Portland Cement Concrete (PCC) OP284SCM50	0.2 - 0.3	10-60 depending on design	15 - 37.5
Portland Cement Concrete (PCC) OP418SCM0	0.2 - 0.3	10-60 depending on design	15 - 37.5
Reflective Coating - Bisphenol A (BPA)	0.2 - 0.3	User Defined	n/a
Reflective Coating - Polyester Styrene	0.2 - 0.3	User Defined	n/a
Reflective Coating - Polyurethane	0.2 - 0.3	User Defined	n/a
Reflective Coating - Styrene Acrylate	0.2 - 0.3	User Defined	n/a
Rubberized Asphalt Concrete (mill and fill)	0.04 - 0.13	5 - 20	2.5 - 6.5
Rubberized Asphalt Concrete (overlay)	0.04 - 0.13	5 - 20	2.5 - 6.5

Sand Seal	0.07 - 0.1	1 - 6	n/a
Slurry Seal	0.07 - 0.1	1 - 10	n/a

[a] Treatment Selection for Flexible Pavements from Pavement Treatment Selection Guide from National Center of for Pavement Preservation (no longer available), Caltrans (2003), Hicks et al. (2000), discussions with California cities and pavement consultants, and UCPRC experience.

2.3.5. Dynamic model for urban albedo

Urban land cover includes buildings, pavements, vegetation, and bare soil. Public organizations and private entities own the paved areas in cities. Part of the paved area is the public pavement network managed by a government agency. Every year a portion of the public pavement network undergoes maintenance to repair it or extend its life. This results in a relatively small fraction of a city's total area that undergoes pavement maintenance or treatment every year. A system diagram depicting these nested land cover domains is shown in Figure 3.

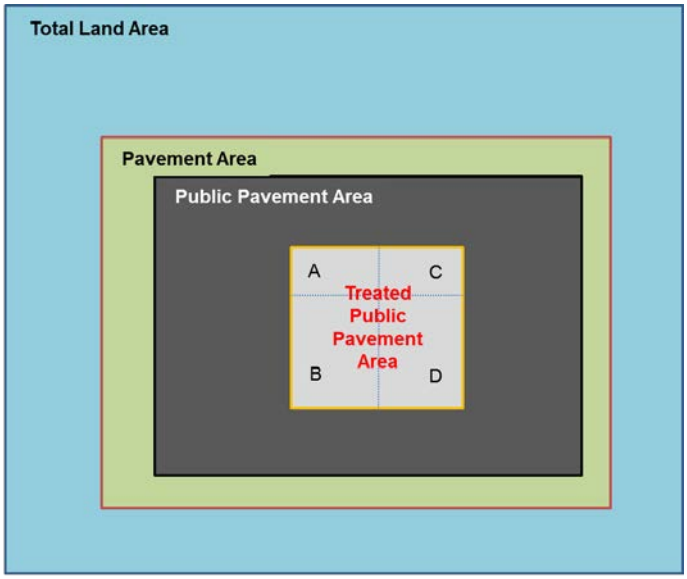

Figure 3. Urban land cover concept, with A, B, C, and D representing different pavement treatments on treated public pavement area.

Every year portions of the public pavement network undergo maintenance. The maintenance treatment is selected based on the existing pavement type, pavement condition, traffic levels, and available funding. Treatments are defined in terms of the material(s) used. The thickness of the materials used for pavement maintenance treatments vary and are specified by the pavement design. However, there are some maintenance treatments where the thickness is not specified because the treatment material is applied at a rate to cover the surfaces, such as slurry seals.

Since the albedos of the maintenance treatments vary, the overall albedo of the public pavement network changes over time. This process can be modeled with a dynamic albedo model, as shown in Eqs. (1)-(4):

$$\alpha_t = (1\text{-}R_{p,t})\ \alpha_{np,t} + R_{p,t}\ \alpha_{p,t} \quad (1)$$

$$\alpha_{p,t} = (1\text{-}R_{pp,t})\ \alpha_{npp,t} + R_{pp,t}\,\alpha_{pp\,t} \quad (2)$$

$$\alpha_{pp,t} = (1\text{-}R_t)\ \alpha_{t\text{-}1} + R_t\,\alpha'_t \quad (3)$$

$$\alpha'_t = \sum n_{i,t}\,\alpha_{i,t} \quad (4)$$

Where:

- $R_{np,t}$ is the total non-pavement area portion in urban land surface in year t;
- $R_{p,t}$ is the total pavement network area portion in urban land surface in year t;
- $R_{pp,t}$ is the total *publicly managed* pavement network portion in urban land surface in year t;
- R_t is the portion of pavement network for treatment in year t;
- $n_{i,t}$ is the portion of treated pavement network which use treatment i in year t;
- α_t is the albedo of total urban area in year t;
- $\alpha_{p,t}$ is the albedo of total pavement area in year t;
- $\alpha_{np,t}$ is the albedo of total non-pavement area in year t;
- $\alpha_{npp,t}$ is the albedo of non-public pavement area in year t;
- $\alpha_{pp,t}$ is the albedo of public pavement area in year t;
- $\alpha_{i,t}$ is the albedo of pavement treatment i in year t;
- α_t is the average albedo of pavement network in year t;
- α'_t is the average albedo of pavement treated in year t;
- i is the pavement treatment type (A, B, C, …); and
- t is the year (1, 2, ..., 50).

For this study we assumed that the albedo of the non-pavement area does not change. Therefore, the focus is on the changes in the albedo of the pavement area, which are evaluated using Eqs. (2)-(4).

2.4. Pavement material life-cycle inventories

Life-cycle assessment (LCA) is used to investigate and quantify the environmental impacts of a product or service within its life cycle. The International Organization for Standardization (ISO) has developed guidelines for conducting LCA (ISO 14040 series [ISO 2006]) and has identified four major steps for any LCA study: goal and scope definition, life-cycle inventory (LCI), life-cycle impact assessment (LCIA), and interpretation. The process begins with defining the goal of the study, which in turn determines the system boundary and scope of study, the duration of the study, and a suitable functional unit. The next step is the inventory stage in which all the inputs and outputs within the system boundary are quantified. Inventories normally consist of input flows of raw materials and energy and output flows of waste and pollution (depending of the system boundary) emissions to air, water, and soil as well as the flow of product output. The input flows of primary energy demand—broken down into renewable energy consumed, non-renewable energy consumed and feedstock energy—and the output flow of particulate matter smaller than 2.5 microns were identified as being important to the goals of this project. These flows were calculated for the cradle-to-gate of the material (extraction from the ground to delivery of the final processed material at the gate of the plant) regardless of the location of where the inputs were used or where the output flows occurred.

Feedstock energy is defined by ISO 14040 as “the heat of combustion of a raw material input that is not used as an energy source to a product system, expressed in terms of higher heating value or lower heating value”. In this study bitumen (asphalt) is an oil-based product that is used as a material and not used as an

energy source, and therefore has high feedstock energy content. Crumb rubber modifier and some other additives in other pavement materials also have feedstock energy. Feedstock energy can dominate the non-renewable energy quantities in pavement LCA. The UCPRC Pavement LCA Guidelines (Harvey et al. 2010) and the FHWA pavement LCA guidelines (Harvey et al. 2016) recommend that feedstock energy be shown separately from other energy flows to identify the use or depletion of oil as a non-renewable energy resource that is not combusted.

LCI results are then classified and categorized into several environmental impact categories such as global warming, acidification, eutrophication, primary energy consumption, and ozone layer depletion. The current study uses the "Tool for Reduction and Assessment of Chemicals and Other Environmental Impacts" (TRACI) 2.1 impact assessment methodology developed by US Environmental Protection Agency (Bare 2012). The following impact indicators were identified to meet the goals of this study: global warming potential (GWP), photochemical ozone creation potential (POCP), and human health particulate (PM2.5). The UCPRC Pavement LCA Guidelines (Harvey et al. 2010) were used as the initial framework for this study, and the FHWA pavement LCA framework (Harvey et al. 2016) was consulted after it was published near the end of this study.

Figure 4 shows the complete life cycle of any pavement section. Materials and construction, and EOL stages were considered in this study for the development of the surface treatment LCIs and LCIAs, use stage impacts due to vehicle fuel consumption were not in the scope of this study. The GaBi software, a commercial LCA software developed by thinkstep, Inc. (GaBi 2014), was used to model each material. The full LCI of each item consists of hundreds of inputs and outputs, while this study is focused on energy consumption, global warming potential, and emissions to air that affect air quality. Table 4 lists the flows and indicators calculated for inclusion in the pLCA tool. Table 5 lists the commonly used materials, energy sources, and transport modes for which LCIs and LCIAs were prepared. LCIs and LCIAs for reflective coatings are presented in the Section 2.4.3.

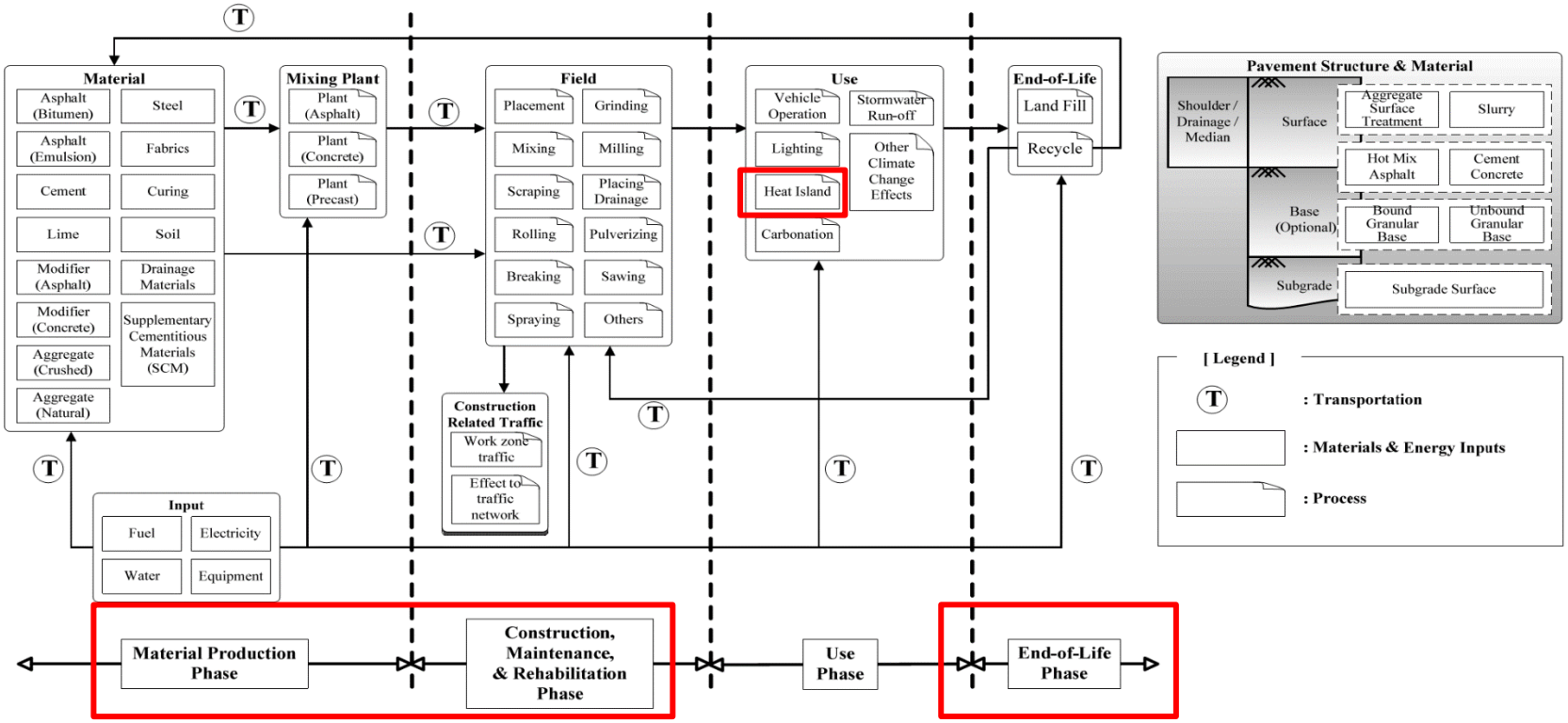

Figure 4. The complete life cycle of a pavement (Harvey et al. 2010) is depicted but the life cycle stages and components considered in this study are outlined in red boxes.

Table 4. Indicators and flows to be used in the final software.

Impact category/inventory	Abbreviation	Unit
Global warming potential	GWP	kg CO_2e
Photochemical ozone creation (smog) potential	POCP	kg O_3e
Particulate matter, less than 2.5 micrometers in diameter	PM2.5	kg
Primary energy demand from renewable & non-renewable sources (net calorific value excluding feedstock energy)	PED (total)	MJ
Feedstock energy	FE	MJ

Table 5. Materials, energy sources, and transport modes considered in the study.

	#	Item
Materials and Energy Sources	1	Aggregate – Crushed
	2	Aggregate – Natural
	3	Bitumen
	4	Bitumen Emulsion
	5	Blast Furnace Slag, Ground & Granulated
	6	Crumb Rubber Modifier (CRM)
	7	Diesel Burned in Equipment
	8	Dowel & Tie Bar
	9	Electricity
	10	Limestone
	11	Natural Gas Combusted
	12	Paraffin (Wax)
	13	Polypropylene Fibers
	14	Portland Cement Admixture, Accelerator
	15	Portland Cement Admixture, Air Enterainer
	16	Portland Cement Admixture, Plasticiser
	17	Portland Cement Admixture, Retarder
	18	Portland Cement Admixture, Superplasticiser
	19	Portland Cement Admixture, Waterproofing
	20	Portland Cement, Regular
	21	Portland Cement, with 19% Slag
	22	Portland Cement, with 50% Slag
	23	Reclaimed Asphalt Pavement (RAP)
	24	Quicklime
	25	Styrene Butadiene Rubber (SBR)
Transport	1	Barge Transport
	2	Heavy Truck (24 Tonne)
	3	Ocean Freighter

2.4.1. Assumptions and details for modeling materials, energy sources, and transport

Assumptions and references used in developing life-cycle inventories and impacts of commonly used materials and energy sources are discussed in this section. LCIs for items not discussed below were taken directly from GaBi or ecoinvent—a comprehensive European life-cycle inventory database included in the GaBi software. Appendix B contains snapshots of all the models developed in GaBi.

Aggregate - crushed

Table 10 in Marceau et al. (2007) was used to model crushed aggregate production in the plant, and is reproduced here as Table 6.

Aggregate - uncrushed

Table 9 in Marceau et al. (2007) was used to model uncrushed aggregate production in the plant, and is reproduced here as

Table 7.

Bitumen

The U.S. Life Cycle Inventory model preloaded in GaBi was used for bitumen, with the electricity in the model modified to reflect the electricity grid mix in California. The feedstock energy of bitumen (for bitumen and bitumen emulsion) we assumed to be 40.2 MJ per kg of residual bitumen.

Bitumen emulsion

Section 6.4 of the Eurobitume LCI report for bitumen (Eurobitume 2012) was used to develop Table 8.

Blast Furnace Slag, Ground & Granulated

The LCI for this item was taken directly from ecoinvent 3.1 database available through GaBi. Refer to end-of-life and recycling section for details on allocation methodology used for blast furnace slag.

Crumb Rubber Modifier (CRM)

A new model in GaBi was developed based on Corti et al. (2004). This model is available in Appendix B.

Electricity

We modeled both the 2012 and a projected electricity grid mix for California. The electricity grid mix for 2012 was taken from the California Energy Almanac website (CEC 2014) and the 2020 projected grid mix was based on the California Renewables Portfolio Standard (RPS) from California Public Utilities Commission (CPUC 2011). The table for 2012 is reproduced here as Table 9 and the electricity grid mix projected for California 2020 is listed in Table 35.

Portland cement

The LCI model for portland cement (PC) was developed based on a Portland Cement Association report (Marceau et al. 2006). As of 2015 the majority of the cement used in California is manufactured in the state; therefore, the electricity sub-model for PC was modified to represent the California grid mix. The standard PC used in California is Type I/II, which includes requirements for mild sulfate resistance. However, after the critical project review of the inventories, it was discovered that the process CO_2 was overestimated in Marceau et al. (2006) due to double counting the emissions from energy production. This was corrected by changing the process CO_2 using Xu et. al. (2016).

Polypropylene Fibers

The LCI for this item was taken directly from GaBi.

Transportation

It was assumed materials used in construction are transported 25 miles by truck from the quarry/mixing plant and that the trucks return empty, resulting in 50 round trip miles. The transportation of asphalt and cement to the mixing plant is included in the inventory for those materials.

Fly ash for use as a supplementary cementitious material (SCM) in concrete is assumed to be transported by truck 350 miles from the primary sources in the four corners area of Arizona and New Mexico to the California border and 80 miles inside California. Steel slag used as an SCM is assumed to be hauled 5,000 miles by marine transport and then 80 miles inside California by truck. It is assumed that all of the truck trips have the trucks return empty resulting in a doubling of the haul distance in the inventory.

End-of-life and recycling

Disposal of a material involves "allocation" and "cut-off." Allocation is the apportioning of environmental burden to different co-products coming from the same process, typically done when the process cannot be subdivided. Typical alternatives for allocation are by mass, by economic value, or by energy content. Cut-off is when some burdens are ignored because they are small enough to be considered insignificant, or because they are defined as being outside the system boundaries. These are two very contentious issues in pavement LCA because decisions made for allocation and cut-off can significantly change and often flip the calculated relative environmental impacts of competitive products, in particular with cement and asphalt. We have followed FHWA's Pavement LCA Framework document to the extent possible.

Most demolished pavement materials are recycled into new pavement materials. Some materials are overlaid (they remain and are covered with new material). When the recycled material is reused in the existing pavement, its processing is considered in the materials model. When the recycled material is not used in one of the treatments, the removal and transport are included. The assumed haul distance to the recycling plant or landfill is 25 miles, resulting in 50 round trip miles. Removal is assumed to occur in one pass of a milling or pulverizing machine. The same impacts have been assumed for removal of all treatments and all thicknesses of treatments. This is a simplification, however, the complexity of determining specific construction processes for each treatment/thickness combination is not warranted by the precision of the pLCA tool.

Details assumed for each treatment are:

- Seal coats (slurries, chip seals, reflective coatings) are very thin and are either covered or milled with the underlying asphalt. Since the pLCA tool assumes continuous use of the same treatment through the 50-year life cycle (a limitation), and seal coats are usually repeatedly placed on top of existing seal coat (no removal of asphalt) the removal and transportation of these materials was cut-off (not included).
- Most asphalt overlays that are removed (milled) go into new asphalt mix. The hot mix asphalt model assumes 15% recycled asphalt content in new asphalt mixes, which is typical in California. Removed asphalt not used in new material is assumed to be used in another life cycle and is cut-off. Removal, transportation and processing of the existing material are part of the model.
- Most existing concrete pavement and pavers are ground up and used as building foundation or parking lot material or as aggregate base in pavements. Removal and transport of the recycled concrete to a recycling plant or landfill is included in the model. The same is assumed for all types of permeable pavement.
- Recycled asphalt pavement (RAP) used in new asphalt mix and fly ash and slag (supplementary cementitious materials, SCM) used in concrete mixes have all of their environmental burdens attributed to their upstream uses (original asphalt pavement; coal burning for electric power; steel production, respectively) which are outside the system boundaries (cut off) and carry no environmental burdens into the pavement. The exception is that the additional processing required to use steel slag as an SCM is included in the model.

- Full-depth reclamation (FDR) and cold-in-place recycling (CIR) treatments process and reuse the existing material in place. Emissions from the construction equipment are included. The full impacts of materials and construction of the new asphalt overlay placed on top of the FDR or CIR are also considered. Each time this treatment is repeated in the life cycle, the new overlay also gets recycled in place.

Table 6. Aggregate-crushed production in plant, reproducing of Table 10 of Marceau et al. (2007).

Fuel or electricity	Total energy used		Energy/ton aggregate		
	Amount	Mbtu (million Btu)	Amount/ton	Btu/ton	kJ/metric ton
Coal	43,000	903,516	0.0000275	577	670
Distillate (light) grade nos. 1, 2, 4, & light diesel fuel, gallon	145,811,400	20,224,041	0.09320	12,920	15,030
Residual (heavy) grade nos. 5 & 6 and heavy diesel fuel, gallon	22,663,200	3,392,681	0.0145	2,167	2,520
Natural gas, 1000 cu ft	5,400,000	5,545,800	0.00345	3,543	4,120
Gasoline used as fuel, gallon	14,700,000	1,837,500	0.00939	1,174	1,370
Electricity, 1000 kWh	4,627,887	15,790,350	0.00296	10,088	11,730
Total	…	47,693,889	…	30,470	35,440

Table 7. Aggregate (uncrushed) production in plant, reproducing Table 9 of Marceau et al. (2007).

Fuel or electricity	Total energy used		Energy/ton aggregate		
	Amount	Mbtu (million Btu)	Amount/ton	Btu/ton	kJ/metric ton
Coal	58,969,600	8,177,697	0.05620	7,793	9,060
Distillate (light) grade nos. 1, 2, 4, & light diesel fuel, gallon	13,234,200	1,981,160	0.01260	1,888	2,200
Residual (heavy) grade nos. 5 & 6 and heavy diesel fuel, gallon	1,400,000	1,437,800	0.00133	1,370	1,590
Gasoline used as fuel, gallon	5,700,000	712,500	0.00543	679	790
Electricity, 1000 kWh	2,525,053	8,615,481	0.00241	8,210	9,550
Total	…	20,924,637	…	19,940	23,190

Table 8. Bitumen emulsion production in plant, from Section 6.4 of Eurobitume (2012).

Production of bitumen emulsion (1 tonne of residual bitumen)		Unit	Bitumen	Emulsifier	HCl	Hot water	Emulsion milling	Total
Raw material	Crude oil	kg	1000	1.1	-	-	-	1001.1
Energy resources	Natural gas	kg	20.1	0.22	0.34	0.08	1.21	21.9
	Crude oil	kg	40.9	1.4	0.4	1.8	0.4	44.9
	Coal	kg	1.03	0.3	0.67	0.07	3.25	5.32
	Uranium	kg	0.00006	0.00002	0.00004	0	0.00023	0.0004

Table 9. Electricity grid mix in California in year 2012 from California Almanac website (CEC 2014).

Fuel Type	Fraction of California electricity grid mix (%)
Coal	7.5
Large hydro	8.3
Natural gas	43.4
Nuclear	9.0
Oil	0.0
Other	0.0
Renewables	15.4
Biomass	2.3
Geothermal	4.4
Small hydro	1.5
Solar	0.9
Wind	6.3
Unspecified	16.4

2.4.2. Summary table of the LCI and LCIA for conventional materials, energy sources, and transport

Table 10 summarizes the major impact categories and inventories for the materials, energy sources, and transport modes discussed in this section.

2.4.3. Life-cycle inventory of reflective coatings (only material production stage)

A number of reflective coatings were identified from our literature search, and from discussions with researchers from Chinese universities. These researchers have worked extensively with reflective coatings for use on pavements to reduce urban heat island effects; see, for example, Cao et al. (2011). Coatings were first divided up into those that were solvent-based and those that were water-based. Solvent-based coatings have longer service lives but may release volatile organic compounds (VOCs) into the atmosphere, to the detriment of both the environment and human health. Water-based coatings have shorter lives, but are relatively benign. The commercially available coatings were then categorized into general types based on chemical composition, with a representative chemistry identified for each general type. The composition of each reflective coating was used to develop its LCA model in GaBi and calculate its LCI (GaBi 2014).

Table 11shows the composition of each coating and the LCI dataset from GaBi (GaBi 2014) that was used to model the process. For most cases, matching LCI datasets were found; in cases where matching datasets were not available, proxy datasets were selected. The table also shows the region from which each LCI dataset is taken. As there are regional differences in technology and processes, US data were given preference. The datasets developed in this project represent cradle-to-gate system boundaries, meaning that all upstream material and energy consumption and emissions and waste are included, from extraction of raw materials to transportation and processing in the plant. The LCIs also include an estimated electricity use of 0.1 MJ/kg to combine the chemicals, which accounts for less than 1% of the total primary energy demand of the coating.

Table 12 summarizes the main LCIA categories and inventory items of interest for the reflective coatings.

2.4.4. Pavement treatment options

Table 13 lists the pavement treatment options that were considered for the study. In this section a brief discussion of each treatment is presented and the assumptions made in modeling are discussed. The section ends with a summary of selected LCI and LCIA of the treatments discussed. Mix designs, construction methods, and other details and assumptions for each treatment are presented below. Most information is taken from the Maintenance Technical Advisory Guide (MTAG) published by Caltrans (2007).

Bonded concrete overlay on asphalt

Bonded concrete overlay on asphalt (BCOA) consists of adding a portland cement concrete (PCC) overlay to an existing asphalt concrete surface. Its thickness ranges from 5 cm (2 in) to more than 20 cm (8 in). BCOA with a thickness of 5 to 10 cm (2 to 4 in) is primarily used in urban areas with light traffic. For the purpose of this study, the default thickness was selected as 12.5 cm (5 in), although the thickness can be input by the tool user. BCOA construction consists of milling the existing asphalt layer (1.3 to 6 cm, assumed 2.5 cm in this study [0.5 to 2 in, assumed 1 in]), sweeping multiple times and air blasting,

wetting the surface, placing the concrete, and finally sawing and sealing of joints every 0.6 to 1.8 m (2 to 6 ft), all these activities were considered in modeling the construction stage except for sawing.

Three different mix designs were considered for BCOAs in this study: BCOA with no, low, and high supplementary cementitious materials (SCM) content.**Error! Reference source not found.** The mix design for high SCM content was obtained from Central Concrete, a ready-mix concrete plant in California. The mix designs for the other two were taken from Barmen et al. (2011).

Table 14 shows mix designs for the BCOA, permeable PCC, and conventional PCCs considered in this study. Each mix design has a code in which the numbers after OP (ordinary portland cement) and SCM represent the amount of each in 1 m^3 of concrete. For example, OP267SCM71 represents a mix with 267 kg of ordinary portland cement and 71 kg of SCM in 1 m^3 of portland cement concrete.

Cape seal

A cape seal is defined by the MTAG as a slurry seal applied over a chip seal.

Chip seal

We assumed that chip seals are constructed with 1.80 L/m^2 (0.40 gal/sy) of bitumen emulsion and 19 kg/m^2 (35 lb/sy) of aggregate. The construction process consists of sweeping, application of asphalt emulsion, spreading of aggregate, embedding of aggregate with pneumatic tire rollers, and a final round of sweeping. Aggregate is assumed to be angular and crushed.

Fog seal

The MTAG states that the emulsion application rate for fog seals is 0.45 to 0.68 L/m^2 (0.10 to 0.15 gal/sy), the average of which was used in this study. Construction consists of sweeping, spraying emulsion, and optional application of sand. We assumed that sand is not used.

Conventional asphalt concrete (mill-and-fill and overlay-only)

Two mix designs were considered for asphalt concrete (also known as hot mix asphalt, or HMA). One was taken from the UCPRC Case Studies Report (Wang et al. 2012) which was based on Hveem design method. It represents a typical mix design used by Caltrans in their rehabilitation projects. Most local governments in California use HMA mix design meeting Caltrans specifications. The second mix design was based on Superpave design method and was taken from (Zhou et al. 2012). The details of both mix designs are available in Table 15. The typical thickness of the asphalt concrete placed we assumed to be 5 cm (2 in). Two options are considered for the use of asphalt concrete. The first option is "mill-and-fill", in which the construction consists of milling (removing) 4.5 cm (1.8 in) of the surface (assumed thickness), applying a prime coat, placing new asphalt concrete on the subgrade using paver, and compacting the layer with three types of roller (vibratory, pneumatic, and static). The second option is "overlay-only", with similar mix design and thickness. The only difference is in the construction stage, where new HMA is placed directly over the old surface (no milling). In either case, the thickness of the new asphalt concrete is a variable that can be changed by the designer.

Conventional interlocking concrete pavement (pavers)

To determine the environmental impacts of pavers, Environmental Product Declarations (EPDs) developed by Angelus Block Inc. (2015) were used. The EPDs reported the impacts for two separate

functional units: m^3 of concrete paver materials, and concrete masonry unit (CMU). We assumed CMU to have the dimensions of 20 by 20 by 40 cm (8 by 8 by 16 in) and 50% voids.

Permeable asphalt concrete pavement

We assumed permeable asphalt concrete consisted of a base of thickness of 15 cm (6 in) made from 100% crushed and angular aggregate, topped with 11 cm (4.2 in) of open-graded asphalt concrete as recommended by Caltrans (2014). The mix design for the HMA layer was taken from Jones et al. (2010) and it was assumed to be 5.9 % asphalt and 94.1% aggregates.

Permeable portland cement concrete

We assumed permeable PCC consisted of a 15 cm (6 in) open-graded portland cement concrete layer on top of a 15 cm (6 in) granular base layer, as recommended by Caltrans (2014) and the mix design was taken from Jones et al. (2010). The mix design is available in Table 14.

Permeable rubberized asphalt concrete pavement

We assumed similar structure and layer thicknesses for both permeable HMA and permeable rubberized HMA (RHMA). The mix design for the RHMA layer was taken from Jones et al. (2010) and it was assumed to be 7.1 % asphalt and 92.9% aggregates.

Portland cement concrete

Three mix designs were considered for PCC: PCC with no, low, and high SCM content. The high SCM content mix design was considered similar to the BCOA with high SCM content. The other two were obtained from contractors in California, one representing a Caltrans' standard mix (OP284SCM50) and the other was a PCC used in a project in Santa Rosa that did not have any SCM. All three mix designs are available in Table 14. The thickness of the PCC layer we assumed to be 44.5 cm (17.5 in) as a default, although the thickness can be modified by the user in the pLCA tool. The construction process consists of grinding of the old asphalt concrete surface, sweeping, and laying down the PCC layer using a paver (the equipment used to deposit a predefined thickness of concrete). Saw cutting and curing were not included in the model.

Reflective coatings

The construction process consists of sweeping the pavement surface, then applying the coating with a tanker. The application rates collected from a literature summary (Li et al. 2014) ranged from 0.5 to 1.5 kg/m^2 (0.9 to 2.7 lb/sy). The average of the range for each coating was used in this study.

Rubberized hot mix asphalt concrete (mill-and-fill and overlay-only)

The mix design for rubberized hot mix asphalt concrete was taken from the UCPRC Case Studies Report (Wang et al. 2012). It represents a typical rubberized hot mix asphalt concrete used by Caltrans in their rehabilitation projects, and is presented in Table 16.

As in the case of conventional asphalt concrete, two options are provided here: mill-and-fill, and overlay-only. The construction process is assumed to be similar to that of conventional asphalt concrete. The thickness of the treatment in each case is assumed to be 5 cm (2 in), but can be changed by the pLCA tool user.

Sand seal

Sand sealing is the application of a bitumen emulsion surfaced with a top layer of sand. A pneumatic roller is often used to stabilize the sand. The range of emulsion application is 0.45 to 1.13 L/m^2 (0.1 to 0.25 gal/sy) and sand is applied at 9.7 to 13.5 kg/m^2 (18 to 25 lb/sy). For both sand and emulsion, the average application rate was used.

Slurry seal

For the type II slurry mix design typically used by California local government, we selected an application rate of 5 to 8 kg/m^2 (10 to 15 lb/sy) of crushed aggregate. We assumed residual asphalt content to be 7.5 to 13.5% aggregate by mass. For both aggregate and residual asphalt content, the average (mid-range) application rate was used.

Table 10. Summary of LCI and LCIA for conventional materials, energy sources, and transport, based on 2012 CA electricity grid mix.

	#	Item	Functional unit	GWP [kg CO2e]	POCP [kg O3e]	PM2.5 [kg]	PED (total) [MJ] *	PED (non-ren) [MJ] **	Feedstock energy [MJ]
Material Production and Energy Sources	1	Aggregate – Crushed	1 kg	3.430E-03	6.532E-04	1.592E-06	6.045E-02	5.242E-02	0.000E+00
	2	Aggregate – Natural	1 kg	2.357E-03	4.040E-04	9.538E-07	4.305E-02	3.651E-02	0.000E+00
	3	Bitumen	1 kg	4.754E-01	8.092E-02	4.098E-04	4.967E+01	4.933E+01	4.020E+01
	4	Bitumen Emulsion	1 kg of Residual Bitumen	5.069E-01	8.229E-02	4.169E-04	5.092E+01	5.044E+01	4.020E+01
	5	Blast Furnace Slag, Ground & Granulated	1 kg	1.028E-01	1.125E-02	1.162E-04	1.966E+00	0.000E+00	0.000E+00
	6	Crumb Rubber Modifier (CRM)	1 kg	2.129E-01	6.901E-03	1.050E-04	4.699E+00	3.599E+00	3.020E+01
	7	Diesel Burned in Equipment	1 gallon	1.194E+01	5.273E+00	9.369E-03	1.645E+02	1.645E+02	0.000E+00
	8	Dowel & Tie Bar	1 Each	3.694E+00	1.303E-01	1.388E-03	4.872E+01	4.199E+01	0.000E+00
	9	Electricity	1 MJ	1.320E-01	4.280E-03	2.538E-05	2.917E+00	2.234E+00	0.000E+00
	10	Limestone	1 kg	4.437E-03	2.108E-04	8.241E-08	7.836E-02	6.795E-02	0.000E+00
	11	Natural Gas Combusted	1 m3	2.408E+00	5.301E-02	1.310E-03	3.835E+01	3.835E+01	0.000E+00
	12	Paraffin (Wax)	1 kg	1.367E+00	7.569E-02	4.704E-04	5.461E+01	5.434E+01	0.000E+00
	13	Polypropylene Fibers	1 kg	2.331E+00	8.654E-02	5.530E-04	8.385E+01	8.107E+01	0.000E+00
	14	Portland Cement Admixture, Accelerator	1 kg	1.263E+00	5.713E-02	1.880E-04	2.280E+01	2.280E+01	0.000E+00
	15	Portland Cement Admixture, Air Enterainer	1 kg	2.664E+00	8.680E+00	2.547E-03	2.100E+00	2.100E+00	0.000E+00
	16	Portland Cement Admixture, Plasticiser	1 kg	2.295E-01	1.338E-02	5.573E-05	4.600E+00	4.600E+00	0.000E+00
	17	Portland Cement Admixture, Retarder	1 kg	2.314E-01	4.229E-02	9.810E-05	1.570E+01	1.570E+01	0.000E+00
	18	Portland Cement Admixture, Superplasticiser	1 kg	7.700E-01	4.549E-02	2.332E-04	1.830E+01	1.830E+01	0.000E+00
	19	Portland Cement Admixture, Waterproofing	1 kg	1.321E-01	4.004E-02	6.735E-05	5.600E+00	5.600E+00	0.000E+00
	20	Portland Cement, Regular	1 kg	8.720E-01	7.284E-02	4.985E-04	5.936E+00	5.584E+00	0.000E+00
	21	Portland Cement, with 19% Slag	1 kg	7.042E-01	2.600E-02	1.778E-04	3.404E+00	3.202E+00	0.000E+00
	22	Portland Cement, with 50% Slag	1 kg	4.449E-01	1.757E-02	1.228E-04	2.751E+00	2.558E+00	0.000E+00
	23	Reclaimed Asphalt Pavement (RAP)	1 kg	7.164E-03	1.394E-03	2.704E-06	1.021E-01	1.021E-01	0.000E+00
	24	Quicklime	1 kg	1.400E+00	3.518E-02	7.107E-04	7.875E+00	7.875E+00	0.000E+00
	25	Styrene Butadiene Rubber (SBR)	1 kg	4.126E+00	1.291E-01	4.477E-04	1.026E+02	1.017E+02	0.000E+00
Transport	1	Barge Transport	1000 kg-km	3.307E-02	9.576E-03	1.962E-05	4.170E-01	4.170E-01	0.000E+00
	2	Heavy Truck (24 Tonne)	1000 kg-km	7.798E-02	1.243E-02	2.492E-05	1.116E+00	1.116E+00	0.000E+00
	3	Ocean Freighter	1000 kg-km	1.833E-02	1.114E-02	1.873E-05	2.311E-01	2.311E-01	0.000E+00

* The total primary energy demand **excluding** the feedstock energy, if feedstock energy is applicable, available, and shown in the table. If feedstock energy is unknown, the PED Total is the total primary energy demand **including** the unknown feedstock energy.

** Same note as above applies to PED (non-renewable)

Table 11. Chemical composition of and LCI dataset used for each coating (GaBi 2014).

Coating	Chemical name	Mass fraction (%)	Representative LCI dataset	Dataset country/ region [a]
A. Polyester styrene (solvent-based)	Unsaturated polyester resin	60	Polyester Resin unsaturated (UP)	DE
	Styrene	24	Styrene	US
	Titanium dioxide	8	Titanium dioxide pigment	US
	Silicon dioxide	4	Silica sand (flour)	US
	Iron oxide	1	Iron oxide ($Fe2O_3$) from iron ore	DE
	Polysiloxane	0.5	Siloxane (cyclic) (from organosilanes)	DE
	Ethylene bis(steramide)	0.5	Ethanediamine	DE
	Cobalt napthenate	2	Cobalt mix	GLO
B. Bisphenol A (BPA, solvent-based)	Bisphenol A epoxy resin	75	Bisphenol A	US
	Titanium dioxide	10	Titanium dioxide pigment	US
	Carbon black	0.5	Carbon black (furnace black; general purpose)	US
	Propylene glycol phenyl ether	3	Dipropyleneglycol dibenzoate plast	EU-27
	Glycerol monostearate	1.5	Stearic acid	DE
	Tetramethylethylenediamine	10	Tetraacetyl ethylenediamine (TAED)	NL
C. Styrene acrylate (water-based)	Styrene	7.7	Styrene	US
	Titanium dioxide	6	Titanium dioxide pigment	US
	Butyl acroylate	13	Butyl acrylate	DE
	Methyl acrylate	5.4	Methyl acrylate from acrylic acid by esterification	DE
	Methacrylic acid	3	Methacrylic acid	US
	Zinc oxide	6	Zinc oxide	GLO
	Ammonium persulfate	0.18	Ammonium sulphate, by product acrylonitrile, hydrocyanic acid	US
	N-dodecyl mercaptan	0.1	Methanthiol (methyl mercaptan)	US
	Ammonium sulfite	0.02	Sodium hydrogen sulfite	EU-27
	Hydroxypropane-1-sulphonate	1.6	Soaping agent (sodium alkyl-benzenesulphonate)	GLO
	Azirdine	1	Hydrazine hydrate/hydrazine	DE
	Ammonium hydroxide	1	Tetramethyl-ammonium hydroxide (TMAH)	US
	Water	55	Water deionized	US
D. Polyurethane (water-based)	cis-1,4-cyclohexylene diisocyanate	8	Isophorone diisocyanate (IPDI)	DE
	Polyester polyols	18	Long Chain Polyether Polyols mix	EU-27
	Titanium dioxide	12	Titanium dioxide pigment	US
	Silicon dioxide	0.6	Silica sand (flour)	US
	Sodium dodecyl sulfate	2	Detergent (fatty acid sulfonate derivate)	GLO
	1,6-Diisocyanatohexane	3	Methylene diisocyanate (MDI)	DE
	2,2-Bis(hydroxymethyl)propionic acid	2	Adipic acid	DE
	Polydimethylsiloxane	0.4	Siloxane (cyclic) (from organosilanes)	DE
	Water	54	Water deionized	US

[a] DE: Germany, EU: Europe, GLO: Global, US: United States

Table 12. Summary of typical LCI and LCIA of reflective coatings by major type.

Item	Functional unit	GWP [kg CO_2e]	POCP [kg O_3e]	PM10 [kg]	PED (total)* [MJ]	PED (non-ren)** [MJ]	Feedstock energy [MJ]
BPA	1 kg	3.733e+00	1.607e-01	1.405e-07	9.076e+01	8.862e+01	n/a
Polyester styrene	1 kg	4.399e+00	2.079e-01	2.234e-06	9.174e+01	8.741e+01	n/a
Polyurethane	1 kg	2.341e+00	1.022e-01	2.197e-07	5.153e+01	4.903e+01	n/a
Styrene acrylate	1 kg	1.557e+00	6.340e-02	3.877e-07	3.663e+01	3.538e+01	n/a

* The total primary energy demand excluding the feedstock energy, where feedstock energy is applicable and available and shown in the table. Otherwise, PED Total is the total primary energy demand including the unknown feedstock energy

** Same note as above applies to PED (non-renewable)

Table 13. Pavement treatments considered in the study and listed in the pLCA tool.

#	Treatment
1	Bonded Concrete Overlay on Asphalt (BCOA) OP139SCM139
2	Bonded Concrete Overlay on Asphalt (BCOA) OP267SCM71
3	Bonded Concrete Overlay on Asphalt (BCOA) OP448SCM0
4	Cape Seal
5	Chip Seal
6	Fog Seal
7	Conventional Asphalt Concrete, Hveem (mill and fill)
8	Conventional Asphalt Concrete, Hveem (overlay)
9	Conventional Asphalt Concrete, Superpave (mill and fill)
10	Conventional Asphalt Concrete, Superpave (overlay)
11	Conventional Interlocking Concrete Pavement (Pavers)
12	Permeable Asphalt Concrete (Only the Asphalt Layer)
13	Permeable Portland Cement Concrete (Only the PCC Layer)
14	Permeable Rubberized Asphalt Concrete (Only the Asphalt Layer)
15	Permeable Section (Only the Crushed Agg Base Layer)
16	Permeable Asphalt Concrete (with Crushed Agg as Base Layer)
17	Permeable Portland Cement Concrete (with Crushed Agg as Base Layer)
18	Permeable Rubberized Asphalt Concrete (with Crushed Agg as Base Layer)
19	Portland Cement Concrete (PCC) OP139SCM139
20	Portland Cement Concrete (PCC) OP284SCM50
21	Portland Cement Concrete (PCC) OP418SCM0
22	Reflective Coating – Bisphenol A (BPA)
23	Reflective Coating – Polyester Styrene
24	Reflective Coating – Polyurethane
25	Reflective Coating – Styrene Acrylate
26	Rubberized Asphalt Concrete (mill and fill)
27	Rubberized Asphalt Concrete (overlay)
28	Sand Seal
29	Slurry Seal

Table 14. BCOA, permeable PCC, and PCC mix designs for 1 m^3 of concrete.

	Code	Cement (kg)	Slag (kg)	Fly Ash (kg)	Coarse Agg (kg)	Fine Agg (kg)	Water (kg)	Fiber (kg)	Accel erator (kg)	Air Entrainer (kg)	Retar der (kg)	Water Redu cer (kg)
BCOA	OP139SCM139	139.4	55.8	83.7	1038.2	816.9	173.3	0.0	0.0	0.0	0.0	0.0
	OP267SCM71	267.0	0.0	71.2	1085.1	763.5	145.4	1.8	0.0	0.0	0.0	0.0
	OP448SCM0	447.9	0.0	0.0	1070.9	598.0	161.3	1.8	0.0	0.6	1.6	1.9
Permeable	OP380SCM0	380.3	0.0	0.0	1594.0	0.0	120.0	0.0	0.0	0.0	0.0	0.0
PCC	OP139SCM139	139.4	55.8	83.7	1038.2	816.9	173.3	0.0	0.0	0.0	0.0	0.0
	OP284SCM50	284.2	0.0	50.4	1067.9	821.7	148.5	0.0	0.0	0.1	0.0	1.2
	OP418SCM0	418.3	0.0	0.0	891.7	868.6	183.9	0.0	4.2	0.0	0.0	3.4

Table 15. HMA with reclaimed asphalt pavement (RAP) mix designs.

Item	**HMA w. RAP, Hveem**	**HMA w. RAP, Superpave**
	Mass fraction (%)	
Aggregate	81	80.2
Coarse	38	32
Fine	57	47.2
Dust	5	1
Asphalt binder	4	4.8
Reclaimed asphalt pavement (RAP)	15	15

Table 16. Rubberized hot mix asphalt concrete mix design.

Item	**Mass fraction (%)**
Aggregate	92.5
Coarse	68
Fine	27
Dust	5
Asphalt Binder	7.5
Bitumen	77.5
CRM	20
Extender oil	2.5
Reclaimed asphalt pavement (RAP)	0

2.5. Local urban climate and air quality modeling

2.5.1. Model

We employ the Weather Research and Forecasting (WRF) Model version 3.5.1 (Skamarock et al 2008). The WRF is a nonhydrostatic, compressible atmosphere model and is coupled to the community Noah land surface model (LSM) (Chen et al. 2001). WRF was set up using three nested domains, using two-way feedback mechanism between the domains, with corresponding spatial resolutions of 36, 12 and 4 km (Figure 5). The inner model domain encapsulates the entire state of California. We employ 30 layers in the vertical from the surface to 10 kPa.

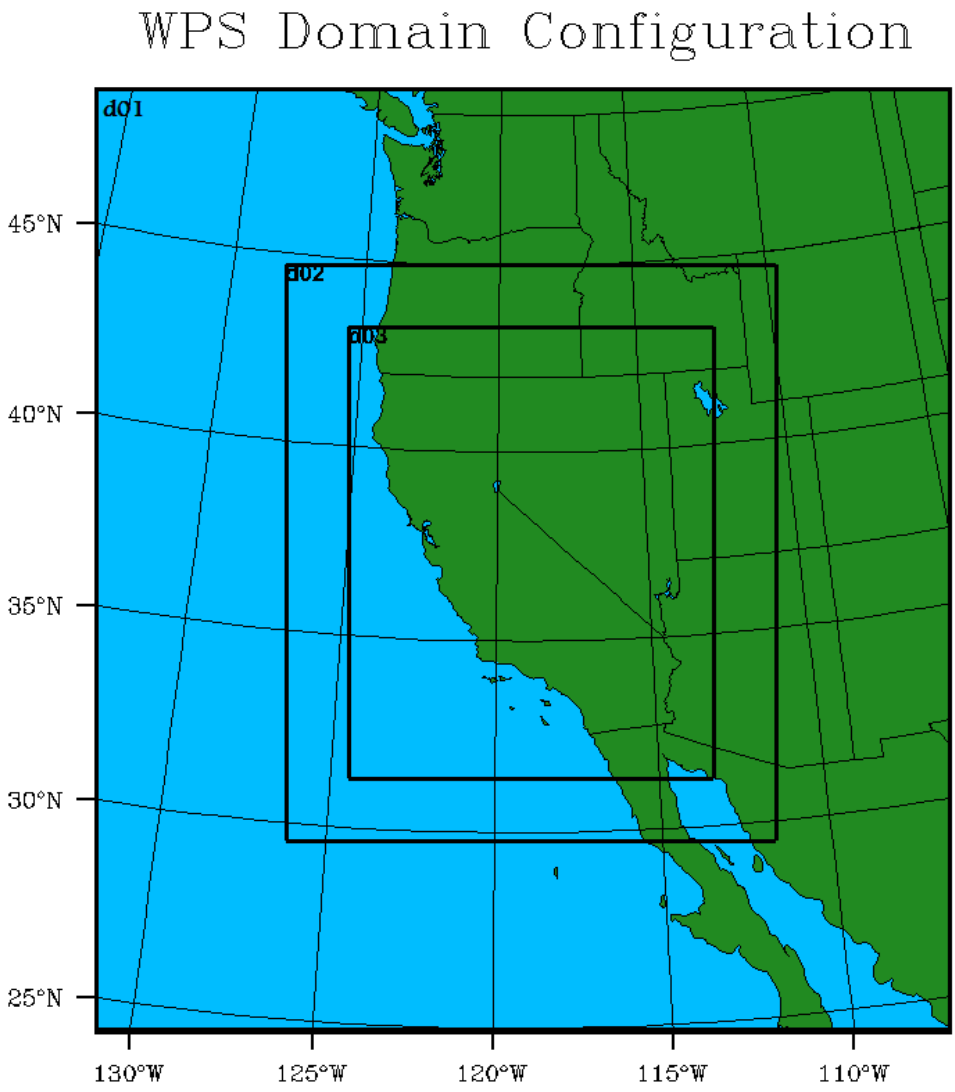

Figure 5. Preview of the 3 nested domains used in the simulations. The entire figure shows the outer domain and the areas labeled as "do2" and "do3" are the inner domains. The innermost domain is "do3" which is the main area of interest and contains the state of California.

The physics of the planetary boundary layer (PBL), cumulus, and cloud microphysics are parameterized using the Yonsei University (YSU) scheme (Hong et al. 2006), Grell scheme (Grell 1993), and WRF Single Moment 6 class (WSM6) scheme (Hong and Lim 2006), respectively. Note that the inner domain does not use the Grell scheme as cumulus is assumed to be resolved at 4 km resolution. A previous study (Zhao et al. 2011) using the same model and spatial resolution over California tested multiple combinations of physics parameterizations. They found that the aforementioned combination of parameterizations led to the lowest root mean square error compared to observations. Longwave and shortwave radiative transfer are simulated using the Rapid Radiative Transfer Model for GCMs (RRTMG) scheme, an update to the Rapid Radiative Transfer Model (RRTM) (Mlawer et al. 1997). RRTMG uses the Monte Carlo Independent Column Approximation (MCICA) method of random cloud overlap, a statistical method to resolve sub-grid scale cloud variability. The single layer Urban Canopy Model (UCM) is used in order to capture the influence of urban canopies on surface-atmosphere interactions. The UCM is described in detail in Chen et al. (2011), and is described briefly here.

In WRF, the single-layer UCM parameterizations are based on Kusaka et al. (2001) and Kusaka and Kimura (2004). These parameterizations are employed in grid cells for which the dominant land cover type is urban. The dominant land cover type for each cell is determined using the MODIS 20 category land-use dataset. Cells that are deemed urban are divided into impervious and pervious portions. Heat and momentum fluxes are determined using the UCM in the impervious portion of the cell, while the Noah LSM is used to determine these fluxes in the pervious portion. The fraction of the grid cell that is impervious is determined using the "urban fraction" parameter explained in the next paragraph. The influences of urban geometry on trapping of shortwave and longwave radiation are taken into account assuming infinitely-long street canyons. The model computes surface skin temperatures for each urban sub-facet (roof, wall, and road) using surface energy balances. Monin-Obukhov similarity theory then predicts sensible heat fluxes from each sub-facet. The sensible heat flux in the impervious portion of the grid cell is subsequently combined with that of the pervious portion, and then transferred to the atmosphere model. Momentum transfer uses stability functions to estimate the canyon drag coefficient and friction velocity. The vertical profile of wind speed is assumed to be exponential. The friction velocities over the impervious and pervious portions of the grid cell are then combined and used in the atmosphere model's boundary layer scheme (Chen et al. 2011).

The fraction of each grid cell that is covered with urban areas (urban fraction) was computed using the United States Geological Survey (USGS) National Land Cover Database (NLCD) (Homer et al. 2007) for 2001. The NLCD data characterizes land cover at 30 m resolution and includes four different urban types: "developed open space" where impervious surfaces account for less than 20% of total cover; "low intensity" where impervious surfaces account for 20% to 49% percent of total cover; "medium intensity" where impervious surfaces account for 50% to 79% percent of total cover; and 'high intensity' where impervious surfaces account for 80% to 100% percent of total cover. Figure 6a shows the urban regions in California that are classified as low, medium, or high intensity. Assuming that these three urban types have corresponding urban fractions of 50, 90, and 95%, respectively, the 30 m NLCD data are aggregated to the WRF grid with resulting urban fractions shown in Figure 6b. Note that another option would have been to derive grid cell urban fraction using the "impervious surface" dataset from NLCD. Details on urban morphology including building height, roof width, road width, and others (see Table 1 in Chen et al. 2011) are obtained using observations from the National Urban Data and Access Portal Tool (NUDAPT) where available (i.e., for portions of Los Angeles, San Diego, Riverside, and Garden Grove). Where NUDAPT observations are unavailable, urban canopy parameters that depend on urban morphology are assumed to be the same as described in Chen et al. (2011). For example, low, medium, and high intensity urban types assume building heights of 5, 7.5, and 10 m, respectively, with corresponding road widths of 8.3, 9.4, and 10 m. Roads are assumed to extend the full width of the urban canyon, with no "setbacks" between roads and buildings. The influence of these assumed urban morphologies on our results are explored in Section 3.4.

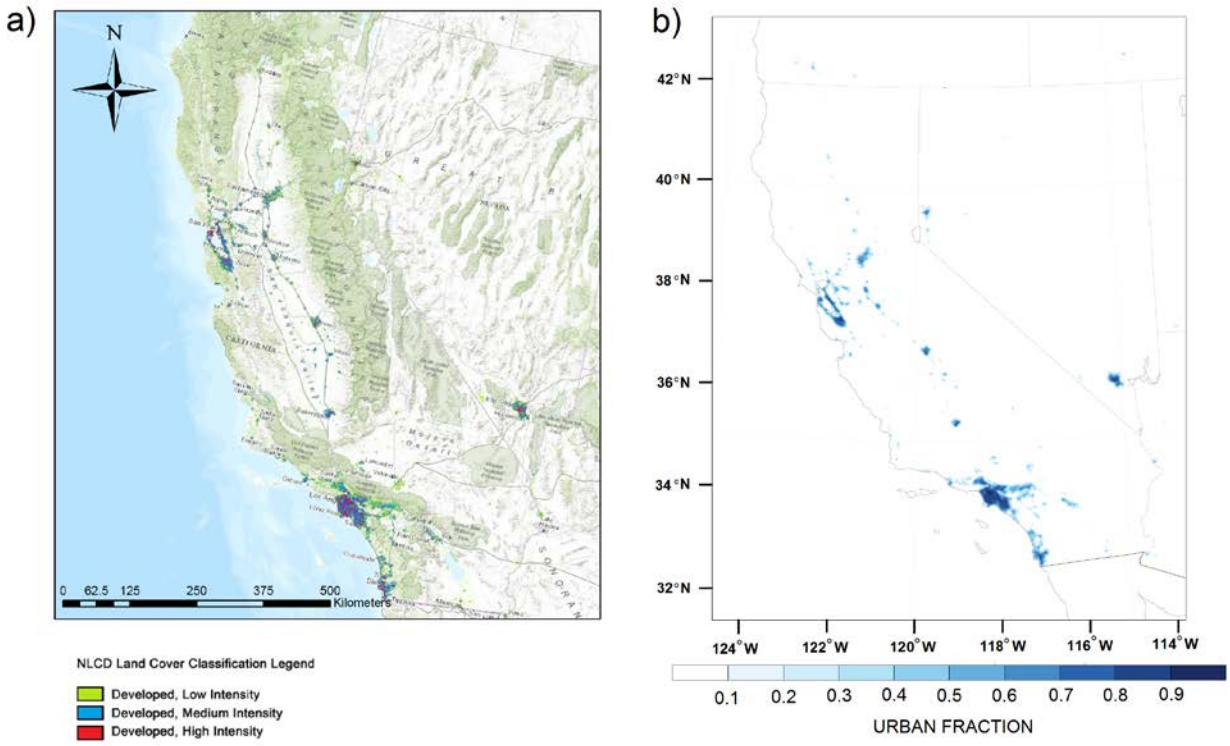

Figure 6. (a) The three urban classification extracted from NLCD database and used in the domain and (b) the resulting urban fraction field extracted from NLCD urban classes.

Roof and wall albedos were assumed to be 0.20. While roof albedo should have negligible effect on the sensitivity of climate to pavement albedo, assumed wall albedo may play a role through reflections between walls and pavements. The mechanics of calculating canyon albedo and the solar heat gain of the urban canyon are detailed in Section 2.5.3.

Boundary and initial conditions are based on the National Center for Environmental Prediction (NCEP) North American Regional Reanalysis (NARR) data. These data have horizontal spatial resolution of 32 km, close to that of the outer domain of the model, and 29 vertical levels ranging from 100 to 10 kPa. Real-time global NCEP sea surface temperature (SST) data are used for the portions of the domain over the Pacific Ocean.

2.5.2. Simulations

To investigate the influence on California climate of the wide spread adoption of cool pavements, three scenarios were simulated, each with a different pavement albedo. The control scenario ('CTRL') assumed a baseline pavement albedo of 0.10. The first perturbation scenario ('COOL_LOW') assumed that cool pavements with albedo 0.20 were deployed in all urban grid cells in California. This pavement albedo represents a case that is technologically achievable in the near term. The second perturbation scenario ('COOL_HIGH') assumed that cool pavements with albedo 0.50 were deployed in all urban grid cells in California. This albedo represents a high estimate that pushes the boundaries of what is likely to be technologically and economically feasible. We include this high pavement albedo case because we strive to quantify a general relationship describing the sensitivity of 2 m air temperature (referred to here as surface air temperature) to pavement albedo. By including this upper bound case, we can check the linearity of the temperature-albedo relationship and ensure that results can be interpolated rather than

extrapolated to other pavement albedos of interest. In this study, we focus on bounding the maximum possible impacts of cool pavements. Thus, most figures compare COOL_HIGH to CTRL, though select results comparing COOL_LOW to CTRL are also presented.

The main analysis period of focus for this study is 1 September 2001 to 31 August 2002, chosen to represent the region without strong El Niño or La Niña conditions. To allow for characterizing uncertainties, we ran three ensemble-members per scenario, for a total of nine simulations. The simulation start dates for each ensemble-member per scenario were 1 March, 1 June, and 1 August 2001, respectively. Thus, for each ensemble-member, a minimum model spin-up time of two months was ensured. The statistical significance of differences between scenarios was assessed using Student's t-test. Here the differences between ensemble-averaged scenarios were compared to variations among each of the three ensemble members per scenario for each grid cell. All presented difference maps omit results for cells that are not significant at the 99.5% confidence level. Spatial averages over cities in California were created using U.S. Census 2000 Topologically Integrated Geographic Encoding and Referencing (TIGER) data (U.S. Census 2002), which provides the boundaries of urban areas in a shapefile.

2.5.3. Albedo

In the single-layer urban canopy model in WRF 3.5.1, the surface temperature of each sub-facet is derived using heat balance equations. Each heat balance includes absorption of shortwave radiation, absorption and emission of longwave radiation, and convective heat flows. The urban part of the grid cell is dry and thus does not include latent heat fluxes. Urban vegetation and corresponding latent heat fluxes are modeled as part of the "natural" pervious portion of the grid cell.

We characterize albedo in four different ways. "Pavement albedo" (ρ_p) describes all pavement types with no distinction between sidewalks, roads, and parking lots. "Urban albedo" (ρ_u) describes the impervious portion of grid cells that are deemed urban. It represents the albedo above the urban canopy and includes contributions from all urban sub-facets (i.e., roofs, pavements, and walls). While we refer to "urban canopy" as the urban part of the grid cell including wall, roof, and pavement, the term "urban canyon" refers to the U-shaped cavity formed by a ground surface and its surrounding walls. The "albedo of the canyon" (including pavements and walls, but excluding roofs) is denoted ρ_c. "Grid cell albedo" (ρ_g) describes the entire grid cell, including both impervious and pervious portions.

The single-layer urban canopy model used in WRF 3.5.1 treats all downwelling sunlight as purely diffuse (note that we discuss limitations to this assumption in Section 4.3.3), and then uses view factors to estimate exchanges of sunlight between the sky, wall, and ground (pavement) sub-facets. The view factor $F_{X\to Y}$ is the fraction of radiant power leaving surface X that is intercepted by surface Y. However, to help explain the derivation of the radiative model, we show first that the radiance (radiant power per unit area) incident on surface Y that originates from surface X is proportional to $F_{Y\to X}$, the view factor from surface Y to surface X.

Let A represent area, J denote outgoing radiance, and I represent incident radiance. If the radiance leaving surface X is J_X, the power leaving surface X is $A_X J_X$., and the power intercepted by surface Y is $F_{X\to Y} A_X J_X$. Applying view factor reciprocity ($A_X F_{X\to Y} = A_Y F_{Y\to X}$), the radiance incident on surface Y is

$$I_Y = (F_{X\to Y} A_X J_X) / A_Y = F_{Y\to X} J_X. \quad (5)$$

The radiance absorbed by the canyon, S_{canyon} (absorbed power per unit sky area) is computed as a weighted average of (a) $S_{ground1}$, the irradiance from the sky absorbed by the ground; (b) S_{wall1}, the

irradiance from the sky absorbed by the walls; (c) $S_{ground2}$, the irradiance from wall reflection that is absorbed by the ground; and (d) S_{wall2}, the irradiance from ground reflection that is absorbed by the walls. Treating the two walls that bound the canyon as a single surface (subscript "wall"),

$$S_{ground1} = J_{sky} F_{ground \rightarrow sky} (1 - \rho_{ground}) \quad (6)$$

$$S_{wall1} = J_{sky} F_{wall \rightarrow sky} (1 - \rho_{wall}) \quad (7)$$

$$S_{ground2} = S_{wall1} [\rho_{wall} / (1 - \rho_{wall})] F_{ground \rightarrow wall} (1 - \rho_{ground}) \quad (8)$$

$$S_{wall2} = S_{ground1} [\rho_{ground} / (1 - \rho_{ground})] F_{wall \rightarrow ground} (1 - \rho_{wall}) \quad (9)$$

Let H, W, and L represent the height, width, and (infinite) length of the canyon. Since the sky area and ground area are each W×L, and the combined wall area is 2×H×L, radiant power absorbed in the canyon per unit sky area is

$$S_{canyon} = [(W \times L) (S_{ground1} + S_{ground2}) + (2 \times H \times L) (S_{wall1} + S_{wall2})] / (W \times L) \quad (10)$$

or

$$S_{canyon} = (S_{ground1} + S_{ground2}) + (2 \times H/W) (S_{wall1} + S_{wall2})] \quad (11)$$

The model calculates the albedo of the canyon as the fraction of solar irradiance entering the canyon that exits the canyon. Neglecting secondary reflections within the canyon, the top of canyon albedo (ρ_c) is estimated as

$$\rho_c = 1 - S_{canyon} / J_{sky} \quad (12)$$

Canyon albedo is a diagnostic variable and, as it is explained later in the Section 4.3.3, is highly correlated to temperature changes from albedo modifications. It can be used as a criterion to extrapolate results simulated here to other values for canyon albedo change. Each grid cell consists of two major parts, urban (a.k.a. "impervious") and vegetative (a.k.a. "pervious"). The albedo of each grid cell is computed as

$$\rho_g = \rho_g f + \rho_v (1 - f) \quad (13)$$

where f is the urban fraction of the grid cell, and ρ_v is the albedo of the vegetative portion of the grid cell. Grid cell albedos (ρ_g) for the CTRL simulation are shown in Figure 7. In California, values of grid cell albedo range from about 0.05 in the forested regions of the state to 0.28 in the desert regions. Raising pavement albedo to 0.20 in COOL_LOW from 0.10 in CTRL increases grid-cell albedo by up to about 0.02 in urban regions around California (Figure 7b). Raising pavement albedo to 0.50 from 0.10 (i.e., [COOL_HIGH – CTRL]) increases grid-cell albedo by up to about 0.08 in the city of Los Angeles (Figure 7c). Spatial variations in grid cell albedo changes are caused by associated variations in urban fraction and urban morphology. We note here that relationships between pavement albedo change and urban albedo (and therefore grid cell albedo) change depend on assumed canyon morphologies, as is further explained in the Section 4.3.3.

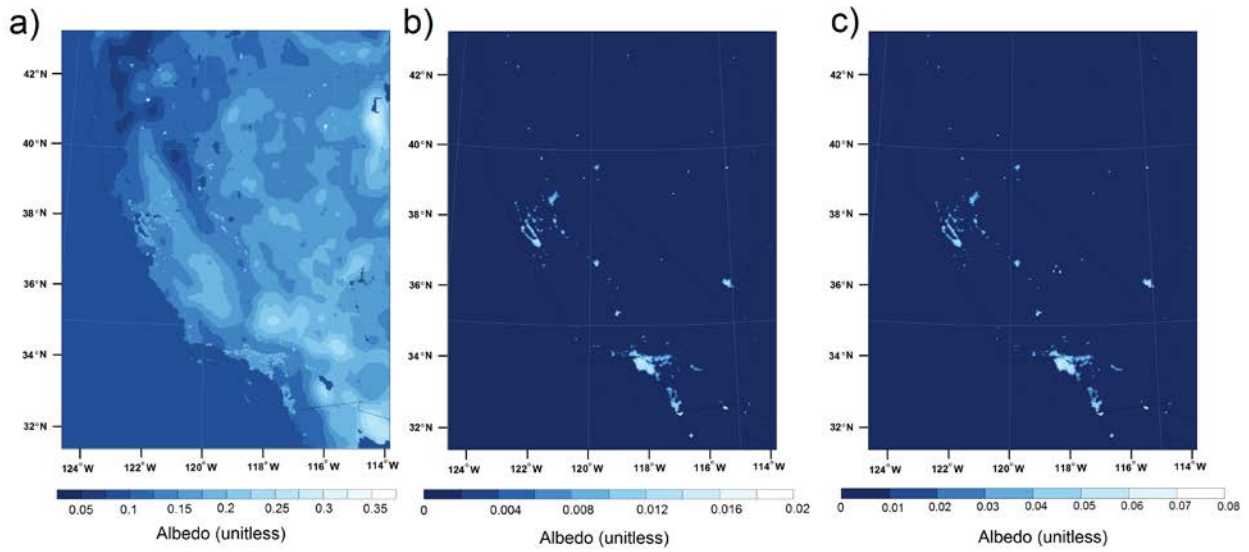

Figure 7. (a) Albedo for control scenario at the start of simulation (Sep); (b) albedo increases from control to scenario B; and (c) albedo increases from control to scenario C.

2.5.4. Ozone air quality

Warmer climate is often associated with elevated ground-level ozone levels (Camalier et al. 2007; Bloomer et al. 2009; see also references cited in the review by Fiore et al. (2012)). This ozone-temperature relationship is governed by multiple pathways, including (a) direct temperature effects on reaction rates and ozone precursor emissions; and (b) close correlation of temperature with other favorable meteorological conditions, such as sunny days and low wind speed (Sillman and Samson 1995; Aw and Kleeman 2003; Kleeman 2007; Steiner et al. 2010; Rasmussen et al. 2013; Pusede et al. 2015). The most important direct effects of temperature are associated with peroxyacetyl nitrate (PAN) chemistry and biogenic emissions of volatile organic compounds (BVOCs). Increasing thermal decomposition rates of PAN under higher temperatures leads to a release of nitrogen oxides (NO_x) and hydroxyl (HO_x) radicals, both of which are precursors to ozone formation. BVOC emissions also tend to increase with temperature. Temperature can also affect other ozone precursors including available water vapor (initiate OH radicals), the evaporative emissions of anthropogenic volatile organic compounds (AVOC), and soil emissions of nitrogen oxides.

To estimate the potential ozone reductions attainable through adoption of cool pavements, we conducted a literature review to assess previously reported values of ozone-temperature sensitivity. Past studies of ozone-temperature sensitivities have focused on air basins in California where ozone concentrations consistently exceed the National Ambient Air Quality Standards. These air basins include the San Francisco Bay Area (SFB), Sacramento Valley (SV), San Joaquin Valley (SJV), and South Coast (SC). Changes in ozone from adoption of cool pavements are subsequently estimated using modeled temperature reductions at 15:00 local standard time (LST) and with best estimates of ozone temperature sensitivity from the literature.

It is important to note that for our assessment, we assume that ultraviolet (UV) reflectance of cool vs standard pavements remain the same. We recognize that increases in UV reflectance would increase the actinic flux and could lead to a rise in ozone concentrations.

2.6. Simulation of building energy use

This section describes the methods used to simulate the effects of cool pavements on the annual cooling, heating, and lighting site energy uses of individual buildings and of the entire building stocks of various California cities. The building energy simulations were performed with 10 different building prototypes that comply with California's 2008 Title 24 building energy efficiency standards. The prototypes were modified to add horizontal surfaces that mimic reflection from public streets adjacent to the buildings, and vertical surfaces that mimic reflection from neighboring buildings. We do not consider reflections from parking lots and private streets in our building simulations because pavements other than public streets lie out of the scope of this study.

The direct effect of cool pavements adjacent to a building was simulated by varying the albedo of the neighboring streets. The indirect effect of changes to the city-mean pavement albedo was evaluated by modifying the weather files used in the simulations. These modified weather files incorporate air temperature changes induced by cool pavements, which in turn were obtained from the urban climate modeling activity.

The results from the building energy simulations were used to fit coefficients to physical models relating the annual cooling, heating, and lighting site energy uses of each prototype to local and city-mean pavement albedos.

To calculate citywide changes in building energy use, we assessed California's current building stock and mapped property types to building prototypes.

The coefficients of the physical model solutions and the results of the building stock assessment are later used by the pavement LCA tool to calculate the site use-stage changes to building energy use in each city. Figure 8 summarizes the methodology that is detailed in this section.

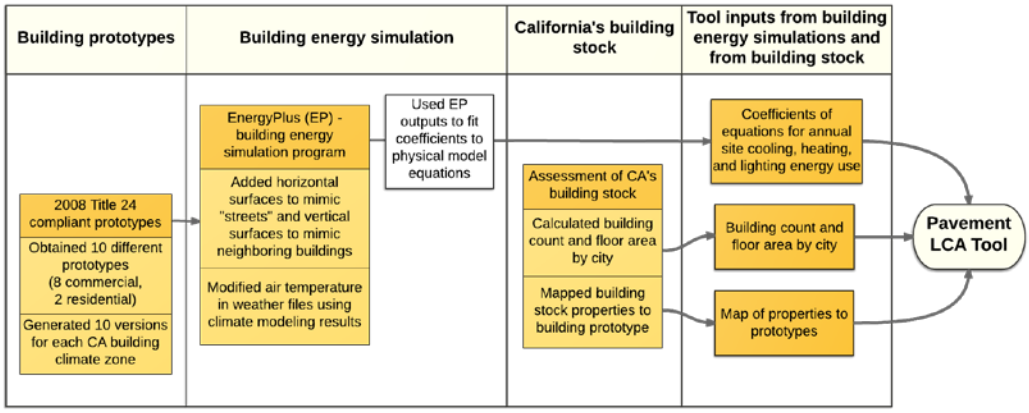

Figure 8. Flowchart of building energy modeling and building stock methodology.

2.6.1. Building prototypes

We simulated building energy consumption with EnergyPlus version 8.5 (EnergyPlus 2003), using building prototypes that detail construction, internal loads, HVAC equipment, and HVAC operation. EnergyPlus calculates the hourly heating and cooling loads that must be met to regulate comfort in the conditioned space, the hourly lighting energy use, and many other facets of the building operation.

Source of residential building prototypes

The United States Department of Energy (DOE) Building Energy Codes Program (BECP) uses two prototypes—single-family home and multi-family apartment building—to evaluate published versions of their code and proposed code changes (PNNL 2014). The building prototypes have attic ductwork and a slab foundation (no basement). We modified these two prototypes to meet the California 2008 Title 24 residential building energy efficiency standards (CEC 2008b), creating one version of each prototype for each of California's 16 building climate zones (BCZs) (Figure 9). The building properties that we modified to meet the Title 24 standards include the following:

- thermal resistances of walls and attic
- thermal transmittance (a.k.a. U-factor, or U-value), solar heat gain coefficient (SHGC), and visible transmittance of windows
- cooling efficiency (seasonal energy efficiency ratio, or SEER) and heating efficiency (annual fuel utilization efficiency, or AFUE)
- HVAC schedule (hours and setpoints)

Other operating schedules (e.g., lighting, occupancy, and miscellaneous plug loads) were unchanged.

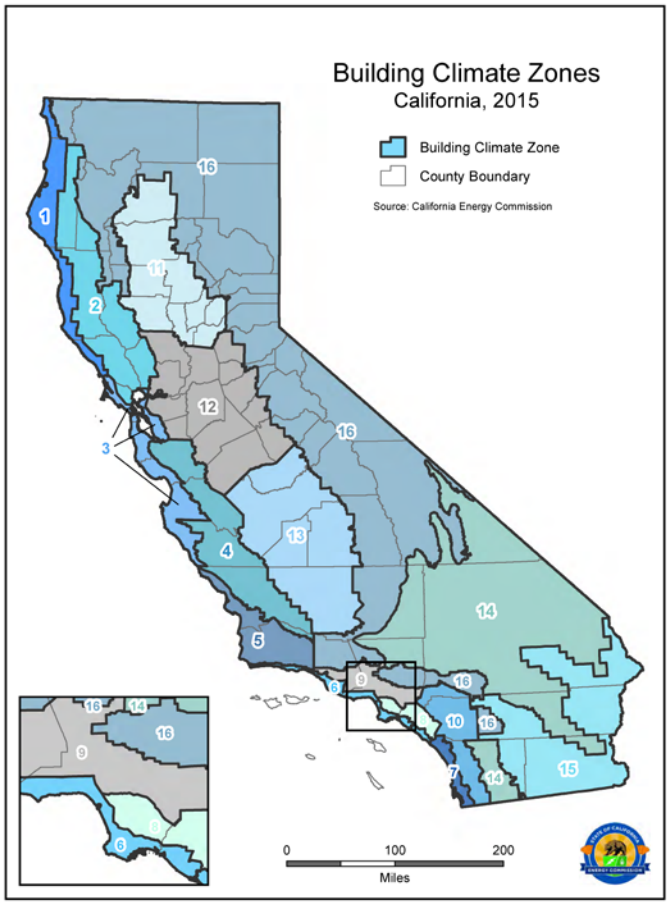

Figure 9. Map of California building climate zones (CEC 2015b).

Source of commercial building types

Past U.S. Department of Energy (DOE) efforts to research building energy efficiency used a suite of 15 commercial building prototypes (Deru et al. 2011). Each prototype complies with ASHRAE Standard 62.1-2004: Ventilation for Acceptable Indoor Air Quality (ASHRAE 2004a) and ASHRAE Standard 90.1-2004: Energy Standard for Buildings Except Low-Rise Residential Buildings (ASHRAE 2004b), which provide standards for energy use, ventilation, and indoor air quality in U.S. commercial buildings. The California Energy Commission (CEC) supplied eight of the 15 DOE commercial building prototypes, adapted to meet 2008 Title 24 nonresidential standards (CEC 2008a). Our collection includes 16 versions of each commercial building prototype, one for each of California's BCZs (Figure 9).

In Section 3.5.1 we compare the energy use intensities of the residential and commercial prototype outputs to those reported by the Commercial Buildings Energy Consumption Survey (CBECS), the Residential Energy Consumption Survey (RECS), and California's Commercial End-Use Survey (CEUS).

Prototype characteristics

Prototype dimensions and construction properties are summarized in Table 17 and 18.

Table 17. Geometries of the prototype buildings.

Building prototype	Floors	Conditioned floor area [1000 m^2]	Footprint area [1000 m^2]	Roof area [1000 m^2]	Wall height [m]	Wall area [1000 m^2]	Window area [1000 m^2]	Window-to-wall area ratio[a] (%)
Single-family home	2	0.22	0.11	0.12	5.18	0.24	0.03	14.1
Apartment building	3	2.01	0.67	0.79	7.77	1.50	0.25	16.4
Large hotel	6	11.35	1.89	1.98	21.6	4.03	1.21	30.2
Large office	13	46.32	3.56	3.56	37.5	11.59	4.64	40.0
Medium office	3	4.98	1.66	1.66	11.89	1.98	0.65	33.0
Primary school	1	6.87	6.8	6.87	4.00	2.51	0.88	35.0
Fast-food restaurant	1	0.23	0.23	0.26	3.05	0.19	0.03	14.0
Retail stand-alone	1	2.29	2.29	2.29	6.10	1.18	0.08	7.1
Strip mall retail	1	2.09	2.09	2.09	5.18	1.18	0.12	10.5
Sit-down restaurant	1	0.51	0.51	0.57	3.05	0.28	0.05	17.1

[a] In calculating the window-to-wall area ratio, the denominator (wall area) omits window area.

Table 18. HVAC systems of the prototype buildings.

Building prototype	Cooling	Heating	Air distribution
Single-family home	Direct expansion unitary system	Gas heating coil	Single zone constant air volume
Apartment building	Direct expansion unitary system	Gas heating coil	Constant air volume
Large hotel	Chiller – air cooled	Boiler	Fan coil unit and variable air volume
Large office	Chiller – water cooled	Boiler	Multizone variable air volume
Medium office	Precision air conditioning unit	Electrical resistance and furnace	Multizone variable air volume
Primary school	Precision air conditioning unit	Boiler	Constant air volume
Fast-food restaurant	Precision air conditioning unit	Furnace	Single zone constant air volume
Retail stand-alone	Precision air conditioning unit	Furnace	Single zone constant air volume
Strip mall retail	Precision air conditioning unit	Furnace	Single zone constant air volume
Sit-down restaurant	Precision air conditioning unit	Furnace	Single zone constant air volume

Adding external surfaces to the prototypes

Neighboring buildings

EnergyPlus has a feature, called *external shading surfaces*, to calculate reflections from and shading by exterior surfaces, such as neighboring buildings.

We added to each building prototype vertical external shading surfaces that represent neighboring buildings. These shading surfaces were assigned albedo 0.20, the same as that of the walls of the modeled buildings.

The distances from the building to the added vertical shading surfaces follow design guidelines specified in the Zoning Code of Sacramento County, or ZCSC (ZCSC 2015). From the guidelines we obtained the widths of the side yards around a building, which depend on building type. With the side yards we determined the distance from the building to the added vertical shading surfaces that represented neighboring buildings. Assuming the neighboring structure has a use similar to that of the modeled building, the distance between a building and its neighbor is twice the side setback. The side and front setbacks vary by building type.

Table 19 summarizes the distance between each prototype building and its vertical shading surfaces.

Table 19. Side and front setbacks of the building prototypes.

Building prototype	Building type category in Sacramento's zoning code	Distance between neighboring buildings [m]	Front yard [m]
Single-family home	Single-family	3.0	6
Apartment building	Multiple-family dwellings	12.2	7.6
Large hotel	Commercial, business, or professional use	15.2	15.3
Large office	Business and professional uses in residential zones	12.2	7.6
Medium office	Business and professional uses in residential zones	12.2	7.6
Primary school	Institutional use	3.7	7.6
Fast-food restaurant	Commercial, business, or professional use	15.2	15.3
Retail stand-alone	Commercial, business, or professional use	15.2	15.3
Strip mall retail	Commercial, business, or professional use	15.2	15.3
Sit-down restaurant	Commercial, business, or professional use	15.2	15.3

Representing local streets

EnergyPlus treats the entire ground around the modeled building as one homogeneous surface. The software is not capable of segmenting the ground into different types of ground surfaces, such as streets and sidewalks. Hence, to isolate the effect of streets on the building energy use, we placed external shading surfaces horizontally around the buildings to represent the local streets. They were placed at a distance from the building that complies with street design standards.

The front yard is the distance from the building to the street's right-of-way. The right-of-way includes the street, street verge (also known as a planting strip, sidewalk buffer, or utility strip), and sidewalk. The front setback distance is the sum of widths of the front yard, street verge, and sidewalk. The front setback width equals the distance from the building to the street. The widths of the front yards were obtained from the ZCSC, while the widths of the sidewalk and the street verge were obtained from the Street Design Standards for the City of Sacramento (DoT Sacramento 2009). Table 20 summarizes these distances for all building prototypes.

Table 20. Distances from building to street and number of sides facing a street, for each prototype building.

Building prototype	Street type	Front yard [m]	Sidewalk and planter [m]	Building to street distance [m]	Building sides facing a street[a]
Single-family home	Residential	6.1	3.5	9.6	1
Apartment building	Residential	7.6	3.5	11.1	1
Large hotel	Boulevard, Commercial	15.2	4.4	19.7, 11.1	2
Large office	Boulevard, Commercial	7.6	4.4	12.0, 11.1	2
Medium office	Commercial	7.6	3.5	11.1	1
Primary school	Residential	7.6	3.5	11.1	3
Fast-food restaurant	Commercial	15.2	3.5	18.7	1
Retail stand-alone	Boulevard	15.2	4.4	64.5	1
Strip mall retail	Boulevard, Commercial	15.2	4.4	64.5, 18.7	2
Sit-down restaurant	Commercial	15.2	3.5	18.7	1

[a] The number of building sides facing a street was determined by comparing the prototype's footprint area to the standard size of a city block in Sacramento (see Section 2.6.1). As an example, since the footprint area of the primary school is 6800 m², which is half the area of a city block, we added streets on three sides of the school prototype.

In Sacramento—the 35th largest U.S. city by population (Infoplease 2015)—a standard city block is 14,400 m². In other major U.S. cities, like Manhattan, NY (1st), Houston, TX (4th), and Portland, OR (24th), the average city block size ranges from 6,000 m² to 22,000 m² (Wikipedia 2015). Since the size of a city block varies widely in the U.S., we use Sacramento's standard city block area (14,000 m²) to represent the size of a city block in California. Unless a building occupies an entire city block, we expect it to face a street on one or two sides. We compared the footprint area of each building prototype to the size of a typical city block to estimate the number of the building sides facing a public street. **Error! Reference source not found.** lists the number of sides (out of four) each building prototype was modified with public "streets."

The streets added to the prototypes varied in width according to street design standards used in various cities in California. Each building prototype was mapped to a street type based on building use and building size. We obtained the dimensions and lane configurations of each street type for the cities of Sacramento (DoT Sacramento 2009), Los Angeles (Ryan Snyder Associates 2011) and San Jose (DoT SAn Jose 2010). Although the street dimensions vary slightly between cities, we selected the street design standards of Sacramento as they are closest to the average of the three cities. **Error! Reference source not found.** details the dimensions and lane configurations of each street type used in each prototype.

Appendix C illustrates the 10 modified building prototypes, including the shading surfaces that represent neighboring walls and "streets".

Table 21. Street descriptions and dimensions assumed for each building prototype.

Building prototype	Street type	Parking lane width [m]	Bike lane width [m]	Travel lane width [m]	Number of travel lanes	Total street width[a] [m]
Single-family home	Residential	0	0	4.6	2	9.1
Apartment building	Residential	0	0	4.6	2	9.1
Large hotel	Boulevard, Commercial	2.1	1.8	3.5	4	22.0, 11.0
Large office	Boulevard, Commercial	2.1	1.8	3.5	4	22.0, 11.0
Medium office	Commercial	2.1	0	3.4	2	11.0
Primary school	Residential	0	0	4.6	2	9.1
Fast-food restaurant	Commercial	2.1	0	3.4	2	11.0
Retail stand-alone	Boulevard	2.1	1.8	3.5	4	22.0
Strip mall retail	Boulevard, Commercial	2.1	1.8	3.5	4	22.0, 11.0
Sit-down restaurant	Commercial	2.1	0	3.4	2	11.0

[a] Some prototypes were modified with streets of different width. In pairs of values, the first is the width of the street added south of the building. The second is the width of the street located in the west side.

Effect of trees

Trees may have a significant effect on the cooling and heating load of a building (Donovan and Butry 2009; Simpson and McPherson 1996). For example, the presence of trees near buildings can reduce the solar flux reflected to walls and windows from pavements, thus diminishing the direct effect of cool pavements. However, in this study we have not included the effect of trees in the building energy analysis.

2.6.2. Building energy simulation

Simulation tools

EnergyPlus (EnergyPlus 2003) is a free building energy simulation program, funded by the U.S. Department of Energy (DOE) Building Technologies Office. We used EnergyPlus version 8.5 to simulate the cooling, heating, lighting, and other building energy uses for each hour of the year. We also employed jEPlus version 1.4 (jEPlus 2012), a parametric EnergyPlus simulation manager, to simplify the process of simulating each model with six different street albedos (0.10, 0.15, 0.20, 0.30, 0.40, and 0.50); we refer to an EnergyPlus model as the software inputs (i.e., building prototype and weather file) required to run a single EnergyPlus simulation. The study required simulating 300 models (10 prototypes × 10 BCZs × 3 weather file versions). We wrote a Python script to manage jEPlus, process the simulation outputs, and analyze the results. The script ran all simulations automatically through jEPlus. It then processed the simulation outputs to extract the annual site cooling, heating, and lighting energy uses. After extracting the annual energy uses, another Python script graphed the energy uses and applied multivariate linear regression analysis to relate the changes in cooling, heating, and lighting energy uses to the changes in local street and city-mean pavement albedos (Section 2.6.3) automatically. The script also helped speed up the process of processing and analyzing the simulation results.

Original weather files

An EnergyPlus simulation requires a weather file that represents the climate in the location specified in the EnergyPlus prototype. We used the most recent California weather files developed by White Box Technologies (WBT 2011). These were released in February 2015, and characterize weather records spanning 1998 to 2009. White Box Technologies created these 85 weather files, collectively called CZ2010, for Title 24 compliance simulations, and provides the CZ2010 weather files in *epw* file format, which is the format required by EnergyPlus. Before the CZ2010 files were released, energy simulations for prototypes in CA used "CTZ2" weather files, one per building climate zone (BCZ), characterizing weather records from the 1950s to the 1980s.

A CZ2010 weather file consists of hourly values over a period of a "typical year". This typical year is an artificial weather year reflecting average conditions between 1998 and 2009. Each month in the weather file consists of actual weather data collected from the weather station and it represents the most typical weather of that month among the 12-year span.

We chose one weather file from the CZ2010 set per climate zone, selecting the same weather stations used to generate CTZ2.

Modified weather files

As mentioned in Section 2.5, this study investigated the influence of widespread adoption of cool pavements in California using three scenarios, each with a different city-mean pavement albedo. The control scenario assumes a baseline pavement albedo of 0.10. The small perturbation scenario assumed cool pavements with albedo 0.20 were deployed in all urban grid cells in California. The large perturbation scenario assumed deployment of cool pavements with albedo 0.50.

We incorporated these results from the climate modeling into the building energy simulations through the weather files. The control scenario uses the original CZ2010 weather files. To represent the small and large perturbation scenarios, we generated two modified versions of the original weather files. The new

versions reflect the hourly urban air temperature differences that results from citywide deployment of cool pavements obtained from the climate modeling.

Incorporating results from climate modeling

Results provided from the climate modeling activity included seasonal hourly values of mean air temperature difference ΔT. The climate modeling team calculated ΔT in each hour of the year by subtracting the air temperature in the control scenario (pavement albedo 0.10) from the air temperature in the large perturbation scenario (pavement albedo 0.50). The seasonal hourly values are obtained by averaging each hour of the day over every day of the season; the seasons are defined as summer (Jun, Jul, Aug); fall (Sep, Oct, Nov); winter (Jan, Feb, Dec); and spring (Mar, Apr, May). As detailed in Section 2.5, the accuracy of the urban climate modeling is greater in large, high-density (high impervious surface fraction) urban areas. These urban areas are also more sensitive to the climate effect of cool pavements. Hence, we obtained ΔT values for only 10 urban areas of California, each representing a different BCZ (3, 4, 7, 8, 9, 10, 12, 13, 14, or 15).

Table 22 lists some of the major cities in these BCZs.

The climate modeling also generated ΔT values that correspond to the small perturbation scenario minus the control scenario. Since these temperature differences were comparable to noise in the climate model, ΔT in the small perturbation scenario was instead calculated by scaling the high perturbation scenario by the ratio of pavement albedo changes, 0.10/0.40 = 0.25.

Table 22. California's major cities in the represented building climate zones (BCZs).

Representative cities	BCZ
Oakland	3
San Jose	4
San Diego	7
Irvine, Anaheim, Santa Ana, Garden Grove	8
Los Angeles	9
Riverside	10
Sacramento	12
Fresno	13
Lancaster	14
Palm Springs	15

Urban canyon geometry used in the climate model

The climate modeling was performed using an urban canyon geometry characteristic of high-intensity urban areas as defined in the National Land Cover Database, or NLCD (Homer et al. 2007). This canyon geometry has a street width of 9.4 m (31 ft) and omits setbacks (canyon floor width equals street width). Wall height is 7.5 m (24.5 ft), and the canyon's length (dimension along the long axis of the street) is treated as infinite. These dimensions were used to represent every urban grid cell in the climate modeling. Table 23 summarizes the dimensions of this NLCD canyon geometry.

Table 23. Urban canyon dimensions used in the climate modeling. These dimensions are specified in the National Land Cover Database.

Canyon	Setback width [m]	Street width [m]	Canyon width [m]	Wall height [m]
NLCD (narrow) canyon	0	9.4	9.4	7.5

Street widths in California cities are generally wider than the street width in this high-intensity residential NLCD canyon geometry (DoT Sacramento 2009). Also, in reality, streets do not extend from wall to wall in an urban canyon. A setback separates the street and wall, which can include a front yard, sidewalk, and/or street verge, as described in Section 2.6.1. Hence, we refer to this NLCD canyon geometry (9.4 m [31 ft.] wide street, 7.5 m [24.5 ft.] high walls, no setbacks) as the *NLCD narrow* canyon.

Another key disparity between the NLCD canyon geometry and the urban geometry of actual cities is the height of the canyon walls, which depends on the type of buildings forming the canyon. While a canyon wall height of 7.5 m (24.5 ft.) is usually a good approximation of a two-level building, a city is composed of buildings that vary widely in height.

Defining realistic canyon geometries

To better represent a city's morphology, we created a new canyon geometry for each of the 10 building prototypes. Each canyon was defined using the street and setback widths used when adding "streets" to the building prototypes, as detailed in Section 2.6.1. Figure 10 shows a general geometry of these urban canyons, and Table 24 defines the dimensions of the 10 canyons. These realistic canyons are wider than the NLCD narrow canyon because their canyon floors have both wide streets and setbacks. Thus, we refer to them as *wide* canyons.

Table 24. Dimensions for canyons defined from modeled building prototypes and streets.

Building prototype	Setback width [m]	Street width [m]	Canyon width [m]	Wall height [m]
Single-family home	6.1	9.1	21.3	5.2
Apartment building	7.6	9.1	24.3	7.8
Large hotel	15.2	22.0	52.4	21.6
Large office	7.6	22.0	37.2	37.5
Medium office	7.6	11.0	26.2	11.9
Primary school	7.6	9.1	24.3	4.0
Fast-food restaurant	15.2	11.0	41.4	3.1
Retail stand-alone	15.2	22.0	52.4	6.1
Strip mall retail	15.2	22.0	52.4	5.2
Sit-down restaurant	15.2	11.0	41.4	3.1

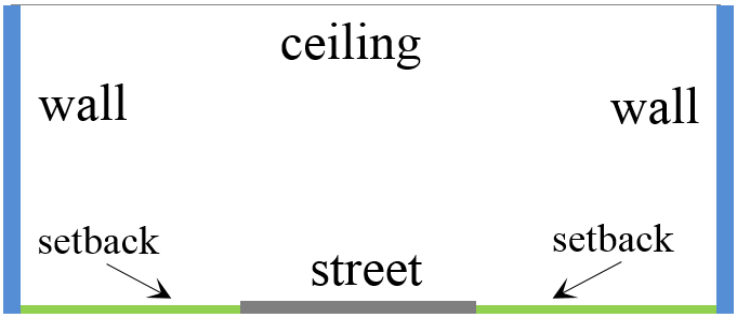

Figure 10. Urban canyon geometry.

Adjusting ΔT obtained from climate modeling

The amount of sunlight that enters and subsequently escapes the canyon depends on the canyon's location, which affects climate and hourly solar position, and the canyon's geometry, which determines how much of the sunlight entering the canyon reaches the floor. This means that canyon albedo (ratio of sunlight leaving the canyon to sunlight entering the canyon) will differ between the narrow canyon and wide canyons. Therefore, the air temperature difference ΔT predicted by the climate modeling applies only to a city populated with narrow canyons, and must be adjusted to describe air temperature changes in wide canyons.

Changing the geometry and surface albedos of an urban canyon may perturb various local atmospheric parameters, such as wind flow, vertical and horizontal mixing, and turbulence kinetic energy (TKE). These parameters may which can affect the surface and near-surface temperatures within the canyon. Assuming these atmospheric parameters remain constant, we expect the near-surface temperatures in the canyon to be proportional to the canyon albedo (Li et al. 2014). To elaborate, the reduction in the near-surface air temperature in a canyon is proportional to the reduction in the canyon's solar heat gain, which in turn is proportional to the decrease in the canyon's solar absorptance. The reduction in solar absorptance is the same as the increase in albedo. Hence, the reduction in air temperature is proportional to the increase in canyon albedo, ρ_c, or simply:

$$\Delta T \propto \Delta \rho_c \tag{14}$$

Our objective is to scale the narrow-canyon temperature change, ΔT_n, obtained from the climate modeling to estimate a wide-canyon temperature change, ΔT_w. Since ΔT is proportional to $\Delta \rho_c$, the scaling factor is

$$\sigma_{\mathrm{n}\to\mathrm{w}} \equiv \frac{\Delta T_{\mathrm{w}}}{\Delta T_{\mathrm{n}}} = \frac{\Delta \rho_{\mathrm{c,w}}}{\Delta \rho_{\mathrm{c,n}}}. \quad (15)$$

We developed an urban canyon albedo model (UCAM) to estimate the canyon albedo from geometry and location (Appendix D). The model calculates the solar radiation that enters through the canyon canopy and the solar radiation that is reflected out of the canyon. It is suited for exploring how the canyon albedo varies with the albedo or geometry of wall, setback, and/or street. Hence, the model can be applied to calculate the rise in canyon albedo as the street is made more reflective.

This led us to define a canyon transmittance, τ. Canyon transmittance is the ratio of the increase in sunlight reflected from canyon to sky upon raising the albedo of a street in the canyon, to the increase in sunlight reflected to the sky upon raising the albedo of the same street not in a canyon. It can be interpreted as the transmittance of sunlight from sky to street to sky. Canyon transmittance should approach unity as canyon height approaches zero, and should never exceed unity.

Let to $\Delta\rho_r$ refer to the change in street albedo (we use the subscript "r" ["road"] for street because the subscript "s" is reserved for "setback"). The change in canyon albedo, $\Delta\rho_c$, upon increasing street albedo by $\Delta\rho_r$ is proportional to the canyon's transmittance, τ. Thus for a given increase in street albedo:

$$\sigma_{\mathrm{n}\to\mathrm{w}} = \frac{\Delta \rho_{\mathrm{c,w}}}{\Delta \rho_{\mathrm{c,n}}} = \frac{\tau_{\mathrm{w}}\ \Delta \rho_{\mathrm{r}}}{\tau_{\mathrm{n}}\ \Delta \rho_{\mathrm{r}}} = \frac{\tau_{\mathrm{w}}}{\tau_{\mathrm{n}}}. \quad (16)$$

We used this ratio of canyon transmittances to scale temperature changes simulated for the narrow canyon to what would be expected in each of the 10 wide canyons.

Thirty-two relevant property types are present in the public records of the County Assessor's offices (see Section 2.7 for details on our assessment of California's building stock using data from the County Assessor's offices). We mapped each of these property types to one of our building prototypes to represent all the relevant buildings in any particular city (Table 26).

We then calculated for each city the fraction of the building stock that was assigned to each building prototype. Using these fractions and the scaling factor ($\sigma_{n\to w}$) for each wide canyon, we calculated a weighted citywide scaling factor, ($\sigma_{n\to \bar{w}}$), which describes the factor to adjust air temperature changes simulated for a city composed of only the narrow canyon to those expected for a city composed of the wide canyons.

Since the albedo of the canyon varies by location, the citywide scaling factor was calculated for each of the BCZs represented by the climate modeling. Table 25 lists $\sigma_{n\to w}$ by BCZ and season. Note that σ_w, the average value of $\sigma_{n\to w}$ over the 10 BCZs, rounds to 2.8 in summer, fall, and spring, and to 2.6 in winter.

Using Eq. (17), we adjusted all the ΔT_n provided by the climate modeling activity and generated new tables of ΔT_w for each of the 10 BCZs.

$$\Delta T_{\bar{\mathrm{w}}} = \sigma_{\mathrm{n}\to\bar{\mathrm{w}}}\ \Delta T_{\mathrm{n}}. \quad (17)$$

Table 25. Scaling factors $\sigma_{n\to\overline{w}}$ from city composed of narrow canyon to city composed of the wide canyons.

Season	Scaling factors, $\sigma_{n\to\overline{w}}$, by building climate zone												
	3	**4**	**7**	**8**	**9**	**10**	**12**	**13**	**14**	**15**	**Min**	**Max**	**Mean**
Fall	2.79	2.80	2.79	2.80	2.79	2.82	2.81	2.82	2.83	2.71	2.71	2.83	2.80
Winter	2.56	2.55	2.62	2.62	2.62	2.65	2.65	2.69	2.68	2.40	2.40	2.69	2.60
Spring	2.79	2.80	2.80	2.79	2.79	2.82	2.81	2.82	2.84	2.72	2.72	2.84	2.80
Summer	2.81	2.82	2.81	2.82	2.82	2.85	2.84	2.85	2.87	2.74	2.74	2.87	2.82

Create modified weather files with adjusted ΔTs

The two modified versions of the weather files were created using the new ΔT_w to adjust dry-bulb air temperature. Each weather file consists of hourly values over the period of a "typical year" (Section 0). The narrow-canyon temperature changes ΔT_n obtained from the climate modeling included four sets of 24 temperature change values (a ΔT_n for each hour of the day) for a representative day in each season. The representative days are in June (for summer season), October (fall), January (winter), and April (spring).[3]

Thus, when scaling the 96 (24 hours × 4 representative days) values of ΔT_n, we obtained 96 adjusted ΔT_w values. To represent the months of the year between those of the representative days, we interpolated for each hour, between the ΔT_w of the representative days. For example, to estimate a representative ΔT_w value for 10:00 AM in each of the months of July, August, and September, we interpolated between the ΔT_w values for 10:00 AM of the representative days in July and October. Thus, we obtained a total of 288 ΔT_w values for a year (24 hours × 12 months). This process was done for each of the 96 ΔT_n values obtained for the 10 California building climate zones.

To modify the dry-bulb air temperature in each weather file, we first grouped the hourly dry-bulb air temperatures in the weather file by month. Then, at each hour of the day for every day of the month, we subtracted from the air temperature in the weather file, the adjusted temperature reductions ΔT_w that corresponds to that hour and that month ΔT_w. In the end, our collection of weather files consisted of the following:

- Original weather files – used in building energy simulations to represent the control scenario
- Modified weather files, small perturbation – used to represent the small perturbation scenario ($\Delta\rho_p = 0.10$)
- Modified weather files, large perturbation – used to represent the large perturbation scenario ($\Delta\rho_p = 0.40$)

[3] Using the climate model output, we attempted to develop a general formulation to predict ΔT_n as a function of individual meteorological variables, including cloud cover or and surface insolation. This proved to not work. We were unable to develop such general formulations due to co-variation of many meteorological variables. Thus teasing out the influence of individual meteorological variables (e.g. only cloud cover) on ΔT_n was impossible. We therefore represent only the first order effect of pavement albedo on temperature seasonally, without considering how e.g. cloud cover and surface insolation impact the ΔT_n – pavement albedo sensitivity.

2.6.3. Physical model

Physical model equations

We propose a physical model to describe the effects of modifying local street albedo and city pavement albedo on the cooling, heating, and lighting energy uses of a building. This model considers two different effects of cool pavements on a building's energy use. The first, or "direct", effect results from modifying the local street albedo, ρ_r, meaning that of the street (or streets) adjacent to the building. Raising load street albedo increases the solar flux incident on walls and windows, which can increase the cooling load and decrease the heating load.[4] The second, or "indirect," effect happens when increasing the city-mean pavement albedo ρ_p reduces the convective heating of the city air. This lowers the city air temperature and changes the air temperature difference across the building envelope. The indirect effect is expected to reduce cooling loads and increase heating loads.

Cooling energy includes both the energy used to chill air and the ventilation energy used to distribute chilled air. Increasing the local street albedo raises the solar flux incident on the walls and windows, which increases the annual cooling load. Assuming the change in the cooling site energy use E_c scales linearly with the change in local street albedo, we can express it as

$$\frac{\partial E_C}{\partial \rho_r} = a_1 . \tag{18}$$

Increasing the city-mean pavement albedo lowers the city air temperature by reducing convective heating of the air. Cooler air decreases the cooling load. Assuming the change in the site cooling energy use scales linearly with the change in city-mean pavement albedo, we can express it as

$$\frac{\partial E_C}{\partial \rho_p} = a_2 . \tag{19}$$

Solving the partial differential equations (18) and (19) yields the linear equation

$$E_C = a_0 + a_1 \rho_r + a_2 \rho_p . \tag{20}$$

We assume the coefficients a_0, a_1, a_2, are constants specific to building and location. Note that a coefficient will be negative if the building energy use decreases as albedo rises. *Heating* energy includes both the energy used to warm air, and the ventilation energy used to distribute warmed air. The prototypes used in this study are heated with natural gas, electricity, or both. *Gas heating* energy includes only gas used to warm air, while *electric heating* energy includes both electricity used to warm air, and electricity used to distribute air that was warmed with either natural gas or electricity. An increase in the incident solar flux on walls and windows from more reflective local streets can also decrease the heating load. If we assume the change in the site gas heating energy use (G_H) changes linearly with the change in ρ_r, we can express it as

$$\frac{\partial G_H}{\partial \rho_r} = b_1 . \tag{21}$$

[4] By cooling the surface of the street, increasing local street albedo also reduces the net longwave (thermal infrared) radiative heat transfer from street to building. This effect may be important, but was not considered because the building energy simulation tool used in this study (EnergyPlus) does not have a mechanism to do so.

Cooler air from the "indirect" effect of cool pavements can also increase the heating load. If we assume the change in the site gas heating energy use scales linearly with the change in ρ_p, we can express it as

$$\frac{\partial G_H}{\partial \rho_p} = b_2 \cdot \tag{22}$$

Solving the partial differential equations (21) and (22) yields the linear equation

$$G_H = b_0 + b_1\ \rho_r + b_2\ \rho_p \cdot \tag{23}$$

Similarly, we derived a linear equation for the site electric heating energy use:

$$E_H = c_0 + c_1\ \rho_r + c_2\ \rho_p \cdot \tag{24}$$

We assume the coefficients b_0, b_1, b_2, c_0, c_1, and c_2 are constants specific to building and location. Increasing the local street albedo increases the solar flux that is reflected from the street and enters through the windows. This rise in sunlight entering through the windows may decrease the need for artificial lighting. Assuming the change in the site lighting energy use (E_L) scales linearly with the change in ρ_r, we can express it as

$$\frac{\partial E_L}{\partial \rho_r} = d_1 \cdot \tag{25}$$

The indirect effect of cool pavements will have no effect on lighting energy use. Hence, we simply solve equation (20) to yield the linear equation

$$E_L = d_0 + d_1\ \rho_r \tag{26}$$

As we assumed for the previous coefficients, we treat d_o and d_1 as constants specific to building and climate.

Regression of physical model coefficients to EnergyPlus simulations

The simulations returned hourly values of energy use for the various HVAC system components over a period of a year. We calculated annual energy use by adding the annual hourly energy uses.

One of the fields from the simulation outputs is the electric cooling energy use. Depending on the prototype, this could refer to any or a combination of chiller, precision air conditioning unit (PACU), or direct exchange (DX) unitary system.

Another field is the gas heating energy use, which refers only to the gas used to heat the conditioned space. Depending on the prototype, the gas heating may involve a boiler or furnace. With the exception of the medium office, all prototypes used gas as their main source for heating. Although the medium office consumed a small amount of gas for heating, it mainly used electric heating coils. The simulation output also provided a field for electric heating energy use.

Another output field is the ventilation energy use. The ventilation system distributed air for both cooling and heating. The ventilation energy had to be separated into that used to distribute cooled air and that used to distribute heated air. In some prototypes (single-family home, sit-down restaurant, and strip mall retail), the cooling and heating system never ran simultaneously. Hence, it was easy to separate the cooling and heating ventilation energies—during the hours when the building was being cooled, ventilation energy was assigned to cooling; while heating, ventilation energy is assigned to heating.

In the other seven prototypes, the cooling and heating system sometimes ran simultaneously. When this happened, the amount of ventilation energy allotted to cooling and heating depended on the fractions of HVAC heat transfer associated with each application. For example, assume that at a given hour in the medium office prototype, the cooling coils remove 1 MJ of heat while the heating coils add 3 MJ of heat. The cooling fraction is 0.25 [1 MJ / (1 MJ + 3 MJ)]; hence, in that hour, 25% of the ventilation energy is assigned to electric cooling and 75% is assigned to electric heating.

Two other output fields of EnergyPlus are the hourly indoor and outdoor lighting energy uses. We considered only the indoor lighting energy use in this study.

The annual site cooling energy use is the sum of the annual electric energy consumed by the cooling system plus the annual ventilation energy allotted to cooling. The annual site gas heating energy use includes gas heating energy, but no ventilation energy. In the case of the medium office, the annual site electric heating is the sum of the electricity used to warm the air and the ventilation energy allotted to heating. For every other prototype, the annual electric heating energy use is equal to the ventilation energy for heating.

We applied multivariate linear regression analysis to the annual site energy uses to find the coefficients of the cooling, heating, and lighting site energy use equations derived from the physical model. This was done for each of the building prototypes and for the different building climate zones. Each prototype was simulated for six different local street albedos (0.10, 0.15, 0.20, 0.30, 0.40, and 0.50). To model the effect of modifying the city-mean pavement albedo, we ran each simulation three times using the three versions of each location's weather file. The total number of simulations was 1,800 (10 building prototypes × 10 building climate zones × 6 local street albedo × 3 weather file versions).

2.6.4. Building-to-street view factors

Assuming an unobstructed view from wall to street (no trees), we used common geometric configurations to calculate the view factors from the prototypes to the streets. The view factor (a.k.a., configuration factor or shape factor) from surface A to surface B () is the fraction of diffuse radiant energy leaving surface A that is intercepted by surface B. View factors depend only on geometry. As such, view factors have been published in the engineering literature for common geometric configurations, many of which are readily available in John Howell's online catalog of configuration factors (Howell 2015).

We treat each street-facing wall of a building as a rectangular surface of height H_w and length L_w with a setback to the street of width W_s. The street is treated as an infinitely long rectangle of width W_r. Figure 11 illustrates the dimensions of the single-family home, setback, and street.

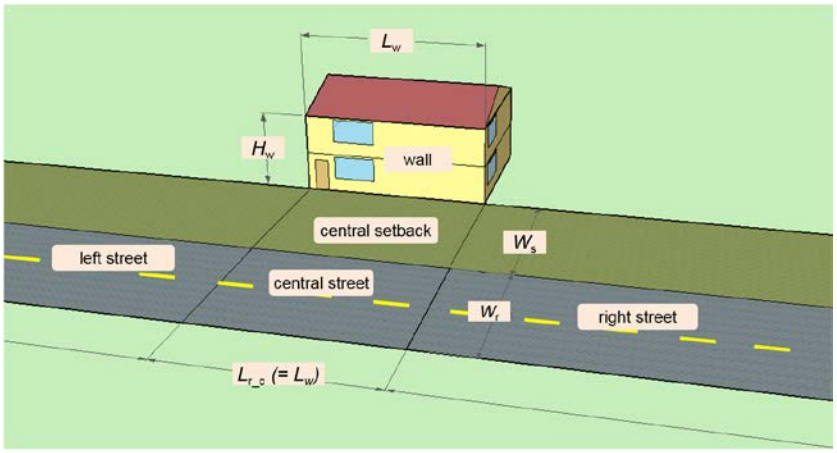

Figure 11. Diagram of single-family home with setback and street.

Let $F_{w\to r}$ represent the wall-to-street view factor, where subscript w refers to wall and subscript r refers road (street). To calculate $F_{w\to r}$, we employed two standard radiation configurations. One configuration was used to find the view factor from the wall to the portion of the street directly in front of the wall, which we call the central street. The second configuration was employed to calculate the view factor from the wall to the left and right sections of the street. See Figure 11 for a diagram of the wall, setback, and street sections used for the view factor calculations.

For the view factor from the wall to the central street, we used the formula for the common geometric configuration of two finite rectangles of same length, having one common edge, and at an angle of 90 ° of each other (Incropera 2007). Hence, the view factor from the wall to the central street portion ($F_{w\to r_c}$) was obtained by subtracting the view factor to the central setback $F_{w\to s_c}$ from the view factor to the central setback + street $F_{w\to(r+s)_c}$:

$$F_{\mathrm{w}\to\mathrm{r_c}} = F_{\mathrm{w}\to(\mathrm{r+s})_\mathrm{c}} - F_{\mathrm{w}\to\mathrm{s_c}} \quad (27)$$

To calculate the view factor from the wall to the left and right sections of the street, we used the view factor formula developed by Ehlert and Smith (1993). The formula gives the view factor from a rectangle to another rectangle in a perpendicular plane, with all boundaries being parallel or perpendicular. Thus with this configuration we obtained the view factors from the wall to the left ($F_{w\to r_1}$) and right ($F_{w\to r_c}$) sections of the street. The total wall-to-street view factor $F_{w\to r}$) was obtained as:

$$F_{\mathrm{w}\to\mathrm{r}} = F_{\mathrm{w}\to r_\mathrm{c}} + F_{\mathrm{w}\to\mathrm{r_l}} + F_{\mathrm{w}\to\mathrm{r_r}} \quad (28)$$

As explained in Section 2.6.1, the modified prototypes do not have streets on all four sides of the building. Using the number of building sides (N) facing a street (Table 20) we estimated the overall building-to-street view factor, $F_{b\to r}$, as:

$$F_{\mathrm{b}\to\mathrm{r}} = F_{\mathrm{w}\to\mathrm{r}} \times N/4 \quad (29)$$

2.7. Assessment of California building stock

With the results from the modeled prototypes we can understand the effect cool pavements have on the energy use in a single building, but to understand the building energy use effect of cool pavements in a city, it is important to know the building stock in that location. In each county, the assessor's office is

responsible for the discovery and assessment of all the properties within their jurisdiction. We used a collection of the public property records for the entire state of California to evaluate the state's building stock.

2.7.1. Obtaining source data

The California Air Resources Board (hereafter, ARB) acquired the public records of commercial and residential properties in the state from each County Assessor's office in California. ARB shared with us these records, which we in turn used to assess the state's building stock. The entire collection includes property data entries up to 2013. Each record includes useful information for each of the properties, which include location (county, city, and ZIP code); floor area; property type (e.g., single-family home, office building); and age. We obtained a total of 12,552,241 records.

2.7.2. Cleaning data

The Assessor's Office in each county locates and assesses all taxable properties in its jurisdiction. In many cases, the property information is collected and recorded manually. This often leads to misspelled information, including the city's name. To correct the inconsistency in city names, we used the ZIP Code Database (USZIPCodes 2015) to pair each reported ZIP code to a city. The cities were renamed by mapping the ZIP codes to cities in the U.S. Census table.

2.7.3. Calculating building count, floor area, and age

To estimate the citywide impact of cool pavements, it is necessary to understand the building stock in the city of interest, such as the size, floor area, and age distributions by property type and location. The building stock data collection provides sufficient information to do this sort of analysis. We first grouped the building stock data by county, city, and property type. The data contains information for all 58 counties in California, and nearly 1,500 cities and towns are represented. Each property is classified into one of 63 types.

After the initial grouping, we calculated the total floor area of each property type in each city. Some building records omit floor area—for example, 12% of single-family homes statewide do not report floor area. Hence, to calculate the total floor area of each property type in each city, we multiplied the mean floor area in that city (for the subset of buildings that report floor area) by the number of buildings to obtain the total floor area. If floor area was absent in every record for a particular property type in a given city, we used the statewide mean floor area for that property type.

The building stock collection also classifies all properties into six general categories: residential, commercial, agricultural, vacant land, industrial, and miscellaneous. The entire building stock was grouped by category to obtain the state-wide floor areas of the residential and commercial buildings—1659 km² (640.5 mi²) (78%) for residential and 469 km² (180 mi²) (22%) for commercial. These values are comparable with the floor area we calculated from the 2009 Residential Energy Consumption Survey (RECS) (EIA 2009) for residential buildings, and from 2006 California Commercial End-Use Survey (CEUS) (Itron Inc. 2006) for commercial buildings.

2.7.4. Mapping property type to building prototype

Sixty-three property types are present in the public records of the County Assessor's offices. Nearly half, including such types as vacant land and agricultural fields, are not relevant to this study. That leaves 32

relevant property types. We mapped each of these remaining property types to one of our building prototypes to represent all the relevant buildings in any particular city (Table 26).

Table 26. Mapping of stock property types to building prototypes.

Building prototype	Stock property types	Building prototype	Stock property types
Single-family home	Single family residence Duplex Triplex Mobile home Trailer park Miscellaneous residential Fraternal organization	Apartment building	Multi-family dwelling (2-4 units) Multi-family res (5+ units) Quadruplex Timeshare Condominium Planned unit development (PUD) Cooperative
Large hotel	Hotel Motel Casino Hospital Convalescent home	Medium office	Store/office combo Medical building Miscellaneous commercial Nursery Veterinary Governmental
Retail stand-alone	Department store Food store Market Bowling alley	Strip mall retail	Shopping center Stores Retail outlet
Fast-food restaurant	Laundry Dry cleaning	Sit-down restaurant	Restaurant Bar Food service
Large office	Financial building Office building	Primary school	School

2.8. Development and operation of the pavement life-cycle assessment decision tool

2.8.1. Overview

The first version of the pavement life-cycle assessment decision tool assesses the energy and environmental consequences of urban pavement choice over a 50-year life cycle (LC). Given the city of interest, the fraction of that city's pavement area to be modified, and two pavement scenarios (each specifying pavement type, service life, and albedo) the tool computes for each scenario two life-cycle impact indicators—global warming potential (CO_2e) and smog potential (kg O_3e)—and three life-cycle flows: PM2.5, primary energy demand without feedstock energy, and feedstock energy. Each of these LCA metrics is defined in Table 4.

These calculations consider in each pavement scenario the contributions to the LCA metrics of pavement material, transport, and construction (the "materials and construction" stage[5]) and those from cooling, heating, and lighting the buildings in the city (the "use" stage). To compare pavement scenarios, the tool

[5] The pLCA tool refers to the materials and construction (MAC) stage as the "non-use" stage.

evaluates the difference in each LCA metric, as well as the differences in annual site electricity used for cooling, lighting, and/or heating [kWh]; and annual site gas used for heating [therm; 1 therm = 100 kBTU = 2.76 m^3 gas = 29.3 kWh]. Each LCA metric and site energy use is tallied by stage element (material, transport, construction, cooling, heating, lighting); subtotaled by stage (materials and construction, use); and summed for the two stages.

The tool also evaluates the differences in two instantaneous environmental metrics: seasonal values of city-mean hourly air temperature at 2 m above ground level (AGL), and city-mean daily max 1 h ozone concentration at 15:00 LST in summer. The environmental metrics are described in Sections 3.4 (air temperature and ozone).

By default, the use-stage LCA metrics and annual site energy uses account for both the "indirect" effect of pavement albedo—the influence of citywide mean pavement albedo on citywide mean air temperature, and the variation of building energy use with that air temperature—and the "direct" effect of pavement albedo, meaning the influence of local street albedo on the energy uses of buildings exposed to sunlight reflected from the street. To disaggregate those phenomena, the tool can be configured to show only direct or only indirect effects of pavement albedo.

The tool lists changes in LCA metrics, annual site energy uses, outdoor air temperature, and ozone concentration, but does not assess whether such changes are significant or cost effective. However, to help the operator compare these results to norms obtained outside the scope of this project, the differences between scenarios in the LCA metrics and the annual site energy uses can be expressed as absolute changes over the entire city, as absolute changes per unit area of pavement modified, or as fractional changes. All results can be graphed, tabulated, and/or exported.

The tool closely follows its initial conceptual design (Figure 12), with the following minor differences:

- Location within California is not used to assess the transport component of the LCA.
- The tool evaluates not only total change in each LCA metric change, but also subtotal (materials and construction, use) and component (material, transport, construction, cooling, heating, lighting) changes.
- The tool can disaggregate use-stage outputs by effect (direct, indirect).

This version of the tool is coded in Python 3 and operates in a jupyter (formerly IPython) notebook that provides a graphical user interface (GUI). It has been developed and tested only for Windows 64-bit computers.

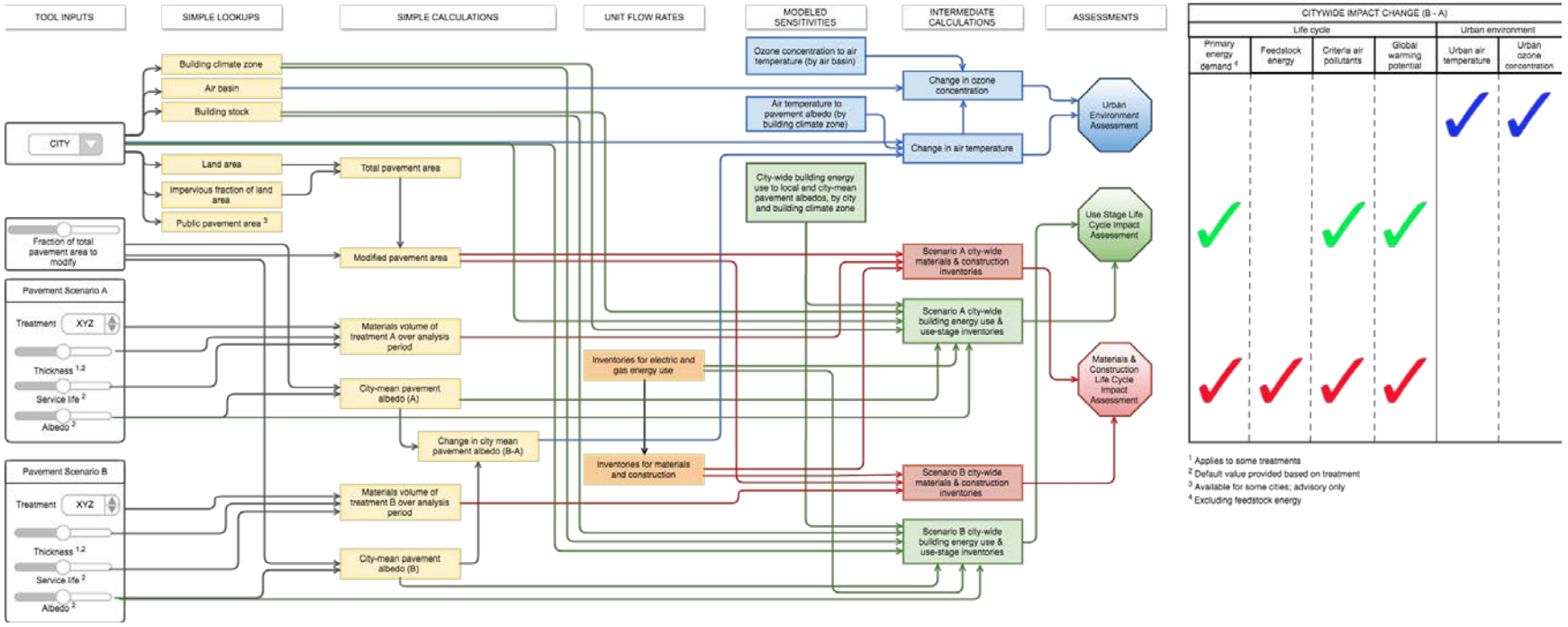

Figure 12. Conceptual design of the pavement life-cycle assessment (pLCA) tool.

2.8.2. pLCA tool assumptions

Several important assumptions were made when developing the datasets and algorithms for the tool. The assumptions are critical for the tool user to keep in mind in order to understand and interpret the results.

Pavement management practices and network

- Current and alternative pavement treatments included in the tool were developed from a phone survey with local governments in California, a literature survey of pavement treatments used by cities outside California, and from discussion with other pavement researchers with expertise in local government applications.
- Most local governments use multiple treatments in their annual program but the tool is simplified to only consider one treatment for entire network at this time.
- Local governments typically treat a portion (about 1 to 20%) of their network annually, resulting in incremental change in albedo over analysis period. The tool currently is simplified to assume that the entire network is treated at once, with instantaneous change of network albedo, maintained over the 50-year analysis period.
- The performance of treatments, which affects replacement frequency, varies. The performance lifetime of treatments is given as a default value and a likely range. The range and default are based on UCPRC experience, literature and survey of local governments.
- For cities with no information about total pavement area, the tool assumes that half of the city's impervious area is pavement.

Pavement albedo values

- Albedo ranges suggested by the tool are based on measurement and engineering judgment from UCPRC.
- While the maximum albedo value found from field measurements reviewed or performed in the current study was 0.37, the tool permits values up to 1.00.

Life-cycle inventories for electricity, natural gas, and pavement materials and construction

- The tool uses LCIs prepared by UCPRC, as detailed in Section 3.3.

2.8.3. Installing and launching the pLCA tool

To use the tool, you will need to

- Install Anaconda 3 for Windows, 64-bit, version 4.1.1 (once)
- Install the pLCA tool sandbox (once)
- Run the pLCA tool (one double-click + one menu instruction)

All software used is free and open source.

Updating Anaconda

The following steps will install and update the Python environment required for the pLCA tool.

- If you have another version of Anaconda, please uninstall it.
- Download the installer for Anaconda 3 for Windows, 64-bit, version 4.1.1, from https://repo.continuum.io/archive/Anaconda3-4.1.1-Windows-x86_64.exe . **Other versions of Anaconda may not work.**
- Run the Anaconda installer, accepting defaults.

Installing the pLCA tool

The following steps will install the pLCA tool.

- Download to your desktop the ZIP archive "pLCA tool sandbox YYYY-MM-DD.zip" from https://goo.gl/zUWq6N . Here YYYY-MM-DD is the date of the most recent release of the tool (e.g., 2017-03-01).
- Expand it to create the folder "pLCA tool sandbox".
- Move this folder to "C:\", yielding "C:\pLCA tool sandbox". The sandbox folder must be placed here. **If you place it elsewhere, the tool as coded will not run.**

Launching the pLCA tool

The following steps will start the pLCA tool.

- Double-click the shortcut "Launch pLCA tool" in folder "C:\pLCA tool sandbox". This will open "pLCA_tool_notebook" in a jupyter Notebook.
- Execute Cell>Run All from the jupyter Notebook menu. This should take less than 10 seconds.

Troubleshooting

It is necessary to install the specified version of Anaconda, to place the sandbox folder at "C:\", and to start the tool as directed. If after meeting these conditions the tool does not run, you may contact the authors for help.

2.8.4. Operating the pLCA tool

This section serves as a simple user guide for the tool.

The reader may find it helpful to run the tool while following the examples in this section. Note that because the tool is updated occasionally to incorporate new data, inputs and outputs displayed by the tool may differ slightly from the screen captures (Figure 13 to Figure 26) shown in this report.

Inputs

The following describes the inputs that are required to run the pLCA tool. Note that each input can be modified at any time. Changing any input triggers recalculation of the outputs, which will take several seconds.

- Select from a dropdown list one of 31 California cities (default value: Sacramento) for which the indirect and direct effects of modifying pavement albedo have been modeled. The tool will advise for that city (a) California building climate zone (1–16); (b) the total pavement area (public and private) (km^2); (c) the fraction of land area covered by pavement (%); and (d) the public pavement area (km^2), and fraction of total pavement area that is public, if public pavement area known (Figure 13).
- Move a slider or enter a value to selects the fraction of total pavement area to modify (default value: 25%). The tool will advise for that city the area of pavement (km^2) that would be modified.
- Define two Pavement Scenarios: base-case scenario A, and alternative scenario B. The following instructions apply to each scenario.
  - Since some pavements have two layers—e.g., a coating over asphalt concrete—the operator can specify in each scenario either a one-layer system, with only an Upper Surface Treatment, or a two-layer system, with an Upper Surface Treatment (in this example, the coating) and a Lower Surface Treatment (in this example, the asphalt concrete). The scenario defaults to an Upper Surface Treatment of "Conventional Asphalt Concrete (mill and fill)", with an albedo of 0.10, and no Lower Surface Treatment (value = "NONE").
  - To specify the Upper Surface Treatment, first select from a dropdown list one of 29 surface treatments for which materials and construction stage LCA metrics are known (Figure 14). The tool will advise for that treatment (a) range of typical albedo (scale 0 – 1); (b) range of typical service life (y); and (c) default value and allowable range of thickness (cm), where applicable. Move sliders or enter values to specify the albedo, service life, and thickness of the Upper Surface Treatment.
  - The procedure for defining a Lower Surface Treatment (Figure 15) is the same as that for defining an Upper Surface Treatment, except that the albedo of the lower treatment is neither described nor set.

Outputs

As described in its overview, the tool evaluates changes in the five LCA metrics, annual site energy uses, outdoor air temperature, and ozone concentration. The radio buttons in the gold box at upper right control whether these results are output as graphs (Figure 16) or tables (Figure 17); expressed as absolute changes [B minus A] (Figure 18), absolute changes per unit pavement area modified [(B minus A) / (pavement area modified)] (Figure 16), or relative changes [(B minus A) / A] (Figure 19); and include direct + indirect (Figure 20), only direct (Figure 21), or only indirect effects (Figure 22) of albedo changes.

It may be difficult to see use-stage changes in the graphs if they are much smaller than materials and construction stage changes (Figure 16). An easy way to focus on use-stage effects is to define the same pavement system in each scenario, varying only the pavement albedo. This zeros the materials and construction stage changes and scales the graphs to the use-stage changes. Figure 20 shows absolute use-stage changes per unit pavement area modified; Figure 23 shows relative use-stage changes.

Note that while *absolute* values [B minus A] of direct, indirect, and combined (direct + indirect) use-stage changes can be compared to each other using any scenario A, *relative* values [(B minus A)/A] of direct, indirect, and combined use-stage changes should be compared to each other only when the pavement albedo in Scenario A is set to 0.10 (the pavement albedo in the unmodified area). This ensures that the Scenario A energy use is the same in all three cases (direct effect, indirect effect, combined effect).
The display defaults to graphs of absolute changes, incorporating both direct and indirect effects. Note that these graphs will appear empty at first because the two Pavement Scenarios have the same initial values.

The "Save…" button in the upper right corner of the gold box will export two files. The first is a comma-delimited text file summarizing the analysis, including its inputs, some intermediate calculations, and all outputs (Figure 24; Figure 25). The second is a multi-page portable document format (PDF) graphic file with vector (line art) editions of all output graphs (Figure 26). The text file and the graphic file each show the LCA metrics and annual energy savings three ways—with direct + indirect, direct only, and indirect only albedo effects.

Example

To illustrate operation of the tool, we consider changing 25% of the total pavement area in Fresno to portland cement concrete—assigned albedo 0.30, thickness 17.5 cm, and a service life of 10 years—from conventional asphalt concrete (mill and fill), to which we assign albedo 0.10, thickness 6 cm, and a service life of 10 years. The inputs and outputs are shown in Figure 13 through Figure 26. The results of this example are discussed in Section 3.6.

After launching the tool as described at the end of Section 2.8.3, we select "Fresno" from the "City" drop-down menu, and move a slider (or enter a number) to set the "Fraction of total pavement area to modify" to 25% (Figure 13, upper left corner; the pavement area fraction control can be seen more clearly in the upper left corner of Figure 14). To define Pavement Scenario A, we set its "Upper surface treatment (UST)" to "Conventional Asphalt Concrete (mill and fill)", and set its "Lower surface treatment (LST)" to "NONE" (Figure 14, center left; the lower surface treatment control can be seen more clearly at center left of Figure 15). We then move sliders (or enter numbers) to set "Pavement albedo" to 0.1, "UST service life" to 10, and pavement thickness to 6 cm in Scenario A (Figure 15, center left). To define Pavement Scenario B, we set its "Upper surface treatment" to "Portland Cement Concrete" and set its "Lower surface treatment" at its default value of "NONE", then set its "Pavement albedo" to 0.3, "UST service life" to 10 years, and its "UST thickness" to 17.5 cm (Figure 16, center right).

Tool outputs are updated within a few seconds each time an input parameter is changed.

There are three columns of radio-button controls in the gold box at the upper right corner of the tool: "Impact change", "Display", and "Effects" (Figure 16). We can view graphs of changes per unit area of pavement modified by selecting the "absolute/m²" radio button to the right of "Impact change" and the "graph" radio button to the right of "Display" (Figure 16). The same results can be tabulated by selecting the "table" radio button next to "Display" (Figure 17). Pressing the "absolute" or "relative" radio button for "Impact change" will make the current graph or table show absolute or relative changes for the entire city (Figure 18 and Figure 19, respectively).

We can focus on use-stage changes by using the same surface treatment in both scenarios, varying only albedo. For example, we can set Scenario B to match Scenario A, then raise the albedo of Scenario B to 0.30 from 0.10 (Figure 20). We can restrict use-stage results to the direct effect or the indirect effect by

selecting the “direct only” or “indirect only” radio button to the right of “Effects” (Figure 21 and Figure 22, respectively). As before, we can see any of these changes expressed as a fraction by selecting the “relative” radio button for “Impact change” (Figure 23).

Pressing the “Save…” button in the gold box at the upper right corner of the tool saves all inputs and outputs of the current case by exporting a comma-delimited table on inputs, intermediate values, and outputs (Figure 24 and Figure 25) and a PDF file containing all output graphs (Figure 26).

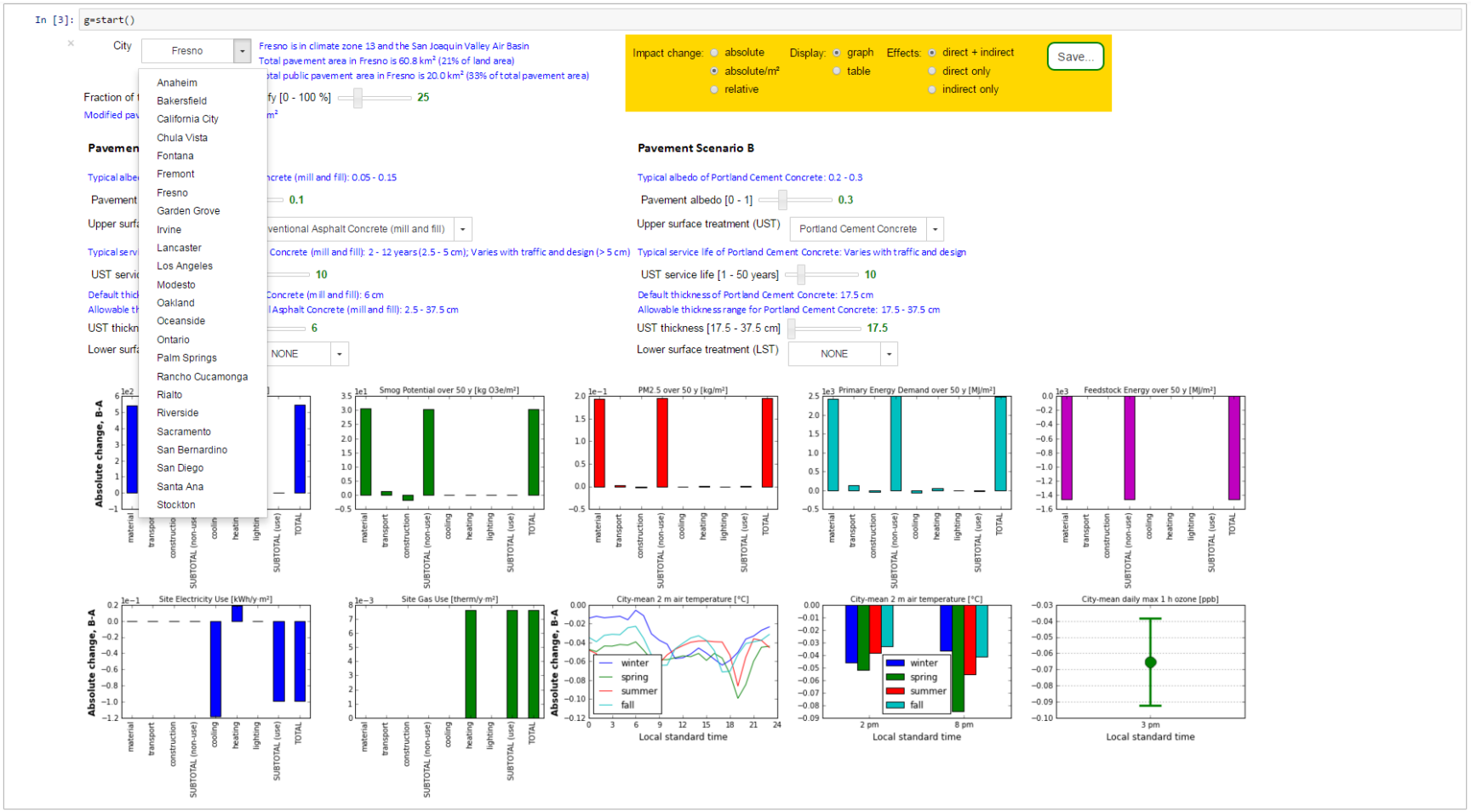

Figure 13. Selecting city from dropdown list in pLCA tool.

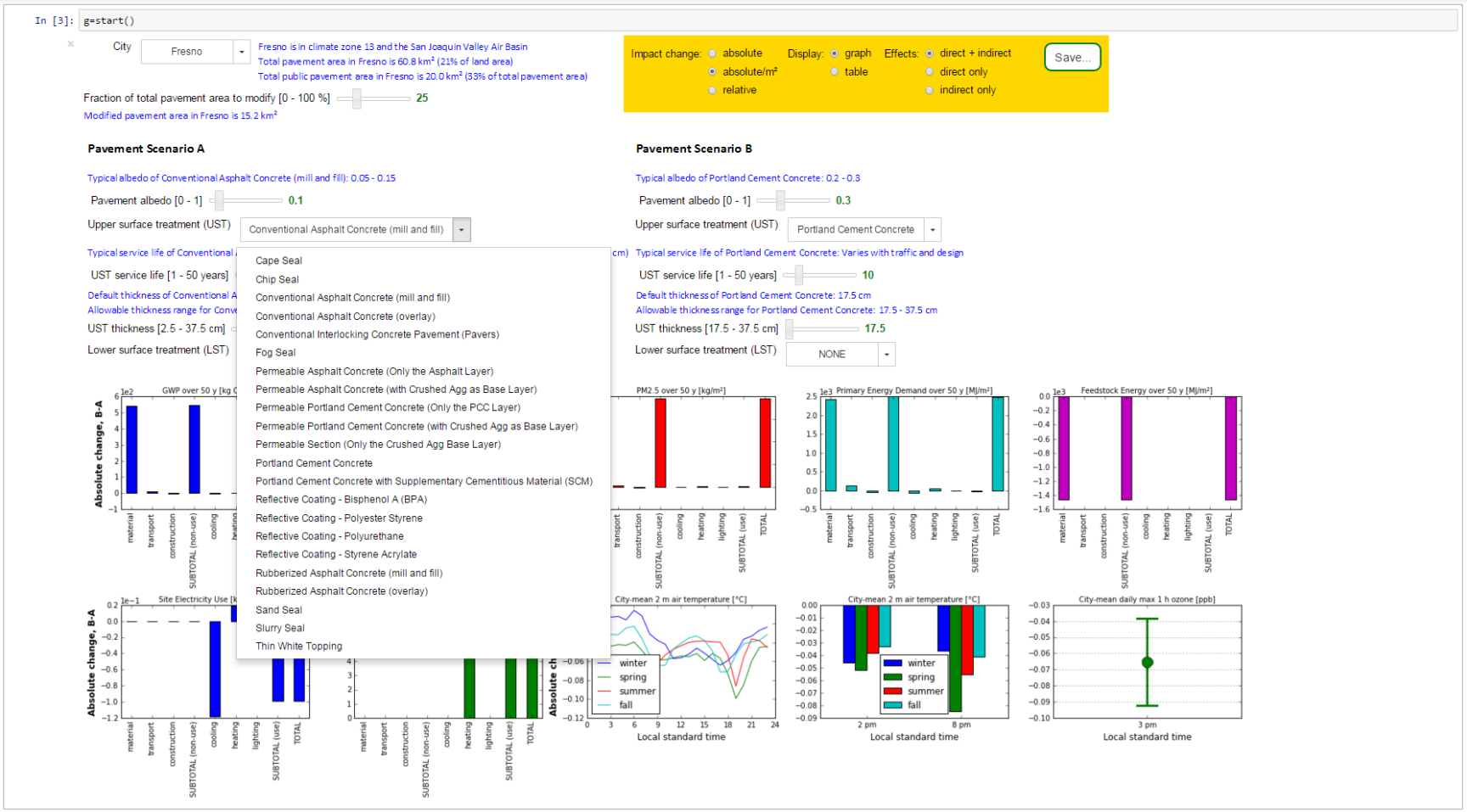

Figure 14. Selecting Scenario A upper surface treatment from dropdown list in pLCA tool. This example compares PCC to AC by defining a one-layer system in Scenario B (UST = PCC; LST = NONE) and a one-layer system in Scenario A (UST = AC; LST = NONE).

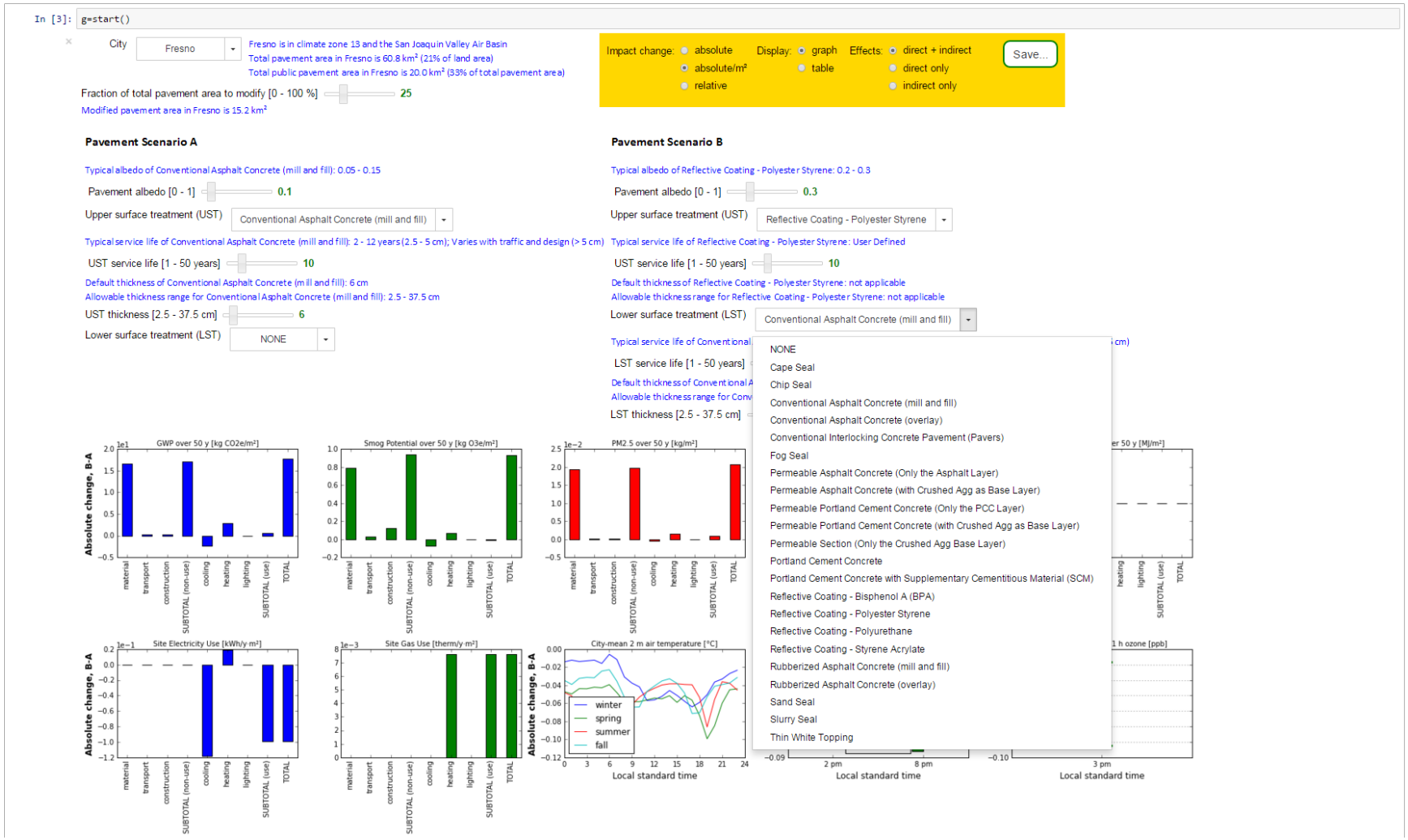

Figure 15. Selecting Scenario B lower surface treatment from dropdown list in pLCA tool. This example evaluates a coating by defining a two-layer system in Scenario B (UST = polyester styrene reflective coating; LST = AC) and a one-layer system in Scenario A (UST = AC; LST = NONE).

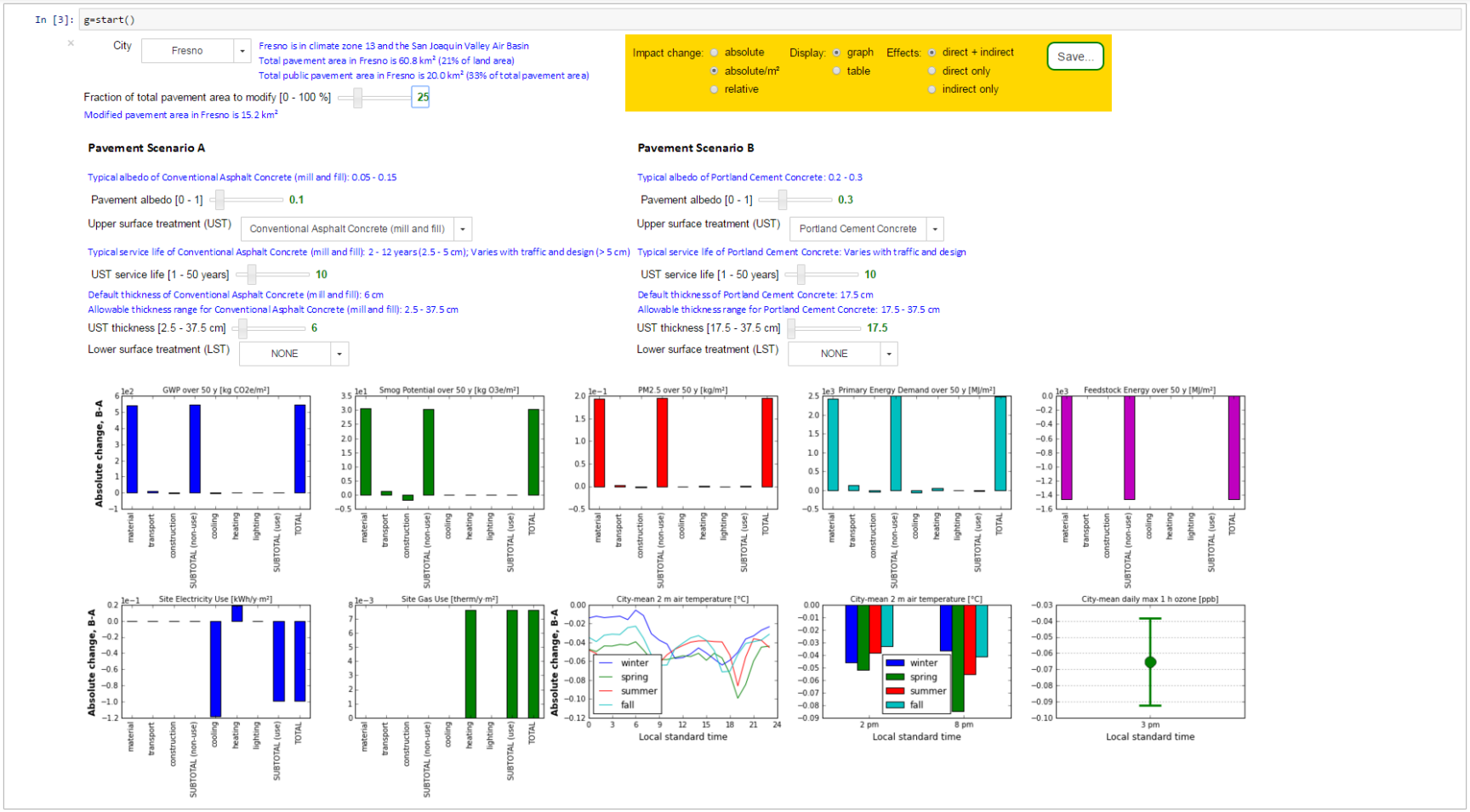

Figure 16. pLCA tool graphing absolute changes per unit area of pavement modified in impacts and site energy uses, for PCC (albedo 0.30) versus AC (albedo 0.10). Both direct and indirect effects are shown in the use stage.

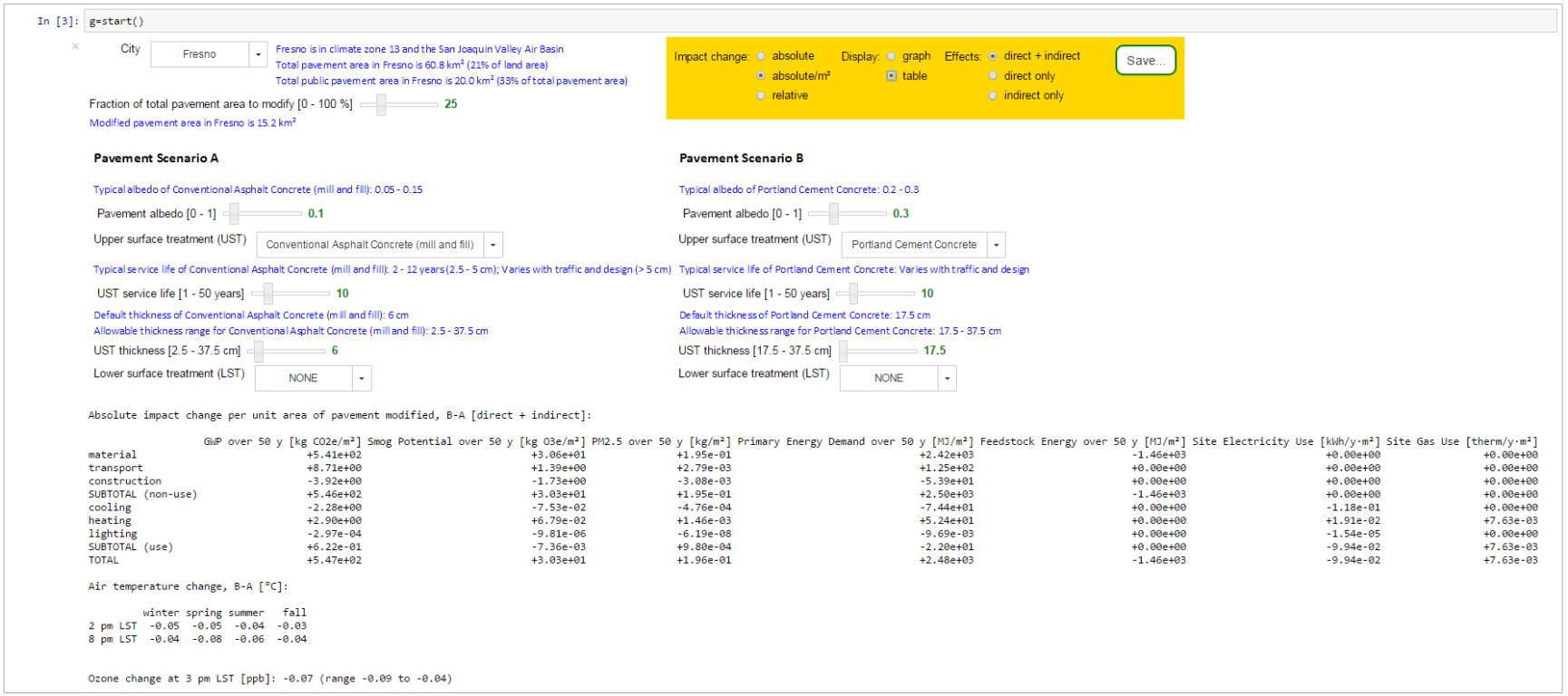

Figure 17. pLCA tool tabulating absolute changes per unit area of pavement modified in impacts and site energy uses, for PCC (albedo 0.30) versus AC (albedo 0.10). Both direct and indirect effects are shown in the use stage.

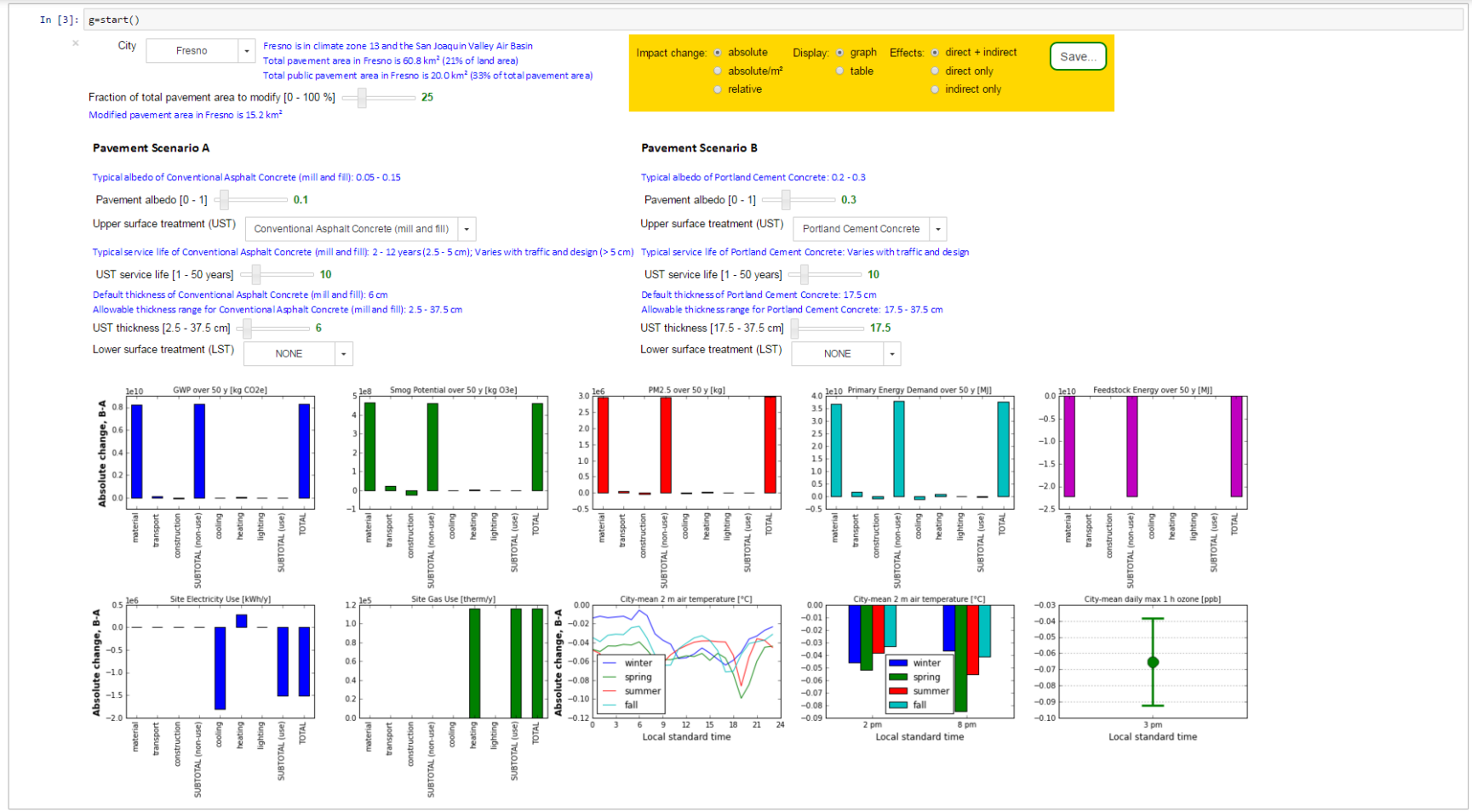

Figure 18. pLCA tool graphing absolute changes in impacts and site energy uses, for PCC (albedo 0.30) versus AC (albedo 0.10). Both direct and indirect effects are shown in the use stage.

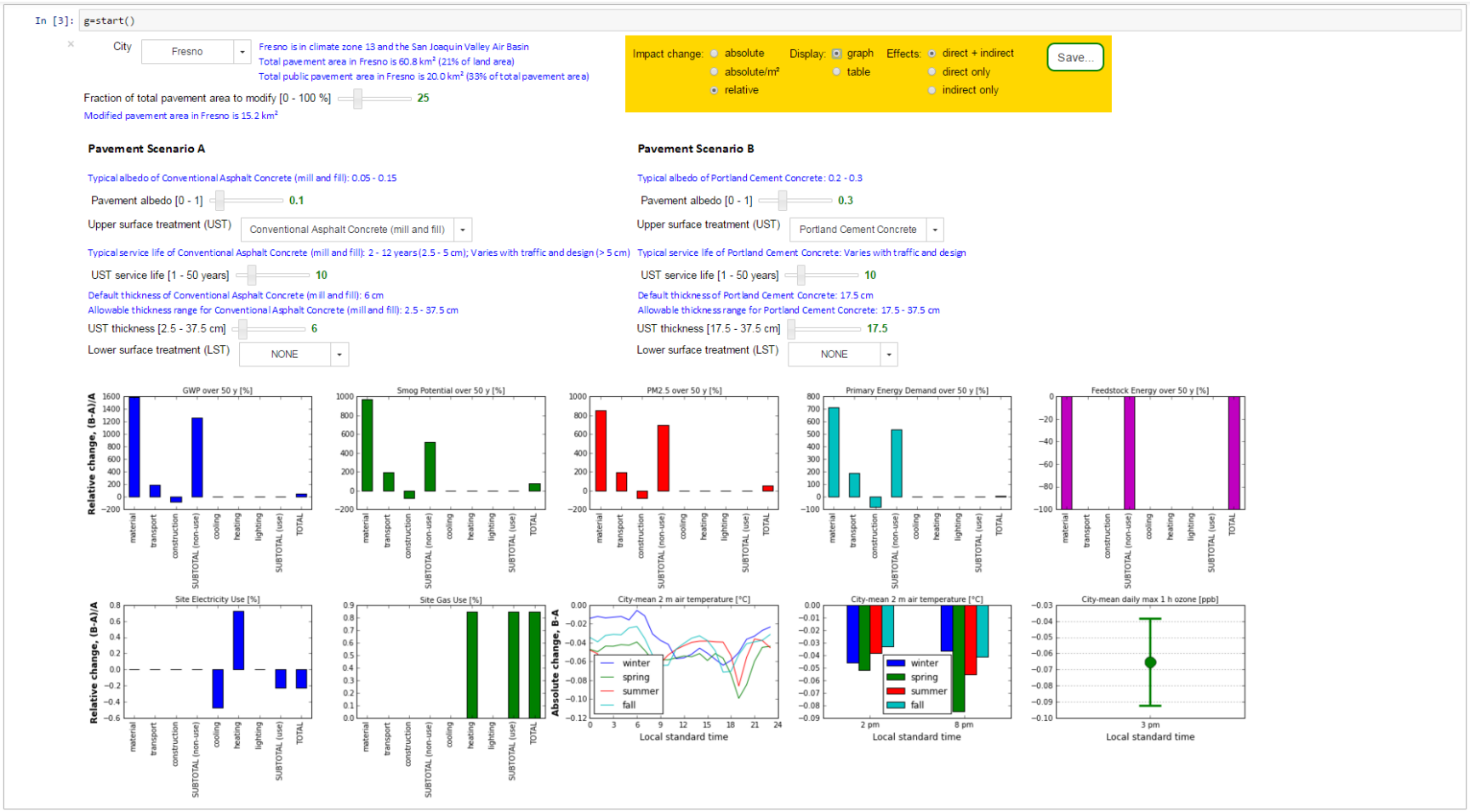

Figure 19. pLCA tool graphing relative changes in impacts and site energy uses, for PCC (albedo 0.30) versus AC (albedo 0.10). Both direct and indirect effects are shown in the use stage.

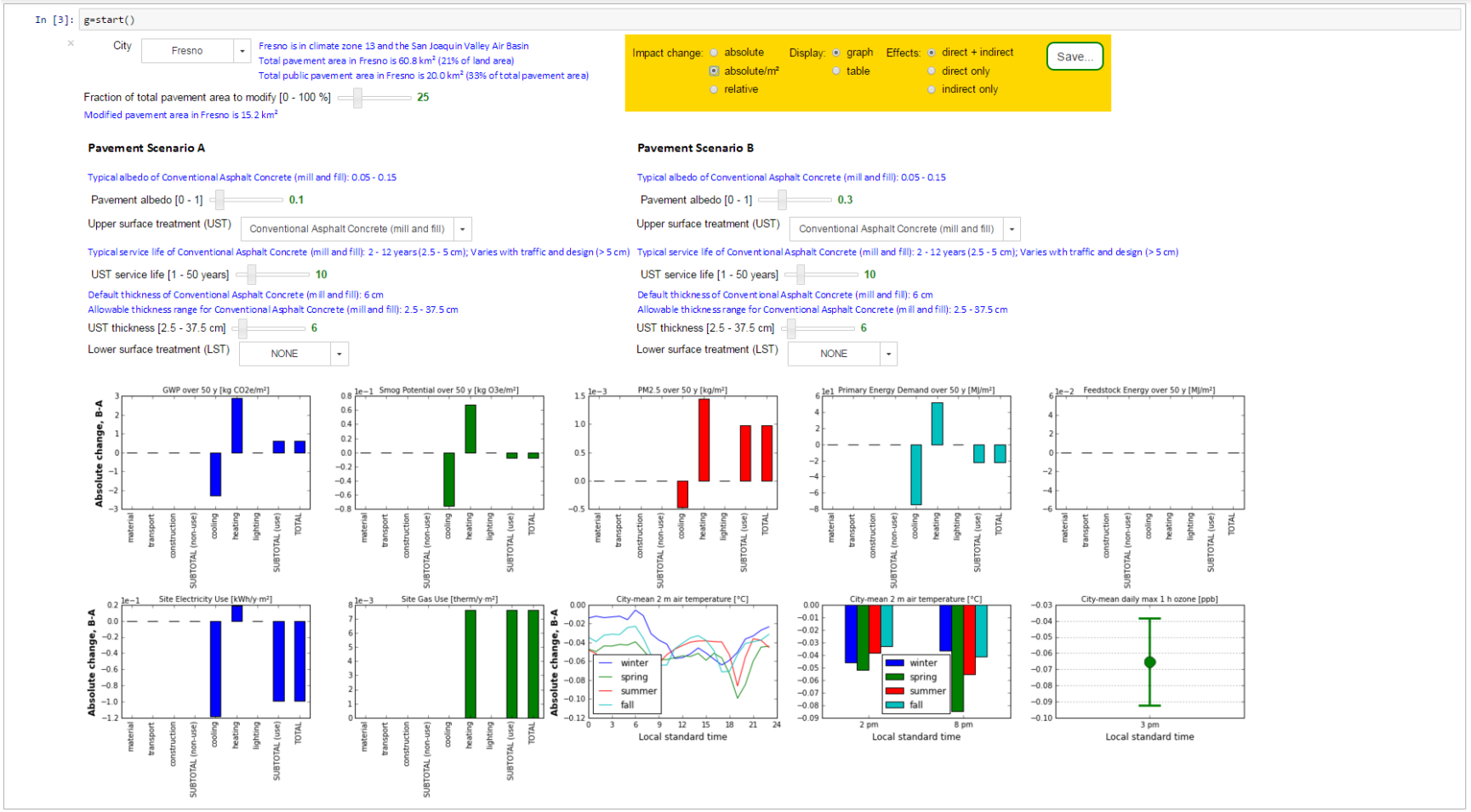

Figure 20. pLCA tool graphing absolute changes per unit area of pavement modified in impacts and site energy uses, varying only albedo (0.30 vs. 0.10). Both direct and indirect effects are shown in the use stage.

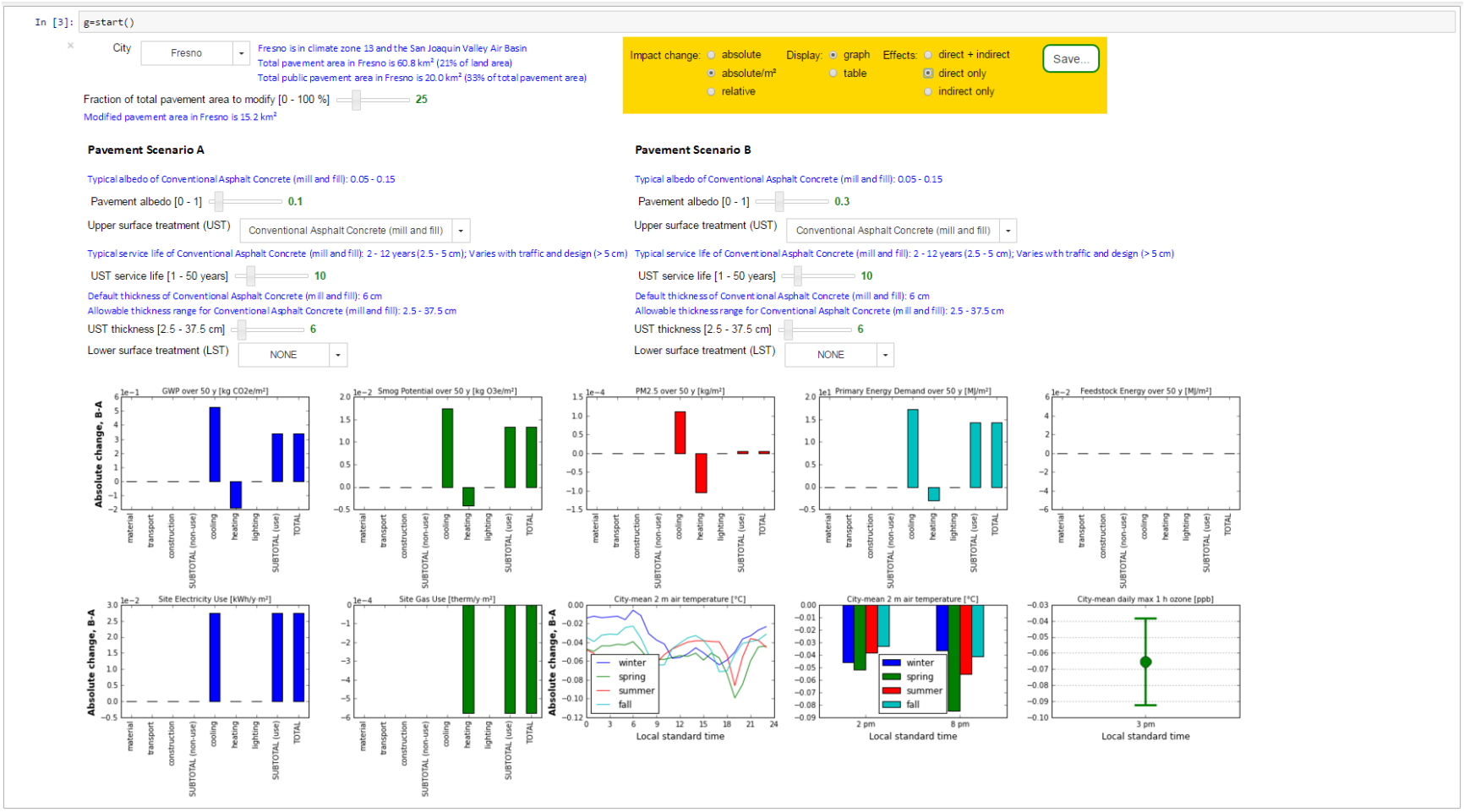

Figure 21. pLCA tool graphing absolute changes per unit area of pavement modified in impacts and site energy uses, varying only albedo (0.30 versus 0.10). Only direct effects are shown in the use stage.

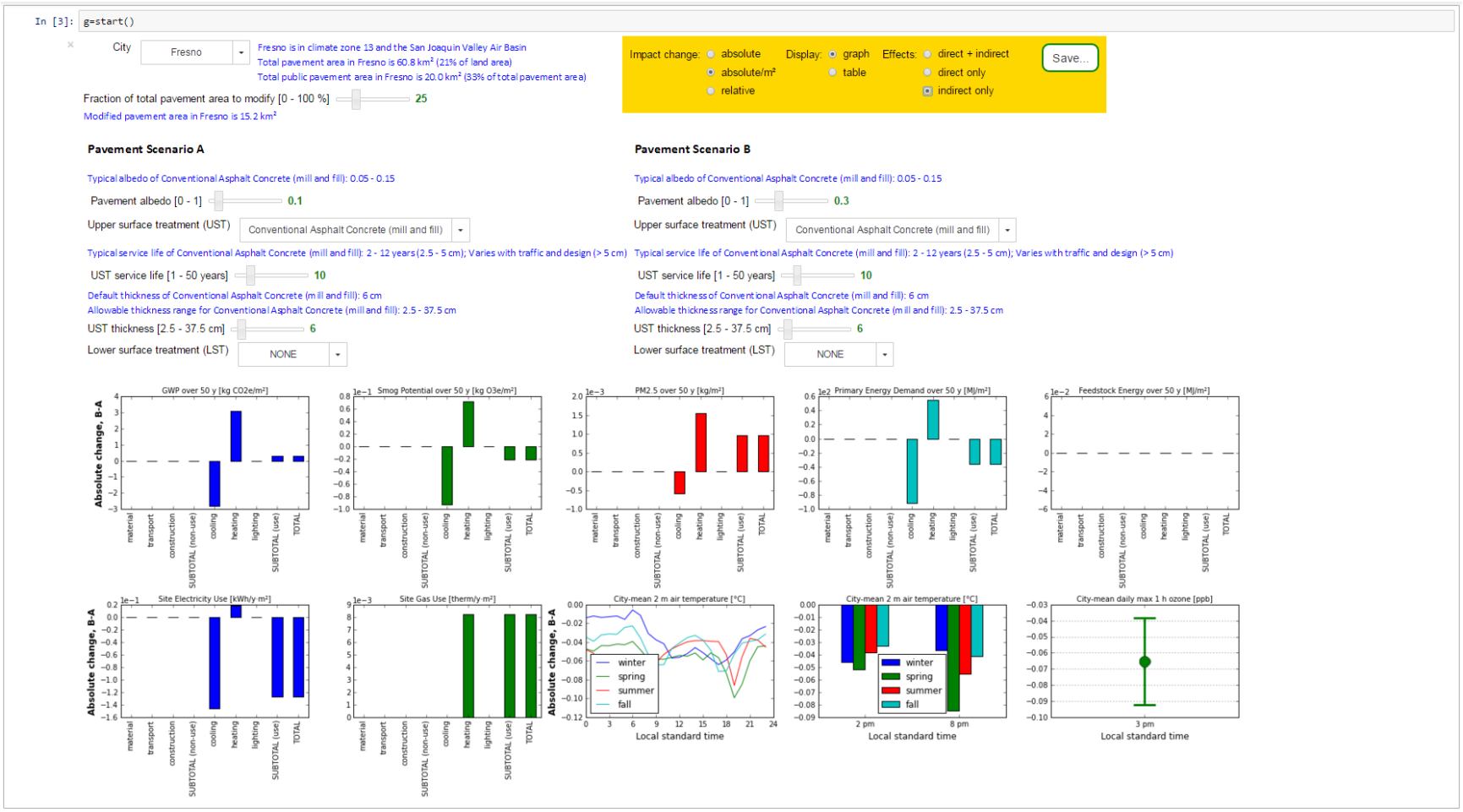

Figure 22. pLCA tool graphing absolute changes per unit area of pavement modified in impacts and site energy uses, varying only albedo (0.30 versus 0.10). Only indirect effects are shown in the use stage.

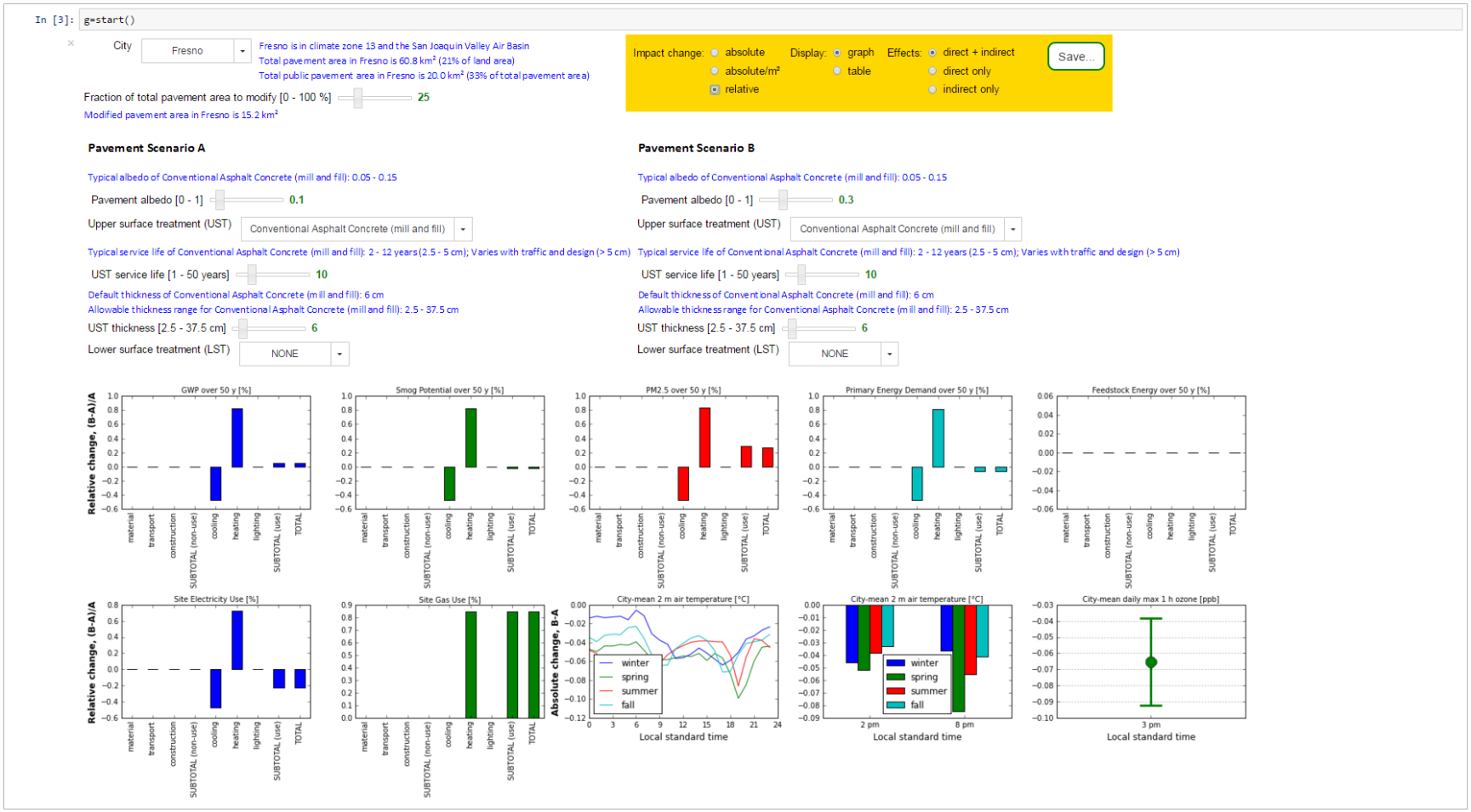

Figure 23. pLCA tool graphing relative changes in impacts and site energy uses, varying only albedo (0.30 versus 0.10). Both direct and indirect effects are shown in the use stage.

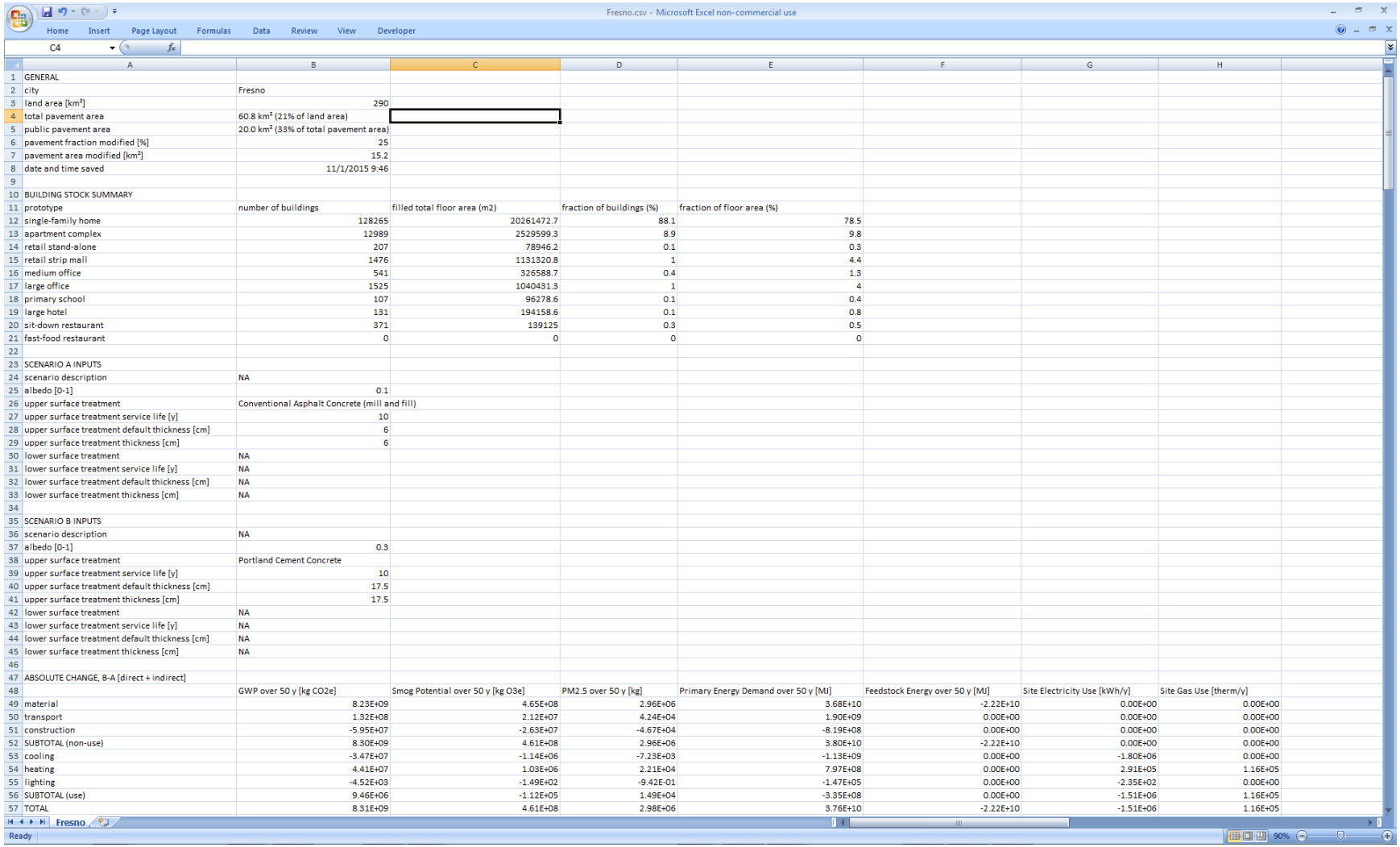

	A	B	C	D	E	F	G	H
1	GENERAL							
2	city	Fresno						
3	land area [km²]	290						
4	total pavement area	60.8 km² (21% of land area)						
5	public pavement area	20.0 km² (33% of total pavement area)						
6	pavement fraction modified [%]	25						
7	pavement area modified [km²]	15.2						
8	date and time saved	11/1/2015 9:46						
9								
10	BUILDING STOCK SUMMARY							
11	prototype	number of buildings	filled total floor area (m2)	fraction of buildings (%)	fraction of floor area (%)			
12	single-family home	128265	20261472.7	88.1	78.5			
13	apartment complex	12989	2529599.3	8.9	9.8			
14	retail stand-alone	207	78946.2	0.1	0.3			
15	retail strip mall	1476	1131320.8	1	4.4			
16	medium office	541	326588.7	0.4	1.3			
17	large office	1525	1040431.3	1	4			
18	primary school	107	96278.6	0.1	0.4			
19	large hotel	131	194158.6	0.1	0.8			
20	sit-down restaurant	371	139125	0.3	0.5			
21	fast-food restaurant	0	0	0	0			
22								
23	SCENARIO A INPUTS							
24	scenario description	NA						
25	albedo [0-1]	0.1						
26	upper surface treatment	Conventional Asphalt Concrete (mill and fill)						
27	upper surface treatment service life [y]	10						
28	upper surface treatment default thickness [cm]	6						
29	upper surface treatment thickness [cm]	6						
30	lower surface treatment	NA						
31	lower surface treatment service life [y]	NA						
32	lower surface treatment default thickness [cm]	NA						
33	lower surface treatment thickness [cm]	NA						
34								
35	SCENARIO B INPUTS							
36	scenario description	NA						
37	albedo [0-1]	0.3						
38	upper surface treatment	Portland Cement Concrete						
39	upper surface treatment service life [y]	10						
40	upper surface treatment default thickness [cm]	17.5						
41	upper surface treatment thickness [cm]	17.5						
42	lower surface treatment	NA						
43	lower surface treatment service life [y]	NA						
44	lower surface treatment default thickness [cm]	NA						
45	lower surface treatment thickness [cm]	NA						
46								
47	ABSOLUTE CHANGE, B-A [direct + indirect]							
48		GWP over 50 y [kg CO2e]	Smog Potential over 50 y [kg O3e]	PM2.5 over 50 y [kg]	Primary Energy Demand over 50 y [MJ]	Feedstock Energy over 50 y [MJ]	Site Electricity Use [kWh/y]	Site Gas Use [therm/y]
49	material	8.23E+09	4.65E+08	2.96E+06	3.68E+10	-2.22E+10	0.00E+00	0.00E+00
50	transport	1.32E+08	2.12E+07	4.24E+04	1.90E+09	0.00E+00	0.00E+00	0.00E+00
51	construction	-5.95E+07	-2.63E+07	-4.67E+04	-8.19E+08	0.00E+00	0.00E+00	0.00E+00
52	SUBTOTAL (non-use)	8.30E+09	4.61E+08	2.96E+06	3.80E+10	-2.22E+10	0.00E+00	0.00E+00
53	cooling	-3.47E+07	-1.14E+06	-7.23E+03	-1.13E+09	0.00E+00	-1.80E+06	0.00E+00
54	heating	4.41E+07	1.03E+06	2.21E+04	7.97E+08	0.00E+00	2.91E+05	1.16E+05
55	lighting	-4.52E+03	-1.49E+02	-9.42E-01	-1.47E+05	0.00E+00	-2.35E+02	0.00E+00
56	SUBTOTAL (use)	9.46E+06	-1.12E+05	1.49E+04	-3.35E+08	0.00E+00	-1.51E+06	1.16E+05
57	TOTAL	8.31E+09	4.61E+08	2.98E+06	3.76E+10	-2.22E+10	-1.51E+06	1.16E+05

Figure 24. Excerpt from CSV text file saved by pLCA tool showing inputs, building stock, and absolute changes in citywide impacts and site energy uses.

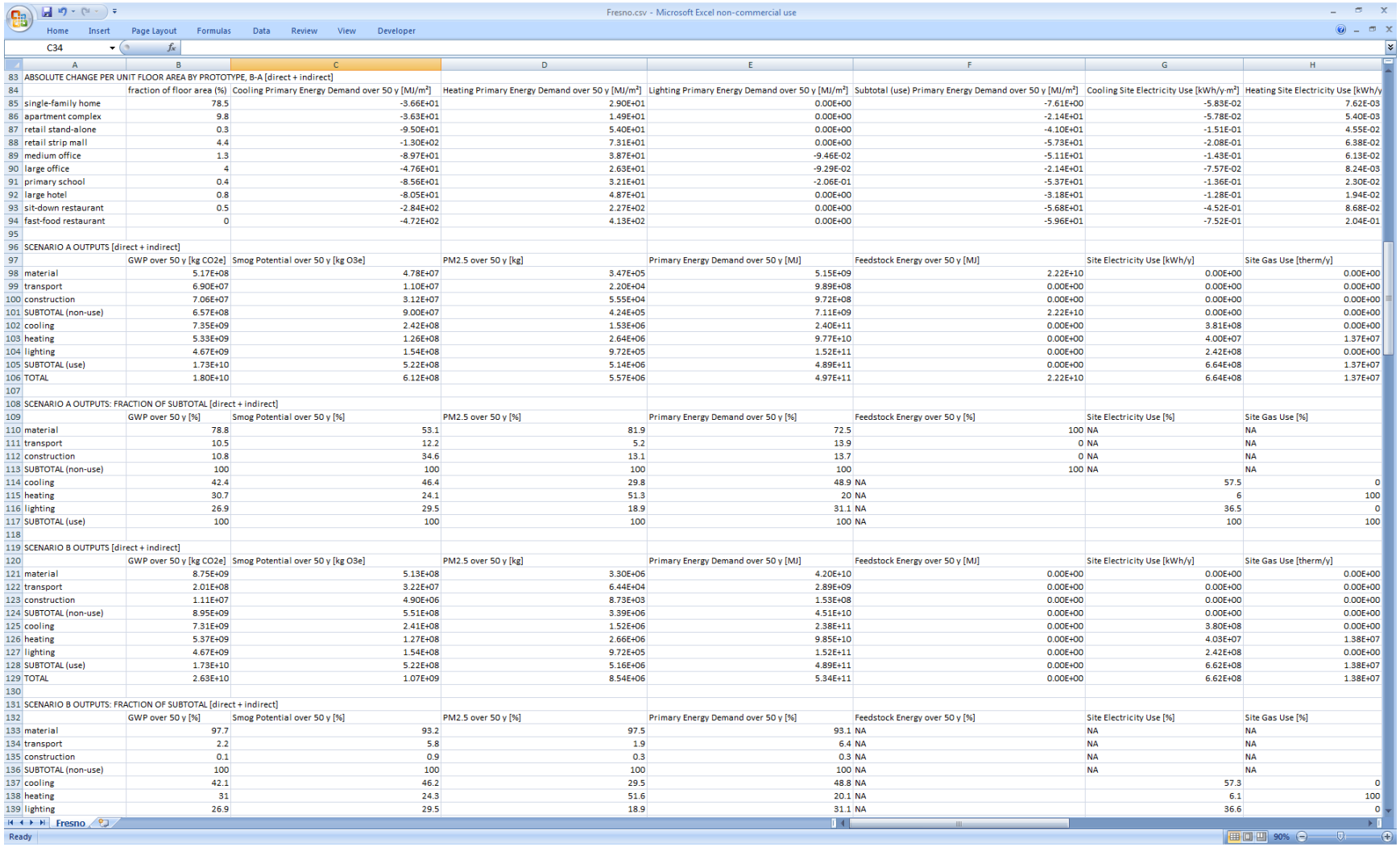

Fresno.csv - Microsoft Excel non-commercial use

Home Insert Page Layout Formulas Data Review View Developer

C34

	A	B	C	D	E	F	G	H
83	ABSOLUTE CHANGE PER UNIT FLOOR AREA BY PROTOTYPE, B-A [direct + indirect]							
84		fraction of floor area (%)	Cooling Primary Energy Demand over 50 y [MJ/m²]	Heating Primary Energy Demand over 50 y [MJ/m²]	Lighting Primary Energy Demand over 50 y [MJ/m²]	Subtotal (use) Primary Energy Demand over 50 y [MJ/m²]	Cooling Site Electricity Use [kWh/y·m²]	Heating Site Electricity Use [kWh/y
85	single-family home	78.5	-3.66E+01	2.90E+01	0.00E+00	-7.61E+00	-5.83E-02	7.62E-03
86	apartment complex	9.8	-3.63E+01	1.49E+01	0.00E+00	-2.14E+01	-5.78E-02	5.40E-03
87	retail stand-alone	0.3	-9.50E+01	5.40E+01	0.00E+00	-4.10E+01	-1.51E-01	4.55E-02
88	retail strip mall	4.4	-1.30E+02	7.31E+01	0.00E+00	-5.73E+01	-2.08E-01	6.38E-02
89	medium office	1.3	-8.97E+01	3.87E+01	-9.46E-02	-5.11E+01	-1.43E-01	6.13E-02
90	large office	4	-4.76E+01	2.63E+01	-9.29E-02	-2.14E+01	-7.57E-02	8.24E-03
91	primary school	0.4	-8.56E+01	3.21E+01	-2.06E-01	-5.37E+01	-1.36E-01	2.30E-02
92	large hotel	0.8	-8.05E+01	4.87E+01	0.00E+00	-3.18E+01	-1.28E-01	1.94E-02
93	sit-down restaurant	0.5	-2.84E+02	2.27E+02	0.00E+00	-5.68E+01	-4.52E-01	8.68E-02
94	fast-food restaurant	0	-4.72E+02	4.13E+02	0.00E+00	-5.96E+01	-7.52E-01	2.04E-01
95								
96	SCENARIO A OUTPUTS [direct + indirect]							
97		GWP over 50 y [kg CO2e]	Smog Potential over 50 y [kg O3e]	PM2.5 over 50 y [kg]	Primary Energy Demand over 50 y [MJ]	Feedstock Energy over 50 y [MJ]	Site Electricity Use [kWh/y]	Site Gas Use [therm/y]
98	material	5.17E+08	4.78E+07	3.47E+05	5.15E+09	2.22E+10	0.00E+00	0.00E+00
99	transport	6.90E+07	1.10E+07	2.20E+04	9.89E+08	0.00E+00	0.00E+00	0.00E+00
100	construction	7.06E+07	3.12E+07	5.55E+04	9.72E+08	0.00E+00	0.00E+00	0.00E+00
101	SUBTOTAL (non-use)	6.57E+08	9.00E+07	4.24E+05	7.11E+09	2.22E+10	0.00E+00	0.00E+00
102	cooling	7.35E+09	2.42E+08	1.53E+06	2.40E+11	0.00E+00	3.81E+08	0.00E+00
103	heating	5.33E+09	1.26E+08	2.64E+06	9.77E+10	0.00E+00	4.00E+07	1.37E+07
104	lighting	4.67E+09	1.54E+08	9.72E+05	1.52E+11	0.00E+00	2.42E+08	0.00E+00
105	SUBTOTAL (use)	1.73E+10	5.22E+08	5.14E+06	4.89E+11	0.00E+00	6.64E+08	1.37E+07
106	TOTAL	1.80E+10	6.12E+08	5.57E+06	4.97E+11	2.22E+10	6.64E+08	1.37E+07
107								
108	SCENARIO A OUTPUTS: FRACTION OF SUBTOTAL [direct + indirect]							
109		GWP over 50 y [%]	Smog Potential over 50 y [%]	PM2.5 over 50 y [%]	Primary Energy Demand over 50 y [%]	Feedstock Energy over 50 y [%]	Site Electricity Use [%]	Site Gas Use [%]
110	material	78.8	53.1	81.9	72.5	100	NA	NA
111	transport	10.5	12.2	5.2	13.9	0	NA	NA
112	construction	10.8	34.6	13.1	13.7	0	NA	NA
113	SUBTOTAL (non-use)	100	100	100	100	100	NA	NA
114	cooling	42.4	46.4	29.8	48.9	NA	57.5	0
115	heating	30.7	24.1	51.3	20	NA	6	100
116	lighting	26.9	29.5	18.9	31.1	NA	36.5	0
117	SUBTOTAL (use)	100	100	100	100	NA	100	100
118								
119	SCENARIO B OUTPUTS [direct + indirect]							
120		GWP over 50 y [kg CO2e]	Smog Potential over 50 y [kg O3e]	PM2.5 over 50 y [kg]	Primary Energy Demand over 50 y [MJ]	Feedstock Energy over 50 y [MJ]	Site Electricity Use [kWh/y]	Site Gas Use [therm/y]
121	material	8.75E+09	5.13E+08	3.30E+06	4.20E+10	0.00E+00	0.00E+00	0.00E+00
122	transport	2.01E+08	3.22E+07	6.44E+04	2.89E+09	0.00E+00	0.00E+00	0.00E+00
123	construction	1.11E+07	4.90E+06	8.73E+03	1.53E+08	0.00E+00	0.00E+00	0.00E+00
124	SUBTOTAL (non-use)	8.95E+09	5.51E+08	3.39E+06	4.51E+10	0.00E+00	0.00E+00	0.00E+00
125	cooling	7.31E+09	2.41E+08	1.52E+06	2.38E+11	0.00E+00	3.80E+08	0.00E+00
126	heating	5.37E+09	1.27E+08	2.66E+06	9.85E+10	0.00E+00	4.03E+07	1.38E+07
127	lighting	4.67E+09	1.54E+08	9.72E+05	1.52E+11	0.00E+00	2.42E+08	0.00E+00
128	SUBTOTAL (use)	1.73E+10	5.22E+08	5.16E+06	4.89E+11	0.00E+00	6.62E+08	1.38E+07
129	TOTAL	2.63E+10	1.07E+09	8.54E+06	5.34E+11	0.00E+00	6.62E+08	1.38E+07
130								
131	SCENARIO B OUTPUTS: FRACTION OF SUBTOTAL [direct + indirect]							
132		GWP over 50 y [%]	Smog Potential over 50 y [%]	PM2.5 over 50 y [%]	Primary Energy Demand over 50 y [%]	Feedstock Energy over 50 y [%]	Site Electricity Use [%]	Site Gas Use [%]
133	material	97.7	93.2	97.5	93.1	NA	NA	NA
134	transport	2.2	5.8	1.9	6.4	NA	NA	NA
135	construction	0.1	0.9	0.3	0.3	NA	NA	NA
136	SUBTOTAL (non-use)	100	100	100	100	NA	NA	NA
137	cooling	42.1	46.2	29.5	48.8	NA	57.3	0
138	heating	31	24.3	51.6	20.1	NA	6.1	100
139	lighting	26.9	29.5	18.9	31.1	NA	36.6	0

Fresno

Ready

90%

Figure 25. Excerpt from CSV text file saved by pLCA tool, showing absolute changes in impacts and site energy uses per unit floor area by building prototype, as well as outputs of Scenarios A and B.

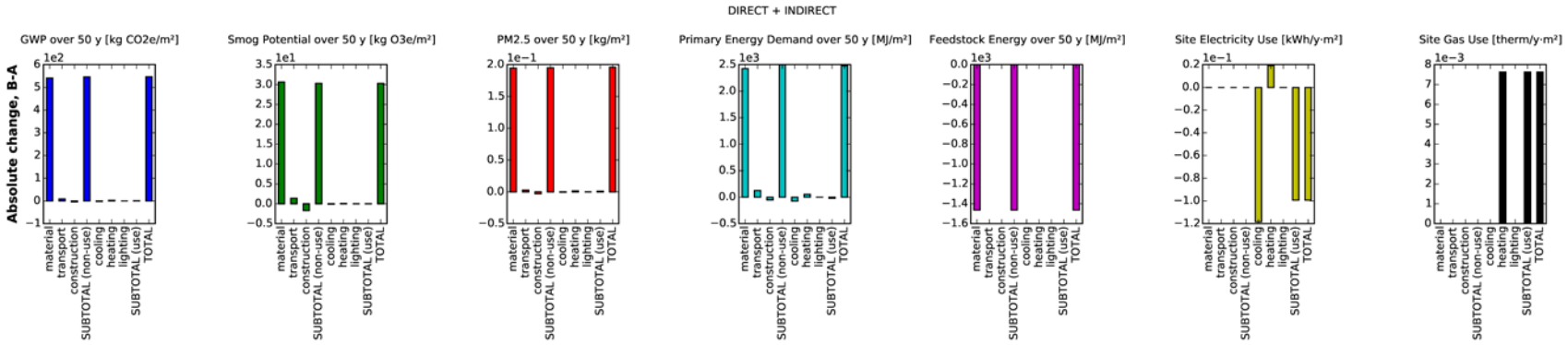

Figure 26. Subset of graphs saved by pLCA tool, showing absolute changes (direct + indirect) in citywide impacts and site energy uses.

2.8.5. Methodology

The tool rapidly evaluates its output by applying the operator's inputs to a series of a data sets pre-complied by the research team. This section describes the data sets and the algorithms used to generate the tool outputs.

Climate zone

The California building climate zone (BCZ) containing each city was found by combining a table of BCZ by ZIP code (CEC 2014) with a table of ZIP code by city (CAZIPCodes 2015) (Table 27).

Table 27. The building climate zones and air basins for the 31 CA cities included in the tool.

City	CA building climate zone	CA air basin*	CA air basin code*
San Jose	4	San Francisco Bay Area	SFB
Sunnyvale	4	San Francisco Bay Area	SFB
San Diego	7	NA	NA
Irvine	8	South Coast	SC
Garden Grove	8	South Coast	SC
Anaheim	8	South Coast	SC
Santa Ana	8	South Coast	SC
Los Angeles	8	South Coast	SC
Canoga Park	9	South Coast	SC
Reseda	9	South Coast	SC
Lake Balboa	9	South Coast	SC
Van Nuys	9	South Coast	SC
Valley Glen	9	South Coast	SC
Burbank	9	South Coast	SC
Glendale	9	South Coast	SC
Pasadena	9	South Coast	SC
East Pasadena	9	South Coast	SC
South Pasadena	9	South Coast	SC
Riverside	10	South Coast	SC
Ontario	10	South Coast	SC
Rancho Cucamonga	10	South Coast	SC
Fontana	10	South Coast	SC
Rialto	10	South Coast	SC
San Bernardino	10	South Coast	SC
Bloomington	10	South Coast	SC
Sacramento	12	Sacramento Valley	SAC
Bakersfield	13	San Joaquin Valley	SJV
Fresno	13	San Joaquin Valley	SJV

Lancaster	14	NA	NA
California City	14	NA	NA
Palm Springs	15	NA	NA

* NA is listed when a city was not contained within one of the four air basins studied. The tool does not report any ozone concentration changes for these cities.

Air basin

USC provided a table identifying the air basin containing each city (Table 27).

Land area and total area

The land area and total area (land + water) of each city were obtained from the 2010 U.S. Census (U.S. Census 2014b). City boundary shape files were also obtained from the 2010 U.S. Census (U.S. Census 2014a).

Pavement area

LBNL calculated the total pavement area (public + private) in each city as the product of city's total area; the city's impervious area fraction, computed with ESRI ArcMap 10.2 as the spatial mean value of the NLCD 2006 Percent Developed Imperviousness (2011 Edition) raster (USGS 2014) within the city's boundary; and the ratio of total pavement area to impervious area, set to 0.5 at the recommendation of USC.

The public pavement area in each city, where available, was taken from a survey conducted by UCPRC (Section 2.2).

Service-life materials and construction stage LCA metrics per unit area of surface treatment

Thinkstep Inc. and UCPRC computed the material, transport, construction, and end-of-life LCA metrics per lane-km of each surface treatment over its service life (Section 3.3). Assuming that each lane is 3.66 m (12 ft.) wide, each service-life LCA metric per lane-km is multiplied by 273.4 lane-km per km² to obtain LCA metric per km².

Other characteristics of surface treatments

UCPRC estimated for each surface treatment the range of typical albedo, range of typical service life, and, where applicable, default value and allowable range of thickness (Table 3).

Use-stage LCA metrics per unit of site energy consumed

UCPRC calculated LCA metrics for each unit of electrical site energy use and gas site energy consumed (Section 3.3).

Assessor's property type stock

LBNL computed the count and mean building floor area in each city of each property type included in records compiled from county assessors across California. The total building floor area (m^2) by property type in each city was then calculated as the product of its count and mean building floor area (Section 2.7). If in a given city no information about building floor area was available for a property type, statewide mean building floor area was for substituted city-mean floor area when calculating total building floor area for that combination of building type and city.

Prototype stock

LBNL mapped each assessor building type to one of 10 building prototypes simulated in this study, discarding several types not readily mapped to any prototype (Section 2.7.4). The total floor area of each prototype in each city was then calculated by summing the total floor areas of the assessor building types mapped to that prototype.

Sensitivity of air temperature change to pavement albedo change

Using long-term, statewide climate simulations to assess the variation of city-mean air temperature with city-mean pavement albedo, USC found a linear relationship between change in air temperature and change in pavement albedo, and calculated hourly coefficients (ratio of air temperature change to pavement albedo change) for each season in each of 31 cities. These coefficients were then adjusted to correct for assumptions that the climate model makes about urban canyon geometry (Section 0).

Sensitivity of ozone concentration change to air temperature change

USC characterized through a literature review the ozone concentration change per unit air temperature change in four major air basins in California (Section 2.5.4).

Variation of building energy use with pavement albedo

LBNL characterized through a suite of EnergyPlus simulations the variations with city-mean pavement albedo (affecting outside temperature) and local street albedo (affecting reflection of sunlight to building) of the cooling, heating, and lighting annual site energy uses of 10 prototype buildings in each of 10 cities. Each city- and prototype-specific energy use per unit floor area was expressed as a linear function of city-mean pavement albedo and local street albedo (Section 3.5.4).

Materials and construction stage LCA metrics (material, construction, transport)

The 50-year material, construction, or transport LCA metric of a surface treatment is calculated as the product of its service-life LCA metric per km^2; the ratio of the 50 y period to its operator-specified service life (y); the ratio of its operator-specified thickness (cm) to the default thickness (cm); and the pavement area modified (km^2). If the treatment has no default thickness, the ratio of operator-specified thickness to default thickness is set to unity.

City-mean pavement albedo

If fraction *f* of the city's total pavement area is modified, the city-mean pavement albedo will be

$$\rho_m = f \times \rho_1 + (1 - f) \times \rho_0, \quad (30)$$

where ρ_1 is the albedo of the upper surface treatment in the modified area, and ρ_0 is the pavement albedo in the unmodified area, assumed to be 0.10.

Annual site energy use

We assume that (a) the modified pavement is distributed evenly across the city, so that all buildings experience the same indirect effect from change in outdoor air temperature; and (b) the fraction of the building stock subject to the direct effects of pavement modification—i.e., the fraction that "sees" modified pavement—is equal to the fraction of total pavement area that is modified, *f*.

The annual site cooling, heating, or electrical energy uses of the city's building stock are then calculated as follows.

Let $e_{i,j}(\rho_m, \rho_r)$ [kWh/m²·y] and $g_{i,j}(\rho_m, \rho_r)$ [therm/m²·y] represent the city-specific annual electricity and gas site energy uses per unit floor area in building prototype *i* for function *j* (cooling, heating, or lighting), where ρ_r is the albedo of the local pavement (streets) seen by the building.

Let $\rho_{r,modified}$ represent the local pavement albedo for the fraction *f* of building stock that sees modified pavement, and $\rho_{r,unmodified}$ represent the local pavement albedo for the fraction (1 – *f*) of building stock that sees unmodified pavement.

- To assess only the direct effect, we set $\rho_m = \rho_0$, $\rho_{r,unmodified} = \rho_0$, and $\rho_{r,modified} = \rho_1$.
- To assess only the indirect effect, we set ρ_m according to Eq. (30), and set $\rho_{r,unmodified} = \rho_{r,modified} = \rho_0$.
- To assess both the direct and indirect effects, we set ρ_m according to Eq. (30), $\rho_{r,unmodified} = \rho_0$, and $\rho_{r,modified} = \rho_1$.

If A_i is the citywide total floor area of buildings mapped to prototype *i*, the citywide annual site electricity use [kWh/y] and gas use [therm/y] for function *j* will be

$$E_j = \sum_i A_i \times \left[f \times e_{i,j}\left(\rho_m, \rho_{r,modified}\right) + (1 - f) \times e_{i,j}\left(\rho_m, \rho_{r,unmodified}\right) \right] \quad (31)$$

and

$$G_j = \sum_i A_i \times \left[f \times g_{i,j}\left(\rho_m, \rho_{r,modified}\right) + (1 - f) \times g_{i,j}\left(\rho_m, \rho_{r,unmodified}\right) \right] \quad (32)$$

respectively.

Use-stage LCA metrics (cooling, heating, lighting)

Let m_e and m_g represent LCA metric per unit site electricity use and per unit site gas energy use, respectively. The 50 y LCII of the city's building stock for function *j* (cooling, heating, or lighting) is

$$M_i = 50 \times \left(m_e E_i + m_g G_i \right) \quad (33)$$

The factor of 50 converts annual site energy use to 50 y site energy use.

Seasonal hourly air temperature changes

The seasonal (winter, spring, summer, fall) hourly air temperature changes between pavement scenarios is calculated by multiplying the change in city-mean pavement albedo by the city-specific sensitivity of air temperature change to pavement albedo change.

Ozone concentration change

The ozone concentration change between pavement scenarios is calculated by multiplying the change in outdoor air temperature at 14:00 LST in summer by the air-basin specific sensitivity of ozone concentration change to air temperature change. If the city selected by the tool user was not contained within one of the four air basins studied, the tool does not report change in ozone concentration.

2.9. Quality control and quality assurance

2.9.1. Project Advisory Team

At the onset of the project, we formed a nine-member Project Advisory Team with expertise in pavements, LCA, climate modeling, building and pavement interactions, and local government (Table 28). The team met twice a year to provide guidance and feedback on the project's methodology and the decision tool. This valuable feedback served as an external check on the project's progress and helped us connect with new resources. For example, advisor Tom Van Dam directed us to find new cement concrete pavement projects for the pavement albedo measurements and helped us develop pavement mx designs.

Table 28. The nine Project Advisory Team members included experts in pavements, LCA, climate modeling, building and pavement interactions, and local government.

Name	Organization	Knowledge/expertise
Donna Chralowicz	City of San Diego	Local government policies, sustainability
Yvonne Hunter	Institute for Local Government	Local government policies
Jan Kleissl	University of California, San Diego	Building/pavement interactions
Ash Lashgari	California Air Resources Board	Air quality, cool roofs, and cool pavements
Matt Machado	Stanislaus County	Local government administration, pavements
Eric Masanet	Northwestern University	LCA
Haider Taha	Altostratus, Inc.	Modeling the effect of cool surfaces (e.g., roof, pavements) on urban climate and air quality
Craig Tranby	Los Angeles Department of Water & Power	Utility programs, cool roofs, local government
Tom Van Dam	NCE	Pavements, cool pavements

2.9.2. Local government pavement management practice

Information regarding local government pavement management practice was collected directly by phone interviews with local government pavement management experts in each of the local government organizations shown in this report. The pavement areas and lane-miles of pavement were cross-checked against values published on the same cities websites, where available.

2.9.3. Life-cycle inventories for pavement materials and building energy sources

The life-cycle inventory data was collected using commercially available and other sources following procedures and in some cases, use of previously developed data published in Wang et al. (2012). The inventories for asphalt pavement have been compared with inventories developed in France (after adjusting for local practices and other factors) by Harvey et al. (2014). The results and approaches have been presented at the Transportation Research Board Annual Meeting in 2015 and to the asphalt and concrete paving industries. The results were critically reviewed by Dr. Santero of thinkstep Inc. as part of his sub-contract to the UCPRC for this project. The life-cycle inventories were evaluated through a formal critical review process following ISO 14040 standards by a committee consisting of Robert Karlsson (chair), Swedish National Road and Transport Research Institute, Jeremy Gregory, Massachusetts Institute of Technology, and Amlan Mukherjee, Michigan Technical University. However, this report and the pLCA tool were not part of the critical review.

Pavement albedo data were collected from the sources cited. They were reviewed with industry and a separate study was funded by the concrete industry to cross-check the albedo ranges in the report with field measurements.

2.9.4. Local urban climate and air quality modeling

We implemented the following measures to help ensure high quality modeling results.

- **Comparison to weather observations.** Our control simulations were evaluated thoroughly by comparing model predictions to weather observations for the same period.
- **Reduction of impact of model noise.** Each of the three scenarios (CTRL, COOL_LOW, COOL_HIGH) is simulated in sets of three ensemble members (three separate simulations) to reduce the impact of model variability on our final results. Further, these ensemble members were used to compute statistics to test whether the temperature changes from albedo modification were statistically significant.
- **Reduction of initial condition dependency.** Each ensemble member has a different start date (within 2 to 3 months of each other) to decrease the dependency of the results on model initial conditions. The output of these ensemble members are then averaged, and variability among ensemble members is used to assess statistical significance.

2.9.5. Building energy simulation

Manual inspection of prototype definitions

We thoroughly inspected the construction properties of all prototypes.

Comparison of modeled and actual building energy use

The EnergyPlus outputs included results for annual cooling and heating energy uses. To test the validity of the model outputs, we compared the annual conditioning energy uses of commercial buildings with those reported in the 2012 Commercial Building Energy Consumption Survey [CBECS] (EIA 2012) and 2006 California Commercial End-Use Survey [CEUS] (CEC 2006), and residential buildings with those reported in the 2009 Residential Energy Consumption Survey [RECS] (EIA 2009). These three surveys (CBECS, RECS, and CEUS) estimate the historical and future energy uses through building energy simulations. Their building energy simulations are calibrated using a small sample of the current building stock. These samples attempt to capture various types of actual buildings and different climate regions. Therefore, energy uses of actual buildings may differ from those reported in these surveys. We use the energy uses from the surveys to verify that our simulation outputs are comparable to the surveys, not to calibrate our simulations.

CBECS is a national sample survey on the stock of US commercial buildings, including their energy-related building characteristics and end-use energy consumption. CBECS uses an engineering model to estimate the amount of electricity, natural gas, and other fuels used for several end-uses, including space heating, cooling, ventilation, lighting, and others. CBECS also includes buildings that may traditionally not be considered commercial, such as schools. The latest full version currently available is CBECS 2012 and was released on August 2016. The finest level of geographic detail available in CBECS is the U.S. Census division. Thus we represent California with the Pacific division, which includes California (75% of the Pacific division population), Alaska (1.4%), Oregon (7.7%), Washington (14%), and Hawaii (2.7%). Note that values do not sum to 100% because of rounding. The population was obtained from the 2010 U.S. Census.

RECS is the residential analog of CBECS. The latest available version is RECS 2009. We utilized these two sources to extract the historical end-use consumption and building age of different building types. RECS data can be segregated by US state, which facilitated access to their California data.

We disaggregated the CBECS and RECS public use microdata by building type, then extracted the results for only the building types that best matched our 10 building prototypes.
Table 29 shows the mapping of CBECS and RECS building stock to the modeled prototypes.

The 2006 California Commercial End-Use Survey (CEUS) is a study of California's commercial sector energy use. The survey captures detailed electricity and gas energy use by building type. This study was generated using a random sample of 2,800 commercial facilities from the service areas of four major California utility companies. This sample represent facilities from different utility service area, building type, and climate regions. The CEUS study then used the details from the survey to calibrate their building energy simulations. They used these building energy simulations to estimate the energy use of 12 different commercial building types in different California climate regions. We used CEUS as a second source to validate the modeled energy uses of our commercial prototypes.
Table 29 shows the mapping of CEUS building stock to the modeled prototypes.

The cooling and heating energy intensities (annual site energy use per unit floor area, in kWh/m^2) reported by CBECS, RECS, and CEUS were compared to the intensities calculated from the building energy modeling. Since the Pacific division includes three states that experience colder climates than California throughout the year (Alaska, Washington, and Oregon), the Pacific conditioning energy use reported by CBECS may underestimate California's cooling load and overestimate its heating load.

Base energy use versus degree-days

We tested the HVAC system response of each building energy prototype to climate by comparing their annual cooling and heating energy uses to annual cooling and heating degree-days. We expect cooling energy use to increase with cooling degree days, and heating energy use to increase with heating degree days.. We selected 18 °C as the reference temperature for calculating cooling degree-days (CDD18C) and heating degree-days (HDD18C) as it is a common reference temperature for calculations of degree-days.

Table 29. Mapping of modeled prototypes to CBECS, RECS, and CEUS building stock (NA = not applicable).

Prototypes	CBECS	RECS	CEUS
Retail strip mall	Strip shopping	NA	Retail
Primary school	Elementary school	NA	School
Large hotel	Hotel	NA	Lodging
Large office	Professional or government office of similar floor area	NA	Large office
Medium office	Professional or government office of similar floor area	NA	Mean of small and large office
Sit-down restaurant	Restaurant	NA	Restaurant
Fast-food restaurant	Fast food	NA	Restaurant
Retail stand-alone	Retail store	NA	Retail
Apartment building	NA	Apartment in Building with 2 - 4 Units; Apartment in building with 5+ units	NA
Single-family home	NA	Single-family detached	NA

Pavement life-cycle assessment decision tool

Over the course of this project, there were 10 versions of the tool released for internal and external review. We completed this alpha testing to review the results, ensure that the various datasets and algorithms were producing results as expected, and check the tool's usability and presentation of results. We completed several internal research team reviews, an internal review with the project sponsors (CA Air Resources Board and CA Department of Transportation), and an external review with the Project Advisory Team. During the review process, several issues were identified internally or brought to the attention of the research team, then fixed. Feature requests not critical to the basic operation of the tool were scheduled for the second phase of the project.

3. Results

3.1. Local government pavement management practice

The results from the pavement management survey with local governments in California are summarized in Table 30. We have three main findings:

- Most local governments treat a small portion of the public street pavement network every year. The eight local governments responding to our survey treat 1.3% to 20% of the network each year (average 6.8%). Note that the respondents were cities, rather than counties.
- The primary pavement treatments used by these local governments include slurry seal, chip seal, cape seal (chip seal followed by micro-surfacing or slurry seal), thin asphalt concrete (AC) or rubberized hot mix asphalt concrete (RHMA) overlay, sand seal, and reconstruction. The latter includes thick asphalt concrete overlay, thick rubberized asphalt concrete overlay, full depth reclamation (FDR), and cold in-place recycling (CIR).
- Slurry seal is the most commonly used treatment. Respondents reported that they use slurry seal for 28% to 82% of their treated pavement area (average 41%) annually. Asphalt overlay is another major treatment used by most local governments, ranging from 13% to 100% of the pavement area treated (average 37%). Chip seal makes up 0.7% to 46% of the pavement area treated (average 5.9%), while cape seal averages less than 1%. Sand seal was used by only one city, which applied it to about 15% of their network each year and used other treatments for the remaining 5% treated each year. The same city also treated a greater percentage of their network each year than any other city surveyed. Reconstruction is used for 3% to 28% of total (average 6.6%). Use of reconstruction as a treatment indicates that pavements have deteriorated to a point at which preservation and maintenance treatments such as slurry seals, chip seals and thin overlays are no longer appropriate.

Table 30. Summary of pavement treatment practice currently used by local governments in California.

City	Public pavement network lane miles (centerline miles) [b]	Portion of network treated every year	Portion of each treatment used in total network treated					
			A. Slurry seal	B. Sand seal	C. Chip seal	D. Cape seal	E. Asphalt overlay	F. Reconstruction (AC, RHMA, FDR, CIR)[c]
Bakersfield	(1,264)	20%	-	75%	-	-	13%	12%
Berkeley	453 (216)	7.4%	31%	-	-	-	41%	28%
Chula Vista	(461)	3.9%	28.3%	-	46.4%	0.5%	21.8%	3%
Fresno [a]	(1,548)	1.3%	-	-	-	-	100%	-
City of Los Angeles	28,000	7.4%	60.7%	-	-		35.4%	3.9%
Richmond	576	5.2%	47.1%	-	0.7%	0.5%	45.9%	5.9%
City of Sacramento	3,065	4.3%	82.4%	-	-	-	17.6%	-
San Jose	4,264	5%	80%	-	-	-	20%	-
Average	-	6.8%	41.2%	9.4%	5.9%	0.1%	36.8%	6.6%

[a] 40 centerline miles of asphalt overlay up to 2009, then 20 centerline miles of asphalt overlay since 2009.
[b] Use multiplier 2.2 to convert centerline miles to lane miles. The lane width is assumed to be 3.7 m (12 ft.).
[c] AC = asphalt concrete, RHMA = rubberized hot mix asphalt concrete, FDR = full-depth reclamation, CIR = partial-depth cold in-place recycling.

3.1.1. Pavement treatment performance life for local streets

Table 3 summarizes the pavement treatment surface materials, the recommendation for their thickness or whether the user should be able to define the thickness, and approximate ranges of expected time between replacement (service life). The ranges of service lives for the typical pavement treatments were generated from the local government survey and UCPRC experience. The service lives for the alternative treatments comes from UCPRC's best judgment.

FDR and CIR are not shown in the table because each has an asphalt or rubberized asphalt surface which defines its albedo.

3.2. Albedo of different pavement materials with data from different sources

3.2.1. Albedo of asphalt concrete overlay (LBNL)

Albedos of asphalt concrete overlays at different ages reported by LBNL are presented in Figure 27. Albedo increases with time to about 0.12 from about 0.04. Albedo changes mostly in the first four years and then tends to stabilize at approximately 0.12.

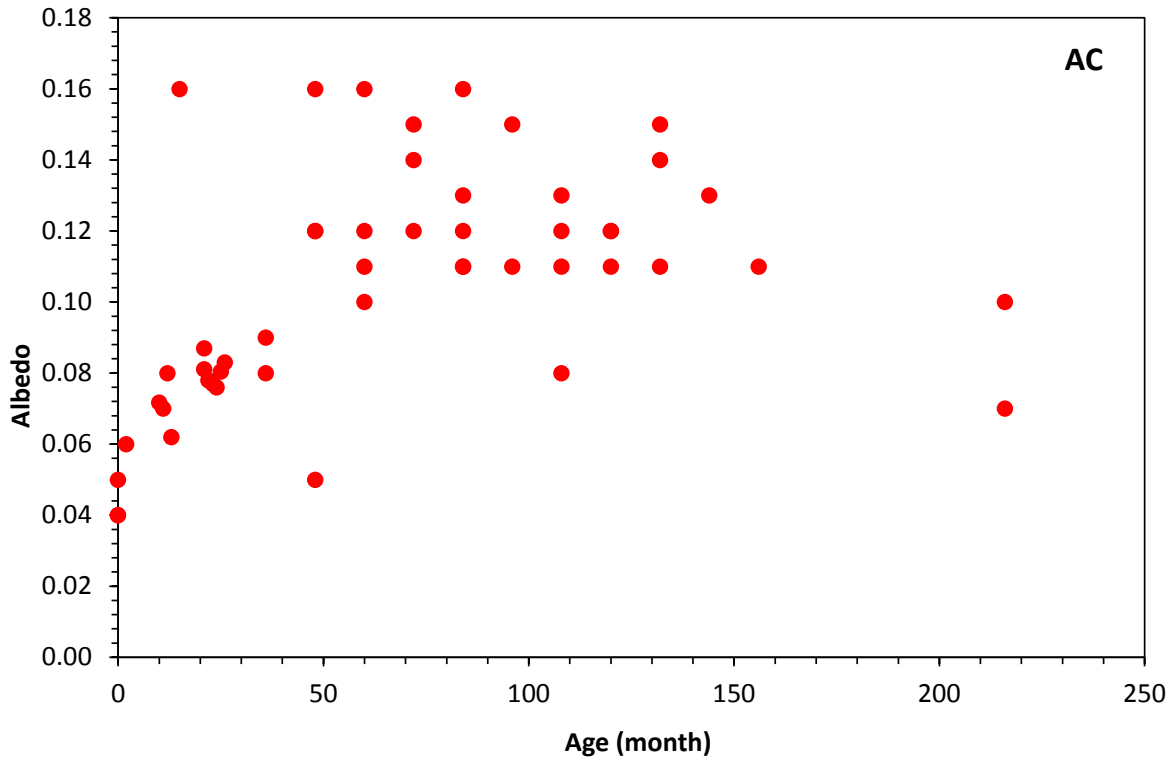

Figure 27. Albedo of asphalt concrete or asphalt overlay from LBNL (Pomerantz et al. 2000).

3.2.2. Albedo of asphalt concrete overlay with reflective coating (LBNL)

The albedos of asphalt concrete overlays with reflective coating from LBNL data are presented in Figure 28. Albedo decreases with time down to 0.20 from 0.46. Albedo change of asphalt concrete with reflective coating happens mostly in the first month and then tends to remain stable at approximately 0.20.

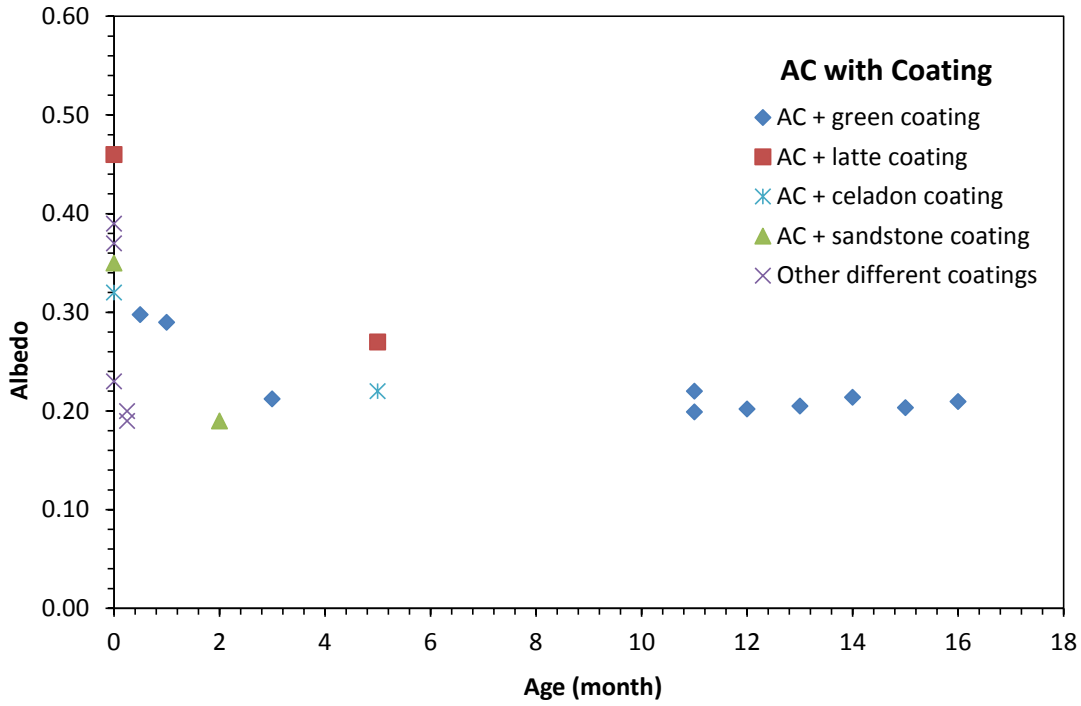

Figure 28. Albedo of asphalt concrete or overlay with reflective coating from LBNL (Gilbert et al. 2014).

3.2.3. Albedo of chip seal (LBNL)

The albedos of chip seals from the LBNL data are presented in Figure 29. The albedos of chip seals decrease with time down to about 0.12 from about 0.20. The albedo change of chip seals happens mostly in the first 10 months and then tends to remain stable at approximately 0.12.

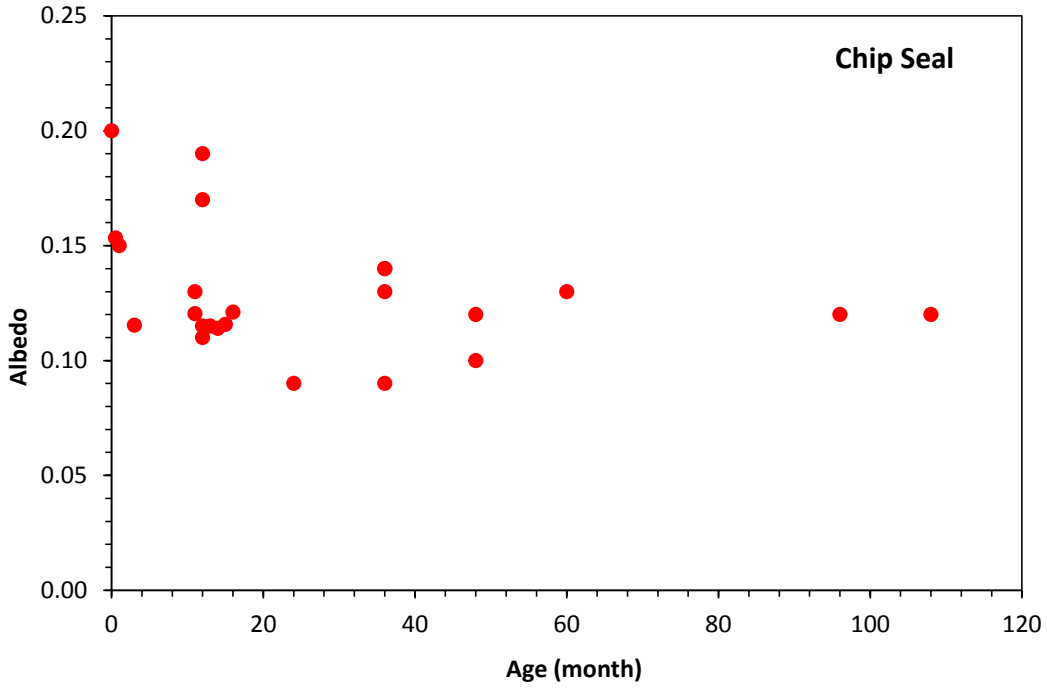

Figure 29. Albedo of chip seal from LBNL (Pomerantz et al. 2003).

3.2.4. Albedos of different types of portland cement concrete (LBNL)

The albedos of various types of portland cement concrete from the LBNL data are presented in Figure 30. The albedos decrease with time down to 0.18 from 0.68. The albedo change happens mostly in the first month and then tends to remain stable at approximately 0.18 on the trafficked street section.

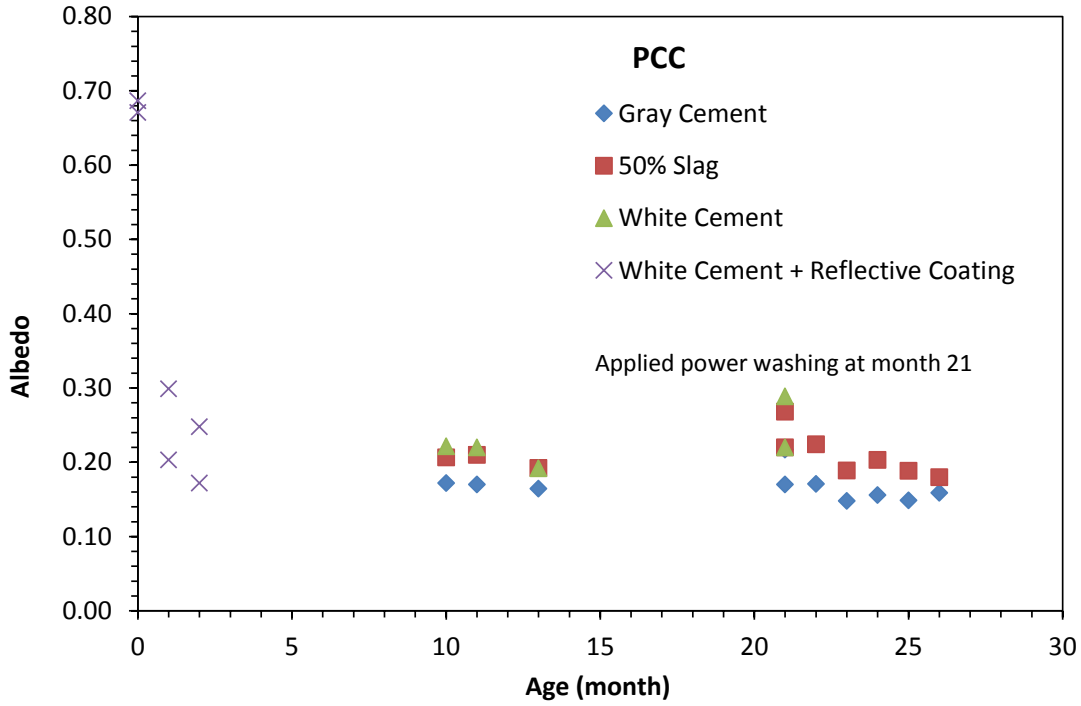

Figure 30. Albedo of portland cement concrete (PCC) from LBNL (Gilbert et al. 2014).

3.2.5. Albedos of asphalt and portland cement concrete (FHWA)

The albedos of asphalt and portland cement concrete from the FHWA project data are presented in Figure 31. These data are from a number of pavement sections around country. As opposed to the time histories measured by LBNL, these are single measurements of a number of surfaces with different ages and in different locations across the U.S. The albedo of asphalt concrete increases with time up to 0.15 from 0.05. The albedo of portland cement concrete decreases with time down to 0.20 from 0.30.

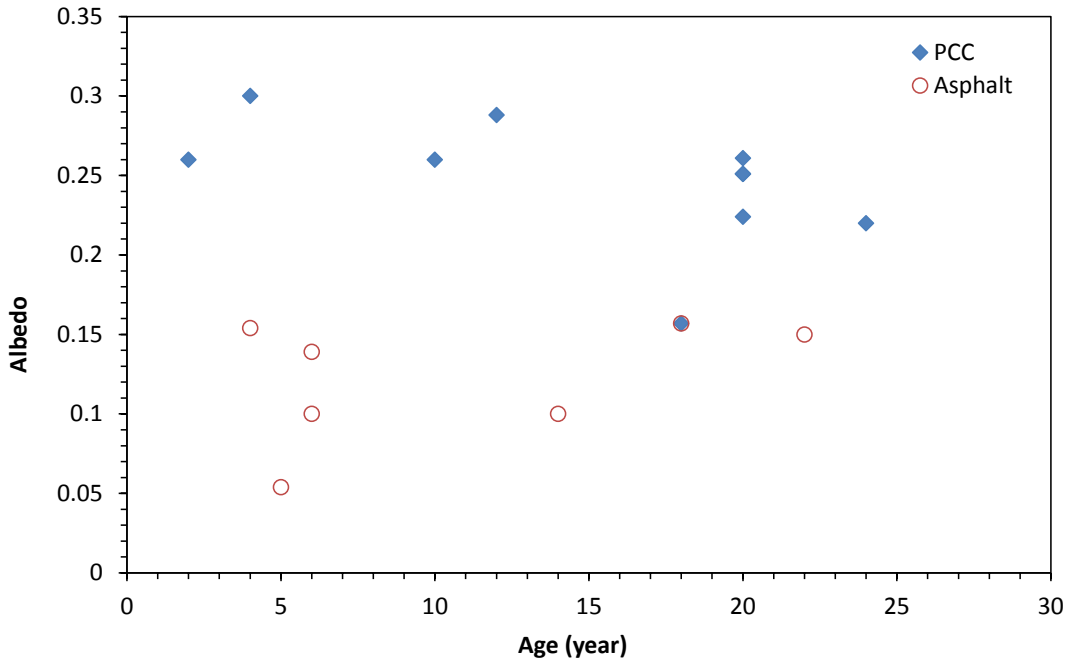

Figure 31. Albedo of asphalt and portland cement concrete from as yet unpublished data from ongoing FHWA project "Quantifying Pavement Albedo".

3.2.6. Albedos of block paver, asphalt and portland cement concrete (UCPRC)

The initial albedo of each of the nine UCPRC test sections (A1-A3, B1-B3 and C1-C3) were measured at 13:00 LST on 19 Sep 2011.

As expected, the asphalt sections have lower albedos (0.09 for B1 and 0.08 for B2 and B3) than the concrete and interlocking concrete pavement (paver) sections. As mentioned previously, sections B2 and B3 have the same open-graded surface material and only their thicknesses are different, and have the same albedo (0.08) as expected. The three concrete sections (C1-C3) have a range of mean albedo of 0.18 to 0.29. The darker open-graded concrete section C2 has a lower albedo of 0.18 compared to the other two concrete sections (0.26 for open-graded C3 and 0.29 for dense-graded C1). The paver sections (A1-A3) have albedos close to those of the more reflective concrete sections (C1 and C3), which are in the range of 0.25 to 0.28. The relatively low albedo of asphalt pavements will result in more absorption of incident solar radiation, and produce a high temperature. In contrast, the concrete and paver pavements generally have a higher albedo.

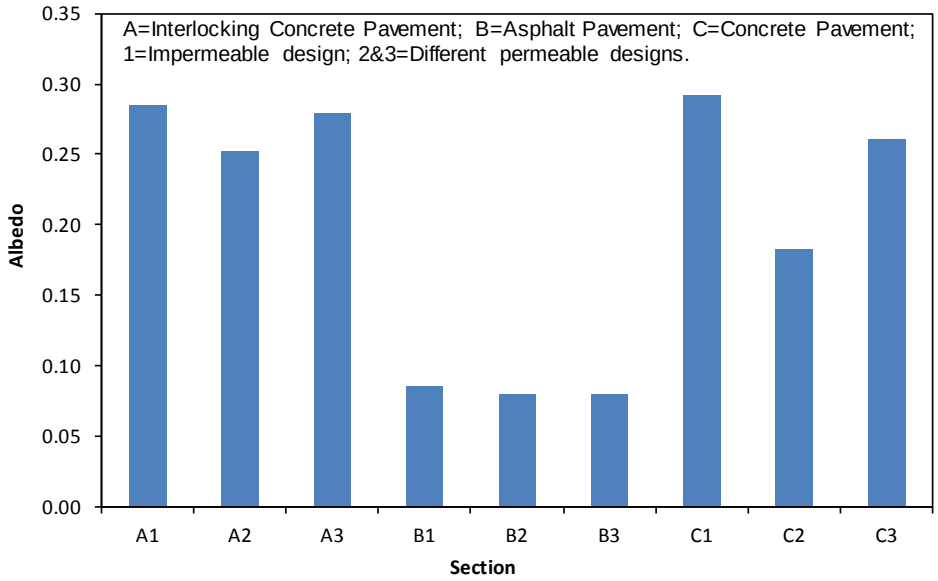

Figure 32. Initial albedo of interlocking concrete pavement (pavers), asphalt concrete, and portland cement concrete from UCPRC data (Li et al. 2013).

Change of albedo over time (UCPRC)

The albedo of pavement surfaces tends to change over time. Figure 33 shows the albedos of the nine test sections measured at 2-month intervals for eight months. These nine test sections were constructed for albedo and temperature testing only and were not open to any type of traffic. As noted, the albedos of concrete pavements (C1-C3, although albedos of C1 and C3 increase slightly in the first month) and interlocking concrete pavers (A1-A3) generally tend to decrease over time; in contrast, the albedos of asphalt pavements (B1-B3) increase slightly over time. The changes in albedo mostly happened in the first month just after the construction.

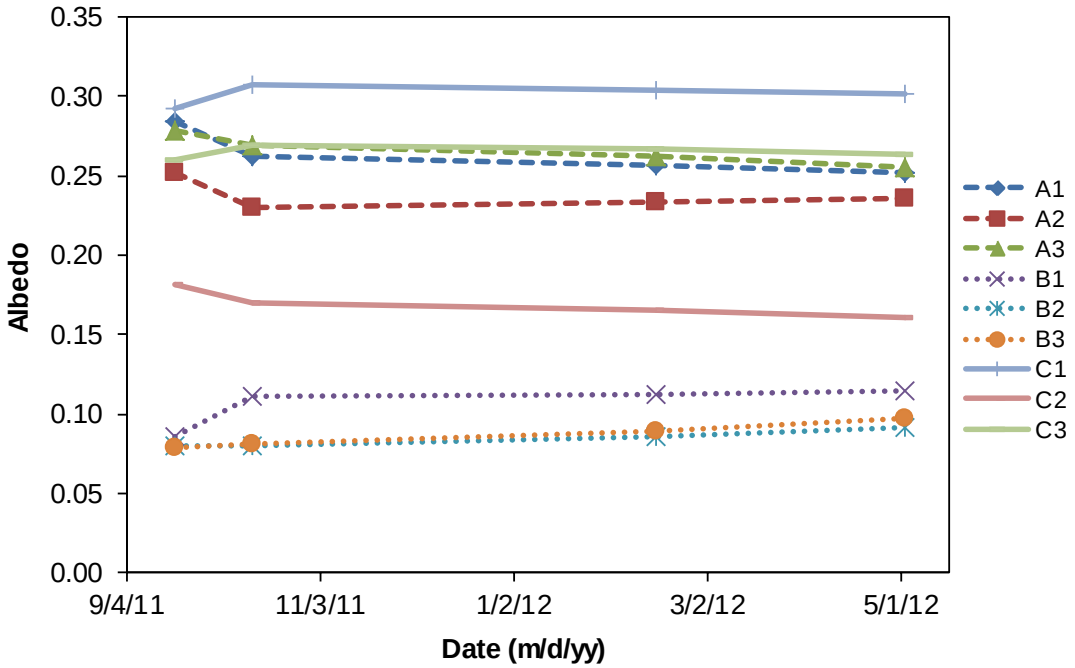

Figure 33. Change of albedo over time with no traffic for the nine experimental test sections of portland cement concrete pavers (A1-A3), asphalt pavements (B1-B3) and cement concrete pavements (C1-C3) (Li et al. 2013).

Albedos of additional pavement sections and materials (UCPRC)

To include additional pavement surface materials for comparison, albedo measurements were performed on asphalt and concrete surfacing materials other than the nine experimental sections (A1-A3, B1-B3 and C1-C3) mentioned previously. These pavements which were city streets and parking lots featured different mix designs from those used in the nine test sections. Moreover, these pavements were between 1 and 5 years old, while the nine experimental test sections were less than 8 months old. Despite their older age, the additional pavement surfaces had not been subjected to much traffic, therefore aging processes related to traffic were not visible. For example, the asphalt covering the aggregate on the pavement surface had not been worn off. Albedos measured on gravel, bare soil and grass are also included for comparison. The results are shown in Figure 34.

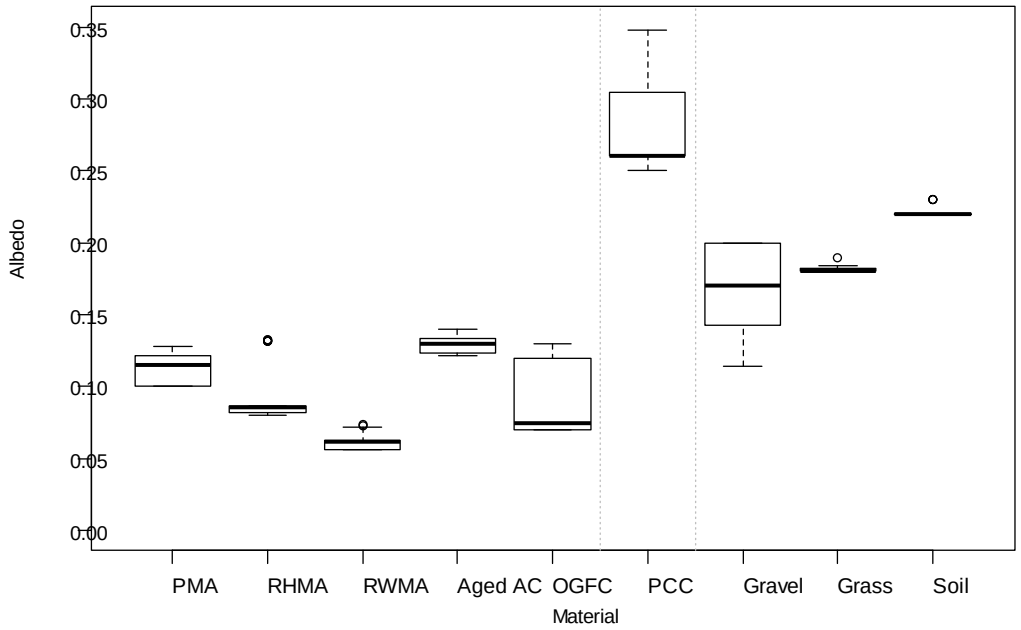

Figure 34. Albedos of additional asphalt and portland cement concrete from UCPRC data with no traffic (Li et al. 2013). PMA = Polymer Modified Asphalt; RHMA = Rubberized Hot Mixed Asphalt; RWMA = Rubberized Warm Mixed Asphalt; Aged AC = Aged Asphalt Concrete; OGFC = Open Graded Friction Course; PCC = Portland Cement Concrete; Gravel = Basalt; Grass = Yellow Lawn; and Soil = Yellow Clay.

The additional types of asphalt pavement materials tested include a polymer modified asphalt (PMA, should not affect the albedo); gap-graded rubberized hot mix asphalt (RHMA, which contains a higher asphalt binder content and recycled tire rubber which is expected to affect the albedo); rubberized warm mix asphalt (RWMA, a different RHMA mix with a "warm mix" additive that should not affect the albedo); an open-graded asphalt friction course (OGFC); and an aged asphalt concrete. The PMA section showed a slightly higher mean albedo of 0.12 compared to 0.08 for the RHMA, and 0.06 for the RWMA. The aged asphalt pavement which was 4 years old had an albedo of 0.14. The newly paved OGFC layer had a lower albedo of 0.07. The lower albedos of the RHMA, RWMA and OGFC compared to the conventional HMA were expected because of their higher asphalt contents, and inclusion of tire rubber in the binder of the RHMA and RWMA. The higher albedo of the aged AC was also expected because of the oxidation of the asphalt.

The extra concrete pavements (PCC) had albedos in the range of 0.25 to 0.35 with an average of 0.26. This is close to the mean albedos of the three concrete pavements in the nine test sections which ranged between 0.18 and 0.29.

The gravel measured in this study is crushed open-graded basalt installed in the yard of the UCPRC facility. It has a maximum aggregate size of 19 mm and is blue/gray in color. This gravel had albedos in the range of 0.12 to 0.22 with an average of 0.18. The bare soil (native yellow clay between the nine test sections) had an albedo of 0.22. The grass (yellow lawn) had an albedo of 0.19.

Albedos of slurry seal, cape seal, fog seal and chip seal and additional PCC and AC sections measured in Davis, California (UCPRC)

Additional field albedo measurements were performed on pavement treatments and some additional PCC and AC sections around Davis, California in May 2014. We targeted sections on city streets. The additional pavement treatments included slurry seal, fog seal, cape seal, and chip seal. The results are

shown in Figure 35. The 5-year-old PCC has an average albedo of 0.26, ranging from 0.23 to 0.27. The 5-year-old AC has an average albedo of 0.12, ranging from 0.09 to 0.13. The 5-year-old slurry seal has an average albedo of 0.08, ranging from 0.07 to 0.10. The 5-year-old chip seal had an average albedo of 0.15, ranging from 0.14 to 0.16. The cape seal (chip seal with micro-surfacing on top) with more than three years of age had an average albedo of 0.06, ranging from 0.05 to 0.15. The fog seal, determined to be between one month to three years old, had an average albedo of 0.06, ranging from 0.04 to 0.07. Referencing all of the albedo measurements from the various sources, we calculated steady-state albedos for the different pavement materials. These values are shown in Table 33.

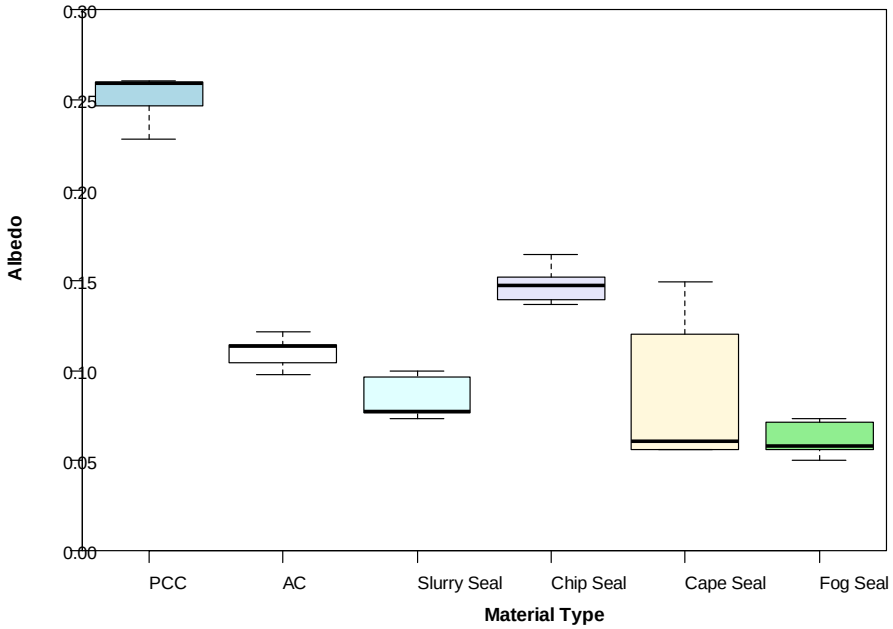

Figure 35. Albedos of slurry seal, cape seal, fog seal, and chip seal and asphalt and portland cement concrete from UCPRC data with traffic. (Note: The PCC was 5 years old; the AC section was 3 to 5 years old; the slurry seal was 5 years old; the chip seal was 5 years or older; the cape seal was 3 years or older; and the fog seal ranged in age from 1 month to 3 years old.)

3.2.7. Pavement albedo simulations

Example dynamic albedo simulation

We performed an example dynamic albedo simulation of pavement management practices for public pavements in a typical California city to demonstrate the equations and process. We made the following assumptions:

- The initial albedo of the public pavement is 0.10.
- Four treatment types are used, named A (e.g., slurry seal), B (e.g., chip seal), C (e.g., asphalt overlay with reflective coating), and D (e.g., reconstruction with concrete), with constant steady-state albedos of 0.10, 0.15, 0.20, and 0.30, respectively.
- The total yearly portion of public pavement network treated is set as a constant of 8% in the analysis term of 50 years.

- The portions of treatments A, B, C and D used for total public pavement network treated are set as constants of 60%, 15%, 15%, and 10%, respectively.

These scenario assumptions are illustrated in Figure 36.

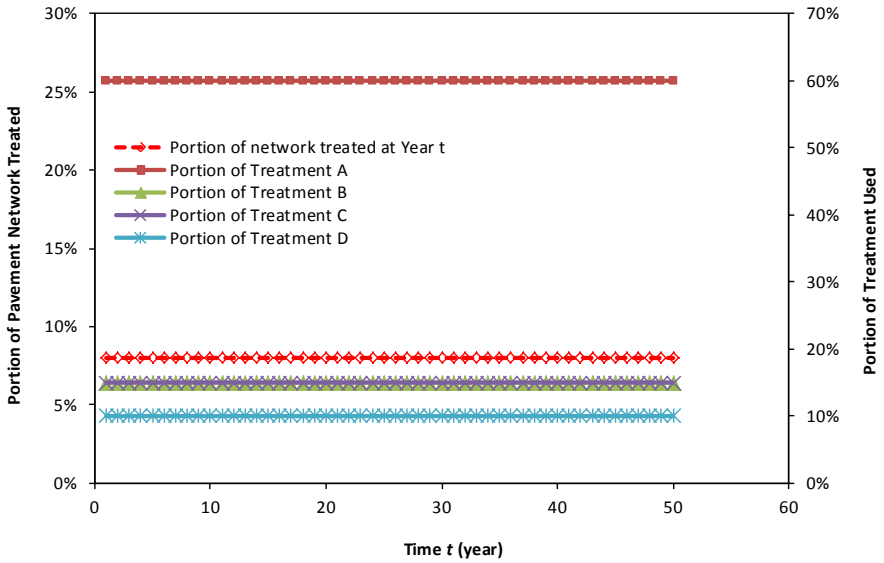

Figure 36. Example of one of the inputs for the dynamic albedo of modeling of citywide pavement albedo. This plot shows the ratio of pavement treatments applied across the public pavement with treatment scenario network for the 50-year analysis period.

The dynamic albedo of public pavement over the 50 years is presented in Figure 37. Since eight percent of the public pavement network undergoes pavement maintenance/preservation with different albedos every year, the average albedo of the entire public pavement network changes over time, as shown in Figure 37. The average albedo increases gradually to 0.14 from 0.10 over the 50 years. It takes approximately 30 years to reach a steady state albedo of 0.14.

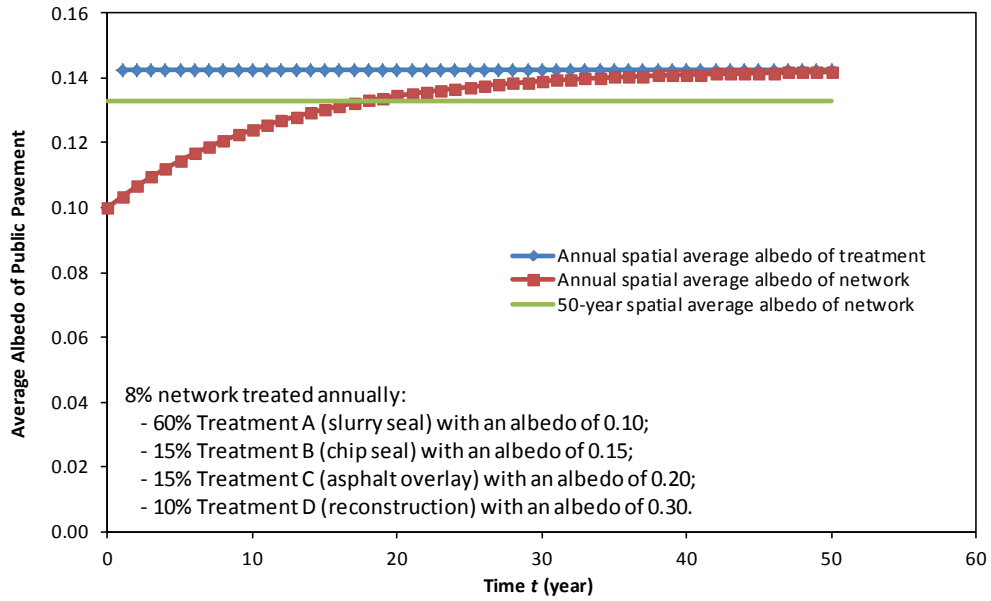

Figure 37. Dynamic albedo of public pavement with treatments for the 50-year analysis period.

Dynamic albedo of public pavement networks with current treatment practices and technologies

The pavement treatment practices, with corresponding albedo, currently used by local governments in California is summarized in Table 32. We performed the dynamic albedo modeling for Bakersfield, Berkeley, Chula Vista, Fresno, Los Angeles, Richmond, Sacramento, and San Jose. We made the following assumptions:

- The initial albedo of the public pavement is 0.10.
- Six main treatment types are used, namely slurry seal (A), sand seal (B), chip seal (C), cape seal (D), asphalt overlay (E), and reconstruction with asphalt (F), with constant steady-state albedos of 0.08, 0.10, 0.15, 0.06, 0.10 and 0.10, respectively.
- The total yearly portion of public pavement network treated is set as constant values from Table 32 for each city in the analysis term of 50 years.

The dynamic albedo modeled results for the City of Chula Vista are presented in Figure 38 as an example. Most of the current pavement materials are asphalt concrete (including asphalt overlay) with an albedo of 0.10, which is the initial value of current pavement network albedo. The current treatment practices used by most local governments are dominated by slurry seals, which have a lower albedo of 0.08. With the current treatment practice and technologies, the average albedos of the public pavement network for most local governments remains constant or decreases slightly over the 50 years. Only the cities that are using a larger portion of chip seal with a higher albedo of 0.15, such as Chula Vista, present a slightly increasing albedo over the 50 years. As summarized in Table 32, the steady-state albedo change of typical pavement networks in the 50 years is relatively low, ranging from -0.01 to 0.02. Across all cities, the 50-year average steady-state albedo for the pavement network remains close to the initial value of the current pavement network albedo, which is 0.1.

Table 31. Summary of steady-state albedo of different pavement treatment materials from different data sources.

Material Type	Albedo (LBNL)		Albedo (FHWA)		Albedo (UCPRC)		Albedo (summarized from data sources shown and considered "typical")	
	Range	Avg.	Range	Avg.	Range	Avg.	Range	Avg.
Asphalt concrete or overlay	0.10-0.15	0.12	0.05-0.15	0.10	0.06-0.15	0.10	0.05-0.15	0.10
Asphalt concrete or overlay with reflective coating	0.20-0.30	0.25	-	-	-	-	0.20-0.30	0.20
Chip seal	0.10-0.2	0.15	-	-	0.14-0.24	0.18	0.10-0.24	0.15
Slurry seal	-	-	-	-	0.07-0.10	0.08	0.07-0.10	0.08
Cape seal	-	-	-	-	0.05-0.15	0.06	0.05-0.15	0.06
Fog seal	-	-	-	-	0.04-0.07	0.06	0.04-0.07	0.06
Sand seal	-	-	-	-	-	-	0.07-0.10	0.08
Portland cement concrete	0.15-0.25	0.20	0.20-0.30	0.25	0.18-0.38	0.25	0.15-0.35	0.25
Conventional interlocking concrete pavement	-	-	-	-	0.25-0.30	0.26	0.25-0.30	0.26
Permeable asphalt pavement	-	-	-	-	0.08-0.12	0.10	0.08-0.12	0.10
Permeable concrete pavement	-	-	-	-	0.18-0.28	0.25	0.18-0.28	0.25
Permeable interlocking concrete pavement	-	-	-	-	0.25-0.30	0.26	0.25-0.30	0.26

Table 32. Summary of pavement treatment practice and albedo currently used by local governments in California.

City	Portion of network treated every year	Portion of each treatment in total treatments (albedo)						Steady-state albedo in 50 years (initial albedo = 0.10)
		A. Slurry seal (0.08)	B. Sand seal (0.10)	C. Chip seal (0.15)	D. Cape seal (0.06)	E. Asphalt overlay (0.10)	F. Reconstruction (AC, RAC, FDR, CIR) (0.10)	
Bakersfield	20%	-	75%	-	-	13%	12%	0.10
Berkeley	7.4%	31%	-	-	-	41%	28%	0.09
Chula Vista	3.9%	28.3%	-	46.4%	0.5%	21.8%	3%	0.12
Fresno	1.3%	-	-	-	-	100%	-	0.10
City of Los Angeles	7.4%	60.7%	-	-	-	35.4%	3.9%	0.09
Richmond	5.2%	47.1%	-	0.7%	0.5%	45.9%	5.9%	0.09
City of Sacramento	4.3%	82.4%	-	-	-	17.6%	-	0.09
San Jose	5%	80%	-	-	-	20%	-	0.09
Average	6.8%	41.2%	9.4%	5.9%	0.1%	36.8%	6.6%	0.10

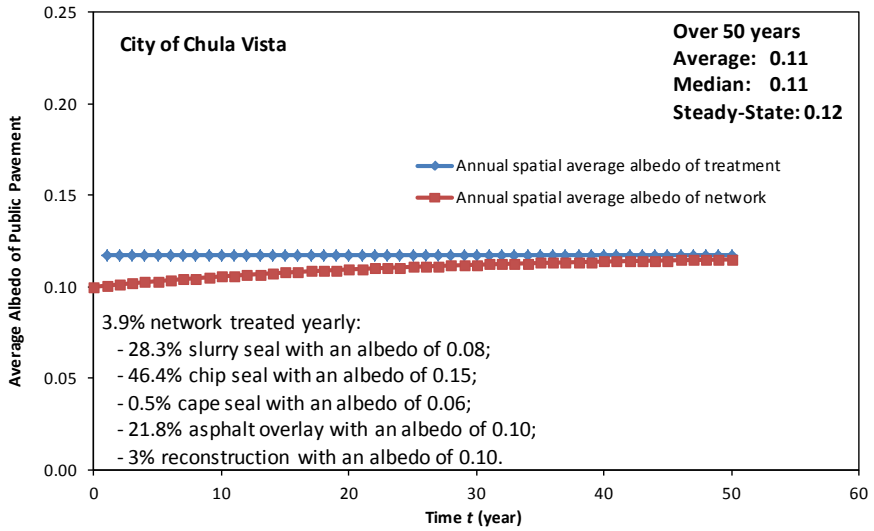

Figure 38. Example dynamic albedo of public pavement with current treatment practice in City of Chula Vista for the 50-year analysis period.

Dynamic albedo of public pavement networks with more reflective treatment practices and technologies

We also simulated the use of more reflective treatments. The scenarios of pavement treatment practice and assumed albedo for these simulations are summarized in Table 33. We made the following assumptions about pavement treatment practices and technologies used by local governments.

- The initial albedo of the public pavement is 0.10.
- The annual portion of network treated is 5%, 10%, and 20% over the 50 years.
- Six main treatment types are used
  - 41.2% slurry seal with an albedo of 0.08;
  - 9.4% sand seal with an albedo of 0.10;
  - 5.9% chip seal with an albedo of 0.15;
  - 0.1% cape seal with an albedo of 0.06;
  - 36.8% asphalt overlay with an albedo of 0.10; and
  - 6.6% reconstruction with an albedo of 0.10.
- Reflective treatment replacements include (a) 20%, 50% and 100% of slurry seal is replaced with reflective material with albedo of 0.25; and (b) 20%, 50% and 100% of asphalt overlay is replaced with reflective material with albedo of 0.30.

Table 33 presents the results of the simulated scenarios. Figure 39 is an example of one of the scenarios showing the dynamic change in citywide public pavement network albedo over 50 years. Since a constant and considerable portion of the public pavement network gets treated with treatments of different albedos every year, the average albedo of the entire public pavement network changes over time. The

average albedo increases gradually from the initial value of 0.10 up to 0.12, 0.15, 0.19, 0.12, 0.16, 0.22, 0.13, 0.17, and 0.23 over the 50 years for the nine scenarios, respectively. It takes approximately 10 to 50 years to reach the steady state with a stable pavement network albedo.

Table 33. Summary of pavement treatment practice and albedo assumed for local governments in California.

Scenario [a]	Portion of network treated every year	Replacement ratio of reflective treatment		Albedo of reflective treatment		Network albedo in 50 years (initial albedo: 0.10)		
		Reflective slurry seal	Reflective asphalt overlay	Reflective slurry seal	Reflective asphalt overlay	Average	Median	Steady-state
1 (5-20)	5%	20%	20%	0.25	0.30	0.12	0.12	0.13
2 (5-50)	5%	50%	50%	0.25	0.30	0.15	0.15	0.17
3 (5-100)	5%	100%	100%	0.25	0.30	0.19	0.21	0.23
4 (10-20)	10%	20%	20%	0.25	0.30	0.12	0.13	0.13
5 (10-50)	10%	50%	50%	0.25	0.30	0.16	0.17	0.17
6 (10-100)	10%	100%	100%	0.25	0.30	0.22	0.23	0.24
7 (20-20)	20%	20%	20%	0.25	0.30	0.13	0.13	0.13
8 (20-50)	20%	50%	50%	0.25	0.30	0.17	0.17	0.17
9 (20-100)	20%	100%	100%	0.25	0.30	0.23	0.24	0.24

[a] (x-y) means that x% of the network is treated each year, y% of slurry seal is replaced with reflective material with albedo of 0.25, and y% of asphalt overlay is replaced with reflective material with an albedo of 0.30.

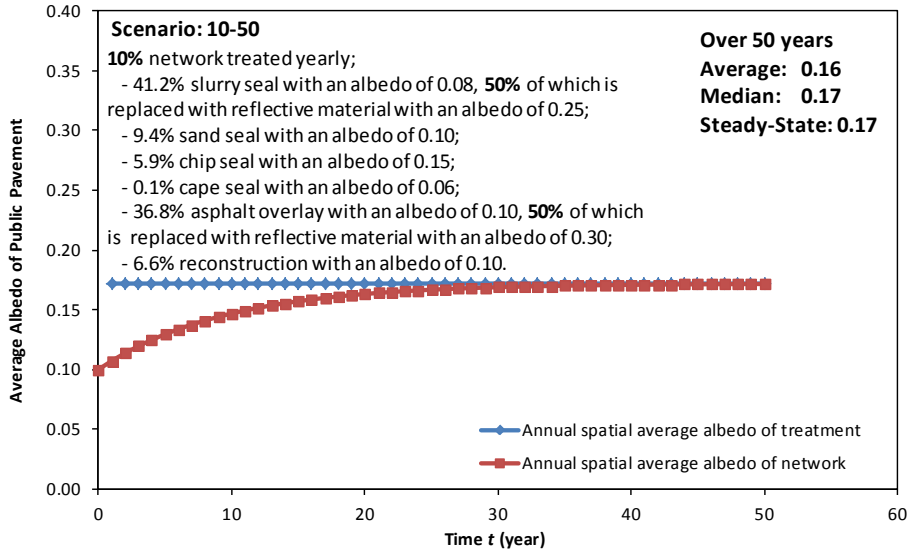

Figure 39. Example dynamic albedo of public pavement with assumed scenario 5 (10-50): 10% network gets treated yearly and 50% of slurry seal and asphalt overlay are replaced with reflective materials for the 50-year analysis period.

3.3. Pavement material and energy sources life-cycle inventories

Table 34 summarizes the main LCIA categories and inventory items of interest for the various treatments. These results were produced with the 2012 California electricity grid mix.

Use of California's Renewable Portfolio Standard

In addition to developing the LCIA with the 2012 electricity grid mix, we also modeled the LCIA categories with the 2020 California RPS electricity grid mix requirements. Since the tool presents results for a 50-year life cycle, we wanted to foresee changes in the grid in the future. The 2020 grid mix was developed based on projected procurement of electricity from renewable sources by the three major investor-owned utilities (IOUs) in California: Pacific Gas & Electric, South California Edison, and San Diego Gas & Electric which is shown in Table 35. While California's Renewables Portfolio Standard (RPS) requires that 33% of the state's electricity come from renewable sources by 2020, only about 28% of the total 2020 generation from these three IOUs is projected to come from renewables (CPUC 2011; PG&E 2014; SCE 2014; SD&E 2014). For the items that electricity process could be updated for grid mix in 2020, new inventories were developed. The models of materials and treatments were updated based on the new electricity grid mix.
Table 36 shows the summary of LCI and LCIAs of the materials for the default thicknesses (where applicable). This table only contains the items for which changing the electricity process in their model was possible. Table 37 is for the surface treatments, updated with the 2020 electricity grid mix.

Table 34. Summary LCI and LCIA of treatments (based on 2012 electricity grid mix, functional unit of 1 ln-km).

#	Item	Functional Unit	Life Cycle Phase	GWP [kg CO2e]	POCP [kg O3e]	PM2.5 [kg]	PED (total)* [MJ]	FE [MJ]
1	Bonded Concrete Overlay on Asphalt (BCOA) OP139SCM139	1 ln-km	material	6.28E+04	5.64E+03	3.71E+01	4.93E+05	0.00E+00
		1 ln-km	transport	1.97E+04	5.29E+03	9.53E+00	2.74E+05	0.00E+00
		1 ln-km	construction	1.54E+03	6.80E+02	1.21E+00	2.12E+04	0.00E+00
		1 ln-km	SUBTOTAL (MAC stage)	8.40E+04	1.16E+04	4.78E+01	7.88E+05	0.00E+00
2	Bonded Concrete Overlay on Asphalt (BCOA) OP267SCM71	1 ln-km	material	1.14E+05	9.78E+03	6.44E+01	8.67E+05	0.00E+00
		1 ln-km	transport	1.52E+04	2.77E+03	5.30E+00	2.16E+05	0.00E+00
		1 ln-km	construction	1.54E+03	6.80E+02	1.21E+00	2.12E+04	0.00E+00
		1 ln-km	SUBTOTAL (MAC stage)	1.31E+05	1.32E+04	7.09E+01	1.10E+06	0.00E+00
3	Bonded Concrete Overlay on Asphalt (BCOA) OP448SCM0	1 ln-km	material	1.89E+05	1.83E+04	1.07E+02	1.38E+06	0.00E+00
		1 ln-km	transport	1.34E+04	2.13E+03	4.28E+00	1.92E+05	0.00E+00
		1 ln-km	construction	1.54E+03	6.80E+02	1.21E+00	2.12E+04	0.00E+00
		1 ln-km	SUBTOTAL (MAC stage)	2.04E+05	2.11E+04	1.13E+02	1.60E+06	0.00E+00
4	Cape Seal	1 ln-km	material	5.03E+03	8.24E+02	4.03E+00	1.05E+05	3.75E+05
		1 ln-km	transport	6.53E+02	1.04E+02	2.09E-01	9.35E+03	0.00E+00
		1 ln-km	construction	1.49E+03	6.56E+02	1.17E+00	2.05E+04	0.00E+00
		1 ln-km	SUBTOTAL (MAC stage)	7.17E+03	1.58E+03	5.40E+00	1.35E+05	3.75E+05
5	Chip Seal	1 ln-km	material	3.64E+03	5.97E+02	2.91E+00	7.60E+04	2.69E+05
		1 ln-km	transport	4.80E+02	7.65E+01	1.53E-01	6.87E+03	0.00E+00
		1 ln-km	construction	8.12E+02	3.59E+02	6.37E-01	1.12E+04	0.00E+00

#	Item	Functional Unit	Life Cycle Phase	GWP [kg CO2e]	POCP [kg O3e]	PM2.5 [kg]	PED (total)* [MJ]	FE [MJ]
		1 ln-km	SUBTOTAL (MAC stage)	4.93E+03	1.03E+03	3.70E+00	9.41E+04	2.69E+05
6	Fog Seal	1 ln-km	material	1.06E+03	1.72E+02	8.73E-01	2.24E+04	8.42E+04
		1 ln-km	transport	1.31E+01	2.08E+00	4.17E-03	1.87E+02	0.00E+00
		1 ln-km	construction	2.14E+02	9.46E+01	1.68E-01	2.95E+03	0.00E+00
		1 ln-km	SUBTOTAL (MAC stage)	1.29E+03	2.69E+02	1.05E+00	2.56E+04	8.42E+04
7	Conventional Asphalt Concrete, Hveem (mill and fill)	1 ln-km	material	2.57E+04	2.36E+03	1.68E+01	1.31E+06	1.01E+06
		1 ln-km	transport	6.65E+03	1.06E+03	2.12E+00	9.51E+04	0.00E+00
		1 ln-km	construction	3.40E+03	1.50E+03	2.67E+00	4.68E+04	0.00E+00
		1 ln-km	SUBTOTAL (MAC stage)	3.57E+04	4.92E+03	2.16E+01	1.45E+06	1.01E+06
8	Conventional Asphalt Concrete, Hveem (overlay)	1 ln-km	material	2.57E+04	2.36E+03	1.68E+01	1.31E+06	1.01E+06
		1 ln-km	transport	3.32E+03	5.30E+02	1.06E+00	4.76E+04	0.00E+00
		1 ln-km	construction	2.09E+03	9.23E+02	1.64E+00	2.88E+04	0.00E+00
		1 ln-km	SUBTOTAL (MAC stage)	3.11E+04	3.82E+03	1.95E+01	1.39E+06	1.01E+06
9	Conventional Asphalt Concrete, Superpave (mill and fill)	1 ln-km	material	2.80E+04	2.78E+03	1.87E+01	1.53E+06	1.22E+06
		1 ln-km	transport	6.65E+03	1.06E+03	2.12E+00	9.51E+04	0.00E+00
		1 ln-km	construction	3.40E+03	1.50E+03	2.67E+00	4.68E+04	0.00E+00
		1 ln-km	SUBTOTAL (MAC stage)	3.81E+04	5.34E+03	2.35E+01	1.68E+06	1.22E+06
10	Conventional Asphalt Concrete, Superpave (overlay)	1 ln-km	material	2.80E+04	2.78E+03	1.87E+01	1.53E+06	1.22E+06
		1 ln-km	transport	3.32E+03	5.30E+02	1.06E+00	4.76E+04	0.00E+00
		1 ln-km	construction	2.09E+03	9.23E+02	1.64E+00	2.88E+04	0.00E+00
		1 ln-km	SUBTOTAL (MAC stage)	3.35E+04	4.23E+03	2.14E+01	1.61E+06	1.22E+06
11	Conventional Interlocking Concrete Pavement (Pavers)	1 ln-km	material	7.66E+04	7.84E+03	1.09E+02	6.81E+05	0.00E+00
		1 ln-km	transport	1.88E+04	2.99E+03	6.00E+00	2.69E+05	0.00E+00
		1 ln-km	construction	1.99E+03	8.78E+02	1.56E+00	2.74E+04	0.00E+00
		1 ln-km	SUBTOTAL (MAC stage)	9.74E+04	1.17E+04	1.17E+02	9.77E+05	0.00E+00
12	Permeable Asphalt Concrete (Only the Asphalt Layer)	1 ln-km	material	5.58E+04	5.83E+03	3.85E+01	3.33E+06	2.32E+06
		1 ln-km	transport	1.22E+04	1.94E+03	3.89E+00	1.74E+05	0.00E+00
		1 ln-km	construction	3.21E+03	1.42E+03	2.52E+00	4.42E+04	0.00E+00
		1 ln-km	SUBTOTAL (MAC stage)	7.12E+04	9.19E+03	4.49E+01	3.55E+06	2.32E+06
13	Permeable Portland Cement Concrete (Only the PCC Layer)	1 ln-km	material	2.14E+05	1.83E+04	1.22E+02	1.50E+06	0.00E+00
		1 ln-km	transport	1.66E+04	2.65E+03	5.31E+00	2.38E+05	0.00E+00
		1 ln-km	construction	1.50E+03	6.63E+02	1.18E+00	2.07E+04	0.00E+00
		1 ln-km	SUBTOTAL (MAC stage)	2.33E+05	2.16E+04	1.29E+02	1.76E+06	0.00E+00
14	Permeable Rubberized Asphalt Concrete (Only the Asphalt Layer)	1 ln-km	material	6.14E+04	6.77E+03	4.33E+01	3.91E+06	2.79E+06
		1 ln-km	transport	1.22E+04	1.94E+03	3.89E+00	1.74E+05	0.00E+00
		1 ln-km	construction	3.21E+03	1.42E+03	2.52E+00	4.42E+04	0.00E+00
		1 ln-km	SUBTOTAL (MAC stage)	7.68E+04	1.01E+04	4.97E+01	4.13E+06	2.79E+06
15	Permeable Section (Only the Crushed Agg	1 ln-km	material	4.95E+03	9.43E+02	2.30E+00	8.72E+04	0.00E+00
		1 ln-km	transport	9.00E+03	1.44E+03	2.88E+00	1.29E+05	0.00E+00
		1 ln-km	construction	4.00E+02	1.76E+02	3.14E-01	5.51E+03	0.00E+00

#	Item	Functional Unit	Life Cycle Phase	GWP [kg CO2e]	POCP [kg O3e]	PM2.5 [kg]	PED (total)* [MJ]	FE [MJ]
		1 ln-km	SUBTOTAL (MAC stage)	1.44E+04	2.55E+03	5.49E+00	2.22E+05	0.00E+00
16	Permeable Asphalt Concrete (with Crushed Agg as Base Layer)	1 ln-km	material	5.92E+04	6.61E+03	3.97E+01	3.32E+06	2.25E+06
		1 ln-km	transport	2.14E+04	3.42E+03	6.85E+00	3.07E+05	0.00E+00
		1 ln-km	construction	3.61E+03	1.59E+03	2.83E+00	4.97E+04	0.00E+00
		1 ln-km	SUBTOTAL (MAC stage)	8.42E+04	1.16E+04	4.93E+01	3.67E+06	2.25E+06
17	Permeable Portland Cement Concrete (with Crushed Agg as Base Layer)	1 ln-km	material	2.23E+05	1.95E+04	1.26E+02	1.61E+06	0.00E+00
		1 ln-km	transport	2.64E+04	4.21E+03	8.43E+00	3.78E+05	0.00E+00
		1 ln-km	construction	1.90E+03	8.40E+02	1.49E+00	2.62E+04	0.00E+00
		1 ln-km	SUBTOTAL (MAC stage)	2.51E+05	2.46E+04	1.36E+02	2.01E+06	0.00E+00
18	Permeable Rubberized Asphalt Concrete (with Crushed Agg as Base Layer)	1 ln-km	material	6.45E+04	7.52E+03	4.43E+01	3.88E+06	2.70E+06
		1 ln-km	transport	2.14E+04	3.42E+03	6.85E+00	3.07E+05	0.00E+00
		1 ln-km	construction	3.61E+03	1.59E+03	2.83E+00	4.97E+04	0.00E+00
		1 ln-km	SUBTOTAL (MAC stage)	8.96E+04	1.25E+04	5.40E+01	4.24E+06	2.70E+06
19	Portland Cement Concrete (PCC) OP139SCM139	1 ln-km	material	8.66E+04	7.77E+03	5.11E+01	6.79E+05	0.00E+00
		1 ln-km	transport	2.71E+04	7.28E+03	1.31E+01	3.77E+05	0.00E+00
		1 ln-km	construction	1.84E+03	8.13E+02	1.44E+00	2.54E+04	0.00E+00
		1 ln-km	SUBTOTAL (MAC stage)	1.16E+05	1.59E+04	6.57E+01	1.08E+06	0.00E+00
20	Portland Cement Concrete (PCC) OP284SCM50	1 ln-km	material	1.65E+05	1.49E+04	9.39E+01	1.17E+06	0.00E+00
		1 ln-km	transport	2.06E+04	3.64E+03	7.03E+00	2.94E+05	0.00E+00
		1 ln-km	construction	1.84E+03	8.13E+02	1.44E+00	2.54E+04	0.00E+00
		1 ln-km	SUBTOTAL (MAC stage)	1.88E+05	1.94E+04	1.02E+02	1.49E+06	0.00E+00
21	Portland Cement Concrete (PCC) OP418SCM0	1 ln-km	material	2.44E+05	2.07E+04	1.38E+02	1.75E+06	0.00E+00
		1 ln-km	transport	1.91E+04	3.05E+03	6.12E+00	2.74E+05	0.00E+00
		1 ln-km	construction	1.84E+03	8.13E+02	1.44E+00	2.54E+04	0.00E+00
		1 ln-km	SUBTOTAL (MAC stage)	2.65E+05	2.46E+04	1.45E+02	2.05E+06	0.00E+00
22	Reflective Coating - Bisphenol A (BPA)	1 ln-km	material	1.04E+04	4.46E+02	2.75E+00	2.52E+05	0.00E+00
		1 ln-km	transport	1.73E+01	2.76E+00	5.53E-03	2.48E+02	0.00E+00
		1 ln-km	construction	2.01E+02	8.88E+01	1.58E-01	2.77E+03	0.00E+00
		1 ln-km	SUBTOTAL (MAC stage)	1.06E+04	5.38E+02	2.91E+00	2.55E+05	0.00E+00
23	Reflective Coating - Polyester Styrene	1 ln-km	material	1.22E+04	5.77E+02	1.42E+01	2.55E+05	0.00E+00
		1 ln-km	transport	1.73E+01	2.76E+00	5.53E-03	2.48E+02	0.00E+00
		1 ln-km	construction	2.01E+02	8.88E+01	1.58E-01	2.77E+03	0.00E+00
		1 ln-km	SUBTOTAL (MAC stage)	1.24E+04	6.68E+02	1.43E+01	2.58E+05	0.00E+00
24	Reflective Coating - Polyurethane	1 ln-km	material	8.66E+03	3.78E+02	3.42E+00	1.91E+05	0.00E+00
		1 ln-km	transport	2.31E+01	3.68E+00	7.38E-03	3.30E+02	0.00E+00
		1 ln-km	construction	2.01E+02	8.88E+01	1.58E-01	2.77E+03	0.00E+00
		1 ln-km	SUBTOTAL (MAC stage)	8.88E+03	4.71E+02	3.58E+00	1.94E+05	0.00E+00

#	Item	Functional Unit	Life Cycle Phase	GWP [kg CO2e]	POCP [kg O3e]	PM2.5 [kg]	PED (total)* [MJ]	FE [MJ]
25	Reflective Coating - Styrene Acrylate	1 ln-km	material	5.76E+03	2.35E+02	1.82E+00	1.36E+05	0.00E+00
		1 ln-km	transport	2.31E+01	3.68E+00	7.38E-03	3.30E+02	0.00E+00
		1 ln-km	construction	2.01E+02	8.88E+01	1.58E-01	2.77E+03	0.00E+00
		1 ln-km	SUBTOTAL (MAC stage)	5.98E+03	3.27E+02	1.99E+00	1.39E+05	0.00E+00
26	Rubberized Asphalt Concrete (mill and fill)	1 ln-km	material	2.76E+04	2.69E+03	1.83E+01	1.57E+06	1.31E+06
		1 ln-km	transport	5.54E+03	8.83E+02	1.77E+00	7.93E+04	0.00E+00
		1 ln-km	construction	3.40E+03	1.50E+03	2.67E+00	4.68E+04	0.00E+00
		1 ln-km	SUBTOTAL (MAC stage)	3.65E+04	5.08E+03	2.28E+01	1.69E+06	1.31E+06
27	Rubberized Asphalt Concrete (overlay)	1 ln-km	material	2.76E+04	2.69E+03	1.83E+01	1.57E+06	1.31E+06
		1 ln-km	transport	2.77E+03	4.42E+02	8.85E-01	3.96E+04	0.00E+00
		1 ln-km	construction	2.09E+03	9.23E+02	1.64E+00	2.88E+04	0.00E+00
		1 ln-km	SUBTOTAL (MAC stage)	3.25E+04	4.06E+03	2.09E+01	1.64E+06	1.31E+06
28	Sand Seal	1 ln-km	material	1.59E+03	2.59E+02	1.26E+00	3.33E+04	1.18E+05
		1 ln-km	transport	2.88E+02	4.58E+01	9.19E-02	4.11E+03	0.00E+00
		1 ln-km	construction	7.99E+02	3.53E+02	6.27E-01	1.10E+04	0.00E+00
		1 ln-km	SUBTOTAL (MAC stage)	2.67E+03	6.57E+02	1.98E+00	4.84E+04	1.18E+05
29	Slurry Seal	1 ln-km	material	1.39E+03	2.27E+02	1.12E+00	2.93E+04	1.06E+05
		1 ln-km	transport	1.73E+02	2.76E+01	5.53E-02	2.48E+03	0.00E+00
		1 ln-km	construction	6.74E+02	2.98E+02	5.29E-01	9.29E+03	0.00E+00
		1 ln-km	SUBTOTAL (MAC stage)	2.24E+03	5.52E+02	1.71E+00	4.11E+04	1.06E+05

* The total primary energy demand **excluding** the feedstock energy, where feedstock energy is applicable and available and shown in the table; otherwise, PED Total is the total primary energy demand **including** the unknown feedstock energy.

Table 35. California's electricity grid mix projection in year 2020 (California Renewable Portfolio Standard 2011).

Item	Fraction of total sales in 2020 (%)
Total renewable	**28.2**
Biomass	1.2
Landfill gas	0.3
Geothermal	2.9
Small hydro	1.6
Solar PV	10.9
Solar thermal	2.3
Wind	9.0
Total non-renewables	**71.8**
Hard coal	6.4
Large hydro	7.0
Natural gas	36.8
Nuclear	7.6
Unspecified	13.9
Total	**100.0**

Table 36. Summary of LCI and LCIA for conventional materials, energy sources, and transport (based on 2020 CA electricity grid mix), only items that their models could be modified and updated with 2020 electricity.

Item	Functional unit	GWP [kg CO_2e]	POCP [kg O_3e]	PM2.5 [kg]	PED total * [MJ]	PED (non-ren) ** [MJ]	Feedstock energy [MJ]
Aggregate - crushed	1 kg	3.13E-03	6.44E-04	1.56E-06	6.72E-02	4.83E-02	0.00E+00
Aggregate - natural	1 kg	2.11E-03	3.97E-04	9.24E-07	4.86E-02	3.32E-02	0.00E+00
Bitumen	1 kg	4.63E-01	8.06E-02	4.08E-04	9.76E+00	8.96E+00	4.02E+01
Bitumen emulsion	1 kg of Residual Bitumen	5.02E-01	8.22E-02	4.16E-04	1.08E+01	1.02E+01	4.02E+01
Crumb rubber modifier (CRM)	1 kg	1.72E-01	5.69E-03	9.99E-05	5.63E+00	3.04E+00	3.02E+02
Portland cement (regular)	1 kg	8.62E-01	7.25E-02	4.97E-04	6.23E+00	5.40E+00	0.00E+00

* The total primary energy demand **excluding** the feedstock energy, where feedstock energy is applicable and available and shown in the table; otherwise, PED Total is the total primary energy demand **including** the unknown feedstock energy.

** Same note as above applies to Primary Energy Demand (PED non-renewable).

Table 37. Summary of LCI and LCIA of treatments (based on 2020 electricity grid mix, functional unit of 1 ln-km).

#	Item	Functional Unit	Life Cycle Phase	GWP [kg CO2e]	POCP [kg O3e]	PM2.5 [kg]	PED (total)* [MJ]	FE [MJ]
1	Bonded Concrete Overlay on Asphalt (BCOA) OP139SCM139	1 ln-km	material	6.18E+04	5.60E+03	3.69E+01	5.13E+05	0.00E+00
		1 ln-km	transport	1.97E+04	5.29E+03	9.53E+00	2.74E+05	0.00E+00
		1 ln-km	construction	1.54E+03	6.80E+02	1.21E+00	2.12E+04	0.00E+00
		1 ln-km	SUBTOTAL (MAC stage)	8.31E+04	1.16E+04	4.77E+01	8.08E+05	0.00E+00
2	Bonded Concrete Overlay on Asphalt (BCOA) OP267SCM71	1 ln-km	material	1.13E+05	9.71E+03	6.41E+01	9.00E+05	0.00E+00
		1 ln-km	transport	1.52E+04	2.77E+03	5.30E+00	2.16E+05	0.00E+00
		1 ln-km	construction	1.54E+03	6.80E+02	1.21E+00	2.12E+04	0.00E+00
		1 ln-km	SUBTOTAL (MAC stage)	1.29E+05	1.32E+04	7.06E+01	1.14E+06	0.00E+00
3	Bonded Concrete Overlay on Asphalt (BCOA) OP448SCM0	1 ln-km	material	1.87E+05	1.81E+04	1.07E+02	1.43E+06	0.00E+00
		1 ln-km	transport	1.34E+04	2.13E+03	4.28E+00	1.92E+05	0.00E+00
		1 ln-km	construction	1.54E+03	6.80E+02	1.21E+00	2.12E+04	0.00E+00
		1 ln-km	SUBTOTAL (MAC stage)	2.02E+05	2.10E+04	1.13E+02	1.65E+06	0.00E+00
4	Cape Seal	1 ln-km	material	4.96E+03	8.22E+02	4.02E+00	1.07E+05	3.75E+05
		1 ln-km	transport	6.53E+02	1.04E+02	2.09E-01	9.35E+03	0.00E+00
		1 ln-km	construction	1.49E+03	6.56E+02	1.17E+00	2.05E+04	0.00E+00
		1 ln-km	SUBTOTAL (MAC stage)	7.10E+03	1.58E+03	5.39E+00	1.37E+05	3.75E+05
5	Chip Seal	1 ln-km	material	3.59E+03	5.96E+02	2.90E+00	7.72E+04	2.69E+05
		1 ln-km	transport	4.80E+02	7.65E+01	1.53E-01	6.87E+03	0.00E+00
		1 ln-km	construction	8.12E+02	3.59E+02	6.37E-01	1.12E+04	0.00E+00
		1 ln-km	SUBTOTAL (MAC stage)	4.88E+03	1.03E+03	3.69E+00	9.53E+04	2.69E+05
6	Fog Seal	1 ln-km	material	1.05E+03	1.72E+02	8.72E-01	2.27E+04	8.42E+04
		1 ln-km	transport	1.31E+01	2.08E+00	4.17E-03	1.87E+02	0.00E+00
		1 ln-km	construction	2.14E+02	9.46E+01	1.68E-01	2.95E+03	0.00E+00
		1 ln-km	SUBTOTAL (MAC stage)	1.28E+03	2.69E+02	1.04E+00	2.58E+04	8.42E+04
7	Conventional Asphalt Concrete, Hveem (mill and fill)	1 ln-km	material	2.52E+04	2.35E+03	1.67E+01	1.32E+06	1.01E+06
		1 ln-km	transport	6.65E+03	1.06E+03	2.12E+00	9.51E+04	0.00E+00
		1 ln-km	construction	3.40E+03	1.50E+03	2.67E+00	4.68E+04	0.00E+00
		1 ln-km	SUBTOTAL (MAC stage)	3.53E+04	4.91E+03	2.15E+01	1.46E+06	1.01E+06
8	Conventional Asphalt Concrete, Hveem (overlay)	1 ln-km	material	2.52E+04	2.35E+03	1.67E+01	1.32E+06	1.01E+06
		1 ln-km	transport	3.32E+03	5.30E+02	1.06E+00	4.76E+04	0.00E+00
		1 ln-km	construction	2.09E+03	9.23E+02	1.64E+00	2.88E+04	0.00E+00
		1 ln-km	SUBTOTAL (MAC stage)	3.06E+04	3.80E+03	1.94E+01	1.40E+06	1.01E+06

9	Conventional Asphalt Concrete, Superpave (mill and fill)	1 ln-km	material	2.75E+04	2.76E+03	1.87E+01	1.55E+06	1.22E+06
		1 ln-km	transport	6.65E+03	1.06E+03	2.12E+00	9.51E+04	0.00E+00
		1 ln-km	construction	3.40E+03	1.50E+03	2.67E+00	4.68E+04	0.00E+00
		1 ln-km	SUBTOTAL (MAC stage)	3.75E+04	5.32E+03	2.35E+01	1.69E+06	1.22E+06
10	Conventional Asphalt Concrete, Superpave (overlay)	1 ln-km	material	2.75E+04	2.76E+03	1.87E+01	1.55E+06	1.22E+06
		1 ln-km	transport	3.32E+03	5.30E+02	1.06E+00	4.76E+04	0.00E+00
		1 ln-km	construction	2.09E+03	9.23E+02	1.64E+00	2.88E+04	0.00E+00
		1 ln-km	SUBTOTAL (MAC stage)	3.29E+04	4.22E+03	2.14E+01	1.62E+06	1.22E+06
11	Conventional Interlocking Concrete Pavement (Pavers)	1 ln-km	material	7.66E+04	7.84E+03	1.09E+02	6.81E+05	0.00E+00
		1 ln-km	transport	1.88E+04	2.99E+03	6.00E+00	2.69E+05	0.00E+00
		1 ln-km	construction	1.99E+03	8.78E+02	1.56E+00	2.74E+04	0.00E+00
		1 ln-km	SUBTOTAL (MAC stage)	9.74E+04	1.17E+04	1.16E+02	9.77E+05	0.00E+00
12	Permeable Asphalt Concrete (Only the Asphalt Layer)	1 ln-km	material	5.46E+04	5.80E+03	3.83E+01	3.35E+06	2.32E+06
		1 ln-km	transport	1.22E+04	1.94E+03	3.89E+00	1.74E+05	0.00E+00
		1 ln-km	construction	3.21E+03	1.42E+03	2.52E+00	4.42E+04	0.00E+00
		1 ln-km	SUBTOTAL (MAC stage)	7.00E+04	9.16E+03	4.48E+01	3.57E+06	2.32E+06
13	Permeable Portland Cement Concrete (Only the PCC Layer)	1 ln-km	material	2.11E+05	1.82E+04	1.22E+02	1.56E+06	0.00E+00
		1 ln-km	transport	1.66E+04	2.65E+03	5.31E+00	2.38E+05	0.00E+00
		1 ln-km	construction	1.50E+03	6.63E+02	1.18E+00	2.07E+04	0.00E+00
		1 ln-km	SUBTOTAL (MAC stage)	2.30E+05	2.15E+04	1.28E+02	1.81E+06	0.00E+00
14	Permeable Rubberized Asphalt Concrete (Only the Asphalt Layer)	1 ln-km	material	6.00E+04	6.73E+03	4.31E+01	3.94E+06	2.79E+06
		1 ln-km	transport	1.22E+04	1.94E+03	3.89E+00	1.74E+05	0.00E+00
		1 ln-km	construction	3.21E+03	1.42E+03	2.52E+00	4.42E+04	0.00E+00
		1 ln-km	SUBTOTAL (MAC stage)	7.54E+04	1.01E+04	4.95E+01	4.16E+06	2.79E+06
15	Permeable Section (Only the Crushed Agg Base Layer)	1 ln-km	material	4.52E+03	9.30E+02	2.24E+00	9.70E+04	0.00E+00
		1 ln-km	transport	9.00E+03	1.44E+03	2.88E+00	1.29E+05	0.00E+00
		1 ln-km	construction	4.00E+02	1.76E+02	3.14E-01	5.51E+03	0.00E+00
		1 ln-km	SUBTOTAL (MAC stage)	1.39E+04	2.54E+03	5.43E+00	2.31E+05	0.00E+00
16	Permeable Asphalt Concrete (with Crushed Agg as Base Layer)	1 ln-km	material	5.76E+04	6.57E+03	3.95E+01	3.35E+06	2.25E+06
		1 ln-km	transport	2.14E+04	3.42E+03	6.85E+00	3.07E+05	0.00E+00
		1 ln-km	construction	3.61E+03	1.59E+03	2.83E+00	4.97E+04	0.00E+00
		1 ln-km	SUBTOTAL (MAC stage)	8.26E+04	1.16E+04	4.91E+01	3.71E+06	2.25E+06
17	Permeable Portland Cement Concrete (with Crushed Agg as Base Layer)	1 ln-km	material	2.19E+05	1.94E+04	1.26E+02	1.68E+06	0.00E+00
		1 ln-km	transport	2.64E+04	4.21E+03	8.43E+00	3.78E+05	0.00E+00
		1 ln-km	construction	1.90E+03	8.40E+02	1.49E+00	2.62E+04	0.00E+00
		1 ln-km	SUBTOTAL (MAC stage)	2.48E+05	2.44E+04	1.36E+02	2.08E+06	0.00E+00

18	Permeable Rubberized Asphalt Concrete (with Crushed Agg as Base Layer)	1 ln-km	material	6.28E+04	7.47E+03	4.41E+01	3.92E+06	2.70E+06
		1 ln-km	transport	2.14E+04	3.42E+03	6.85E+00	3.07E+05	0.00E+00
		1 ln-km	construction	3.61E+03	1.59E+03	2.83E+00	4.97E+04	0.00E+00
		1 ln-km	SUBTOTAL (MAC stage)	8.78E+04	1.25E+04	5.38E+01	4.27E+06	2.70E+06
19	Portland Cement Concrete (PCC) OP139SCM139	1 ln-km	material	8.52E+04	7.71E+03	5.09E+01	7.07E+05	0.00E+00
		1 ln-km	transport	2.71E+04	7.28E+03	1.31E+01	3.77E+05	0.00E+00
		1 ln-km	construction	1.84E+03	8.13E+02	1.44E+00	2.54E+04	0.00E+00
		1 ln-km	SUBTOTAL (MAC stage)	1.14E+05	1.58E+04	6.55E+01	1.11E+06	0.00E+00
20	Portland Cement Concrete (PCC) OP284SCM50	1 ln-km	material	1.63E+05	1.48E+04	9.36E+01	1.22E+06	0.00E+00
		1 ln-km	transport	2.06E+04	3.64E+03	7.03E+00	2.94E+05	0.00E+00
		1 ln-km	construction	1.84E+03	8.13E+02	1.44E+00	2.54E+04	0.00E+00
		1 ln-km	SUBTOTAL (MAC stage)	1.85E+05	1.93E+04	1.02E+02	1.54E+06	0.00E+00
21	Portland Cement Concrete (PCC) OP418SCM0	1 ln-km	material	2.41E+05	2.05E+04	1.37E+02	1.82E+06	0.00E+00
		1 ln-km	transport	1.91E+04	3.05E+03	6.12E+00	2.74E+05	0.00E+00
		1 ln-km	construction	1.84E+03	8.13E+02	1.44E+00	2.54E+04	0.00E+00
		1 ln-km	SUBTOTAL (MAC stage)	2.62E+05	2.44E+04	1.45E+02	2.12E+06	0.00E+00
22	Reflective Coating - Bisphenol A (BPA)	1 ln-km	material	1.04E+04	4.46E+02	2.75E+00	2.52E+05	0.00E+00
		1 ln-km	transport	1.73E+01	2.76E+00	5.53E-03	2.48E+02	0.00E+00
		1 ln-km	construction	2.01E+02	8.88E+01	1.58E-01	2.77E+03	0.00E+00
		1 ln-km	SUBTOTAL (MAC stage)	1.06E+04	5.38E+02	2.91E+00	2.55E+05	0.00E+00
23	Reflective Coating - Polyester Styrene	1 ln-km	material	1.22E+04	5.77E+02	1.42E+01	2.55E+05	0.00E+00
		1 ln-km	transport	1.73E+01	2.76E+00	5.53E-03	2.48E+02	0.00E+00
		1 ln-km	construction	2.01E+02	8.88E+01	1.58E-01	2.77E+03	0.00E+00
		1 ln-km	SUBTOTAL (MAC stage)	1.24E+04	6.68E+02	1.43E+01	2.58E+05	0.00E+00
24	Reflective Coating - Polyurethane	1 ln-km	material	8.66E+03	3.78E+02	3.42E+00	1.91E+05	0.00E+00
		1 ln-km	transport	2.31E+01	3.68E+00	7.38E-03	3.30E+02	0.00E+00
		1 ln-km	construction	2.01E+02	8.88E+01	1.58E-01	2.77E+03	0.00E+00
		1 ln-km	SUBTOTAL (MAC stage)	8.88E+03	4.71E+02	3.58E+00	1.94E+05	0.00E+00
25	Reflective Coating - Styrene Acrylate	1 ln-km	material	5.76E+03	2.35E+02	1.82E+00	1.36E+05	0.00E+00
		1 ln-km	transport	2.31E+01	3.68E+00	7.38E-03	3.30E+02	0.00E+00
		1 ln-km	construction	2.01E+02	8.88E+01	1.58E-01	2.77E+03	0.00E+00
		1 ln-km	SUBTOTAL (MAC stage)	5.98E+03	3.27E+02	1.99E+00	1.39E+05	0.00E+00
26	Rubberized Asphalt Concrete (mill and fill)	1 ln-km	material	2.68E+04	2.67E+03	1.82E+01	1.59E+06	1.31E+06
		1 ln-km	transport	5.54E+03	8.83E+02	1.77E+00	7.93E+04	0.00E+00
		1 ln-km	construction	3.40E+03	1.50E+03	2.67E+00	4.68E+04	0.00E+00
		1 ln-km	SUBTOTAL (MAC stage)	3.57E+04	5.05E+03	2.27E+01	1.71E+06	1.31E+06

27	Rubberized Asphalt Concrete (overlay)	1 ln-km	material	2.68E+04	2.67E+03	1.82E+01	1.59E+06	1.31E+06
		1 ln-km	transport	2.77E+03	4.42E+02	8.85E-01	3.96E+04	0.00E+00
		1 ln-km	construction	2.09E+03	9.23E+02	1.64E+00	2.88E+04	0.00E+00
		1 ln-km	SUBTOTAL (MAC stage)	3.17E+04	4.04E+03	2.08E+01	1.65E+06	1.31E+06
28	Sand Seal	1 ln-km	material	1.56E+03	2.58E+02	1.26E+00	3.38E+04	1.18E+05
		1 ln-km	transport	2.88E+02	4.58E+01	9.19E-02	4.11E+03	0.00E+00
		1 ln-km	construction	7.99E+02	3.53E+02	6.27E-01	1.10E+04	0.00E+00
		1 ln-km	SUBTOTAL (MAC stage)	2.65E+03	6.57E+02	1.98E+00	4.89E+04	1.18E+05
29	Slurry Seal	1 ln-km	material	1.38E+03	2.26E+02	1.12E+00	2.97E+04	1.06E+05
		1 ln-km	transport	1.73E+02	2.76E+01	5.53E-02	2.48E+03	0.00E+00
		1 ln-km	construction	6.74E+02	2.98E+02	5.29E-01	9.29E+03	0.00E+00
		1 ln-km	SUBTOTAL (MAC stage)	2.22E+03	5.52E+02	1.70E+00	4.15E+04	1.06E+05

* The total primary energy demand **excluding** the feedstock energy, where feedstock energy is applicable and available and shown in the table; otherwise, PED Total is the total primary energy demand **including** the unknown feedstock energy.

3.4. Local urban climate and air quality modeling

3.4.1. Model evaluation

We evaluate the 'CTRL' simulation by comparing simulated surface air temperature and accumulated weekly precipitation to weather observations from the National Climatic Data Center (NCDC) Global Surface Summary of the Day (GSOD). Data from 105 weather stations in California were used in the evaluation. Histograms of simulated and observed daily mean temperatures indicate that the model reproduces the observed temperatures well but with a slightly narrower distribution (Figure 7a). Assessing the spatial variation in bias (model minus observation) indicates that the model captures well the daily mean temperatures in the Sacramento and San Joaquin Valley, and has larger biases in the coastal portions of Los Angeles and the San Francisco Bay area, as well as the desert regions in the southeastern portion of California. The overall mean bias for the entire state of California is -0.30 °C. Precipitation is quite well modeled though weeks with < 5 mm of precipitation are more frequent than indicated by observations, and weeks with ≥ 5 mm are less frequent than indicated by observations. Similar to daily mean temperatures, biases in precipitation are low in most parts of the Sacramento and San Joaquin Valley, while coastal regions show relatively larger biases. The overall mean normalized bias in weekly accumulated precipitation during the wet season (November to March) was 150%.

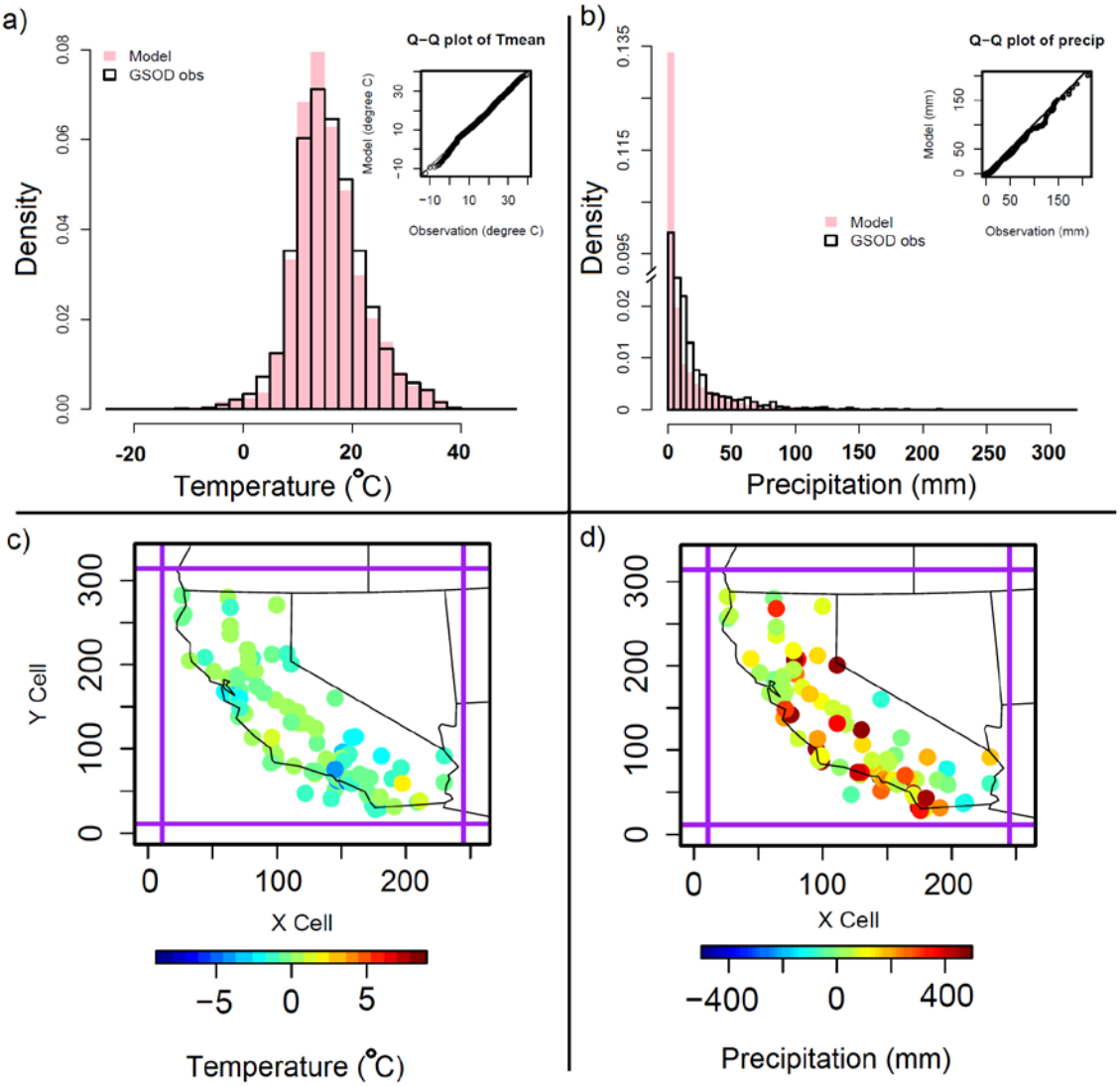

Figure 40. Model evaluation for daily mean temperature and precipitation of control scenario and NCDC global observation data showing (a) Probability Density Function (PDF) for daily mean temperature; (b) spatial distribution of bias for daily mean temperature; (c) PDF for model results and observed data; and (d) spatial distribution of bias for precipitation. The purple lines in the bottom panels bound the model domain.

3.4.2. Spatially resolved climate response to cool pavement adoption

The effect of increasing pavement albedo to 0.50 from 0.10 on surface air temperature (air temperature near the top of the urban canopy) is shown in Figure 41. Temperature changes are shown for the hottest time of day (14:00 LST), and in the evening (20:00 LST) when the magnitude of the air temperature heat island (urban temperature minus surrounding rural temperature) is often observed to be at a maximum (Oke 1982). Only differences that are significant at 99.5% confidence interval are shown. Widespread deployment of cool pavements reduces surface air temperatures in the urban parts of California including the Los Angeles Basin, San Diego, San Francisco Bay Area, and cities in the Sacramento and San Joaquin Valleys. Temperature reductions of up to 0.32 °C and 0.25 °C are simulated at 14:00 LST for summer and winter, respectively (summer and winter are defined as June-July-August and

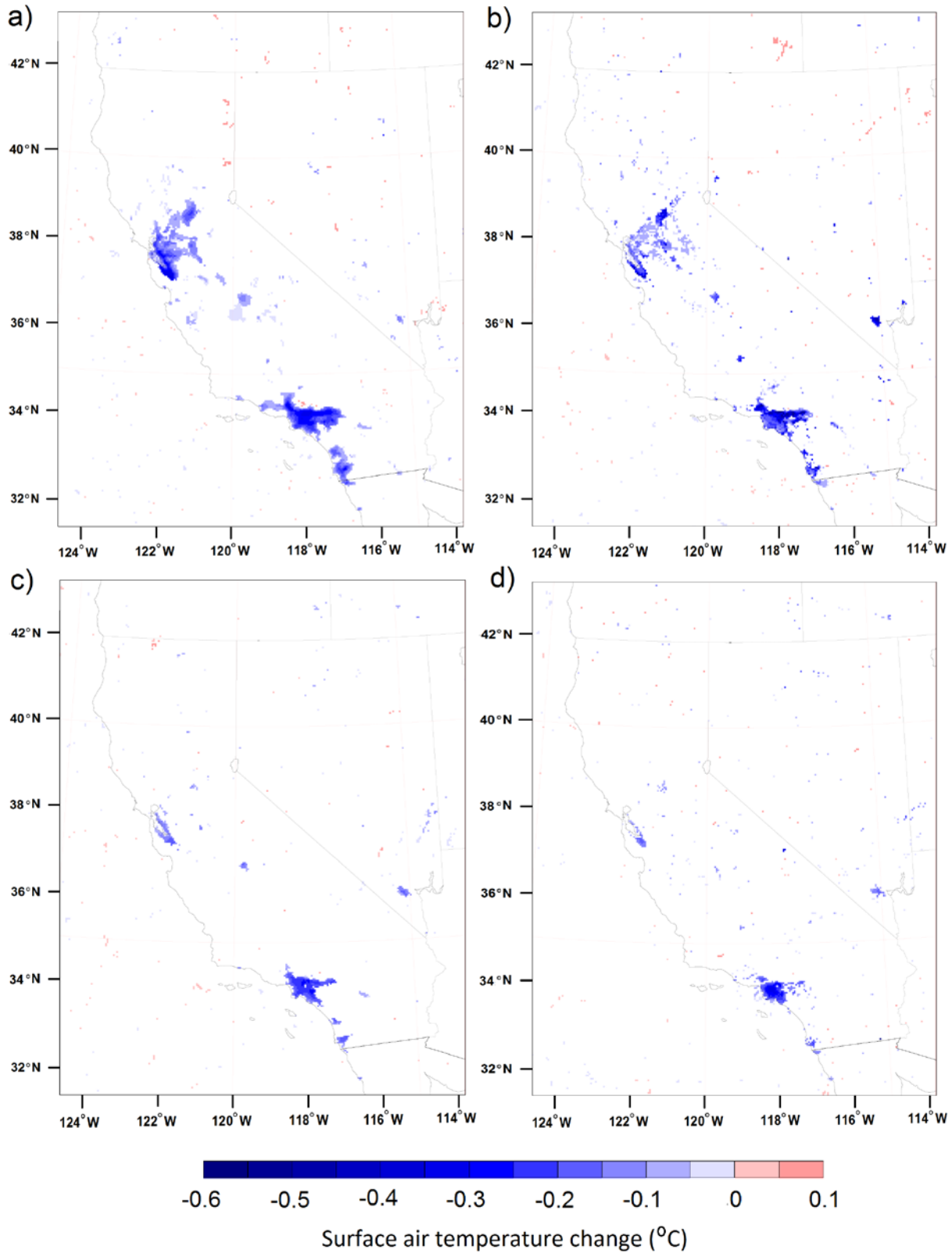

Figure 41. Cooling effects of cool pavements (COOL-CTRL), showing (a) summer average at 14:00 LST; (b) summer average at 20:00 LST; (c) winter average at 14:00 LST; and (d) winter average at 20:00 LST.

December-January-February, respectively). Corresponding temperature reductions at 20:00 are 0.62 °C and 0.32 °C. The absolute values of temperature reductions are smaller in winter versus summer, a consequence of the fact that insolation at the surface is decreased in winter and therefore changes in the albedo play a smaller role on temperatures. In the Los Angeles basin, temperature reductions are stronger in the inland versus coastal regions. This occurs because the effects of cool pavements accumulate as the dominant winds flow from west to east.

Raising pavement albedo increases net (upward – downward) all-wave (short-wave + long-wave) radiance at the top of the model in the urban parts of California by up to about 45 W m^{-2} in summer and 25 W m^{-2} in winter (Figure 42). These increases in radiation are larger in summer than winter due to the increased solar irradiance at the surface during summer. While boosting the surface albedo increases the reflected shortwave radiation at the surface, corresponding increases in total upward radiation at the top of model can be muted for two reasons: (1) short-wave radiation that is reflected from the surface can be scattered and absorbed by gases, aerosols, and clouds in the atmosphere prior to reaching the top of model (Zhang et al. 2016); and (2) surface temperature reductions caused by increasing pavement albedo lead to decreases in upward long-wave radiation.

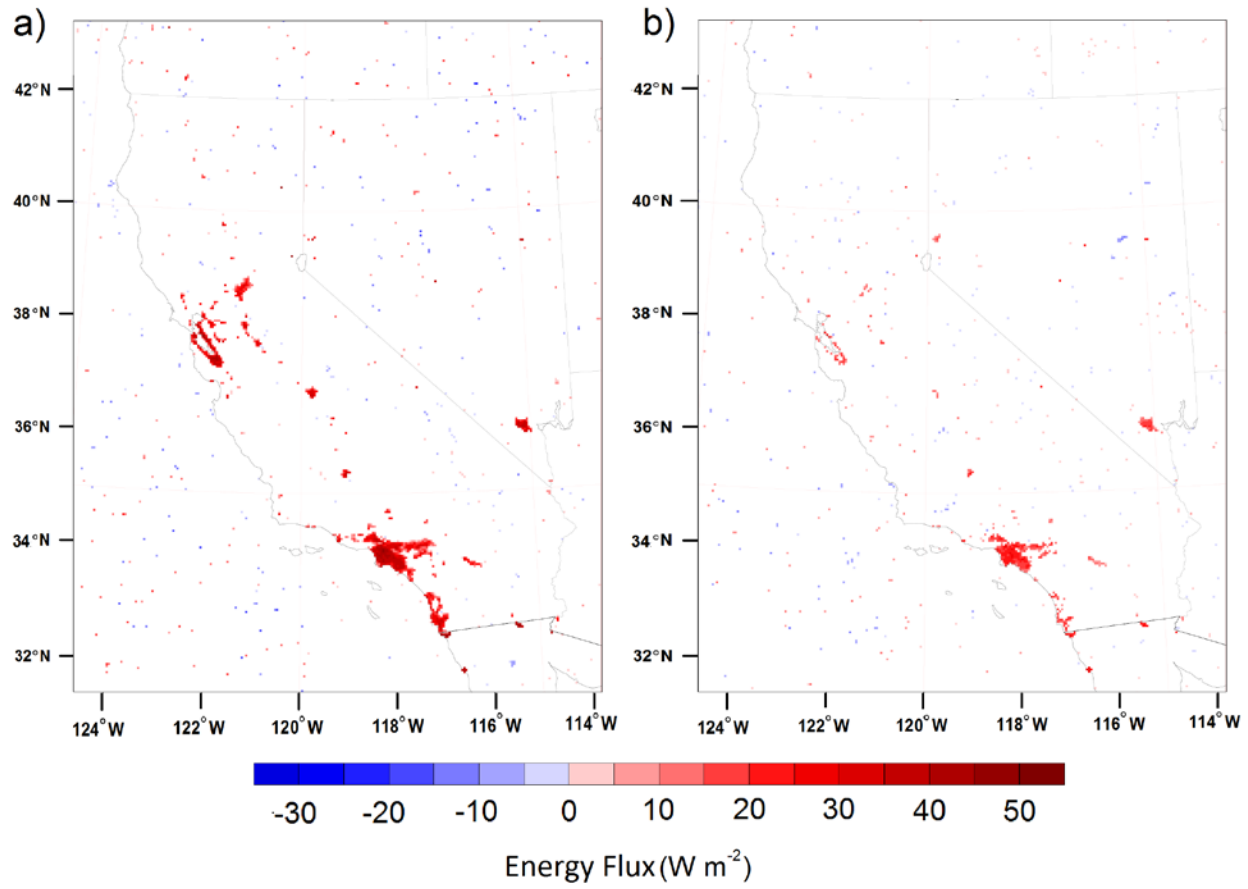

Figure 42. Upwelling all-wave (short-wave + long-wave) radiance at top of model (10,000 Pa pressure level), showing (a) summer average at 14:00 LST and (b) winter average at 14:00 LST.

3.4.3. Diurnal cycles

Diurnal cycles of seasonal mean temperature differences for (COOL_HIGH – CTRL) are shown for two example cities (Los Angeles and Sacramento) in Figure 43. In order to investigate the temperature impacts of

cool pavement adoption in the urban parts of the city, spatial means are weighted by corresponding grid-cell values for urban fraction. For all seasons, the largest temperature reductions are simulated in the late morning between about 9:00 and 11:00 LST, and in evening between about 16:00 and 20:00 LST. While one might expect the largest temperature decreases to occur at noon when solar irradiance peaks, or around 14:00 LST when absolute temperatures are highest, we find that the magnitudes of temperature decreases are closely coupled to the height of the planetary boundary layer (PBL) (Figure 43). This occurs because convective heat transfer from the surface to atmosphere can have a more pronounced impact on the temperature of the boundary layer when PBL height is lower. Thus, the largest temperature reductions occur in the late morning since solar irradiance is relatively strong, and PBL height is relatively low compared to diurnal maximum values that occur in the early afternoon. Similarly, in the evening, differences in the solar heat gain accumulated throughout the day for cool versus standard pavements, which lead to larger temperature differences as PBL height decreases. The mentioned evening peak is consistent with past studies showing that the magnitude of the air temperature heat island effect reaches a maximum after sunset (e.g. Oke 1982).

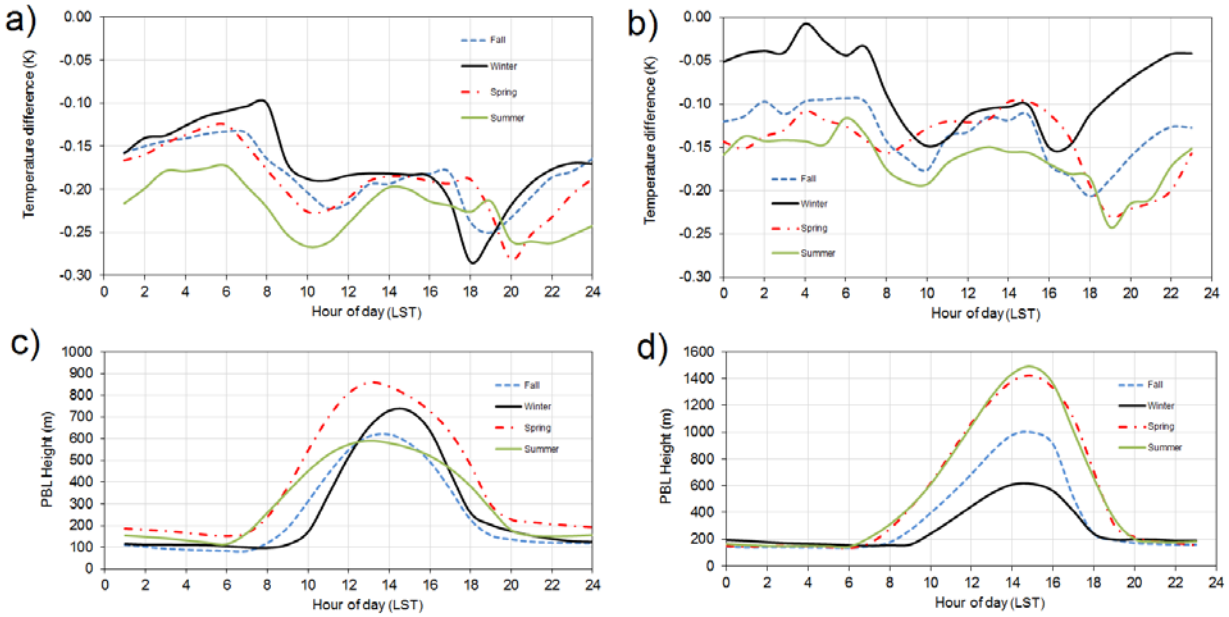

Figure 43. Seasonal diurnal profiles for cooling effects of albedo modifications and planetary boundary layer height (PBLH) showing (a) seasonal diurnal temperature difference averaged spatially over Los Angeles city (COOL_HIGH - CTRL); (b) seasonal diurnal temperature difference averaged spatially over Sacramento (COOL HIGH - CTRL); (c) seasonal diurnal profile of PBLH for CTRL scenario averaged spatially over LA; and (d) seasonal diurnal profile of PBLH for CTRL scenario averaged spatially over Sacramento.

Diurnal cycles of changes in surface energy fluxes for (COOL_HIGH – CTRL) are shown for an example city (Los Angeles) in Figure 44. Widespread adoption of cool pavements reduces net (downward – upward) short-wave radiation due to increases in the reflected short-wave radiative flux. The maximum reduction in net short-wave radiation of 43 W m^{-2} occurs at noon when solar irradiance is highest. Sensible heat fluxes are reduced throughout the day with maximum decreases of about 30 W m^{-2} just after noon. Changes to latent heat fluxes are small relative to other flux changes, as expected. Surface temperature reductions throughout the day are associated with decreases in net (upward – downward) long-wave radiation. The ground heat flux (downward positive) is reduced during the day, associated with cooler surface temperatures decreasing the heat transferred from the surface to the ground. However, the ground heat flux increases at night, likely because the surface temperature differential for (COOL_HIGH – CTRL) is lower than the corresponding temperature differential for the subsurface. Since ground heat fluxes are generally upward at night, a smaller reduction in surface temperature than in ground temperature would lead to smaller upward ground heat fluxes after

adopting cool pavements (and thus increases in downward positive ground heat flux). This occurs as ground temperatures are dependent on ground heat accumulation throughout the entire day, whereas surface temperatures are expected to be less dependent on albedo after the sun goes down. A similar diurnal cycle in ground heat flux was reported for widespread deployment of cool roofs by Li et al. (2014).

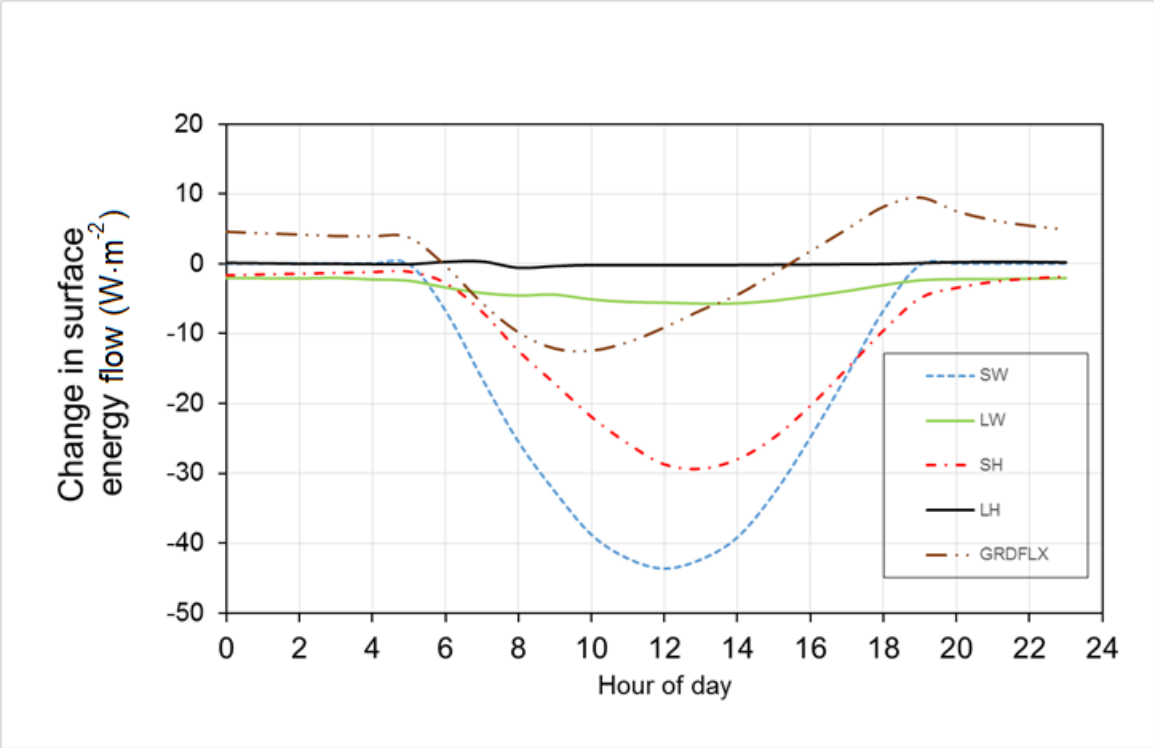

Figure 44. Diurnal cycle of changes in the surface energy flux (COOL_HIGH - CTRL) averaged spatially over the city of Los Angeles and temporally over summer.

3.4.4. Ozone

Ozone concentration changes per unit temperature change (m_{O3}, in parts per billion by volume per K or ppbV K^{-1}) have been quantified in the literature using the slope of the best linear fit of ozone concentration and temperature with long-term observational data (e.g., Mahmud et al. 2008; Bloomer et al. 2009; Steiner et al. 2010) and through direct model perturbation simulations (e.g., Steiner et al. 2006; Millstein and Harley 2009; Rasmussen et al. 2013). The concentration of ozone varies with underlying emissions of NO_x and volatile organic compounds (VOCs), as well as meteorological conditions (reviewed in, e.g., Steiner et al. 2010 and Rasmussen et al. 2013). The concentration of ozone therefore differs by region and changes with assumed emissions that change by year. Steiner et al. (2010) also noted that ozone is not consistent within all temperature ranges, diminishing and even turning negative at high temperatures (i.e., > 313 K) due to chemical and biophysical feedbacks.

In our review of the literature reporting ozone concentration, we assess only studies in regions within California and assuming conditions relevant to recent emission conditions (i.e., since the year 2000). The air basins of interest included the South Coast (SC), Sacramento Valley (SAC), San Joaquin Valley (SJV), and San Francisco Bay Area (SFB). Both observational and modeling studies are included in our review. Their findings are tabulated for the four California air basins along with the relevant chemical and physical processes considered in each study (Table 38). We found that ozone concentration falls generally in the 1-4 ppb K^{-1} range. m_{O3} under future year emission scenarios were also reported in Rasmussen et al. (2013). These future

values were smaller (<1 ppb K^{-1}), with considerable in-region variability in the South Coast air basin (Table 39). For the purposes of the pLCA tool, we used the following ranges for m_{O3} in each region: SC = 1.8 to 3.4 ppb K^{-1}, SAC = 1.2 to 1.8 ppb K^{-1}, SJV = 1 to 2.4 ppb K^{-1}, and SFB = 2.3 to 4.1 ppb K^{-1}.

All studies other than Rasmussen et al. (2013) diagnose either the mean of daily maximum 1-h ozone, or the mean of ozone concentrations at 15:00 LST, which is the time of day often observed to have maximum ozone concentrations (Steiner et al. 2006).

The range of ozone concentration changes due to the temperature reductions are calculated using the low and high ozone sensitivity to the temperature reductions, derived from previous studies, and the 14:00 LST temperature reductions averaged over the year (Table 40). Temperature reductions are calculated for 14:00 LST, since the photochemistry reactions are more active in this time due to the high temperature. To calculate the range of ozone concentration changes, the scaled temperature reductions for the revised canopy are used. These temperature reductions are derived using the model results and the scaling factors that are a function of modified urban canyon morphology, described in Section 0.

Table 38. Ozone to temperature sensitivity derived from the literature.

Air basin	O_3-T sensitivity (ppb/K)	Emission year	Study type	Pathways	Reference	Notes
SFB	2.3	2000-2005	observation	Reaction, BVOC, AVOC, NOx, meteorology	Steiner et al. 2010	-7.8 ppb/K for T>313K. 1 h peak ozone June 1 to October 31.
	4.1	2000	model	reaction, BVOC, moisture	Steiner et al. 2006	Bay area. Ozone at 15:00 LT driven by meteorology July 29 to August 3, 2000.
SAC	1.8	2000-2005	observation	Reaction, BVOC, AVOC, NOx, meteorology	Steiner et al. 2010	0.4 ppb/K for T>314K. 1 h peak ozone June 1 to October 31.
	1.2	2000	model	reaction, BVOC, moisture	Steiner et al. 2006	Sacramento. Ozone at 15:00 LT driven by meteorology July 29 to August 3, 2000.
SJV	2.4	2000-2005	observation	Reaction, BVOC, AVOC, NOx, meteorology	Steiner et al. 2010	0.4 ppb/K for T>314K. 1 h peak ozone June 1to October 31.
	2.6, 2.4, and 2.2	2000, 2005, and 2010	model	reaction, BVOC, moisture	Rasmussen et al. 2013	Median value from 18 urban receptors. 8 h average O_3 (10:00-18:00 LDT) driven by meteorology over July 25 to 27, 2005.
	1.0	2000-2004	observation	reaction, BVOC, meteorology	Mahmud et al. 2008	Used T850* reanalysis data. single site at Hanford. Peak 1 h ozone May to October.
	1.2	2000	model	reaction, BVOC, moisture	Steiner et al. 2006	Fresno region. Ozone at 15:00 LT driven by meteorology July 29 to August 3, 2000.
SC	3.4	2000-2005	observation	Reaction, BVOC, AVOC, NOx, meteorology	Steiner et al. 2010	-8.5 ppb/K for T>313K. 1 h peak ozone. June 1 to October 31.
	3.5, 2.0, and 1.6	2000, 2005, and 2010	model	reaction, BVOC, moisture	Rasmussen et al. 2013	Median value from 26 urban receptors. 8 h average O_3 (10:00-18:00 LDT) driven by meteorology September 7 to 9, 1993.
	3.0	2000-2004	observation	reaction, BVOC, meteorology	Mahmud et al. 2008	Used T850 reanalysis data, single site at Upland. Peak 1 h ozone May to October.
	1.8	2005	model	reaction, BVOC, moisture	Millstein and Harley 2009	Basin wide average for 1 h peak ozone over July 14 to 19, 2005.

* T850: the temperature at an elevation of 850-mbar pressure.

Table 39. Ozone to temperature sensitivity projected to 2020 (median value and associated range).

Region	O_3-T sensitivity (ppb/K)	Emission year	Study type	Pathways	Reference	Notes
SJV	0.9 (ranging from 0 to 1.5)	2020	model	reaction, BVOC, moisture	Rasmussen et al. 2013	18 urban receptors. 8 h average O_3 (10:00-18:00 LDT).
SC	0.8 (ranging from -0.8 to 11.8)	2020	model	reaction, BVOC, moisture	Rasmussen et al. 2013	26 urban receptors. 8 h average O_3 (10:00-18:00 LDT).

Table 40. Estimated changes in annual mean surface air temperatures and 1 hour ozone, scaling factors, and sensitivities for cities investigated in the current research. Air basins (used for estimated changes in ozone) and building climate zones (used for calculations of building energy changes) are also shown for each city.

City	Air basin	Building climate zone	Annual mean temperature difference at 14:00 LST (K)	Scaling factors	Annual mean temperature difference at 14:00 LST, scaled for realistic canyon (K)	Ozone-temperature sensitivity lower estimate. Mean daily max 1 hour ozone* (ppb/K)	Ozone-temperature sensitivity upper estimate. Mean daily max 1 hour ozone* (ppb/K)	1 hour ozone increase with lower bound sensitivity* (14:00 LST in ppb)	1 hour ozone increase with higher bound sensitivity (14:00 LST in ppb)
San Jose	SFB	4	-0.31	2.79	-0.87	NA	NA	NA	NA
Sunnyvale	SFB	4	-0.31	2.79	-0.87	NA	NA	NA	NA
San Diego	NA	7	-0.13	2.80	-0.38	NA	NA	NA	NA
Los Angeles	SC	8	-0.20	2.82	-0.56	1.8	3.4	-1.01	-1.91
Irvine	SC	8	-0.11	2.82	-0.32	1.8	3.4	-0.57	-1.08
Anaheim	SC	8	-0.24	2.82	-0.68	1.8	3.4	-1.23	-2.32
Santa Ana	SC	8	-0.19	2.82	-0.55	1.8	3.4	-0.99	-1.87
Garden Grove	SC	8	-0.22	2.82	-0.62	1.8	3.4	-1.12	-2.11
Canoga Park	SC	9	-0.25	2.81	-0.70	1.8	3.4	-1.26	-2.39
Reseda	SC	9	-0.25	2.81	-0.70	1.8	3.4	-1.26	-2.39
Lake Balboa	SC	9	-0.25	2.81	-0.70	1.8	3.4	-1.26	-2.39
Van Nuys	SC	9	-0.25	2.81	-0.70	1.8	3.4	-1.26	-2.39

Valley Glen	SC	9	-0.25	2.81	-0.70	1.8	3.4	-1.26	-2.39
Burbank	SC	9	-0.25	2.81	-0.71	1.8	3.4	-1.27	-2.40
Glendale	SC	9	-0.23	2.81	-0.65	1.8	3.4	-1.17	-2.21
Pasadena	SC	9	-0.27	2.81	-0.75	1.8	3.4	-1.35	-2.55
East Pasadena	SC	9	-0.25	2.81	-0.70	1.8	3.4	-1.26	-2.39
South Pasadena	SC	9	-0.25	2.81	-0.70	1.8	3.4	-1.26	-2.39
Riverside	SC	10	-0.23	2.79	-0.64	1.8	3.4	-1.14	-2.16
Ontario	SC	10	-0.24	2.79	-0.67	1.8	3.4	-1.21	-2.29
Rancho Cucamonga	SC	10	-0.29	2.79	-0.80	1.8	3.4	-1.44	-2.72
Fontana	SC	10	-0.25	2.79	-0.70	1.8	3.4	-1.26	-2.38
Rialto	SC	10	-0.27	2.79	-0.76	1.8	3.4	-1.37	-2.59
San Bernardino	SC	10	-0.25	2.79	-0.71	1.8	3.4	-1.28	-2.41
Bloomington	SC	10	-0.24	2.79	-0.66	1.8	3.4	-1.19	-2.25
Sacramento	SAC	12	-0.15	2.81	-0.43	1.2	1.8	-0.51	-0.77
Bakersfield	SJV	13	-0.09	2.82	-0.24	1.0	2.4	-0.24	-0.58
Fresno	SJV	13	-0.11	2.82	-0.30	1.0	2.4	-0.30	-0.73
Lancaster	NA	14	-0.09	2.76	-0.25	NA	NA	NA	NA
California City	NA	14	-0.09	2.76	-0.25	NA	NA	NA	NA
Palm Springs	NA	15	-0.07	2.78	-0.19	NA	NA	NA	NA

* NA is listed when a city was not contained within one of the four air basins studied. The tool does not report any ozone concentration changes for these cities.

3.5. Building energy modeling

3.5.1. Comparison of modeled and actual building energy use

The cooling and heating energy use intensities reported by CBECS, RECS, and CEUS were compared to the intensities calculated from the building energy modeling. RECS data can be disaggregated by state, and CEUS is a California study, but the smallest geographic unit available in CBECS is the U.S. Census division. Thus to estimate the California energy use intensities using CBECS, we selected their data from the Pacific division, which includes California (74.7% of the Pacific division population), Alaska (1.4%), Oregon (7.7 %), Washington (13.5%), and Hawaii (2.7%).

In Table 41 we report California's mean annual site cooling energy use intensities (annual site energy use per unit floor area, in kWh/m²) calculated from the EnergyPlus simulations. Population varies widely across the state's climate zones. Hence, these values of California's mean site cooling energy use intensities were weighted by climate zone population. These are compared with values reported in CBECS and RECS for new stock (CBECS period 2000-2012; RECS period 2000-2009) and all stock. The table also compares the modeled commercial buildings to CEUS. For the residential prototypes, the cooling energy intensities calculated from the EnergyPlus simulations matched well with the intensities computed from all of California's residential stock in RECS. Some of the simulated commercial prototypes have cooling intensities that match the intensities from CEUS; the other commercial prototypes have intensities matching those from CBECS.

Table 41. Comparing electric cooling energy intensity of modeled prototypes to values reported by CBECS, RECS and CEUS.

	California's site cooling energy intensity [kWh/m²]					
Building type	**EnergyPlus models weighted by CZ population**	**CBECS[a] new stock**	**RECS new stock**	**CBECS all stock**	**RECS all stock**	**CEUS all stock**
Retail strip mall	26.39	18.13	NA[b]	15.19	NA	26.05
Primary school	18.98	14.58	NA	13.99	NA	13.79
Large hotel	22.12	5.8	NA	8.48	NA	28.41
Large office	16.6	9.22	NA	16.71	NA	42.08
Medium office	25.29	9.22	NA	16.71	NA	36.42
Sit-down restaurant	43.21	47.99	NA	41.47	NA	67.89
Fast-food restaurant	56.42	64.22	NA	56.55	NA	67.89
Retail stand-alone	22.15	20.17	NA	14.62	NA	26.05
Apartment building	9.07	NA	6.93	NA	7.62	NA
Single-family home	8.06	NA	10.1	NA	8.2	NA

[a] CBECS values describe commercial buildings from the Pacific division of the U.S. Census.
[b] NA = Not Applicable

Table 42 reports California's mean site gas and electric heating energy use intensities. The medium office prototype is the only one that uses electricity as its main source for heating. Thus, the table reports electric heating intensity for the medium office and gas heating intensity for all other prototypes. The heating intensities calculated for most of the prototypes are much smaller than the heating intensities obtained from CBECS, CEUS, and RECS. This is probably due to the high air tightness of the envelope

of the simulated buildings—high air tightness decreases the heat loss from the conditioned space to the exterior. The simulated prototypes had more stringent construction standards than those observed in many of the buildings in California's current building stock. Thus, the prototypes have greater air tightness than many current buildings in the state.

Table 42. Comparing heating energy intensity of modeled prototypes to values reported by CBECS, RECS and CEUS.

	California's site gas or electric heating energy intensity [kWh/m²]					
Building type	**EnergyPlus models weighted by BCZ population**	**CBECS new stock**	**RECS new stock**	**CBECS all stock**	**RECS all stock**	**CEUS all stock**
Retail strip mall	8.29	67.8	NA[a]	119	NA	8.93
Primary school	6.58	62.3	NA	156	NA	29.8
Large hotel	24.9	3.14	NA	14.1	NA	21.7
Large office	7.48	34.6	NA	66.1	NA	51.2
Medium office (electric heating)	15.6	6.32	NA	25.2	NA	11.2
Sit-down restaurant	66.6	77.25	NA	74.3	NA	22.9
Fast-food restaurant	97.0	109	NA	54.9	NA	22.9
Retail stand-alone	12.4	51.0	NA	58.8	NA	8.93
Apartment building	3.69	NA	64.9	NA	54.4	NA
Single-family home	14.0	NA	64.9	NA	42.6	NA

[a] NA = not applicable

3.5.2. Base energy use versus degree days

As one way to verify the correct modeling of the HVAC equipment of each prototype, we compared the base energy use by climate zone to degree days at 18 °C (we selected 18 °C as it is a common reference temperature for calculation of cooling degree days and heating degree days.) Figure 45 show cooling source energy use intensities versus cooling degree-days at 18 °C (CDD18C). The 10 prototypes were paired by the use of the building—retail, residential, restaurant, office, and others (hotel and school). Note that in each plot, both curves follow the same trend and increase with CDD18C. In each pair of prototypes, the curves have similar slopes, but the difference in magnitudes is due to differences in plug loads and internal loads. The residential and restaurant buildings are the prototypes that show the best correlation between cooling source energy intensities and CDD18C.

Figure 46 shows heating source energy use intensity versus heating degree-days at 18 °C (HDD18C). In Figure 46 the 10 prototypes were paired the same way as in Figure 45. As expected, the heating energy use intensities show good correlation with HDD18C.

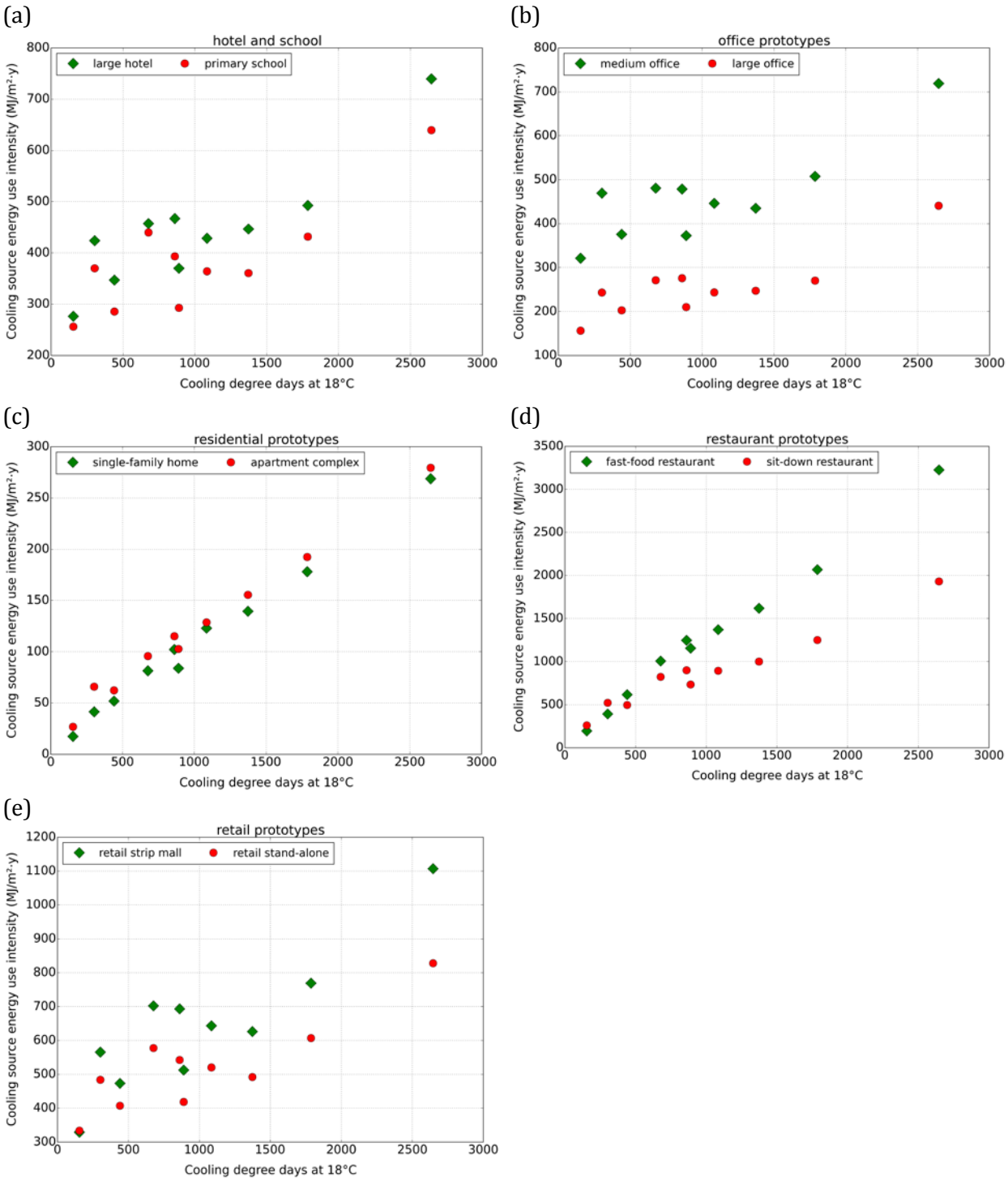

Figure 45. Cooling source energy use intensity versus cooling degree days.

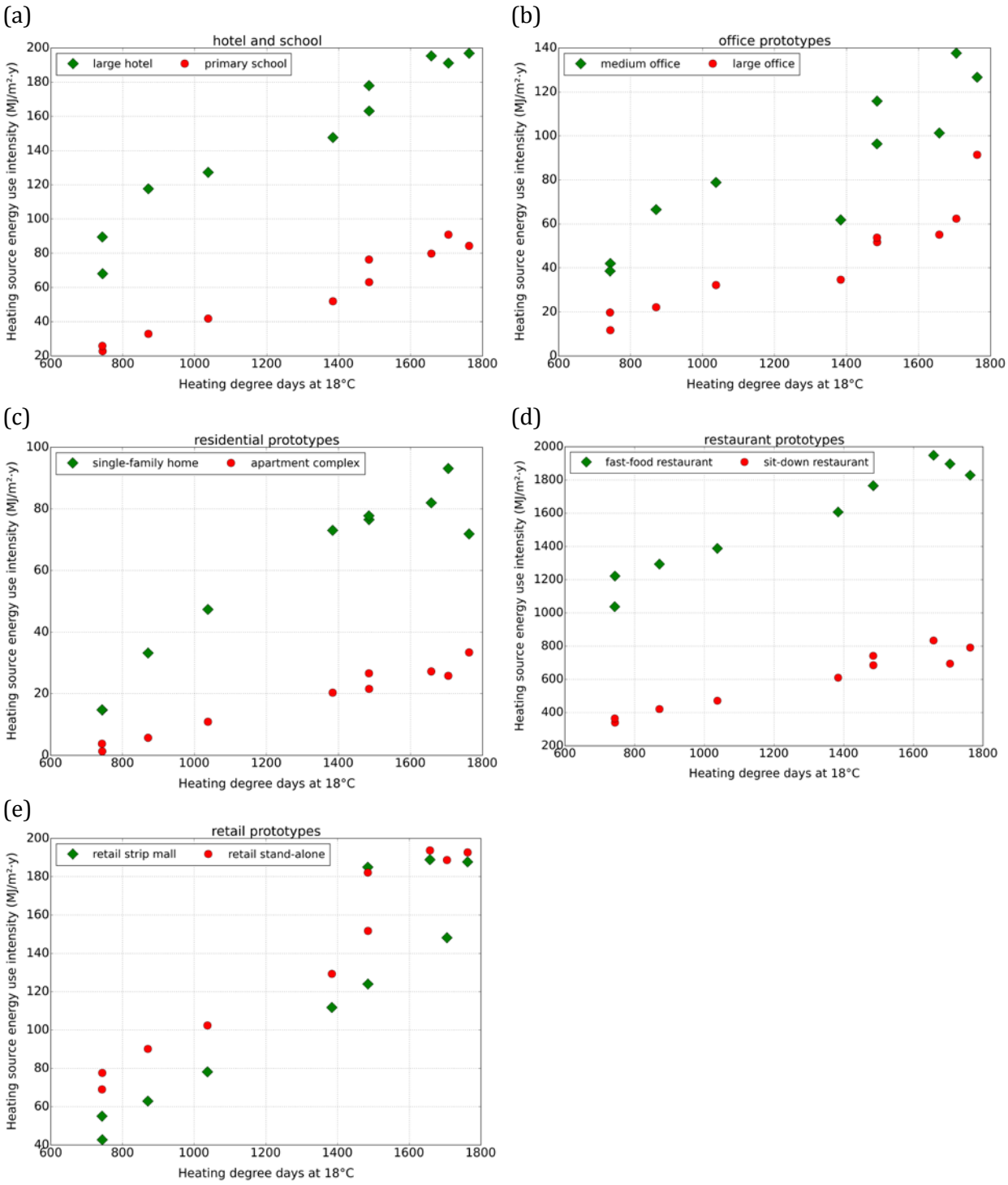

Figure 46. Heating source energy use intensity versus heating degree days.

3.5.3. Building-to-road view factors

lists for each building prototype, the calculated view factors from the wall to different sections of the floor. The table includes the building-to-road view factors, which were calculated following the steps described in Section 2.6.4. The view factors were calculated using the wall height given in Table 17, and the road and setback widths listed in Table 20.

Each prototype had a different window-to-wall ratio. Hence, we normalized the direct effects by the window-to-wall ratio so they can be properly compared. Once normalized, it is possible to find a climate-specific relationship between the direct effect of cool roads and the building-to-road view factor. Figure 47 shows this relationship for the direct effect in cooling energy use for BCZs 9 and 13. The slope of the curve varies by climate zone; for cooling, it ranged between 2.3% and 3.2% per 0.10 increase in road albedo. For the effect on heating energy use, the slopes were opposite in sign, and smaller in magnitude (-2.5% to -0.6% per 0.10 increase in road albedo).

Table 43. View factors by building prototype.

Prototype	**Wall to setback (F_{w-s})**	**Wall to (setback + road) (F_{w-sr})**	**Wall to road (F_{w-r})**	**Building to road (F_{b-r})**
Single-family home	0.373	0.430	0.057	0.014
Apartment building	0.342	0.406	0.064	0.016
Large office	0.133	0.246	0.113	0.057
Medium office	0.282	0.372	0.090	0.023
Primary school	0.413	0.450	0.037	0.028
Fast-food restaurant	0.458	0.472	0.014	0.004
Retail stand-alone	0.422	0.460	0.038	0.010
Retail strip mall	0.434	0.462	0.028	0.014
Sit-down restaurant	0.459	0.472	0.013	0.003

(a) (b)

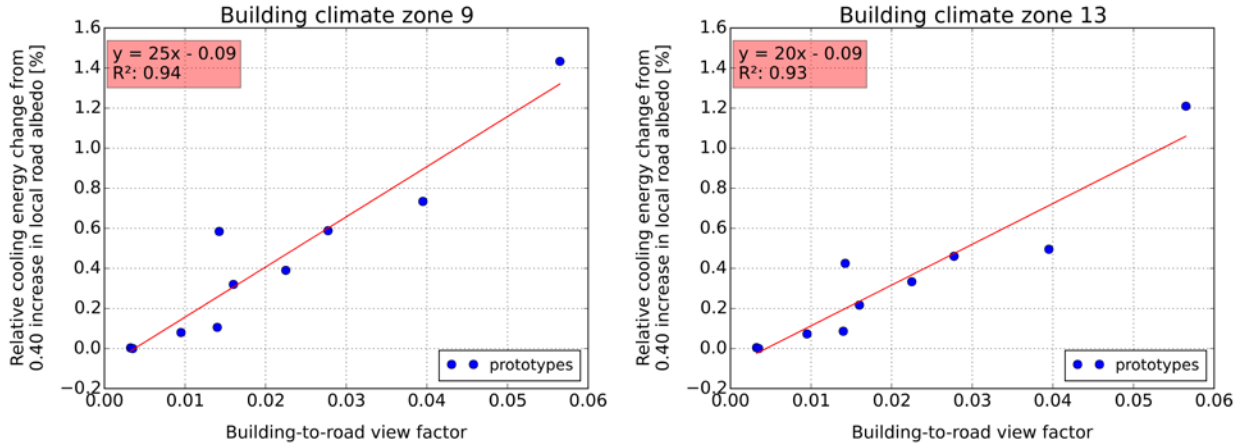

Figure 47. Direct effect from cool pavements normalized by window-to-wall ratio versus building-to-road view factor, for BCZ 9 and BCZ 13.

3.5.4. Modeling output results

Coefficients to physical model solutions

We applied multivariate linear regression analysis to the EnergyPlus simulation results to test the energy equations derived from the physical model and estimate their coefficients. Here we present a subset of the coefficients. Table 44 shows the site cooling, heating, and lighting coefficients for the sit-down restaurant, retail strip mall, and single-family home prototypes in climate zone 13, represented by the city of Fresno. The coefficients labeled *e* represent electric site energy use in units of MWh/y, and the coefficients *g* are for gas site energy use in units of therm/y. Site energies can be expressed in MJ using conversion factors of 3600 MJ/kWh or 105.5 MJ/therm. This table is a subset of a complete coefficient table that covers the cooling, heating and lighting coefficients for the 10 building prototypes and 10 modeled building climate zones. The full table can be found in the *input tables* folder of the pLCA tool sandbox.

Table 44. Coefficients of physical model solutions for prototypes sit-down restaurant, retail strip mall, and single-family home, in BCZ 13 (represented by Fresno).

Prototype	Use	e0 [MWh/y]	e1 [MWh/y]	e2 [MWh/y]	g0 [therm/y]	g1 [therm/y]	g2 [therm/y]
Sit-down restaurant	cooling	43.2	0.002	-4.67	0.000	0.000	0.000
	heating	10.4	-0.006	0.925	1710	-0.143	327
	lighting	20.4	0.000	0.000	0.000	0.000	0.000
Retail strip mall	cooling	110	0.384	-9.12	0.000	0.000	0.000
	heating	22.9	0.032	3.00	1060	-4.23	268
	lighting	102	0.000	0.000	0.000	0.000	0.000
Single-family home	cooling	3.40	0.102	-0.432	0.000	0.000	0.000
	heating	0.231	0.001	0.04	1423	-2.050	24.4
	lighting	1.35	0.000	0.000	0.000	0.000	0.000

Direct effect versus indirect effect of cool pavements

We compared the individual contributions to energy use from both the indirect and direct effects of cool pavements, as well as their overall effect. For this purpose, we defined the base case and three modified cases as follows:

- Base case: Original local road albedo (ρ_r = 0.10), original city-mean pavement albedo (ρ_p = 0.10)
- Case 1 (direct effect only): Modified local road albedo, original city-mean pavement albedo (ρ_p = 0.10)
- Case 2 (indirect effect only): Original local road albedo (ρ_r = 0.10), modified city-mean pavement albedo
- Case 3 (direct + indirect effects): Modified local road albedo, modified city-mean pavement albedo

When only fraction *f* of the city's pavement is modified, the city's mean pavement albedo is calculated as

$$\rho_{p,city} = f \cdot \rho_{p,modified} + (1 - f) \cdot \rho_{p,original} \quad (34)$$

To demonstrate, let us assume a scenario in which the albedo of 25% of the pavement in a city within climate zone 12 increases from 0.10 to 0.40. Table 45 shows the cooling savings from Cases 1, 2, and 3 relative to the base case for each building. The base case represents site cooling energy use normalized by the conditioned floor area (kWh/m²·y). The table compares the savings from Cases 1, 2, and 3 relative to the base case.

Table 45. Comparing savings of site cooling energy intensity when modifying the albedo of 25% of the city's pavement from 0.10 to 0.40 in BCZ 12 (represented by Sacramento).

Prototype	Base case: ρ_r = 0.10, ρ_p = 0.10 [kWh/m²·y]	Fractional savings in site cooling energy intensity (%)		
		Case 1: ρ_r = 0.40, ρ_p = 0.10	Case 2: ρ_r = 0.10, ρ_p = 0.175	Case 3: ρ_r = 0.40, ρ_p = 0.175
Single-family home	6.98	-0.29	1.33	1.04
Apartment complex	8.54	-0.25	1.15	0.89
Retail stand-alone	34.8	-0.03	0.65	0.62
Retail strip mall	42.6	-0.03	0.71	0.69
Medium office	31.0	-0.07	0.75	0.69
Large office	17.5	-0.16	0.83	0.66
Primary school	24.4	-0.10	0.88	0.78
Large hotel	30.8	-0.15	0.74	0.59
Sit-down restaurant	61.1	0.00	1.01	1.01
Fast-food restaurant	96.1	0.00	1.07	1.07

Table 46 shows the site gas heating energy savings in the same scenario. These results, for both cooling and heating, describe the general trend observed in all climate zones. During the cooling season, the single-family home and apartment building are scheduled with daytime indoor temperatures higher than the commercial buildings. Hence, these two residential buildings have lower daytime cooling intensities than the other prototypes. Since their base case cooling energy uses are much lower, the direct effect penalties of cool pavements are more noticeable (see fractional savings in Case 1 in Table 45).

Table 46. Comparing savings of site gas heating energy intensity when modifying the albedo of 25% of the city's pavement from 0.10 to 0.40 in BCZ 12 (represented by Sacramento).

Prototype	Base case: ρ_r = 0.10, ρ_p = 0.10 [therm/m²·y]	Fractional savings in site gas heating energy intensity (%)		
		Case 1: ρ_r = 0.40, ρ_p = 0.10	Case 2: ρ_r = 0.10, ρ_p = 0.175	Case 3: ρ_r = 0.40, ρ_p = 0.175
Single-family home	0.610	0.10	-1.23	-1.13
Apartment complex	0.189	0.11	-1.74	-1.63
Retail stand-alone	0.638	0.01	-1.11	-1.10
Retail strip mall	0.546	0.03	-1.61	-1.58
Medium office	0.006	0.78	-2.07	-1.29
Large office	0.345	-0.13	-1.48	-1.61
Primary school	0.342	0.04	-1.40	-1.36
Large hotel	1.131	0.08	-1.05	-0.98
Sit-down restaurant	4.759	0.00	-1.04	-1.04
Fast-food restaurant	8.794	0.00	-0.88	-0.88

3.6. Results of pavement strategy guidance tool development

The following example serves only to illustrate use of the tool. It does not provide design guidance or draw all possible conclusions.

We consider changing 25% of the total pavement area in Fresno to portland cement concrete—assigned albedo 0.30, thickness 17.5 cm, and a service life of 10 years—from conventional asphalt concrete (mill and fill), to which we assign albedo 0.10, thickness 6 cm, and a service life of 10 years. Figure 16 shows the inputs and the graphical outputs. The latter report absolute change per unit area of pavement modified, and include both the direct and indirect use-stage effects of the albedo change.

Inspection of the first four graphs shows that the materials and construction-stage changes to GWP, smog potential, PM2.5, and PED greatly exceed the corresponding use-stage changes, and each of these impacts is dominated by its material element. We also note that the reduction in material feedstock energy (about 1,500 MJ/m²) is about 60% of the increase in material PED (about 2,400 MJ/m²).

The use-stage changes are hard to see on this graph, which is scaled to the much larger materials and construction stage changes. One solution is to view the tabular display (Figure 17). However, a convenient alternative is to use the same surface treatment in each scenario, varying only pavement albedo. In that case, the materials and construction stage changes will be zero, and the graphs will be scaled to the use-stage metrics. After setting the surface treatment in Scenario B equal to that in Scenario A, retaining in Scenario B only the elevated pavement albedo of 0.30, we can readily see absolute use-stage changes per unit area of pavement modified (Figure 20) and relative use-stage changes (Figure 23). The *absolute* change graphs are best for comparing changes in the three components of the use stage (cooling, heating, and lighting) to one another. For example, Figure 20 shows that the magnitude of the cooling GWP reduction is less than that of the heating GWP increase, while the magnitude of the cooling PED reduction is greater than that of the heating PED increase. It also shows that the lighting-related changes are negligible, and that when summed over all three components of the use stage, GWP increases and PED decreases.

Each *relative* change graph provides context by showing the fraction by which an LCA metric changes. For example, Figure 23 indicates that the 74 MJ/m² pavement reduction in LC cooling PED shown in Figure 20 corresponds to a 0.5% decrease in the LC cooling PED of the building stock in Fresno.

Researchers may wish to disaggregate the use-stage changes into those resulting from the direct effect (change in sunlight reflected from pavements to buildings) and those arising from the indirect effect (change in city-mean air temperature). For example, Figure 22 shows the indirect effect LC changes per unit pavement area modified. In the absence of the direct effect, the reduction in LC cooling PED rises to 92 from 74 MJ/m² pavement. 3.6

The exported data tables provide further insight into the citywide changes in use-stage indicators. For example, the table at the top of Figure 25 (rows 83-94) shows floor area fractions, and the absolute changes per unit floor area in LCA metrics and site energy uses, by prototype. We can see that the two residential prototypes (single-family home and apartment complex) compose nearly 88% of the floor area in Fresno, with single-family homes alone representing 79% of floor area. Hence, citywide changes will be dominated by the results for single-family homes. For example, expressed per unit floor area, the savings in use-stage PED over 50 years for the single-family home is only 7.6 MJ/m². This is nearly an order of magnitude smaller than the 57 MJ/m² savings experienced by the retail strip mall, which at 4.3% of citywide floor area is the most prevalent commercial building type.

4. Discussion

4.1. Pavement albedo

The following presents our main findings from the investigation into pavement albedo:

- The most commonly used pavement treatments currently have relatively low steady-state albedo, ranging from 0.05 to 0.15 with average of 0.10 for asphalt concrete, and from 0.10 to 0.24 with average of 0.15 for chip seal. Albedos for slurry seals were measured in Davis, California and ranged from 0.07 to 0.10, with an average of 0.08. Albedos for cape seals measured in the City of Davis ranged from 0.05 to 0.15, with an average of 0.06. Albedos for fog seals measured in the City of Davis ranged from 0.04 to 0.07, with an average of 0.06. Data are not available for sand seals. For experimental coatings, albedos are from 0.20 to 0.30 with average of 0.25 for asphalt concrete with reflective coating, and from 0.15 to 0.35 with average of 0.25 for concrete with reflective coating.
- Experience to date on experimental sections placed by LBNL indicates that although the initial albedo of treatment with reflective coatings can be very high (e.g., up to 0.70), the albedo will decrease very quickly to a low value due to weathering and tracking.

4.2. Pavement material life-cycle inventories

The main findings from the development of the pavement life-cycle inventories include the following:

- Among the materials production, transportation and construction stages, materials production typically had the greatest impacts across each of the indicators and flows considered in this study. For most materials, the greatest impacts come from the binders (asphalt, cement, etc.) which make up a small portion of the material by mass and volume.
- In general, impacts and flows increase with treatment thickness.
- The use of a concrete mix design with supplementary cementitious materials and other changes intended to reduce environmental impacts generated less than half the GHG produced by the conventional portland cement concrete mix with same thickness. However, most local governments in California do not currently include SCM in their concrete paving materials.
- The reflective coatings had higher environmental impacts and flows that did other treatments of similar thickness (chip seals, slurry seals).

4.3. Local urban climate and air quality

4.3.1. Sensitivity of air temperature change to urban fraction and linearity of simulations

City-mean temperature changes for (COOL_HIGH – CTRL) and (COOL_LOW – CTRL) are plotted versus the city-mean urban fraction in Figure 48. Note that unlike other figures presented in this paper,

city-means in this case include all pixels within the city boundary and are not weighted by urban fraction. In general, deployment of cool pavements leads to larger air temperature reductions in cities with higher mean urban fractions. Figure 48 also shows least-squares linear regressions of surface air temperature change to urban fraction for (COOL_HIGH – CTRL) and (COOL_LOW – CTRL). These regressions indicate that for (COOL_LOW – CTRL), the temperature reduction per 0.1 increase in urban fraction is 0.055 and 0.043 °C for 14:00 LST and daily means, respectively. Corresponding temperature reductions for (COOL_HIGH – CTRL) are 0.24 and 0.22 °C. The fact that the temperature reductions for (COOL_HIGH – CTRL) are about 4 times higher than those for (COOL_LOW – CTRL) shows that the sensitivity of air temperature change to increase in pavement albedo is nearly constant, since the corresponding pavement albedo changes are 0.10 and 0.40. Scatter about the trend lines represents variation in the sensitivity of air temperature change to albedo change, and is caused by widely varying baseline climates for cities around California. For example, sensitivity of air temperature to albedo is expected to be higher for cities with lower wind speeds and less cloud cover. Scatter is also caused by variation in the size of each city. This occurs because the effects of cool pavements accumulate as winds flow over the city, an effect that can amplify the sensitivity of air temperature to albedo change for larger cities.

4.3.2. Sensitivity of air temperature to grid cell albedo and comparison to other studies

Results reported here are compared to other relevant studies. Millstein and Menon (2011) investigated the temperature reductions attainable from widespread deployment of cool roofs and pavements in cities around the United States. They used WRF version 3.2.1 to simulate the entire country at 25 km resolution for 12 years. An urban canopy model was not implemented and thus each urban grid cell was represented as a 2D surface without including the effects of the urban canopy on surface-atmosphere interactions. In Millstein and Menon, the urban albedo (ρ_u) was increased by 0.19, achieved by increasing roof albedo by 0.25 and pavement albedo by 0.15. For comparison, our increases in pavement albedo of 0.4 led to increases of ρ_u ranging from 0.069 to 0.086 across all urban grid cells in California. Given the different treatments of urban grid cells in our study versus Millstein and Menon means that we cannot directly compare the sensitivity of temperature difference to roof/pavement albedo difference. Rather, we compare temperature difference to grid cell albedo (ρ_g) difference. Figure 49 shows air temperature difference versus change in grid cell albedo for each city investigated in our study and each city reported in Millstein and Menon (see their Table 1). To make results more comparable, city-mean values shown for our study are not weighted by urban fraction in this figure. Using results from our investigation, linearly regressing temperature versus albedo change leads to a slope of 3.2, implying surface air temperature reductions of 0.32 °C per 0.10 increase in grid cell albedo. An equivalent analysis of the results reported in Millstein and Menon suggests very similar temperature reductions of 0.34 °C per 0.10 increase in albedo. These are both consistent with that reported in Santamouris (2014), who reviewed a number of past studies [Synnefa et al. (2008), Sailor (1995), Rosenfeld et al. (1995), Rosenfeld et al. (1998), Millstein and Menon (2011), Sailor et al. (2002), Zhou and Shepherd (2010), Taha (2008a), Lynn et al. (2009, Taha (2008c)], and found that average ambient temperatures are expected to be reduced by 0.30 °C per 0.10 increase in albedo (i.e. what we refer to as grid cell albedo). Note that Santamouris (2014) does not include past studies that single out the urban temperature impacts of cool pavements since no such studies existed.

Taha (2013) is the only other study to our knowledge that has investigated the urban temperature impacts of cool pavements. Taha simulated the impacts of increasing the albedo of driveways, sidewalks, and parking lots by 0.10 and 0.20. Corresponding peak (i.e. both spatially and temporally) temperature reductions in Los Angeles were about 0.25 °C and 0.50 °C, respectively. These results are not directly comparable to our study since he reports only peak temperature reductions.

Another recent study (Taleghani et al. 2016) compared the impacts of adopting heat mitigation strategies (i.e., cool roofs, cool pavements, green roofs, and street trees) on neighborhood scale temperatures and pedestrian thermal comfort. This study implemented a micrometeorological model with a spatial resolution of 3 m, orders of magnitude higher resolution than that of the regional climate model used in our research. They found that increasing pavement albedo by 0.3 decreased surface air temperatures by up to about 2 °C, which is larger than the temperature reductions reported in our research. There are important differences in methodology between our study and that of Taleghani et al. For example, Taleghani et al. simulated one extreme heat day, while our longer simulations are "climatological" and thus represent a variety of meteorological regimes. In addition, due to model limitations on domain size, the high resolution simulations carried out in Taleghani et al. could only be performed for a neighborhood, and not an entire city or state. Thus, these results may be dependent on the neighborhood selected for the study and not transferable. The higher spatial resolution of the micrometeorological model allowed for more detailed characterizations of land cover as compared to the regional climate model used in the current research. It also allowed for better resolving the air flows between buildings than the regional climate model used in our research, which parameterizes the urban canopy using only one layer in the vertical. We suggest that the temperature reduction from cool pavements may be dependent on the spatial scale of the model used. Note also that Taleghani et al. explored the impacts of heat mitigations strategies on pedestrian thermal comfort, which is beyond the scope of the current study.

4.3.3. Influence of assumed urban morphology on climate response

The single layer urban canopy parameterization employed in this study assumes that canyons are infinitely long without any spacing between walls and pavements (see Figure 2 in Chen et al. [2011]). The pavement is assumed homogeneous with no distinction between roadways and sidewalks. Building "setbacks" (gaps between streets and buildings) are not resolved. Adding these details to the urban canopy model would change the relationship between pavement albedo and urban albedo. Since we are ultimately interested in the influence of changes in pavement (street) albedo on climate, we now explore the sensitivity of our results to assumed urban morphology, and develop modified temperature responses from cool pavements using more realistic canyon geometries derived using data that became available after the WRF simulations were complete.

Since albedo modifications are implemented only in the urban part of the grid cell, we can write

$$\Delta\rho_g = f^* \Delta\rho_u \tag{35}$$

Changes in urban albedo and pavement albedo can also be related by

$$\frac{\Delta\rho_{u_2}}{\Delta\rho_{p\ 2}} = \frac{K_2}{K_1} \cdot \frac{\Delta\rho_{u_1}}{\Delta\rho_{p\ 1}} \tag{36}$$

where K is the ratio of change in urban albedo to the pavement albedo change, and subscripts 1 and 2 denote estimates of this proportionality for either two different assumed urban canyon morphologies, or two different modeling methods. Note that K is independent of urban fraction.

Figure 50 illustrates the relationship of urban albedo to pavement albedo difference for the three canyon geometries (e.g., building heights and street widths) associated with NLCD urban classifications (Section 2.5.1), and the limiting case assuming 2D urban surfaces with no canyon. The slopes of each line represent values for K corresponding to each assumed morphology as calculated using the single layer urban canopy model in WRF 3.5.1. As the ratio of building height to street width increases (as occurs

from low to high density), the urban albedo increase attained from raising pavement albedo is diminished. The upper bound for the impact of pavement albedo modification on urban albedo is set by assuming there is no canyon. Combining equations (35) and (36), we attain:

$$\frac{\Delta\rho_g}{\Delta\rho_{p_2}} = \frac{K_2}{K_1} \cdot \frac{\Delta\rho_g}{\Delta\rho_{p_1}} \tag{37}$$

This expresses the proportionality of grid cell albedo to pavement albedo. Note that this proportionality again does not depend on urban fraction.

As discussed previously, comparing the slopes for COOL_LOW – CTRL and COOL_HIGH – CTRL in Figure 48 indicates that the sensitivity of surface air temperature to pavement albedo is approximately constant in each modeled city. Thus, to generalize the sensitivity of surface air temperature to pavement albedo for any urban canyon configuration of choice, we can compare *K* values assumed in our WRF modeling (i.e. *K*1) to newly derived *K* values for various morphologies (i.e. *K*2 in equation (37)). Scaled estimates of surface air temperature can then be attained for newly assumed canyon morphologies by scaling city-mean surface air temperature differences derived using WRF (Table 40) by the ratio *K*2/*K*1. Note that to attain city specific results, city-mean temperature-albedo sensitivities and *K*1 values should be used (*K*1 values for each city can differ because of different relative amounts of low, medium, and high intensity urban land cover, and potential incorporation of NUDAPT data).

We note also that in the single layer urban canopy parameterization employed here, urban albedo is not a function of canyon orientation. Instead, the mean results after considering eight different typical canyon orientations are used. Further, close inspection of the default model code in the single-layer urban canopy model of WRF3.5.1 highlights that sunlight entering the top of the urban canyon is assumed to be 100% diffuse. This means that shading of pavements by buildings is not resolved since the solar beam is not separately tracked.

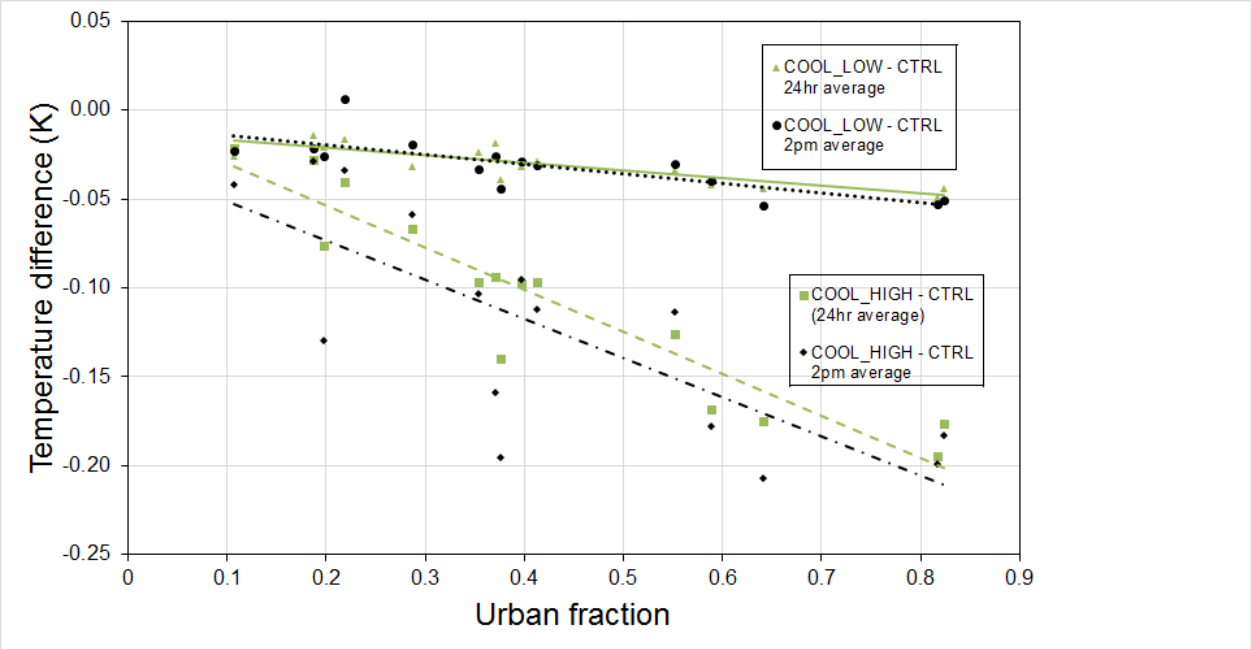

Figure 48. Average temperature reductions of different cities graphed against each city average urban albedo. Each point represents a city. The temperature reductions are calculated from the difference of COOL_HIGH and COOL_LOW scenarios from CTRL scenario. Green color shows the 24 h average and black color shows 14:00 LST temperature reductions.

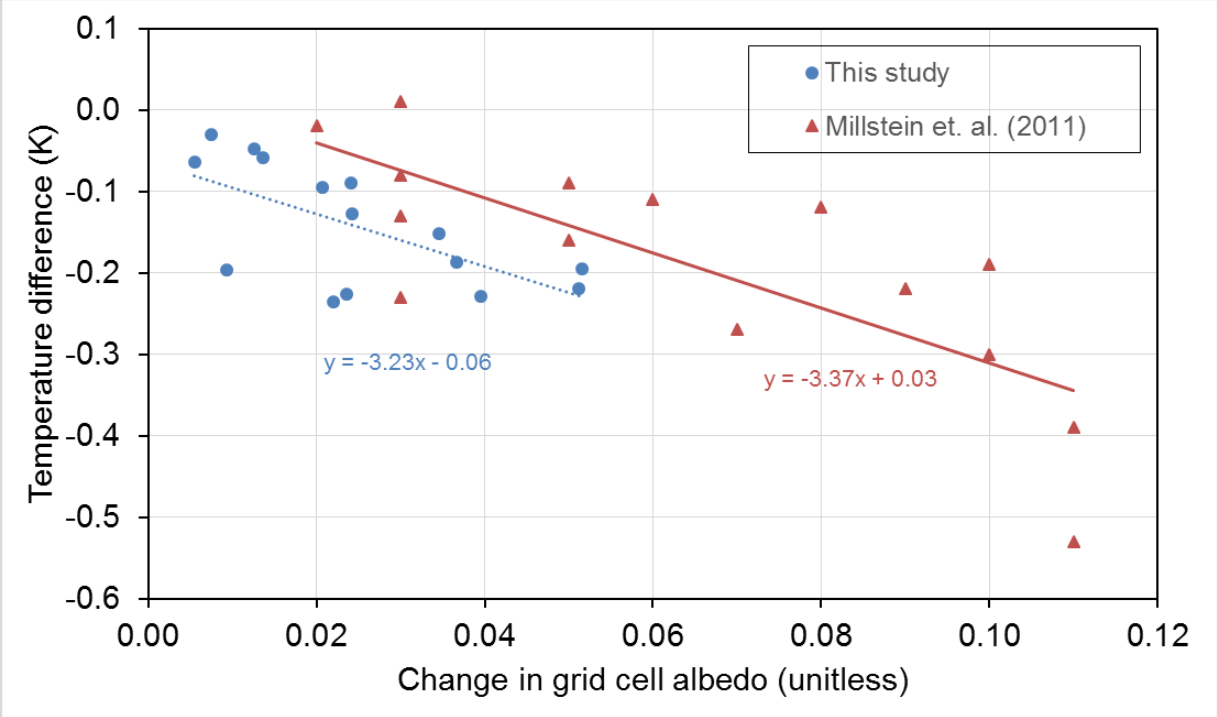

Figure 49. Comparison between the temperature reductions in current study and Millstein et al. (2011). Each point represents a different city. The temperature reductions in each city are graphed versus the changes in model grid cell albedo. Linear regression of the cities in each study with the equation of the regression is shown.

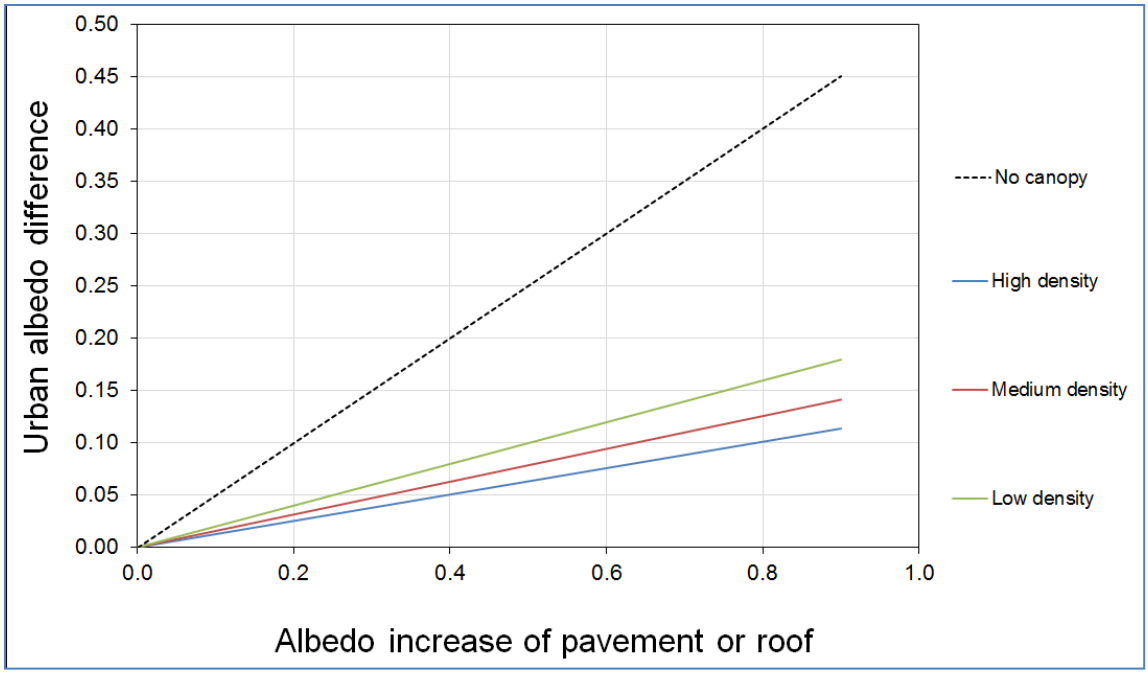

Figure 50. Comparing the changes in the urban albedo made by modifications in different sub-facets of canopy, between different densities of urban area. The dashed line shows the changes in the urban albedo, when there is no canyon (very wide canyon).

4.4. Building energy modeling

4.4.1. Comparison of modeled and actual building energy use

Comparing the energy intensities modeled in this study with EnergyPlus to the energy intensities reported in CBECS, RECS, and CEUS surveys served to corroborate the prototypes outputs are comparable to the state's documented energy. For each building type, the energy intensities vary widely within the surveys, which provide a range of realistic energy intensities. For cooling, the modeling results nearly match either or both of the survey results.

For heating, the modeling results are generally much lower than the CBECS and RECS results. One reason for this is that in the case of commercial buildings, CBECS values include much colder states like Alaska, Washington, and Oregon. When comparing the heating from the modeling with the CEUS results, the energy intensities match better; we expected this since CEUS is a study done solely for California. Another reason the heating energy intensities from the EnergyPlus simulations were lower than those reported in the surveys is the stricter construction standards on insulation and greater airtightness of the prototypes, thus reducing the need for heating energy. The modeling results of the two restaurants are four (sit-down restaurant) to 10 (fast-food restaurant) times larger than the survey values, but the CBECS survey suggest many restaurants also use electric heating. When we compared the gas heating source energy of the modeled restaurants to CBECS' restaurants electric heating source energy, we found an excellent match.

4.4.2. Represent vintage of California's building stock

The most common period of construction of California's building stock is between 1970 and 1979 (Appendix E). The building prototypes do not precisely represent the current building stock because the prototypes were simulated following 2008 Title 24 Standards. The prototypes were modeled with higher HVAC efficiency and better envelope insulation than what is found in typical current buildings. Hence, the simulations may have underestimated the direct and indirect building energy effects of cool pavements.

To represent the current building stock fully, we would have had to generate a new set of prototypes with 30+ year old typical construction properties (e.g., envelope insulation and HVAC system efficiencies). It would also require a detailed understanding of the building stock age in each California city. Simulation time would have doubled.

4.5. Pavement strategy guidance tool development

Again, the project objective was to develop sub-models for the life-cycle inventories, local climate effect, and building energy impacts, and incorporate the results into a draft decision tool. Therefore, we have only performed a cursory assessment of the results so are unable to discuss the policy and regulatory implications of the results or offer guidance on pavement management practices.

4.5.1. Comparison between pLCA tool results and the top-down approach for citywide building energy use

The pLCA tool calculates the use-stage building energy use effects through a detailed bottom-up methodology. By comparison, the methodology developed by Pomerantz et al. (2015) is top-down (TD). However, comparing the bottom-up building energy use effects derived with the pLCA tool to results calculated using the TD methodology outlined in Pomerantz et al. (2015) is a helpful way to validate the pLCA tool's findings.

If we apply the TD method to Sacramento and increase pavement albedo by 0.20, we come up with building energy use savings of less than 1.6 kWh/y·m^2. This estimate is an upper limit because several parameters are not considered in the TD approach, such as the winter heating penalty and winds from outside the city. Considering the omission of these other parameters, the top-down approach is in approximate agreement with the pLCA results. For the Sacramento example, the pLCA tool predicts electrical savings of about 0.1 kWh/y·m^2. This is also the order of magnitude saving implied in a top-down study of the Los Angeles Basin (Rosenfeld et al. 1998). All of these results indicate that the electrical energy savings due to the use of cooler pavements are modest.

5. Summary and Conclusions

We completed the first version of the pLCA tool. The various sub-models have been developed and used to generate the tool's backend datasets and algorithms. The tool features a user interface that allows the creation of two pavement treatment scenarios to compare their 50-year life cycle environmental effects. This includes the embodied energy and environmental effects from the extraction/manufacturing of the pavement materials, transportation of the materials to the city, and pavement construction in the materials and construction stage, and the removal and transportation of pavement materials to the landfill or recycling center in the EOL stage. The tool also reports the use-stage effects from changing pavement albedo, including changes to the local air temperature, citywide building energy, and local ozone.

Below are summaries and conclusions for the individual sub-models and investigations.

5.1. Local government pavement management practice

Local governments were surveyed to determine their pavement management practices with respect to how much of their networks they treated each year and what kinds of treatments they used. This information was needed to provide realistic data for users of the tool to consider when running scenarios for application of different pavement treatments.

- Most of the local government survey respondents treat a small portion of the public street pavement network every year, ranging from 1.3% to 20% with an average of 6.8%. The survey consisted of responses from cities as opposed to counties.
- The main pavement treatments used by local governments include slurry seal, chip seal, cape seal (chip seal plus micro-surfacing or slurry seal), asphalt or rubberized asphalt overlay, sand seal, and reconstruction which can include thicker overlays or in-place recycling with an overlay surface.
- Slurry seal is the major treatment used by the local government respondents, ranging from 28% to 82% of mileage treated with an average of 41.2%. Asphalt overlay is another major treatment, ranging from 13% to 100% of mileage treated with an average of 36.8%. Other treatments are used less frequently. Reconstruction is used on average as 6.6% of the total treatment, ranging from 3% to 28%.

5.2. Pavement albedo

Albedos for different pavement treatments were gathered from all available literature and some additional measurements were made in order to fill gaps in the literature. This information was needed to provide reasonable values for user of the tool to consider when running scenarios.

- Most currently utilized pavement treatments have relatively low steady-state albedo, ranging from 0.05 to 0.15 with average of 0.10 for asphalt concrete, and from 0.10 to 0.24 with average of 0.15 for chip seal. Albedos for slurry seals, cape seals and fog seals are generally lower. Experimental treatments include asphalt concrete with reflective coating with albedo from 0.20 to 0.30 with average of 0.25 and portland cement concrete with different surfaces ranging from 0.15 to 0.35 with average of 0.25.

- Although the initial albedo of treatments with reflective coating can be very high (e.g. up to 0.70), the albedo will decrease very quickly down to a value similar to the underlying pavement with currently available technologies for which information was available.
- With the pavement treatment practice and albedo currently used by local governments in California, most of the current pavement materials are asphalt concrete (including asphalt overlay) with an albedo of 0.10, which is the initial value of current pavement network albedo. Treatment practices used most local governments are dominated by slurry seal, which has a lower albedo of 0.08. With the current treatment practice and technologies, the average albedos of the public pavement network for most local governments remain constant or decrease slightly over a 50-year simulation period. Only the cities that are using a larger portion of higher albedo chip seal (e.g., Chula Vista) show a slight increase in albedo over the 50 years. The steady-state albedo change of pavement network in the 50 years is relatively low, ranging from -0.01 to 0.02 from the initial value of current pavement network albedo of 0.10. The average steady-state albedo of the pavement network in the 50 years across local governments therefore remains close to the initial value of current pavement network albedo, which is 0.10.
- Scenarios for changes in pavement treatment practice to use treatments with higher albedo were simulated for local governments in California. Sensitivity analysis was done for scenarios with different percentages of the network treated each year and different percentages of higher albedo treatment in the annual treatment program. The average albedo increases gradually from the initial value of 0.10 up to 0.12 to 0.23 over the 50-year analysis period for the nine scenarios. It takes approximately 10 to 50 years to reach the steady state with a stable network albedo. Due to the small portion of pavement network currently treated every year with treatments of relatively low steady-state albedo, the final steady-state albedo increase of pavement network in the 50 years is relatively low, ranging from 0.03 to 0.14. The 50-year average increase of the pavement network albedo is even lower, ranging from 0.02 to 0.12.

5.3. Reflective coatings

The available literature on the albedo and service life of reflective coatings, primarily used on asphalt surfaces, was investigated. The literature was utilized to provide reasonable values for tool users to consider when creating various pavement treatment scenarios. New life-cycle inventories were created for reflective coatings as part of this project because they were not available in the literature.

- Reflective coatings currently available fall into two categories: solvent-based coatings and water-based coatings. Solvent-based coatings have longer lives but may release volatile organic compounds (VOCs) into the atmosphere, with a negative impact on both the environment and human health. Water-based coatings have relatively shorter lives, but have less environmental impact.
- The durability of reflective coatings needs to be improved in order for them to be used more widely on low- and high-traffic volume streets.
- The emissions and potential toxicity from reflective coatings should be measured and evaluated to ensure limited negative environmental impacts.

5.4. Pavement material life-cycle inventories

To assemble California-specific values for use in the tool, life-cycle inventories and impacts of major input materials and energy sources were either developed through modeling in GaBi or adopted from available and reliable datasets (GaBi, ecoinvent, literature). These datasets and models were modified to reflect local practice and technologies better. The California electricity grid mix was modeled for the current grid mix and the Renewables Portfolio Standard (RPS) requirement of 33% of electricity from renewable resources by 2020.

Major findings from the life-cycle inventories were:

- Impacts of surface treatments (material production, transportation, and construction) can be relatively high compared to the impacts during the use stage in buildings. Therefore, surface treatment can be responsible for a large portion of the total impacts during the analysis period. Consequently, pavement life and the resultant replacement rate for treatments will have a large influence on total impacts and flows because pavement life will dictate the number of times a surface treatment will be applied during the analysis period.
- Impacts and flows are generally correlated with the thickness of the treatment and most of the impacts come from the materials' production for the binders (cement, asphalt) in the pavement material mixes. Most asphalt paving materials used in California use some reclaimed asphalt pavement (RAP) typically resulting in about 10 to 15% virgin binder replacement.
- The use of a concrete mix design with supplementary cementitious materials (SCMs) and other changes intended to reduce environmental impacts generated less than half the GHG produced by the conventional portland cement concrete mix with same thickness. This is because production of conventional portland cement is carbon-intensive and it is the main source of total GHG emissions in production of portland cement concrete. SCMs such as fly ash, slag cement, and silica foam are by-products of other industrial processes and therefore, bear less environmental impacts compared to conventional cement and can significantly reduce environmental impacts of portland cement concrete production. Currently, most local governments in California do not use SCMs in their concrete paving materials. Caltrans requires use of some SCMs, typically in the range of 20 to 25% cementitious replacement, in their concrete paving materials. Cement contents in concrete paving materials can also be reduced by changes in mix design practices.
- The reflective coatings had higher environmental impacts and flows that did other treatments of similar thickness (chip seals, slurry seals).
- The 2020 RPS electrical grid mix greatly reduces the environmental impacts and flows from electricity used for building cooling.

5.5. Local urban climate modeling and air quality analysis

This study investigated the effects of increasing pavement albedo on near-surface air temperature measured at the bottom of an urban canyon.

- The results show the largest temperature reductions at night, when the surface air temperature urban heat island is at its peak, and also in morning, when the incoming solar radiation is relatively high and planetary boundary layer height is low. The maximum summer time average temperature reduction at night (20:00 LST) is 0.62 K.

- The temperature reductions based on the albedo modifications of the pavement increases as the average urban fraction of the city increases. The temperature reductions also show a linear relation between the "temperature reductions sensitivity to urban fraction" and the albedo modifications applied to pavements with the sensitivity of 0.24 K for 24 h averaged associated with 0.40 albedo increase and 0.055 for 0.10 albedo increase in pavements.

5.6. Building energy modeling

In this study, we simulated the effects on cooling, heating, and lighting annual energy use from the widespread adoption of cool pavements. The direct effect of cool pavements was simulated by modifying building prototypes with adjacent streets. To incorporate the indirect effect of cool pavements, we used the temperature change results from the urban climate modeling.

- The base energy uses of all building prototypes were compared with cooling degree days (CDD18C) and heating degree days (HDD18C). The cooling energy use in all building prototypes increased with CDD18C and heating energy use increased with HDD18C.
- The direct effect of cool pavements is proportional to the building-to-street view factor. The direct effect in cooling energy use increases with building-to-street view factor, while the direct effect in heating energy use decreases with building-to-street view factor.
- As an illustration case, we calculated the savings of each building prototype when modifying the albedo of 25% of Sacramento's pavement to 0.40 from 0.10. The indirect effect of the cool pavement contributed more to the cooling and heating energy uses than the direct effect.
- The energy simulations were done on prototypes that follow 2008 Title 24 Standards. However, the average year of construction for California's current building stock lies between 1970 and 1979. Hence, the simulations may have underestimated the direct and indirect building energy effects of cool pavements. On the contrary, results may have been overestimated by not considering the impact of trees, parked cars, and traffic.

6. Recommendations

This section is divided into next steps for the pLCA tool and recommendations for additional related research.

6.1. Next steps for pLCA tool

We achieved the project objective by developing the first version of the pLCA tool. However, the tool needs some further refinements in future versions to make it accessible for general use and to update some of its features to improve usability. These refinements were originally planned for the second stage of the project. We recommend the following analyses and improvements.

- Create a panel of urban planners, local government sustainability managers, and pavement professionals who would use the tool to explore the environmental consequences of different pavement management decisions. This project focused only on the development of the tool. Therefore, a separate effort to develop, analyze and assess realistic scenarios is important before the tool is shared more broadly. This effort would provide an additional external quality check on the results and assumptions, identify potential areas for further research, and help future tool users understand how to interpret the results.
- Continue to update tool to improve its functionality and ease-of-use, to (1) make it more applicable and flexible for intended users; (2) improve its ease-of-use by creating a web-based application; (3) adjust granularity of data to improve specificity of results; and (4) enhance the presentation and communication of the results.
- Create a more detailed user guide based on ARB and tool user feedback.
- Partner with a local government organization to pilot the tool. We recommend finding a local government interested in evaluating different pavement management practices as a climate mitigation/adaptation strategy. The partnership would help the local government organization use the tool and interpret the results, and provide invaluable feedback to improve the tool.
- Perform life-cycle cost analysis (LCCA) studies to determine the cost of the different pavement strategies considered in the tool. Use the LCCA results to determine the cost-effectiveness of the use of cool pavements to reduce environmental and human impacts for comparison with the cost-effectiveness of other strategies. This has been done in Santero et al. 2013 to compare the cost-effectiveness of different strategies for reducing the impacts of concrete pavements.
- Produce tool guidance that has instructions for the periodic updates and maintenance to the tool and the back-end data. Because of continually changing conditions, assumptions on which the tool and sub-models are based may become obsolete over time.
- Consider inclusion in the tool of use-stage consequences unrelated to albedo change, such as vehicle-pavement interaction, that would provide a more complete perspective.
- Compare actual energy consumption data for a city with the results from the pLCA tool for a single day and one year. This test of the results would verify the building energy modeling methodology and allow easier scaling of the results.
- Evaluate the extent to which cool pavements can counter future climate warming by incorporating additional local climate scenarios into the tool. The current tool evaluates

results based on current climate conditions. However, new future climate warming scenarios could be developed based on existing studies in California for 2050. The results for the new scenarios will help local governments understand the climate adaptation potential of cool pavements for their jurisdictions.

- Update the building prototypes utilized for the development of the building energy modeling results to include older vintages. The mean period of construction of California's building stock is 1970-1979. The tool will then be updated to give use-stage results specific to the current state's building stock.
- Include the consequences of the visible reflectance of pavement on street lighting energy use in the tool. There are studies that note a relationship between pavement reflectance and street lighting. The effects would need to be studied in more detail to understand how they vary in CA cities with different urban design configurations.
- Research the effect of pavement albedo on pedestrian comfort and include the results in the tool. Previous studies would help inform the research to understand the sensitivity of pavement albedo on pedestrian comfort in CA cities.

6.2. Additional research recommendations

We have identified several research recommendations that are an extension from this project.

- Additional data are needed regarding how pavement surfaces age, including the degradation of albedo and their typical service life. This could include experimental work and modeling efforts to evaluate pavement albedo changes and service life under different traffic, climate and maintenance conditions. A Federal Highway Administration study is nearing publication which includes a nation-wide survey of pavement albedos for a wide variety of materials.
- Cool pavements are still an emerging technology and thus would greatly benefit from further research and development to increase albedo, improve durability, and ease installation.
- Track the location of environmental effects in the pavement life cycle, such as spatial distribution of emissions other than those having global effects
- Find more data regarding uncertainty of the inventories used in this study and regionalized data for asphalt production (expected in the next few years), which should be used to update the first-order estimates presented in the tool and for more extensive sensitivity analysis.
- Consider greenhouse emission timing using the work of Kendall (2012) when assessing global warming potential.
- We have shown that raising pavement albedo increases the solar flux incident on walls and windows. However, small modifications to a building's envelope can outweigh the cooling penalties associated with the direct effect of cool pavements. For future research, we propose quantifying how small modifications to the solar absorptance of walls and to the solar heat gain coefficient of windows influence the direct effect of cool pavements. The presence of trees near buildings may also have an important effect on the pavement-reflected solar flux that strike walls and windows, and thus affect building energy, so should be investigated further.
- Neither climate modeling nor the building energy modeling considered parked vehicles and traffic, which could affect the city-mean and local pavement albedo. Thus, a future study can evaluate the effect of vehicles on citywide pavement albedo.

- The tool does not take into account any shading by vegetation on pavements; therefore, additional research should be conducted to evaluate how trees alter the direct effect of cool pavements.
- Further analysis is suggested to study the influence of temperature reductions on the local air quality and the effects of cool pavements on other pollutants, such as semi-volatile aerosols, in each city. The research could investigate shifts in coastal wind patterns induced by reduction of land-ocean temperature differences.
- By cooling the surface of the street, increasing local street albedo also reduces the net longwave (thermal infrared) radiative heat transfer from street to building. This effect may be important, and was not considered in this project. Follow on research could investigate this effect further.
- The tool models the reduction of citywide air temperature from cool pavements. However, the adoption of a suite of urban heat mitigation strategies (cool roofs, cool pavements, and urban forestry) might further reduce air temperatures. In addition, there have been few field experiments to measure real world temperature reductions. Therefore, we suggest implementing a pilot project to evaluate the real-time benefits from the suite of mitigation strategies properly.

7. References

Akbari H, Matthews HD, Seto D. 2012. The long-term effect of increasing the albedo of urban areas. *Environmental Research Letters* 7(2), 024004 (10 pp).

Akbari H, Menon S, Rosenfeld A. 2009. Global cooling: increasing world-wide urban albedos to offset CO_2. *Climatic Change* 94(3), 275-286.

Akbari H, Pomerantz M, Taha H. 2001. Cool surfaces and shade trees to reduce energy use and improve air quality in urban areas. *Solar Energy* 70(3), 295-310.

Akbari H, Rose LS, Taha H. 1999. Characterizing the fabric of the urban environment: A case study of Sacramento, California. Technical Report LBNL-44688, Lawrence Berkeley National Laboratory, Berkeley, CA. http://dx.doi.org/10.2172/764362

Akbari H, Rose, LS. 2008. Urban surfaces and heat island mitigation potentials. *Journal of the Human-Environmental* System 11(2), 85-101.

Angelus Block Inc. 2015. Environmental Product Declaration Angelus Block Concrete Masonry Units. Angelus Block Inc., Sun Valley, CA. Retrieved 2015-12-10 from http://www.angelusblock.com/docs/Angelus_Block_CMU_Type_III_EPD.pdf

ASHRAE. 2004a. *ANSI/ASHRAE/IES Standard 62.1-2004 – Ventilation for Acceptable Indoor Air Quality: ASHRAE Standard.* American Society of Heating, Refrigerating, and Air-Conditioning Engineers. Atlanta, GA.

ASHRAE. 2004b. *ANSI/ASHRAE/IES Standard 90.1-2004 – Energy Standard for Buildings Except Low-Rise Residential Buildings: ASHRAE Standard.* American Society of Heating, Refrigerating, and Air-Conditioning Engineers. Atlanta, GA.

ASTM International. 2012. E903-12(2012): Standard test method for solar absorptance, reflectance, and transmittance of materials using integrating spheres. West Conshohocken, PA.

ASTM International. 2014. C1549-14(2014): Standard test method for determination of solar reflectance near ambient temperature using a portable solar reflectometer. West Conshohocken, PA.

ASTM International. 2015. E1918-06(2015): Standard test method for measuring solar reflectance of horizontal and low-sloped surfaces in the field. West Conshohocken, PA.

Aw J, Kleeman MJ. 2003. Evaluating the first-order effect of intraannual temperature variability on urban air pollution. *Journal of Geophysical Research* 108 (D12), 4365 (20 pp).

Bare J. 2012. Tool for the Reduction and Assessment of Chemical and Other Environmental Impacts (TRACI). TRACI Version 2.1 User's Guide. EPA/600/R-12/554 2012. Environmental Protection Agency, Cincinnati, OH. Retrieved 2015-12-15 from https://www.pre-sustainability.com/download/TRACI_2_1_User_Manual.pdf

Barman M, Vandenbossche J, Mu F, Gatti K. 2010. Compilation and Review of Existing Performance Data and Information. Minnesota Department of Transportation St. Paul, MN.

Bloomer BJ, Stehr JW, Piety CA, et al. 2009. Observed relationships of ozone air pollution with temperature and emissions. *Geophysical Research Letters* 36(9), L09803 (5 pp).

Bobes-Jesus V, Pascual-Muñoz P, Castro-Fresno D, Rodriguez-Hernandez J. 2013. Asphalt solar collectors: a literature review. *Applied Energy* 102, 962-970.

CalEPA, CDPH. 2013. Preparing California for extreme heat: guidance and recommendations. California Environmental Protection Agency and California Department of Public Health, Sacramento, CA. Retrieved 2015-12-05 from http://www.climatechange.ca.gov/climate_action_team/reports/Preparing_California_for_Extreme_Heat.pdf

Caltrans. 2008. Maintenance Technical Advisory Guide (MTAG) Volume I - Flexible Pavement Preservation Second Edition. California Department of Transportation, Sacramento, CA. Retrieved 2015-12-10 from http://www.dot.ca.gov/hq/maint/MTA_GuideVolume1Flexible.html

Caltrans. 2014. Pervious Pavement Design Guide. California Department of Transportation, Sacramento, CA. Retrieved 2015-12-10 from http://www.dot.ca.gov/hq/oppd/stormwtr/bmp/DG-Pervious-Pvm_082114.pdf

Caltrans. 2016. California Public Road Data 2014, Statistical Information Derived from the Highway Performance Monitoring System. California Department of Transportation, Sacramento, CA. Retrieved 2016-11-30 from http://www.dot.ca.gov/hq/tsip/hpms/.

Caltrans. 2003. Caltrans Maintenance Technical Advisory Guide (TAG), Chapter 2 Framework for Treatment Selection. California Department of Transportation, Sacramento, CA. Retrieved 2016-11-20 from http://www.dot.ca.gov/hq/maint/mtag/ch2_treatment_section.pdf

Caltrans. 2011. 2010 California Public Road Data. California Department of Transportation, Sacramento, CA. Retrieved 2016-11-30 from www.dot.ca.gov/hq/tsip/hpms/hpmslibrary/hpmspdf/2010PRD.pdf

Camalier L, Cox W, Dolwick P. 2007. The effects of meteorology on ozone in urban areas and their use in assessing ozone trends. *Atmospheric Environment* 41(33), 7127-7137.

Cao X, Tang B, Zhu H, Zhang A, Chen S. 2011. Cooling Principle Analyses and Performance Evaluation of Heat-Reflective Coating for Asphalt Pavement. *Journal of Materials in Civil Engineering*, 10.1061/(ASCE)MT.1943-5533.0000256, 1067-1075.

CARB. 2016. California Greenhouse Gas Emission Inventory – 2016 Edition. California Air Resources Board, Sacramento, CA. Retrieved 2016-07-27 from http://www.arb.ca.gov/cc/inventory/data/data.htm

CARB. 2014a. Greenhouse Gas Reductions from Ongoing, Adopted and Foreseeable Scoping Plan Measures. California Environmental Protection Agency – Air Resources Board. March 2014. Retrieved 2016-09-30 from https://www.arb.ca.gov/cc/inventory/data/bau.htm

CARB. 2014b. First Update to the Scoping Plan – Pursuant on the Framework. Pursuant to AB 32 The California Global Warming Solutions Act of 2006. California Environmental Protection Agency – Air Resources Board. May 2014. Retrieved 2016-09-30 from https://www.arb.ca.gov/cc/scopingplan/document/updatedscopingplan2013.htm

CAZIPCodes. 2015. California Zip Code List, ZIP Codes to go. Retrieved 2015-12-10 from http://www.zipcodestogo.com/California/

CEC. 2006. Our changing climate: assessing the risks to California. Publication CEC-500-2006-077, California Energy Commission, Sacramento, CA. Retrieved 2015-12-05 from http://www.energy.ca.gov/2006publications/CEC-500-2006-077

CEC. 2008a. Nonresidential compliance manual. Publication CEC-400-2008-017-CMF-Rev 1, California Energy Commission, Sacramento, CA. Retrieved 2015-12-10 from http://www.energy.ca.gov/title24/standards_archive/

CEC. 2008b. Residential compliance manual. Publication CEC-400-2008-016-CMF-Rev 1, California Energy Commission, Sacramento, CA. Retrieved 2015-12-10 from http://www.energy.ca.gov/title24/standards_archive/

CEC. 2014. Total electricity system power. California Energy Commission, Sacramento, CA. Retrieved 2015-12-10 from http://energyalmanac.ca.gov/electricity/total_system_power.html

CEC. 2015a. Climate Zones by ZIPcode List. California Energy Commission, Sacramento, CA. Retrieved 2-15-12-10 from http://www.energy.ca.gov/maps/renewable/BuildingClimateZonesByZIPCode.xlsx

CEC. 2015b. California Building Climate Zone Areas. California Energy Commission, Sacramento, CA. Retrieved 2015-12-10 from http://www.energy.ca.gov/maps/renewable/building_climate_zones.html

Chen F, Dudhia J. 2001. Coupling an advanced land-surface/ hydrology model with the Penn State/NCAR MM5 modeling system. Part I: model description and implementation. *Mon. Weather Rev*. 129(2001), 569-585.

Chen F, Kusaka H, Bornstein R, Ching J, Grimmond CSB, Grossman-Clarke S, Loridan T, Manning KW, Martilli A, Miao S, Sailor D, Salamanca FP, Taha H, Tewari M, Wang X, Wyszogrodzki AA, Zhang C. 2011. The integrated WRF/urban modeling system: development, evaluation, and applications to urban environmental problems. *International Journal of Climatology* 31, 273-288.

Corti A, Lombardi L. 2004. End life tyres: Alternative final disposal processes compared by LCA. *Energy* 29(12), 2089-2108.

CPUC. 2011. California Renewables Portfolio Standard. California Public Utilities Commission, Sacramento, CA. Retrieved 2015-05-04 from http://www.cpuc.ca.gov/PUC/energy/Renewables/

Deru M, Field K, Studer D, Benne K, Griffith B, Torcellini P, Liu B, Halverson M, Winiarski D, Rosenberg M, Yazdanian M, Huang J, Crawley D. 2011. US Department of Energy commercial reference building models of the national building stock. Technical report NREL/TP-5500-46861, National Renewable Energy Laboratory, Golden, CO. Retrieved 2015-12-10 from http://energy.gov/eere/buildings/commercial-reference-buildings

Donovan GH, Butry D. 2009. The value of shade: Estimating the effect of urban trees on summertime electricity use. *Energy and Buildings* 41, 662-668.

DoT Sacramento. 2009. Design and Procedures Manual: Section 15 - Street Design Standards. Department of Transportation, City of Sacramento. Retrieve 2015-12-10 from http://portal.cityofsacramento.org/Public-Works/Resources/Publications

DoT San Jose. 2010. Geometric Design Guidelines. Department of Transportation, City of San Jose, CA. Retrieved 2015-12-10 from https://www.sanjoseca.gov/index.aspx?NID=1882

ecoinvent. Life Cycle Inventory Database. Swiss Centre for Life Cycle Inventories, Zurich, Switzerland. Available at http://www.ecoinvent.org/

Ehlert JR, Smith TF. 1993. View factors for perpendicular and parallel rectangular plates. *Journal of Thermophysics and Heat Transfer* 7(1), 173-175.

EIA. 2003. Commercial Building Energy Consumption Survey (CBECS) – public use microdata. US Energy Information Administration, Washington, DC. Retrieved 2016-09-01 from http://www.eia.gov/consumption/commercial/data/2012/

EIA. 2009. Residential energy consumption survey (RECS) – public use microdata. US Energy Information Administration Washington, DC. Retrieved 2015-12-10 from http://www.eia.gov/consumption/residential/data/2009/

EnergyPlus. 2003. EnergyPlus version 8.5. Downloaded from https://energyplus.net/

Eurobitume. 2012. Life Cycle Inventory: Bitumen. Eurobitume, Brussels, Belgium. Retrieved 2015-12-10 from http://www.eurobitume.eu/homepage/focus/eurobitume-life-cycle-inventory-bitumen

Fiore AM, Naik V, Spracklen DV, et al. 2012. Global air quality and climate. *Chemical Society Reviews* 41(19) 6663-6683.

GaBi. 2014. Life Cycle Assessment Software Version 6.3. PE Order Number PEA-11128 Thinkstep, Leinfelden-Echterdingen, Germany.

Georgescu M, Moustaoui M, Mahalov A, Dudhia J. 2013. Summer-time climate impacts of projected megapolitan expansion in Arizona. *Nature Climate Change* 3, 37-41.

Gilbert H, Levinson R, Mandel B, Millstein D, Pomerantz M, Rosado P. 2014. Urban Heat Island Mitigation Phase 2 (Cool Communities: Phase 2). Publication CEC-500-2015-018, California Energy Commission, Sacramento, CA. Retrieved 2015-12-05 from http://www.energy.ca.gov/2015publications/CEC-500-2015-018/

Grell GA. 1993. Prognostic evaluation of assumptions used by cumulus parameterizations. *Mon. Wea. Rev.* 121, 764-787.

Harvey J, Kendall A, Lee IS, Santero N, Van Dam T, Wang T. 2010. Pavement Life Cycle Assessment Workshop: Discussion Summary and Guidelines. UCPRC-TM-2010-03, University of California Pavement Research Center, Davis, CA. Retrieved 2015-12-10 from http://www.ucprc.ucdavis.edu/P-LCA/resources.html

Harvey J, Kendall A, Lee IS, Santero N, Van Dam T, Wang T. 2011. Pavement life cycle assessment workshop, May 5–7, 2010 in Davis, California, USA. *The International Journal of Life Cycle Assessment* 16(9), 944–946.

Harvey J, Saboori A, Dauvergne M, Steyn W, Jullien A, Li H. 2014. Comparison of new pavement construction GHG and energy impacts in different regions. Proceedings of the International Symposium on Pavement LCA 2014, Davis, CA, October 14-16 2014. Retrieved 2015-12-10 from http://www.ucprc.ucdavis.edu/P-LCA2014/Papers.aspx

Harvey JT, Meijer J, Ozer H, Al-Qadi I, Saboori A, & Kendall A. 2016. Pavement Life-Cycle Assessment Framework. Technical report # FHWA-HIF-16-014. Prepared for Federal Highway Administration, Washington DC. Retrieved 2016-09-30 from http://www.fhwa.dot.gov/pavement/sustainability/hif16014.pdf

Hicks RG, Seeds SB, Peshkin DG. 2000. Selecting a preventative maintenance treatment for flexible pavements. Prepared for Foundation for Pavement Preservation, Washington, DC. Retrieved 2016-11-30 from https://www.wsdot.wa.gov/NR/rdonlyres/F27BCD0A-793C-48EF-A795-6C57136C4437/0/PavementPreservation.pdf

Homer C, Dewitz J, Fry J, Coan M, Hossain N, Larson C, Herold N, McKerrow A, VanDriel J, and Wickham J. 2007. Completion of the 2001 National Land Cover Database for the Conterminous United States. Photogrammetric Engineering and Remote Sensing, Vol. 73, No. 4, pp 337-341.

Hong SY, Lim JOJ. 2006. The WRF single-moment 6-class microphysics scheme (WSM6), *J. Korean Meteorol. Soc.* 42, 129-151.

Hong SY, Noh Y, Dudhia J. 2006. A new vertical diffusion package with an explicit treatment of entrainment processes. *Mon. Weather Rev.* 134, 2318-2341.

Howell J. 2015. A catalog of radiation heat transfer configuration factors, 3rd edition. University of Texas, Austin. http://www.thermalradiation.net/indexCat.html

Incropera FP. 2007. *Fundamentals of Heat and Mass Transfer, 6th Edition.* Section 13.1.1 - Radiation exchange between surfaces. Wiley & Sons.

Infoplease. 2015. Top 50 cities in the U.S. by population and rank. Retrieved 2015-11-24 from http://www.infoplease.com/ipa/a0763098.html

International Organization for Standardization. 2006. ISO 14040(2010): Environmental management—Life cycle assessment—Principles and framework. International Organization for Standardization, Geneva, Switzerland.

Itron Inc. 2006. California commercial end-use survey (CEUS). Publication CEC-400-2006-005, California Energy Commission, Sacramento, CA. Retrieved 2015-12-05 from http://www.energy.ca.gov/ceus

jEPlus. 2012. jEPlus – An EnergyPlus simulation manager for parametrics. Downloaded 2014-05-10 from http://www.jeplus.org/wiki/doku.php

Jones D, Harvey J, Li H, Want T, Wu R, Campbel B. 2010. Laboratory Testing and Modeling for Structural Performance of Fully Permeable Pavements: Final Report. UCPRC-RR-2010-01, University of California Pavement Research Center, Davis, CA.

Kendall, A. 2012. Time-adjusted global warming potentials for LCA and carbon footprints. *International Journal of Life Cycle Assessment* 17, 1042-1049.

Kleeman, MJ. 2007. A preliminary assessment of the sensitivity of air quality in California to global change. *Climatic Change* 87(S1), 273-292.

Kusaka H, Kimura F. 2004. Coupling a single-layer urban canopy model with a simple atmospheric model: Impact on urban heat island simulation for an idealized case. *Journal of the Meteorological Society of Japan* 82, 67-80.

Kusaka H, Kondo H, Kikegawa Y, Kimura F. 2001. A simple single-layer urban canopy model for atmospheric models: Comparison with multi-layer and slab models. *Boundary-Layer Meteorology* 101, 329-358.

Lenke L, Graul R.1986. Development of runway rubber removal specifications using friction measurement and surface texture for control. The Tire Pavement Interface, ASTM STP 929, MG Pottinger and TJ Yagger, Eds, American Society of Testing and Materials, 72-88.

Li D, Bou-Zeid E, Oppenheimer, M. 2014. The Effectiveness of Cool and Green roofs as Urban Heat Island Mitigation Strategies, *Environmental Research Letters* 9(5), 055002, 16 pp.

Li D, Bou-Zeid E. 2014. Quality and Sensitivity of High-resolution Numerical Simulation of Urban Heat Islands, *Environmental Research Letters* 9(5), 055001, 14 pp.

Li H, Harvey J, Kendall A, 2013. Field measurement of albedo for different land cover materials and effects on thermal performance. *Building and Environment* 59, 536-546.

Li H, Saboori A, Cao X. 2014. Reflective coatings for cool pavements: information synthesis and preliminary case study for life cycle assessment. Proceedings of the International Symposium on Pavement LCA 2014, Davis, CA, October 14-16 2014. Retrieved 2015-12-10 from http://www.ucprc.ucdavis.edu/P-LCA2014/Papers.aspx

Lynn BH, Carlson TN, Rosenzweig C, Goldberg R, Druyan L, Cox J, Gaffin S, Parshall L, Civerolo K. 2009. A modification to the Noah LSM to simulate heat mitigation strategies in the New York city metropolitan area. *Journal of Applied Meteorology and Climatology* 48, 200-216.

Mahmud A, Tyree M, Cayan D, et al. 2008. Statistical downscaling of climate change impacts on ozone concentrations in California. *Journal of Geophysical Research* 113, D21103 (12 pp).

Marceau M, Nisbet MA, Van Geem MG. 2006. Life cycle inventory of portland cement manufacture. PCA R&D serial no. 2095b, Portland Cement Association, Skokie, IL. Retrieved 2015-12-10 from http://www.nrmca.org/taskforce/item_2_talkingpoints/sustainability/sustainability/sn2095b%20-%20cement%20lci%202006.pdf

Marceau M, Nisbet MA, Van Geem MG. 2007. Life Cycle Inventory of Portland Cement Concrete. PCA R&D serial no. 3007, Portland Cement Association, Skokie, IL. Retrieved 2016-07-26 from www.nrmca.org/taskforce/item_2_talkingpoints/sustainability/sustainability/sn3011%5B1%5D.pdf

Mayor's Office of Sustainability. 2015. Los Angeles Climate Action Report: Updated 1990 Baseline and 2013 Emissions Inventory Summary. City of Los Angeles. Retrieved 2016-09-30 from http://www.lamayor.org/sites/g/files/wph446/f/landing_pages/files/pLAn%20Climate%20Action-final-highres.pdf

Millstein DE, Harley RA. 2009. Impact of climate change on photochemical air pollution in Southern California. *Atmospheric Chemistry and Physics* 9(11), 3745-3754.

Millstein DE, Menon S. 2011. Regional climate consequences of large-scale cool roof and photovoltaic array deployment. *Environmental Research Letters* 6, 034001, 9pp.

Mlawer EJ, Taubman SJ, Brown PD, Iacono MJ, Clough SA. 1997. Radiative transfer for inhomogeneous atmospheres: RRTM, a validated correlated-k model for the longwave. Journal of Geophysical Research 102, 16663-16682.

NLCD. 2000. National Land Cover Dataset. United States Geological Survey, Washington, DC. Retrieved 2015-12-10 from http://pubs.er.usgs.gov/publication/fs10800

NovaLynxCorporation. 240-8104 Albedometer. Nova Lynx Corporation, Grass Valley, CA. Available at http://novalynx.com/store/pc/240-8104-Albedometer-11p509.htm

NREL. 2013. Measurement and Instrumentation Data Center Solar Position Calculator. National Renewable Energy Laboratory, Golden, CO. Retrieved 2015-12-10 from http://www.nrel.gov/midc/solpos/spa.html

Oke TR. 1982. The energetic basis of the urban heat island. *Q.J.R. Meteorol. Soc.*, 108, 1-24.

PG&E. 2014. 2013 Preliminary Annual 33% RPS Compliance Report of Pacific Gas and Electric Company (U 39 E) (Public Version). Pacific Gas and Electric Company, San Francisco, CA. Retrieved 2014-09-07 from http://www.cpuc.ca.gov/RPS_Reports_Docs

PNNL. 2014. Residential Prototype Building Models. Pacific Northwest National Laboratory, Richland, WA. Retrieved 2015-12-10 from https://www.energycodes.gov/development/residential/iecc_models

Pomerantz M, Akbari H, Chen A, Taha H, Rosenfeld AH. 1997. Paving materials for heat island mitigation. Technical Report LBL-38074, Lawrence Berkeley National Laboratory, Berkeley, CA. http://dx.doi.org/10.2172/291033

Pomerantz M, Akbari H, Harvey J. 2000. Cooler reflective pavements give benefits beyond energy savings: durability and illumination. Proceedings of the ACEEE Summer Study on Energy Efficiency in Buidings, Asilomar, CA, August 20-25 2000. Retrieved 2015-12-10 from http://aceee.org/files/proceedings/2000/data/papers/SS00_Panel8_Paper24.pdf

Pomerantz M, B Pon, H Akbari, SC Chang. 2000. The Effect of Pavements' Temperatures on Air Temperatures in Large Cities. Technical Report LBNL-45370, Lawrence Berkeley National Laboratory, Berkeley, CA. Retrieved 2015-12-10 from https://heatisland.lbl.gov/publications/effect-pavements-temperatures-air

Pomerantz M, Rosado PJ, Levinson R. 2015. A simple tool for estimating city-wide annual electrical energy savings from cooler surfaces. *Urban Climate* 14(2), 315-325.

Pomerantz, M., H. Akbari, S-C. Chang, R. Levinson, and B. Pon. 2003. Examples of Cooler Reflective Streets for Urban Heat-Island Mitigation: Portland Cement Concrete and Chip Seals. Technical Report LBNL-49283, Lawrence Berkeley National Laboratory, Berkeley, CA. Retrieved 2015-12-10 from https://heatisland.lbl.gov/publications/examples-cooler-reflective-streets

Pouget S, Sauzéat C, Benedetto H, Olard F. 2012. Viscous energy dissipation in asphalt pavement structures and implication for vehicle fuel consumption. *Journal of Materials in Civil Engineering* 24(5), 568-576.

Pusede SE, Steiner AL, Cohen RC. 2015. Temperature and recent trends in the chemistry of continental surface ozone. *Chemical Reviews* 115(10), 3898-3918.

Rasmussen DJ, Hu J, Mahmud A, et al. 2013. The ozone–climate penalty: past, present, and future. *Environmental Science & Technology* 47(24), 14258-14266.

Rosenfeld AH, Akbari H, Bretz S, Fishman BL, Kurn DM, Sailor D, Taha H. 1995. Mitigation of urban heat islands: materials, utility programs, updates. *Energy and Buildings* 22, 255-265.

Rosenfeld AH, Akbari H, Romm JJ, Pomerantz M. 1998. Cool communities: strategies for heat island mitigation and smog reduction. *Energy and Buildings* 28(1), 51-62.

Rosenzweig C, Solecki W, Slosberg R. 2006. Mitigating New York City's heat island with urban forestry, living roofs, and light surfaces. New York State Energy Research and Development Authority, Albany NY. Retrieved 2015-12-10 from http://www.giss.nasa.gov/research/news/20060130/103341.pdf

Rossum GV, Drake FL. 2001. Python Reference Manual. PythonLabs. Virginia. Retrieved 2015-12-10 from http://www.python.org

Ryan Snyder Associates. 2011. Los Angeles County Model Design Manual for Living Streets. Ryan Snyder Associates, Transportation Planning for Livable Communities. Retrieved 2015-12-10 from http://www.modelstreetdesignmanual.com/

Sailor DJ, Kalkstein LS, Wong E. 2002. The potential of urban heat island mitigation to alleviate heat related mortality: methodological overview and preliminary modeling results for Philadelphia. Proceedings of the 4th Symposium on the Urban Environment, vol. 4. May 2002, Norfolk, VA, 68–69.

Sailor DJ. 1995. Simulated urban climate response to modifications in surface albedo and vegetative cover. *Journal of Applied Meteorology* 34, 1694–1700.

Santamouris M. 2014. Cooling the cities - A review of reflective and green roof mitigation technologies to fight heat island and improve comfort in urban environments. *Solar Energy* 103, 682-703.

Santero N, Horvath A. 2009. Global warming potential of pavements. *Environmental Research Letters* 4, 034011, 7pp.

Santero N, Masanet E, Horvath A. 2011. Life-cycle assessment of pavements. Part I: Critical review. Resources, *Conservation and Recycling* 55, 801–809.

Santero, N., Loijos, A., & Ochsendorf, J. 2013. Greenhouse gas emissions reduction opportunities for concrete pavements. *Journal of Industrial Ecology* 17, 859-868.

SCE. 2014. Southern California Edison Company's (U 338-E) 2013 Preliminary Annual 33% Report (Public Version). Southern California Edison Company, Rosemead, CA. Last retrieved 2014-09-03 from: http://www.cpuc.ca.gov/RPS_Reports_Docs

SDG&E. 2014. 2013 Preliminary Annual 33% RPS Compliance Report. San Diego Gas and Electric Company, San Diego, CA. Retrieved 2014-09-03 from http://www.cpuc.ca.gov/RPS_Reports_Docs

Sillman S, Samson PJ. 1995. Impact of temperature on oxidant photochemistry in urban, polluted rural and remote environment. *Journal of Geophysical Research* 100(D6), 11497-11508.

Simpson JR, McPherson EG. 1996. Potential of tree shade for reducing residential energy use in California. *Journal of Arboriculture* 22(1) 10-18.

Skamarock WC, Klemp JB, Dudhia J, Gill DO, Barker DM, Duda MG, Huang XY, Wang W, Powers JG. 2008. A description of the advanced research WRF version 3. NCAR Tech. Note NCAR/TN 475 STR, 125, National Center for Atmospheric Research, Boulder, CO. Retrieved 2015-12-10 from http://www2.mmm.ucar.edu/wrf/users/docs/arw_v3.pdf

Steiner AL, Davis AJ, Sillman S, et al. 2010. Observed suppression of ozone formation at extremely high temperatures due to chemical and biophysical feedbacks. Proceedings of the National Academy of Sciences of the United States of America 107(46), 19685-19690.

Steiner AL, Tonse S, Cohen RC, et al. 2006. Influence of future climate and emissions on regional air quality in California. *Journal of Geophysical Research* 111(D18303), (22 pp).

Synnefa A, Dandou A, Santamouris M, Tombrou M. 2008. On the use of cool materials as a heat island mitigation strategy. *Journal of Applied Meteorology Climatology* 47, 2846–2856.

Taha H. 2008a. Meso-urban meteorological and photochemical modeling of heat island mitigation. *Atmospheric Environment* 42 (38), 8795– 8809.

Taha H. 2008b. Urban surface modification as a potential ozone airquality improvement strategy in California: A mesoscale modeling study. *Boundary-Layer Meteorology* 127, 219–239.

Taha H. 2013. Meteorological, emissions and air-quality modeling of heat-island mitigation: recent findings for California, USA. *International Journal of Low-Carbon Technologies Advance*, 0, 1-12.

Taha H. 2008c. Episodic performance and sensitivity of the urbanized MM5 (uMM5) to perturbations in surface properties in Houston TX. *Boundary-Layer Meteorology*, 127, 193–218.

Taleghani M, Sailor D, Ban-Weiss GA. 2016 Micrometeorological simulations to predict the impacts of heat mitigation strategies on pedestrian thermal comfort in a Los Angeles neighborhood. *Environmental Research Letters* 11, 024003, 12pp.

U.S. Census. 2002. 2000 TIGER/Line Shapefiles. Retrieved 2015-12-13 from http://www.census.gov/geo/maps-data/data/tiger-data.html

U.S. Census. 2014a. 2010 TIGER/Line Shapefiles: Places (2010). Retrieved 2015-12-10 from http://www.census.gov/cgi-bin/geo/shapefiles2010/main

U.S. Census. 2014b. Table GCT-PH1 Population, Housing Units, Area, and Density: 2010 - State -- Place and (in selected states) County Subdivision. Retrieved 2015-12-10 from http://factfinder.census.gov/faces/nav/jsf/pages/index.xhtml

USEPA. 2008. Reducing urban heat islands: Compendium of strategies, Chapter 1 – Heat Island Basics. U.S. Environmental Protection Agency, Washington, DC. Retrieved 2015-12-14 from http://www.epa.gov/sites/production/files/2014-06/documents/basicscompendium.pdf

USGS. 2014. NLCD 2006 Percent Developed Imperviousness (2011 Edition). Multi-Resolution Land Characteristics Consortium, United States Geological Survey, Menlo Park, CA. Retrieved 2015-12-10 from http://gisdata.usgs.gov/TDDS/DownloadFile.php?TYPE=nlcd2006&FNAME=nlcd_2006_impervious_2011_edition_2014_10_10.zip

USZIPCodes. 2015. Zip Code Database. Retrieved 2015-12-10 from http://www.unitedstateszipcodes.org/zip-code-database/

Wang T, Lee IS, Kendall A, Harvey J, Lee EB, Kim, C. 2012. Life Cycle Energy Consumption and GHG Emission from Pavement Rehabilitation with Different Rolling Resistance. *Journal of Cleaner Production* 33, 86-96.

WBT. 2011. White Box Technologies – weather data for energy calculations. Retrieved 2015-12-10 from http://weather.whiteboxtechnologies.com/

Wikipedia 2015. City block. In *Wikipedia*. Retrieved 2015-12-10 from https://en.wikipedia.org/wiki/City_block

Xi F, Davis SJ, Ciais P, Crawford-Brown D, Guan D, Pade C, Shi T, Syddall M, Lv J, Ji L, Bing L. 2016. Substantial global carbon uptake by cement carbonation. *Nature Geoscience*. Dec 1;9(12):880-3.

Xu X, Wildnauer M, Gregory J, Kirchain R. 2016. Accounting for Variation in Life Cycle Inventories: The Case of Portland Cement Production in the US. InRewas 2016 (pp. 145-149). Springer International Publishing.

ZCSC. 2015. Sacramento County Zoning Code. Sacramento County, CA. Retrieved 2015-12-10 from http://www.per.saccounty.net/LandUseRegulationDocuments/Pages/Sacramento%20County%20Zoning%20Code.aspx

Zhang J, Zhang K, Liu J, Ban-Weiss GA. 2016. Revisiting the climate impacts of cool roofs around the globe using an earth system model. *Environmental Research Letters* 11, 084014, 12 pp.

Zhao Z, Chen SH, Kleeman MJ, Tyree MJ, Cayan D. 2011. The Impact of Climate Change on Air Quality-Related Meteorological Conditions in California. Part I: Present Time Simulation Analysis. *Journal of Climate* 24, 3344-3361.

Zhou J, Signore J, Harvey J. 2012. Superpave Implementation Phase I: Determining Optimum Binder Content. UCPRC-TM-2012-03, University of California Pavement Research Center, Davis, CA.

Zhou YZJ, Shepherd M. 2010. Atlanta's urban heat island under extreme heat conditions and potential mitigation strategies. *Natural Hazards* 52, 639–668.

8. Appendices

Appendix A

A Full literature review

The full literature review for cool pavements and pavement life-cycle assessment can be found online at http://goo.gl/jqKtC3.

Appendix B

B Screenshots of the pavement life-cycle inventory models in GaBi

Figure B-1. Aggregate-crushed plan in GaBi.

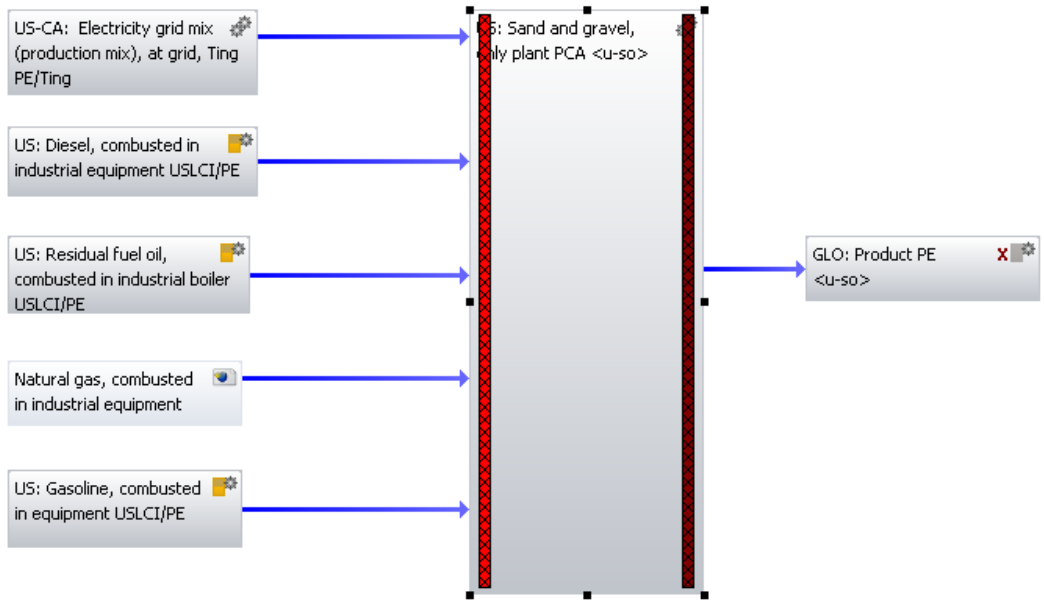

Figure B-2. Aggregate-uncrushed plan in GaBi.

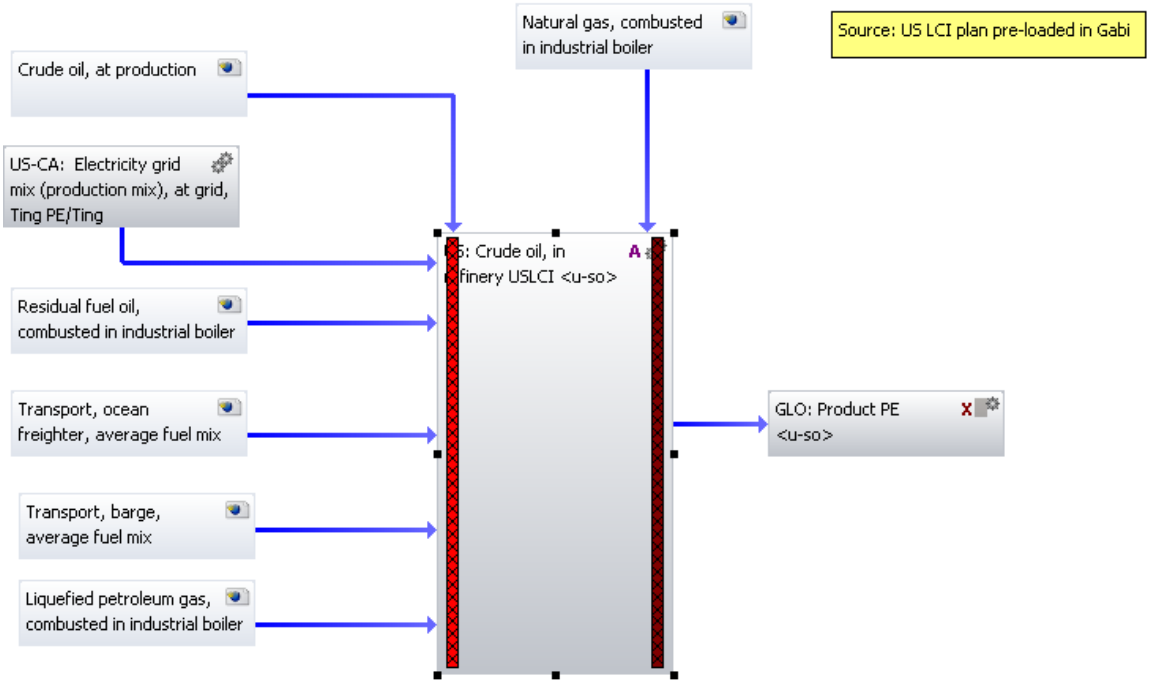

Figure B-3. Bitumen plan in GaBi.

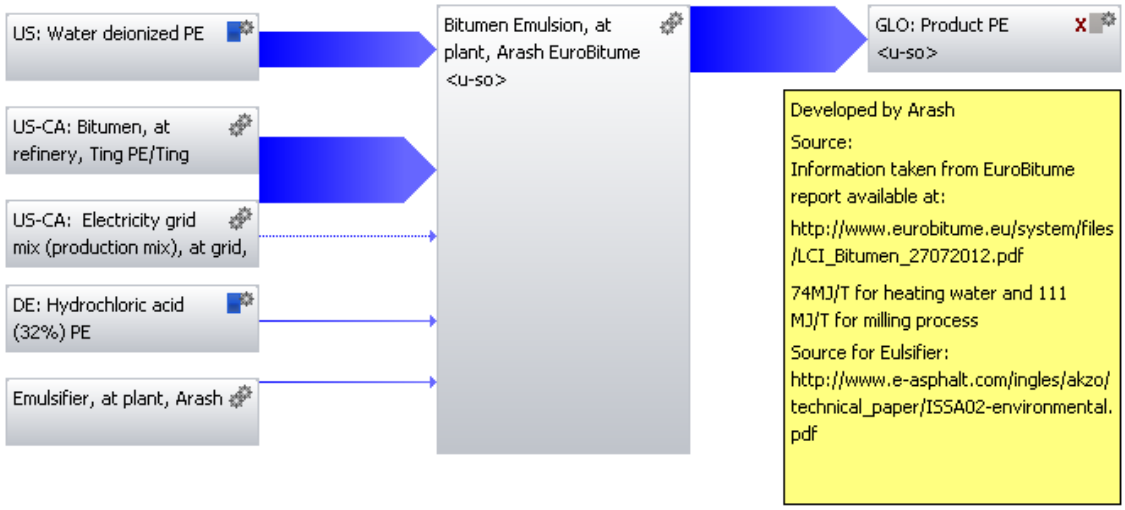

Figure B-4. Bitumen emulsion plan in GaBi.

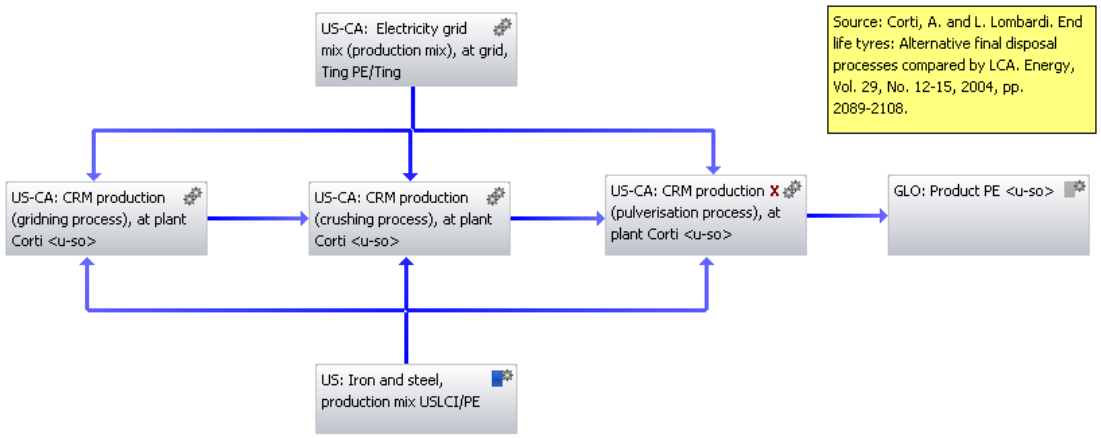

Figure B-5. CRM plan in GaBi.

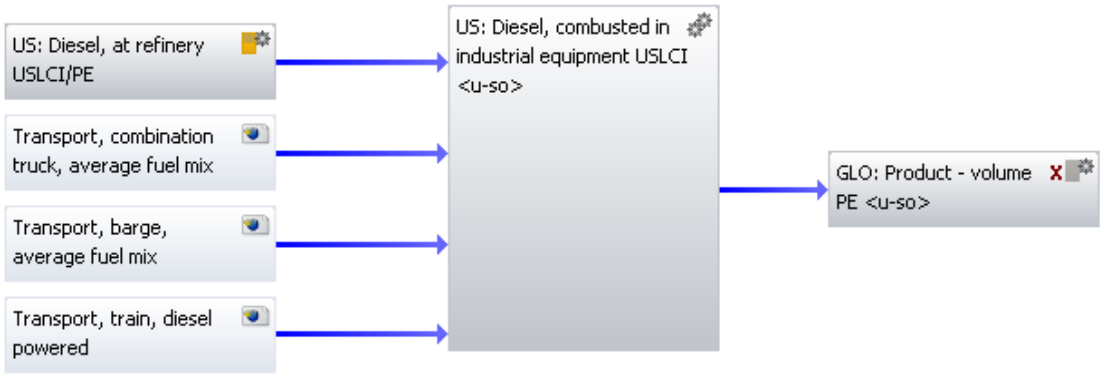

Figure B-6. Diesel combusted in industrial equipment plan in GaBi.

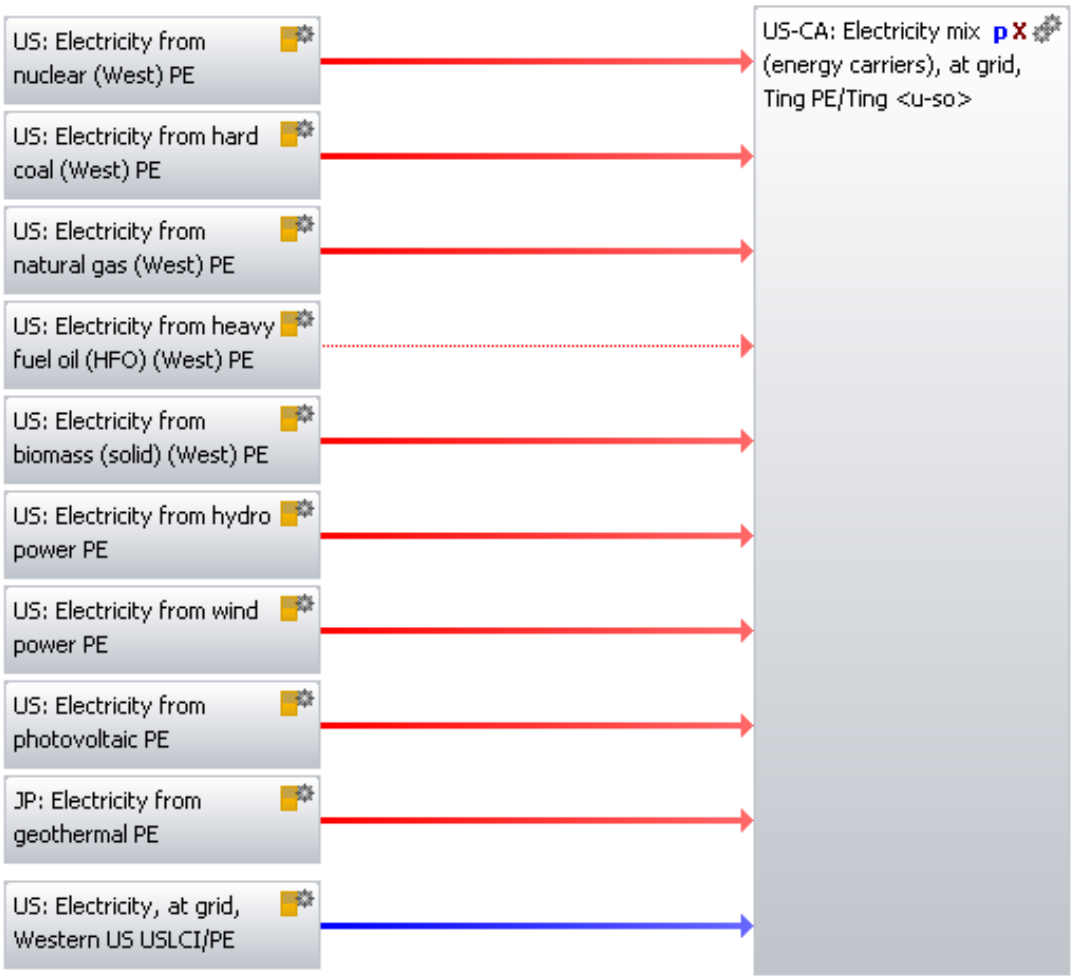

Figure B-7. Electricity plan in GaBi.

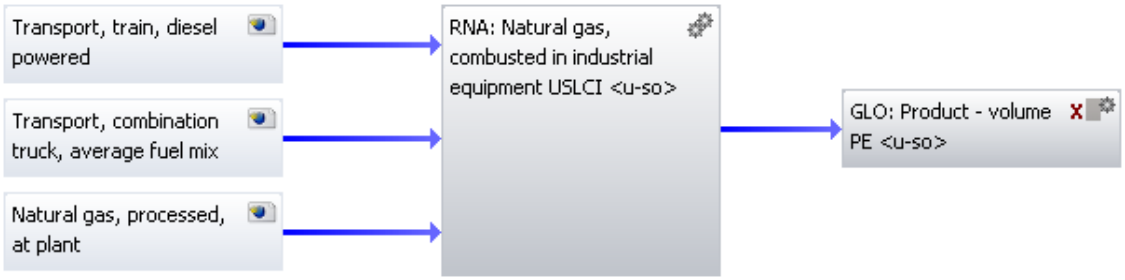

Figure B-8. Natural gas combusted in industrial equipment plan in GaBi.

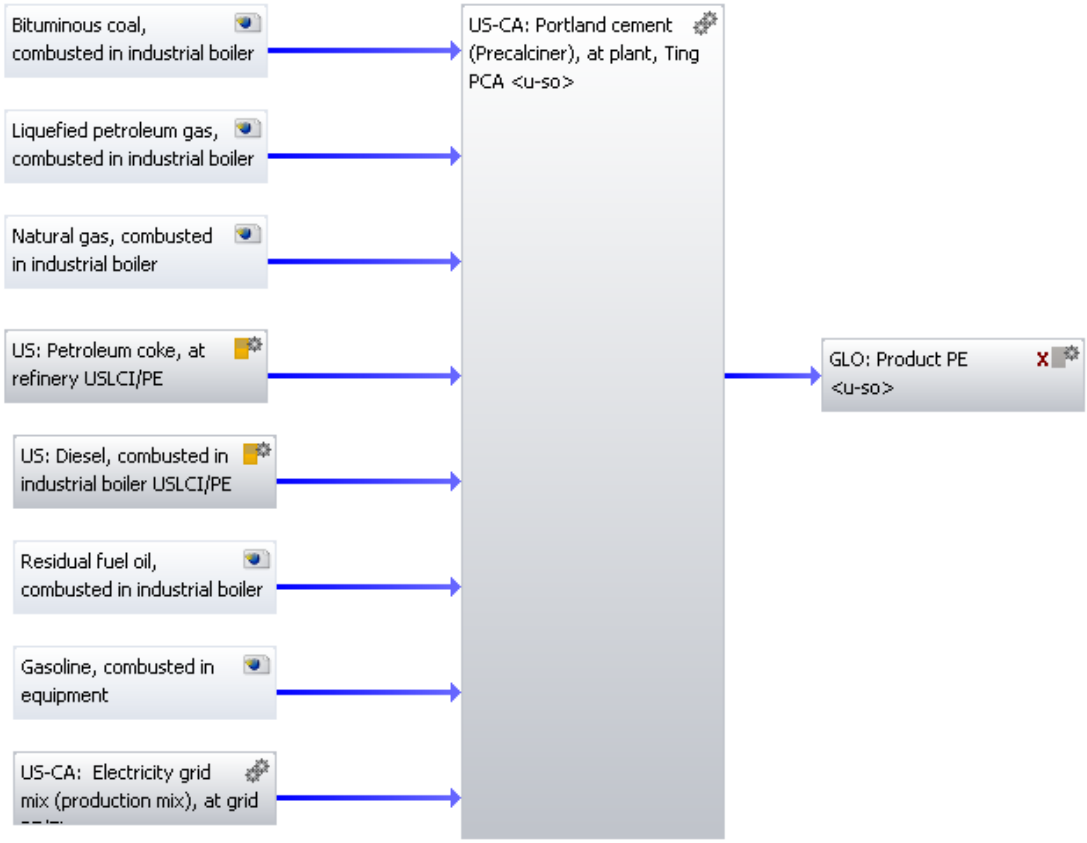

Figure B-9. Regular portland cement plan in GaBi.

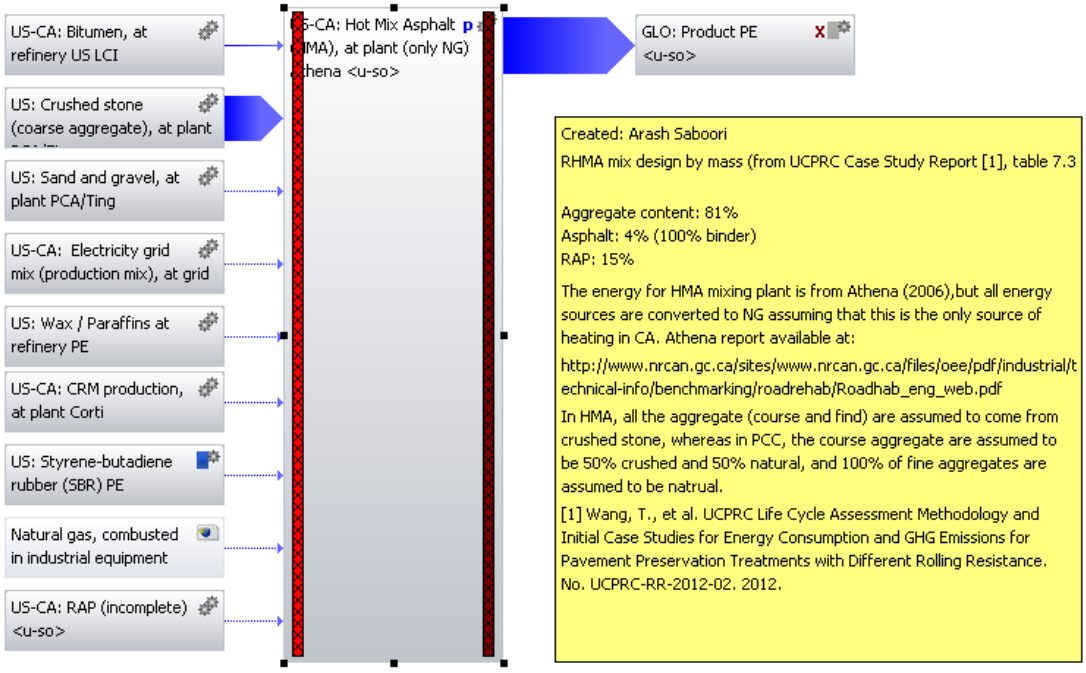

Figure B-10. HMA plan in GaBi.

Appendix C

C Prototype schematics

Table C-1 shows schematics of the 10 modified building energy model prototypes. The vertical purple surfaces represent the wall of a neighboring building of the same height as the modeled prototype. The horizontal purple surfaces represent the local roads. The setback width and dimensions for the neighboring walls and roads follow the Sacramento County Zone Code (ZCSC) (ZCSC 2015). Note that the illustrations of the large hotel and large office do not show the horizontal and vertical purple surfaces; these two prototypes were simulated with the walls and roads, but the buildings were not rendering correctly in our 3D modeling software.

Table C-1. Illustration of modified prototypes. The purple surfaces represent the roads (horizontal surfaces) and neighboring buildings (vertical surfaces). The illustrations of the large hotel and large office omit the horizontal and vertical surfaces because they were not rendering correctly in our 3D modeling software.

Large hotel	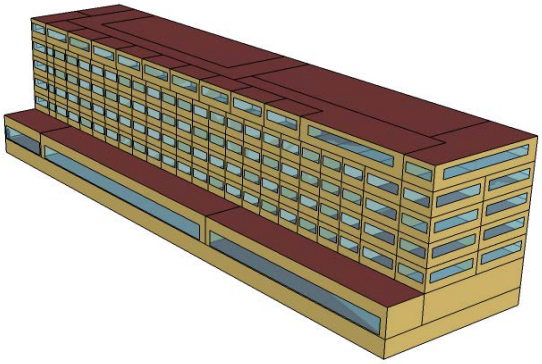
Large office	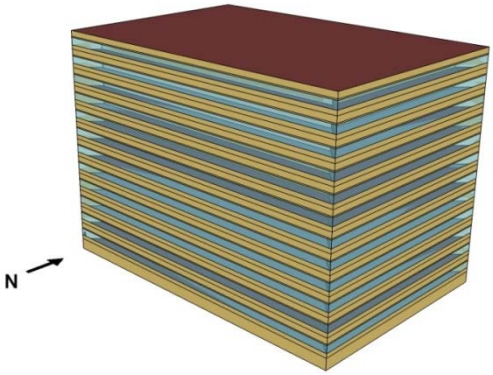

Medium office

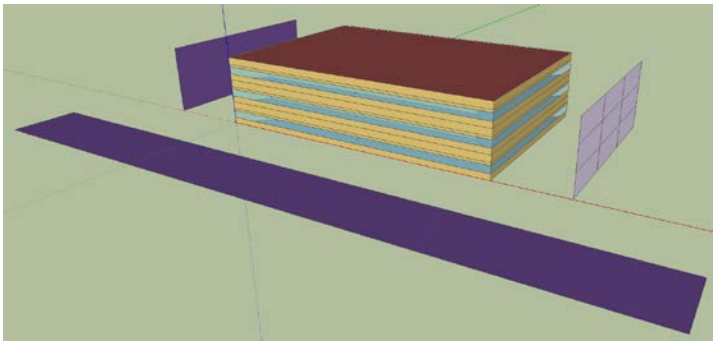

Fast-food restaurant

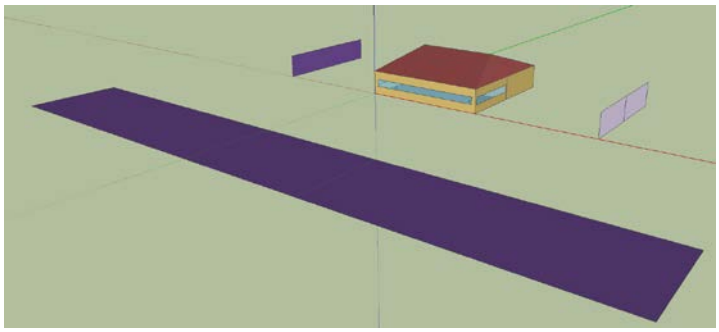

Sit-down restaurant

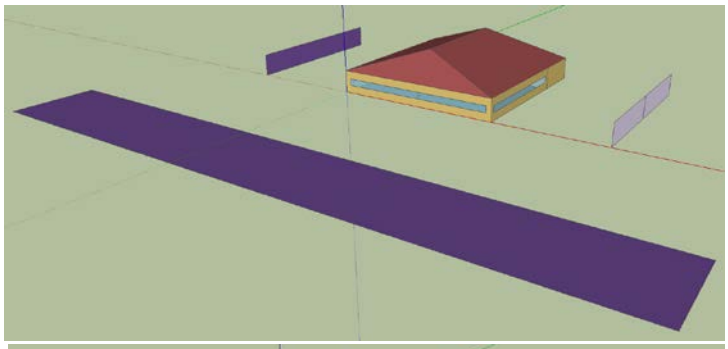

Retail stand-alone

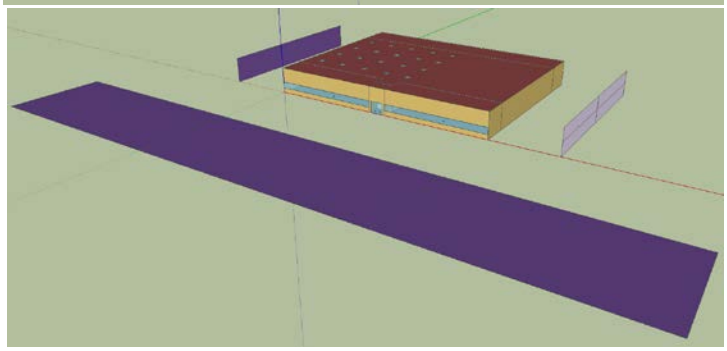

Strip mall retail

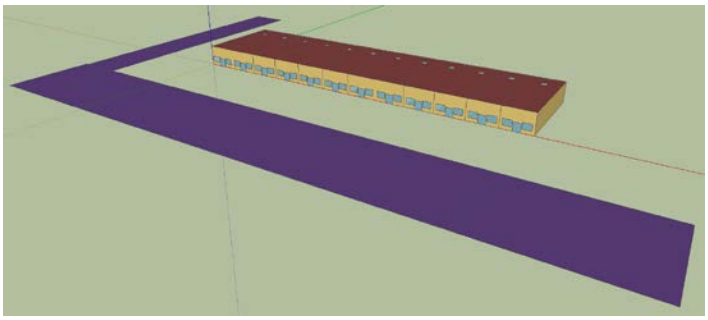

Primary school

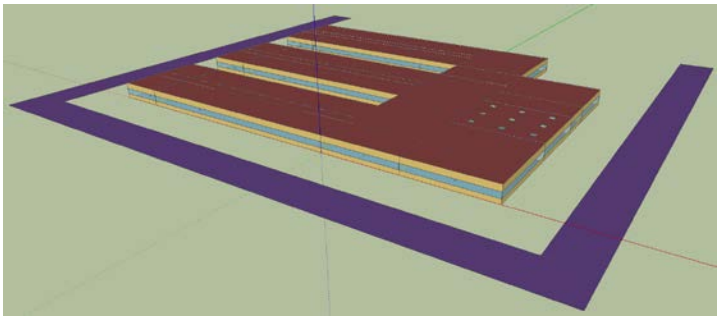

Apartment building

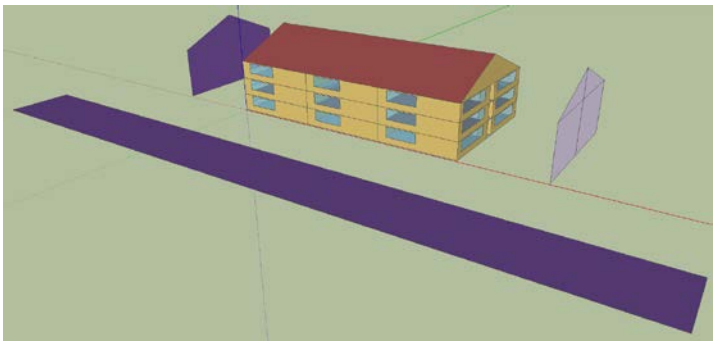

Single-family home

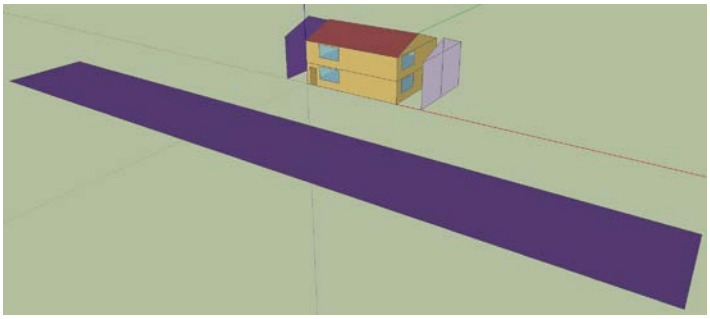

Appendix D

D Urban Canyon Albedo Model

D.1 Overview

We present a three-reflection urban canyon albedo model (UCAM). A three-reflection model is one that it tracks up to three reflections from canyon surfaces. The model treats the canyon as of infinite length with a floor composed of a street and surrounding setbacks. The dimension and albedo of the canyon surfaces (street, setback, and walls) can be varied, and allows for the canyon being oriented either north-south (N-S) or east-west (E-W). The model also considers the solar position to address the radiative effect of shadows casted by the canyon walls. The air between the surfaces is assumed non-absorbing, and all surfaces are treated as Lambertian (purely diffuse) reflectors.

The proposed UCAM calculates the amount of radiant solar power per unit of canyon length [W/m] (hereafter, 'flux'; symbol *J*) that flows downward through the canyon ceiling. The model computes the flux that is reflected from the surfaces—walls, setbacks, and street—and exits through the ceiling. Canyon albedo is computed as the ratio of upward to downward flux through the canyon ceiling.

D.2 Theory

D.2.1 Canyon geometry

The proposed UCAM defines the canyon geometry as shown in Figure D-1. Surface 1 is the canyon floor, while surface 2 is the canyon ceiling; floor width w_1 equals ceiling width w_2. The canyon floor includes a central street (dashed gray line) and two setbacks of equal width (dashed green lines). The floor is divided into *N* small segments of equal width w_0, with any particular segment referred to as surface 0. Based on location, each segment is identified as part of the street or part of a setback.

Surfaces 3 and 4 are the left and right walls, assumed to be of equal height ($h_3 = h_4$). Each wall may be partially shaded at times. Surfaces 3u and 4u refer to the unshaded section of each wall, with heights h_{3u} and h_{4u}, respectively.

Surfaces 5 and 6 are the canyon's light sources. Surface 5 (sun) is the source of beam (a.k.a. direct) sunlight. Surface 6 (sky) is the source of diffuse sunlight.

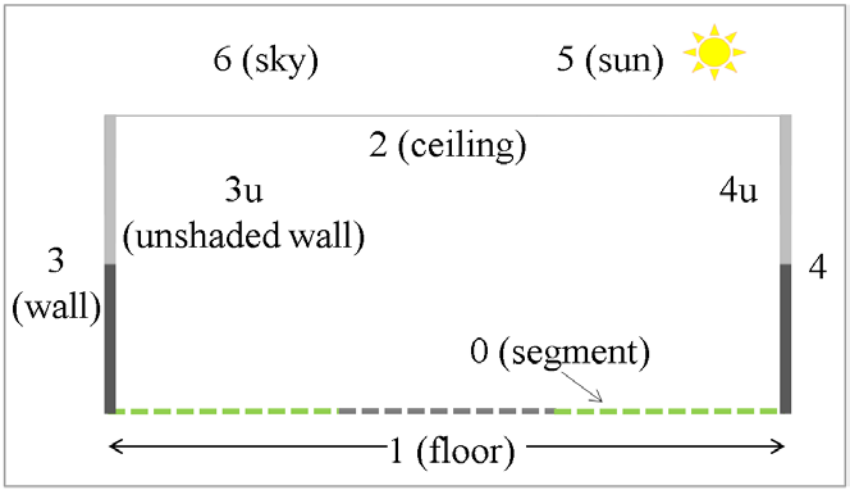

Figure D-1. Elements of the urban canyon (surfaces 0 – 4) and its light sources (surfaces 5 and 6).

D.2.2 Shadow on canyon floor

During the day, the canyon walls may partially or completely shade the canyon floor. The width of the canyon w_c is equal to the street width w_{st} plus twice the setback width w_{sb}. The width of the canyon floor shadow, w_s, depends on sun position and canyon orientation. To illustrate, Figure D-2 shows the shadow cast by a 10 m high wall over a 30 m wide floor (10 m street + two 10 m setbacks) in Sacramento, CA on October 21 at 08:00 local standard time (LST). The street extends N-S (panel a) and E-W (panel b).

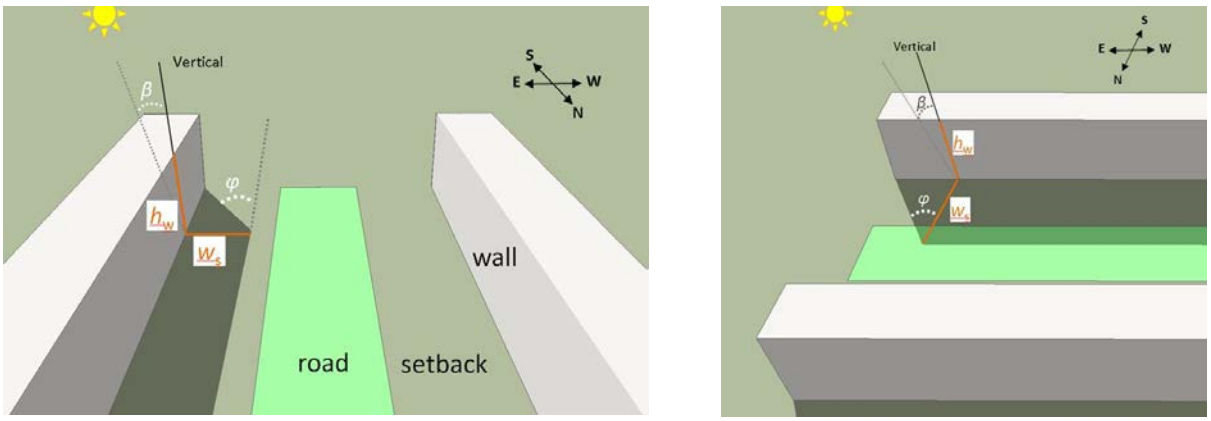

(a) (b)

Figure D-2. Illustration of a wide canyon located in Sacramento, California, on October 21 at 8:00 LST. The canyon is oriented (a) N-S and (b) E-W. The street width, setback width, and wall height are 10 m each. The variables shown are canyon width (w_s), wall height (h_w), azimuth angle (ϕ), and zenith angle (β).

When the canyon runs N-S,

$$w_s = h_w \tan\beta \sin\phi \qquad \text{(D-1)}$$

where h_w is the height of the wall, β is the solar zenith angle, and ϕ is the solar azimuth angle (measured clockwise from south).

When the canyon runs E-W,

$$w_s = h_w \tan\beta \cos\phi \ . \qquad \text{(D-2)}$$

When the shadow is wider than the canyon, the wall facing the sun may be partially shaded by the other wall. The height of the shaded portion h_s is

$$h_s = \frac{h_w \left(w_s - w_c\right)}{w_s} \qquad \text{(D-3)}$$

and the height of the unshaded portion h_u is

$$h_u = h_w - h_s \ . \qquad \text{(D-4)}$$

D.2.3 Solar fluxes

The proposed UCAM calculates all fluxes that enter the canyon and escape through the ceiling after no more than three reflections. To calculate the fluxes, the model uses the sun position, canyon orientation, albedo and dimension of canyon elements, and hourly beam and diffuse horizontal solar irradiances. The fluxes that escape the canyon after the first, second, or third reflection are listed in Table D-1, Table D-2, and Table D-3, respectively. In the flux formulas, ρ_X is the albedo (solar reflectance) of surface X. J_2 is the diffuse sky flux entering through the ceiling; and $J_{5\to0}$, $J_{5\to3u}$, and $J_{5\to4u}$ are the beam solar flux to a sunlit floor segment, to the sunlit portion of the left wall, and to the sunlit portion of the right wall, respectively.

The dimensions of the canyon elements are used to calculate the view factors. A view factor (a.k.a. configuration factor or shape factor) $F_{X\to Y}$ to surface Y from surface X is the fraction of radiant energy leaving surface X that is intercepted by surface Y.

The fluxes that strike a floor segment (surface 0) are calculated independently for each floor segment. According to its location, the segment is assigned the albedo of either the setback or the road. The proposed three-reflection UCAM computes the total upward flux as the sum of all the fluxes listed in in Table through Table including the fluxes that strike each floor segment. Canyon albedo is then computed as the ratio of upward to downward flux through the canyon ceiling. Section D.2.6 gives additional details on how to calculate the solar fluxes and the canyon albedo. Section D.2.7 details calculation of the view factors.

Table D-1. Fluxes that escape the canyon after the first reflection.

Flux	Flux description	Flux formula
2 to 3 to 2	ceiling to left wall to ceiling	$J_2 \cdot F_{2\to3} \cdot \rho_3 \cdot F_{3\to2}$
2 to 4 to 2	ceiling to right wall to ceiling	$J_2 \cdot F_{2\to4} \cdot \rho_4 \cdot F_{4\to2}$
2 to 0 to 2	ceiling to segment to ceiling	$J_2 \cdot F_{2\to0} \cdot \rho_0 \cdot F_{0\to2}$
5 to 0 to 2	sun to sunlit left wall to ceiling	$J_{5\to0} \cdot \rho_0 \cdot F_{0\to2}$
5 to 3u to 2	sun to sunlit right wall to ceiling	$J_{5\to3u} \cdot \rho_3 \cdot F_{3u\to2}$
5 to 4u to 2	sun to segment to ceiling	$J_{5\to4u} \cdot \rho_4 \cdot F_{4u\to2}$

Table D-2. Fluxes that escape the canyon after the second reflection.

Flux	Flux description	Flux formula
2 to 3 to 4 to 2	ceiling to left wall to right wall to ceiling	$J_2 \cdot F_{2\to3} \cdot \rho_3 \cdot F_{3\to4} \cdot \rho_4 \cdot F_{4\to2}$
2 to 4 to 3 to 2	ceiling to left wall to segment to ceiling	$J_2 \cdot F_{2\to4} \cdot \rho_4 \cdot F_{4\to3} \cdot \rho_3 \cdot F_{3\to2}$
2 to 3 to 0 to 2	ceiling to right wall to left wall to ceiling	$J_2 \cdot F_{2\to3} \cdot \rho_3 \cdot F_{3\to0} \cdot \rho_0 \cdot F_{0\to2}$
2 to 4 to 0 to 2	ceiling to right wall to segment to ceiling	$J_2 \cdot F_{2\to4} \cdot \rho_4 \cdot F_{4\to0} \cdot \rho_0 \cdot F_{0\to2}$
2 to 0 to 3 to 2	ceiling to segment to left wall to ceiling	$J_2 \cdot F_{2\to0} \cdot \rho_0 \cdot F_{0\to3} \cdot \rho_3 \cdot F_{3\to2}$
2 to 0 to 4 to 2	ceiling to segment to right wall to ceiling	$J_2 \cdot F_{2\to0} \cdot \rho_0 \cdot F_{0\to4} \cdot \rho_4 \cdot F_{4\to2}$
5 to 0 to 3 to 2	sun to sunlit left wall to right wall to ceiling	$J_{5\to0} \cdot \rho_0 \cdot F_{0\to3} \cdot \rho_3 \cdot F_{3\to2}$
5 to 0 to 4 to 2	sun to sunlit left wall to segment to ceiling	$J_{5\to0} \cdot \rho_0 \cdot F_{0\to4} \cdot \rho_4 \cdot F_{4\to2}$
5 to 3u to 4 to 2	sun to sunlit right wall to left wall to ceiling	$J_{5\to3u} \cdot \rho_3 \cdot F_{3u\to4} \cdot \rho_4 \cdot F_{4\to2}$
5 to 3u to 0 to 2	sun to sunlit right wall to segment to ceiling	$J_{5\to3u} \cdot \rho_3 \cdot F_{3u\to0} \cdot \rho_0 \cdot F_{0\to2}$
5 to 4u to 3 to 2	sun to segment to left wall to ceiling	$J_{5\to4u} \cdot \rho_4 \cdot F_{4u\to3} \cdot \rho_3 \cdot F_{3\to2}$
5 to 4u to 0 to 2	sun to segment to right wall to ceiling	$J_{5\to4u} \cdot \rho_4 \cdot F_{4u\to0} \cdot \rho_0 \cdot F_{0\to2}$

Table D-3. Fluxes that escape the canyon after the third reflection.

Flux	Flux description	Flux formula
2 to 0 to 3 to 4 to 2	ceiling to segment to left wall to right wall to ceiling	$J_2 \cdot F_{2\to0} \cdot \rho_0 \cdot F_{0\to3} \cdot \rho_3 \cdot F_{3\to4} \cdot \rho_4 \cdot F_{4\to2}$
2 to 0 to 4 to 3 to 2	ceiling to segment to right wall to left wall to ceiling	$J_2 \cdot F_{2\to0} \cdot \rho_0 \cdot F_{0\to4} \cdot \rho_4 \cdot F_{4\to3} \cdot \rho_3 \cdot F_{3\to2}$
2 to 0 to 3 to 0 to 2	ceiling to segment to left wall to segment to ceiling	$J_2 \cdot F_{2\to0} \cdot \rho_0 \cdot F_{0\to3} \cdot \rho_3 \cdot F_{3\to0} \cdot \rho_0 \cdot F_{0\to2}$
2 to 0 to 4 to 0 to 2	ceiling to segment to right wall to segment to ceiling	$J_2 \cdot F_{2\to0} \cdot \rho_0 \cdot F_{0\to4} \cdot \rho_4 \cdot F_{4\to0} \cdot \rho_0 \cdot F_{0\to2}$

2 to 3 to 4 to 3 to 2	ceiling to left wall to right wall to left wall to ceiling	$J_2 \cdot F_{2\to3} \cdot \rho_3 \cdot F_{3\to4} \cdot \rho_4 \cdot F_{4\to3} \cdot \rho_3 \cdot F_{3\to2}$
2 to 3 to 4 to 0 to 2	ceiling to left wall to right wall to segment to ceiling	$J_2 \cdot F_{2\to3} \cdot \rho_3 \cdot F_{3\to4} \cdot \rho_4 \cdot F_{4\to0} \cdot \rho_0 \cdot F_{0\to2}$
2 to 3 to 0 to 3 to 2	ceiling to left wall to segment to left wall to ceiling	$J_2 \cdot F_{2\to3} \cdot \rho_3 \cdot F_{3\to0} \cdot \rho_0 \cdot F_{0\to3} \cdot \rho_3 \cdot F_{3\to2}$
2 to 3 to 0 to 4 to 2	ceiling to left wall to segment to right wall to ceiling	$J_2 \cdot F_{2\to3} \cdot \rho_3 \cdot F_{3\to0} \cdot \rho_0 \cdot F_{0\to4} \cdot \rho_4 \cdot F_{4\to2}$
2 to 4 to 3 to 4 to 2	ceiling to right wall to left wall to right wall to ceiling	$J_2 \cdot F_{2\to4} \cdot \rho_4 \cdot F_{4\to3} \cdot \rho_3 \cdot F_{3\to4} \cdot \rho_4 \cdot F_{4\to2}$
2 to 4 to 3 to 0 to 2	ceiling to right wall to left wall to segment to ceiling	$J_2 \cdot F_{2\to4} \cdot \rho_4 \cdot F_{4\to3} \cdot \rho_3 \cdot F_{3\to0} \cdot \rho_0 \cdot F_{0\to2}$
2 to 4 to 0 to 3 to 2	ceiling to right wall to segment to left wall to ceiling	$J_2 \cdot F_{2\to4} \cdot \rho_4 \cdot F_{4\to0} \cdot \rho_0 \cdot F_{0\to3} \cdot \rho_3 \cdot F_{3\to2}$
2 to 4 to 0 to 4 to 2	ceiling to right wall to segment to right wall to ceiling	$J_2 \cdot F_{2\to4} \cdot \rho_4 \cdot F_{4\to0} \cdot \rho_0 \cdot F_{0\to4} \cdot \rho_4 \cdot F_{4\to2}$
5 to 0 to 3 to 4 to 2	sun to segment to left wall to right wall to ceiling	$J_{5\to0} \cdot \rho_0 \cdot F_{0\to3} \cdot \rho_3 \cdot F_{3\to4} \cdot \rho_4 \cdot F_{4\to2}$
5 to 0 to 4 to 3 to 2	sun to segment to right wall to left wall to ceiling	$J_{5\to0} \cdot \rho_0 \cdot F_{0\to4} \cdot \rho_4 \cdot F_{4\to3} \cdot \rho_3 \cdot F_{3\to2}$
5 to 0 to 3 to 0 to 2	sun to segment to left wall to segment to ceiling	$J_{5\to0} \cdot \rho_0 \cdot F_{0\to3} \cdot \rho_3 \cdot F_{3\to0} \cdot \rho_0 \cdot F_{0\to2}$
5 to 0 to 4 to 0 to 2	sun to segment to right wall to segment to ceiling	$J_{5\to0} \cdot \rho_0 \cdot F_{0\to4} \cdot \rho_4 \cdot F_{4\to0} \cdot \rho_0 \cdot F_{0\to2}$
5 to 3u to 4 to 3 to 2	sun to sunlit left wall to right wall to left wall to ceiling	$J_{5\to3u} \cdot \rho_3 \cdot F_{3u\to4} \cdot \rho_4 \cdot F_{4\to3} \cdot \rho_3 \cdot F_{3\to2}$
5 to 3u to 4 to 0 to 2	sun to sunlit left wall to right wall to segment to ceiling	$J_{5\to3u} \cdot \rho_3 \cdot F_{3u\to4} \cdot \rho_4 \cdot F_{4\to0} \cdot \rho_0 \cdot F_{0\to2}$
5 to 3u to 0 to 3 to 2	sun to sunlit left wall to segment to left wall to ceiling	$J_{5\to3u} \cdot \rho_3 \cdot F_{3u\to0} \cdot \rho_0 \cdot F_{0\to3} \cdot \rho_3 \cdot F_{3\to2}$
5 to 3u to 0 to 4 to 2	sun to sunlit left wall to segment to right wall to ceiling	$J_{5\to3u} \cdot \rho_3 \cdot F_{3u\to0} \cdot \rho_0 \cdot F_{0\to4} \cdot \rho_4 \cdot F_{4\to2}$
5 to 4u to 3 to 4 to 2	sun to sunlit right wall to left wall to right wall to ceiling	$J_{5\to4u} \cdot \rho_4 \cdot F_{4u\to3} \cdot \rho_3 \cdot F_{3\to4} \cdot \rho_4 \cdot F_{4\to2}$
5 to 4u to 3 to 0 to 2	sun to sunlit right wall to left wall to segment to ceiling	$J_{5\to4u} \cdot \rho_4 \cdot F_{4u\to3} \cdot \rho_3 \cdot F_{3\to0} \cdot \rho_0 \cdot F_{0\to2}$
5 to 4u to 0 to 3 to 2	sun to sunlit right wall to segment to left wall to ceiling	$J_{5\to4u} \cdot \rho_4 \cdot F_{4u\to0} \cdot \rho_0 \cdot F_{0\to3} \cdot \rho_3 \cdot F_{3\to2}$
5 to 4u to 0 to 4 to 2	sun to sunlit right wall to segment to right wall to ceiling	$J_{5\to4u} \cdot \rho_4 \cdot F_{4u\to0} \cdot \rho_0 \cdot F_{0\to4} \cdot \rho_4 \cdot F_{4\to2}$

D.2.4 Canyon transmittance

Canyon transmittance τ_{canyon} is defined as the ratio of (a) the increase in sunlight reflected through the canyon ceiling upon raising the albedo of a street in the canyon, to (b) the increase in sunlight reflected upon raising the albedo of the same street not in a canyon. It can be interpreted as the transmittance of sunlight from canyon ceiling to street to canyon ceiling.

Let τ_{down} represent the fraction of sunlight downwelling from the sun and sky that travels from ceiling to floor, from ceiling to wall to street, or from ceiling to wall to opposite wall to street. Similarly, let τ_{up}

represent the fraction of sunlight reflected from the street that travels from street to ceiling, from street to wall to ceiling, or from street to wall to opposite wall to ceiling.

Neglecting reflection of light from street to wall to floor, and from street to wall to opposite wall to floor, increasing by $\Delta\rho_{st}$ the albedo of a street of width w_{st} inside a canyon will increase the upflux through the canyon ceiling by

$$\Delta J_{up,inside} = I_g \ \tau_{down} \ w_{st} \ \Delta\rho_{st} \ \tau_{up} \ . \tag{D-5}$$

Increasing by $\Delta\rho_r$ the albedo of the same street *outside* a canyon will increase its upflux by

$$\Delta J_{up,outside} = I_g \ w_{st} \ \Delta\rho_{st} \ . \tag{D-6}$$

Therefore

$$\tau_{canyon} \equiv \frac{\Delta J_{up,inside}}{\Delta J_{up,outside}} = \frac{I_g \ \tau_{down} \ w_{st} \ \Delta\rho_{st} \ \tau_{up}}{I_g \ w_{st} \ \Delta\rho_{st}} = \tau_{down} \ \tau_{up} \ . \tag{D-7}$$

Canyon transmittance should approach unity as canyon height approaches zero, and should never exceed unity. The proposed UCAM is used to calculate the increase in upflux through the ceiling upon increasing the albedo of a street in the canyon:

$$\Delta J_{up,inside} = J_{out}(\rho_{st,\,modified}) - J_{out}(\rho_{st,\,original}) \tag{D-8}$$

where

$$\rho_{st,\,modified} = \rho_{st,\,original} + \Delta\rho_{st} \ . \tag{D-9}$$

D.2.5 Scaling factor

Changing the geometry and surface albedos of an urban canyon may perturb various local atmospheric parameters such as wind flow, vertical and horizontal mixing, and TKE. These parameters may affect the surface and near-surface temperatures. Assuming the atmospheric parameters remain constant, we expect changes in near-surface air temperature to be proportional to changes in the albedo of the canyon surfaces [Li et al. 2014]. To elaborate, the reduction in the near-surface air temperature is proportional to the reduction in the canyon's solar heat gain, which in turn is proportional to the decrease in the canyon's solar absorptance. The reduction in canyon solar absorptance is the same as the increase in canyon albedo. Hence, the reduction in near-surface air temperature is proportional to the increase in flux reflected from the canyon ($\Delta J_{up,inside}$), or simply

$$\Delta T \propto \Delta J_{up,inside} \ . \tag{D-10}$$

Climate models can be used to predict the reduction in air temperature upon increasing the street albedo in a canyon. However, this change in air temperature applies only to a city with the canyon geometry defined in the climate model, and must be adjusted to describe air temperature changes that will occur in a city with different canyon geometries.

To illustrate, assume that the climate model was used to obtain the air temperature change from modifying the street albedo in a city composed of narrow canyons (canyons with no setbacks). The narrow-canyon temperature change ΔT_n may need to be scaled to estimate temperature changes ΔT_w from wide canyons (canyons with setbacks), where subscripts *n* and *w* refer to narrow and wide canyons, respectively. Assuming ΔT is proportional to $\Delta J_{up,inside}$, we define a canyon reflection scaling factor $\sigma_{n\to w}$ to relate the air temperature changes in a wide canyon to those in a narrow canyon:

$$\Delta T_{\mathrm{w}} = \sigma_{\mathrm{n}\to\mathrm{w}}\ \Delta T_{\mathrm{n}} \tag{D-11}$$

where

$$\sigma_{\mathrm{n}\to\mathrm{w}} \equiv \frac{\Delta T_{\mathrm{w}}}{\Delta T_{\mathrm{n}}} = \frac{\Delta J_{\mathrm{up,inside,w}}}{\Delta J_{\mathrm{up,inside,n}}}\ . \tag{D-12}$$

The increase in canyon-reflected flux $\Delta J_{\mathrm{up,inside}}$ upon raising street albedo by $\Delta\rho_{\mathrm{st}}$ is proportional to τ_{canyon}. If the wide and narrow canyons have the same street width and the same increase in street albedo, then

$$\Delta J_{\mathrm{up,outside,w}} = \Delta J_{\mathrm{up,outside,n}} = I_{\mathrm{g}}\ w_{\mathrm{st}}\ \Delta\rho_{\mathrm{st}} \tag{D-13}$$

and the scaling factor equals the ratio of canyon transmittance:

$$\sigma_{\mathrm{n}\to\mathrm{w}} = \frac{\Delta J_{\mathrm{up,inside,w}}}{\Delta J_{\mathrm{up,inside,n}}} = \frac{\tau_{\mathrm{canyon,w}}\ \Delta J_{\mathrm{up,outside,w}}}{\tau_{\mathrm{canyon,n}}\ \Delta J_{\mathrm{up,outside,n}}} = \frac{\tau_{\mathrm{canyon,w}}}{\tau_{\mathrm{canyon,n}}}\ . \tag{D-14}$$

Citywide scaling factor. The shapes of urban canyons can vary between cities and within a city. However, they can be estimated from the city's street design standards and building stock. First, several wide canyons are defined, each with geometries that represent a particular city region and dimensions that follow the street design guidelines of that region. Next, we compute a canyon reflection scaling factor for each wide canyon to relate the air temperature changes in the wide canyon to those in a narrow canyon. Each building of the city is then mapped to one of the newly defined wide canyons. Finally, a citywide scaling factor ($\sigma_{\mathrm{n}\to\overline{\mathrm{w}}}$) can be calculated as the average of the scaling factors of each wide canyon weighted by the number of buildings assigned to each wide canyon. The citywide scaling factor can be used in Eq. (D-11) to scale the changes in air temperature of a city modeled entirely with the narrow canyon to the city composed of the more realistic wide canyons.

D.2.6 Additional details for calculating solar fluxes and canyon albedo

D.2.6.1 Solar irradiances

The model calculates the flux that enters the canyon and is intercepted by the walls and floor. It takes as inputs global horizontal irradiance I_{g} [W/m²] and diffuse horizontal irradiance I_{d} [W/m²]. Annual hourly mean global and diffuse horizontal irradiances are available for over 1,000 sites in the United States from the National Renewable Energy Laboratory's Typical Meteorological Year, version 3 (TMY3) data sets (Wilcox and Marion 2008). The beam (a.k.a. direct) horizontal irradiance I_{b} is then calculated as

$$I_{\mathrm{b}} = I_{\mathrm{g}} - I_{\mathrm{d}} \tag{D-15}$$

and the beam normal solar irradiance I_{bn} is

$$I_{\mathrm{bn}} = \frac{I_{\mathrm{b}}}{\cos\beta}\ . \tag{D-16}$$

Using these solar irradiances and the algorithm detailed next, the model can then calculate the flux that is reflected from the canyon through the ceiling, and calculate the canyon albedo.

D.2.6.2 Downward diffuse solar flux intercepted by the canyon surfaces

The diffuse solar flux entering through the ceiling is

$$J_2 = I_{\mathrm{d}}\ w_{\mathrm{c}}\ . \tag{D-17}$$

The fraction of J_2 that strikes a floor segment is

$$J_{2\to 0} = J_2\ F_{2\to 0} \tag{D-18}$$

where $F_{2\to 0}$ is the view factor to a floor segment from the canyon ceiling. The model iterates through the segments to obtain each value of $J_{2\to 0}$.

The fractions of J_2 that are intercepted by the left wall $J_{2\to 3}$ and by the right wall $J_{2\to 4}$ are

$$J_{2\to 3} = J_2\ F_{2\to 3} \tag{D-19}$$

and

$$J_{2\to 4} = J_2\ F_{2\to 4} \tag{D-20}$$

where $F_{2\to 3}$ and $F_{2\to 4}$ are the view factors from ceiling to left wall and from ceiling to right wall, respectively.

D.2.6.3 Downward beam solar flux intercepted by the canyon surfaces

When a floor segment is unshaded, the beam flux from the solar disc intercepted by the segment is

$$J_{5\to 0} = I_{\mathrm{b}}\ w_0\ . \tag{D-21}$$

The model compares the shadow width (w_{s}) to the segment's distance from each canyon wall to determine whether the segment is unshaded. If segment is in shade, $J_{5\to 0} = 0$. The model iterates through the segments to obtain each value of $J_{5\to 0}$.

The ASHRAE Handbook–Fundamentals (ASHRAE 2009) details how to calculate the downward beam solar irradiance incident on a tilted surface $I_{\mathrm{t,b}}$. Let θ represent angle of incidence. For vertical surfaces (tilt angle 90 °) such as walls, the beam tilt irradiance is

$$I_{\mathrm{t,b}} = I_{\mathrm{bn}}\ \cos\theta \tag{D-22}$$

when $\cos\theta > 0$; otherwise, the surface is in shade. The wall may also be partially or fully shaded by the opposite wall at certain times of the day. For walls or section of walls that are in shade, $I_{\mathrm{t,b}} = 0$.
The cosine of the incidence angle is

$$\cos\theta = \cos(90° - \beta)\ \cos(\phi - \Psi) \tag{D-23}$$

where Ψ is the surface azimuth angle. Thus the beam flux to the unshaded section of wall k from the sun (surface 5) is

$$J_{5\to k\mathrm{u}} = I_{\mathrm{t,b}}\ h_{k\mathrm{u}}\ \cos\theta_k \tag{D-24}$$

where $h_{k\mathrm{u}}$ is the height of the unshaded portion of wall k and θ_k is the angle of incidence for wall k .

This equation yields the fluxes from the sun to the unshaded portion of the left wall, $J_{5\to 3u}$, with unshaded height h_{3u}; and to the unshaded portion of the right wall, $J_{5\to 4u}$, with unshaded height h_{4u}. The magnitudes of $J_{5\to 0}$, $J_{5\to 3u}$, and $J_{5\to 4u}$ depend on wall orientation and solar position. For example, an urban canyon whose length extends E-W has one wall facing north (surface azimuth angle of 180 °) and the other facing south (0 °). For canyons whose length extends N-S, one wall faces east (-90 °) and the other faces west (90 °). Solar position (zenith and azimuth angles) can be obtained from NREL's Solar Position Calculator (NREL 2013) by location, date, and time, or computed following ASHRAE (2009).

D.2.6.4 Example of calculating the canyon-reflected solar fluxes

The albedo ρ_X is the fraction of the incoming flux that is reflected from canyon surface X. The view factor $F_{X\to Y}$ is the fraction of the reflected flux leaving surface X that is intercepted by surface Y. Using the albedo of every canyon surface and the view factors from each surface to all other surfaces, we calculated all of the fluxes that are listed in Table D-1 through Table D-3. As an example, the two-reflection flux from the sun (surface 5) to a floor segment (0) to the left wall (3) to the canyon ceiling (2) is

$$J_{5\to 0\to 3\to 2} = J_{5\to 0}\ \rho_0\ F_{0\to 3}\ \rho_3\ F_{3\to 2}\,. \tag{D-25}$$

This approach was used to calculate all one-, two-, and three-reflection fluxes.

D.2.6.5 Canyon albedo

For the three-reflection proposed UCAM, the upward flux leaving the canyon, J_{up}, is the sum of all fluxes listed in Table D-1 through Table D-3, including all fluxes that are intercepted by each floor segment. The downward flux entering the canyon is

$$J_{down} = w_2\ I_g \tag{D-26}$$

where w_2 is the width of the canyon ceiling. Hence, the canyon albedo ρ_c is the ratio of upward flux to downward flux:

$$\rho_c \equiv \frac{J_{up}}{J_{down}}\ . \tag{D-27}$$

The daily mean canyon albedo is

$$\overline{\rho}_c = \frac{\int_{day} J_{down}(t)\ \rho_c(t)\ dt}{\int_{day} J_{down}(t)\ dt} \tag{D-28}$$

where t is time.

D.2.7 View factor calculations

View factor formulas have been presented in the engineering literature for most common geometric configurations (Howell 2015). All the view factors required in the proposed UCAM can be calculated from published formulas.

Ceiling to wall

Consider two infinitely long perpendicular plates sharing a common edge (e.g. the geometry formed by the canyon ceiling and a canyon wall in Figure D-1). If horizontal surface X has width *w* and vertical surface Y has height *h*, the view factor to Y from X is

$$F_{X\to Y} = \frac{1}{2}\left(1 + \frac{h}{w} - \sqrt{1+\left(\frac{h}{w}\right)^2}\right) . \qquad \text{(D-29)}$$

(Howell 2015, Equation C-3). This formula yields the view factors from the canyon ceiling (surface 2, width w_2) to the entire left wall (surface 3, height h_3); to the entire right wall (surface 4, height h_4); to the unshaded portion of the left wall (surface 3u, height h_{3u}); and to the unshaded portion of the right wall (surface 4u, height h_{4u}). These view factors are $F_{2\to3}$, $F_{2\to4}$, $F_{2\to3u}$, and $F_{2\to4u}$ respectively.
View factor reciprocity relates view factors (F) and areas (A), such that

$$A_X\, F_{X\to Y} = A_Y\, F_{Y\to X} . \qquad \text{(D-30)}$$

View factors $F_{3\to2}$, $F_{4\to2}$, $F_{3u\to2}$, and $F_{4u\to2}$ can be obtained from this relation.

Ceiling to floor

The sum of view factors from a given surface to itself and all other surfaces is unity. Thus from the canyon ceiling (surface 2),

$$F_{2\to1} + F_{2\to2} + F_{2\to3} + F_{2\to4} = 1 . \qquad \text{(D-31)}$$

By symmetry, $F_{2\to3} = F_{2\to4}$. Meanwhile, $F_{2\to2}$ is zero since the surface 2 does not see itself. Hence, the ceiling-to-floor view factor is

$$F_{2\to1} = 1 - 2\times F_{2\to3} . \qquad \text{(D-32)}$$

Segment to ceiling

The view factor from a floor segment to sky varies by segment. As the model iterates through the segments, it calculates their view factor to the sky using the “crossed-string method” (Hottel 1954). Figure D-3. illustrates how the method is applied to calculate the segment-to-sky view factor. The model calculates the distances L_x, L_w, L_y, and L_z for each segment.

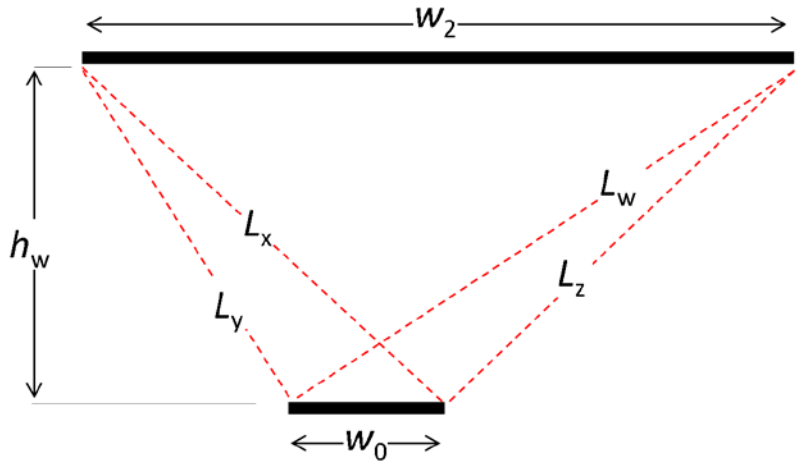

Figure D-3. Crossed-string method applied to segment-to-ceiling view factors.

The equation (Howell 2015, section C-2a) is derived from this method and used to calculate the segment-to-ceiling view factors:

$$F_{0\to 2} = \frac{L_x + L_w - L_y - L_z}{2w_0} \quad . \tag{D-33}$$

Segment to wall

Consider an infinitely long plate S_1 at an angle α from another non-adjacent infinitely long plate S_2. If the plates are perpendicular, the formula for this configuration (Figure D-4a) can be simplified to

$$F_{S_1\to S_2} = \frac{\left(a_1^{\,2} - b_2^{\,2}\right)^{1/2} + \left(a_2^{\,2} + b_1^{\,2}\right)^{1/2} - \left(a_2^{\,2} + b_2^{\,2}\right)^{1/2} - \left(a_1^{\,2} + b_1^{\,2}\right)^{1/2}}{2\left(a_2 - a_1\right)} \tag{D-34}$$

(Howell 2015, section C-5a). This formula is used by the model to calculate the view factor from each wall to each floor segment. Given the position of the segment relative to each wall (Figure D-4b), $F_{3\to 0}$, $F_{3u\to 0}$, $F_{4\to 0,}$ and $F_{4u\to 0}$ are calculated as follows:

$$F_{3\to 0} = F_{S_1\to S_2}(a_1 = 0, a_2 = h_w, b_1 = x_1, b_2 = x_2) \tag{D-35}$$

$$F_{4\to 0} = F_{S_1\to S_2}(a_1 = 0, a_2 = h_w, b_1 = w_c - x_2, b_2 = w_2 - x_1) \tag{D-36}$$

$$F_{3u\to 0} = F_{S_1\to S_2}(a_1 = h_w - h_{3u}, a_2 = h_w, b_1 = x_1, b_2 = x_2) \tag{D-37}$$

$$F_{4u\to 0} = F_{S_1\to S_2}(a_1 = h_w - h_4, a_2 = h_w, b_1 = w_2 - x_2, b_2 = w_2 - x_1) \tag{D-38}$$

Note that x_1 and x_2 vary by segment, while h_{3u} and h_{4u} vary by time of day.

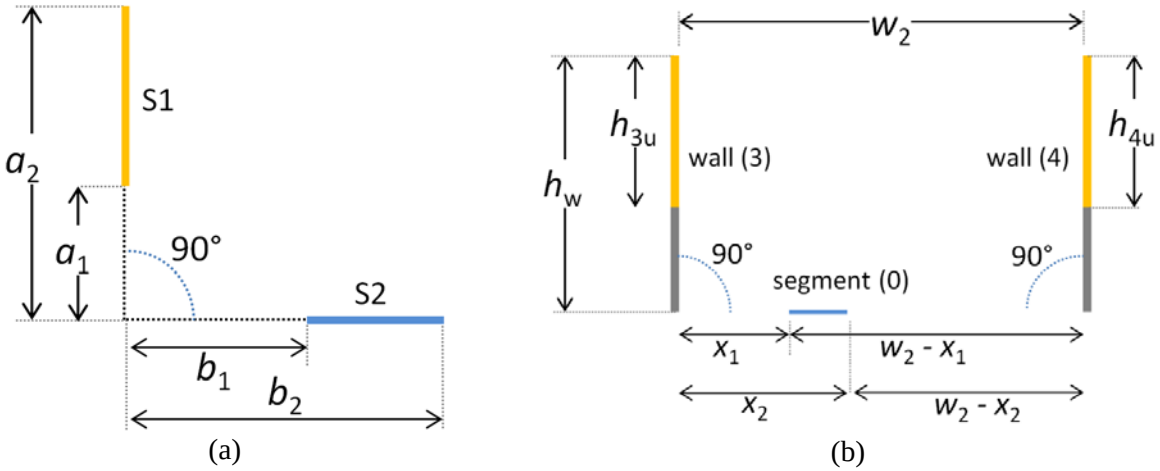

Figure D-4. Diagram of dimensions and variables used to calculate segment to wall view factors.

Applying view-factor reciprocity, segment-to-wall view factors are calculated as

$$F_{0\to 3} = \frac{h_3 F_{3\to 0}}{w_0} \tag{D-39}$$

$$F_{0\to 4} = \frac{h_4 F_{4\to 0}}{w_0}. \tag{D-40}$$

Wall to wall

The "cross-string method" described in the Section D.2.7, can also be used to calculate the view factors from one wall (or section of wall) to the opposite wall (or section of opposite wall). Thus, Eq. D-29 and the canyon dimensions given in Figure D-4 were used to obtain the view factors from one canyon wall to the opposite wall ($F_{3\to 4}$ and $F_{4\to 3}$), and from the unshaded portion of each wall to the opposite wall ($F_{3u\to 4}$ and $F_{4u\to 3}$).

D.3 References

ASHRAE 2009. Chapter 14: Climatic Design Information. *2009 ASHRAE Handbook—Fundamentals (SI)*.

Hottel, HC. 1954. Radiant Heat Transmission. William H. McAdams 3rd Edition. pp 55-125. McGraw-Hill Book Co., New York.

Howell JR. 2015. A catalog of radiation configuration factors. McGraw-Hill Book Co., New York. Retrieved 2015-12-10 from http://www.thermalradiation.net/tablecon.html

Li D, Bou-Zeid E, Oppenheimer M. 2014. The effectiveness of cool and green roofs as urban heat island mitigation strategies. *Environmental Research Letters* 9(5), 055002 (16 pages).

NREL. 2013. Measurement and Instrumentation Data Center Solar Position (SOLPOS) Calculator. National Renewable Energy Laboratory, Golden, CO. Retrieved 2015-12-10 from http://www.nrel.gov/midc/solpos/spa.html

Wilcox S, Marion W. 2008. User's Manual for TMY3 Data Sets, NREL/TP-581-43156. National Renewable Energy Laboratory, Golden CO. Retrieved 2015-12-10 from http://rredc.nrel.gov/solar/old_data/nsrdb/1991-2005/tmy3

Appendix E

E Assessing the age of California's building stock

The Commercial Building Energy Consumption Survey (CBECS) groups the year of construction for commercial building stock into 10-year periods. The Residential Energy Consumption Survey (RECS) is the residential analog of CBECS and does a similar classification for residential buildings. Table E-1 gives the mean period of construction as obtained by CBECS and RECS for the building types that were mapped to the EnergyPlus prototypes that were used for the study (Table 26).

The age of the state's building stock was also calculated using the property data collection from California's Assessor's office. The collection includes over 12.5 million records of properties in the state. Table E-2 lists the relevant property types for this study and their state-wide age.

Table E-1. Mean period of construction for different building types as reported by CBECS and RECS.

Building type	Mean period of construction
Professional office [a]	1970 to 1979
Government office [a]	1970 to 1979
Mixed-use office [a]	1980 to 1989
Elementary school [a]	1970 to 1979
Fast food [a]	1980 to 1989
Restaurant [a]	1970 to 1979
Hotel [a]	1980 to 1989
Retail store [a]	1970 to 1979
Strip shopping mall [a]	1980 to 1989
Single-family detached [b]	1970 to 1979
5+ units apartment complex [b]	1970 to 1979

[a] Source: CBECS 2012.
[b] Source: RECS 2009.

Table E-2. Mean year of construction of building stock reported by the Assessor's office.

Building type	Mean year of construction	Building type	Mean year of construction
Store/office combo	1961	Bowling alley	1970
Department store	1970	Clubs, fraternal organizations	1954
Restaurant, bar, food service	1967	Governmental, public	1950
Financial building	1971	School	1960
Food store, market	1973	Multi-family res (5+ units)	1957
Hospitals, convalescent homes	1965	Condominium, PUD	1982
Hotel/motel	1958	Cooperative	1944
Laundry, dry cleaning	1959	Duplex	1958
Medical buildings	1972	Multi-family dwelling (2-4 units)	1984
Mobile home parks, trailer parks	1981	Mobile home	1973
Miscellaneous commercial	1953	Miscellaneous residential	1951
Nursery	1961	Quadruplex	1962
Office building	1968	Single-family residence	1969
Shopping center	1980	Time share	1991
Stores, retail outlet	1958	Triplex	1943